frontiers
RESEARCH TOPICS

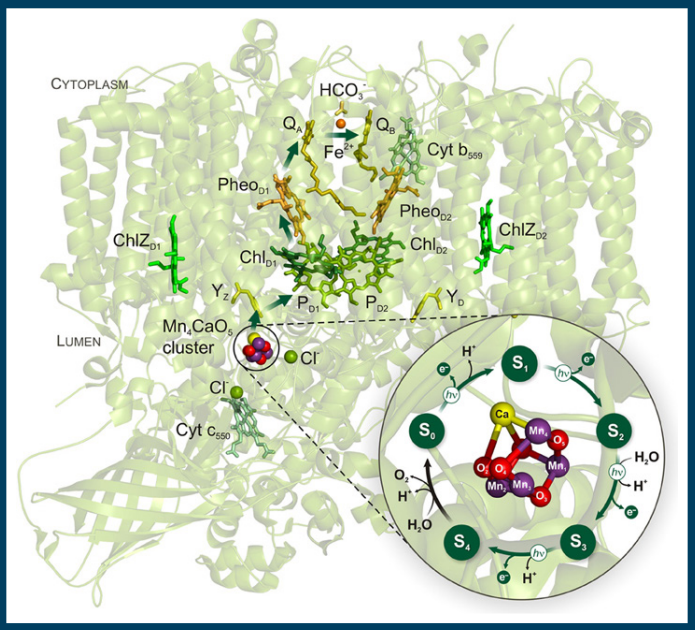

CURRENT CHALLENGES IN PHOTOSYNTHESIS: FROM NATURAL TO ARTIFICIAL

Topic Editors
Harvey J. M. Hou, Suleyman I. Allakhverdiev, Mohammad Mahdi Najafpour and Govindjee

frontiers in PLANT SCIENCE

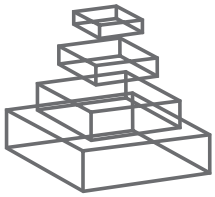

frontiers

ISSN 1664-8714
ISBN 978-2-88919-286-1
DOI 10.3389/978-2-88919-286-1

ABOUT FRONTIERS

Frontiers is more than just an open-access publisher of scholarly articles: it is a pioneering approach to the world of academia, radically improving the way scholarly research is managed. The grand vision of Frontiers is a world where all people have an equal opportunity to seek, share and generate knowledge. Frontiers provides immediate and permanent online open access to all its publications, but this alone is not enough to realize our grand goals.

FRONTIERS JOURNAL SERIES

The Frontiers Journal Series is a multi-tier and interdisciplinary set of open-access, online journals, promising a paradigm shift from the current review, selection and dissemination processes in academic publishing.
All Frontiers journals are driven by researchers for researchers; therefore, they constitute a service to the scholarly community. At the same time, the Frontiers Journal Series operates on a revolutionary invention, the tiered publishing system, initially addressing specific communities of scholars, and gradually climbing up to broader public understanding, thus serving the interests of the lay society, too.

DEDICATION TO QUALITY

Each Frontiers article is a landmark of the highest quality, thanks to genuinely collaborative interactions between authors and review editors, who include some of the world's best academicians. Research must be certified by peers before entering a stream of knowledge that may eventually reach the public - and shape society; therefore, Frontiers only applies the most rigorous and unbiased reviews.
Frontiers revolutionizes research publishing by freely delivering the most outstanding research, evaluated with no bias from both the academic and social point of view.
By applying the most advanced information technologies, Frontiers is catapulting scholarly publishing into a new generation.

WHAT ARE FRONTIERS RESEARCH TOPICS?

Frontiers Research Topics are very popular trademarks of the Frontiers Journals Series: they are collections of at least ten articles, all centered on a particular subject. With their unique mix of varied contributions from Original Research to Review Articles, Frontiers Research Topics unify the most influential researchers, the latest key findings and historical advances in a hot research area!
Find out more on how to host your own Frontiers Research Topic or contribute to one as an author by contacting the Frontiers Editorial Office: researchtopics@frontiersin.org

CURRENT CHALLENGES IN PHOTOSYNTHESIS: FROM NATURAL TO ARTIFICIAL

Topic Editors:
Harvey J. M. Hou, Alabama State University, USA
Suleyman I. Allakhverdiev, Russian Academy of Sciences, Russia
Mohammad Mahdi Najafpour, Institute for Advanced Studies in Basic Sciences, Iran
Govindjee, University of Illinois at Urbana-Champaign, USA

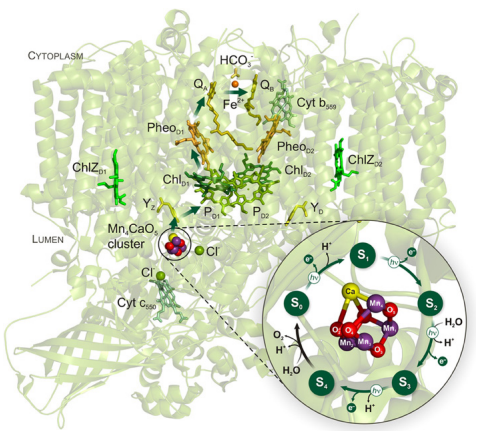

Principles of artificial photosynthesis. Figure taken from: Shevela D and Messinger J (2013) Studying the oxidation of water to molecular oxygen in photosynthetic and artificial systems by time-resolved membrane-inlet mass spectrometry. *Front. Plant* Sci. 4:473. doi: 10.3389/fpls.2013.00473

Jules Verne (1828-1905), author of Around the World in Eighty Days (1873) and Journey to the Center of the Earth (1864), wrote in 1875

"I believe that water will one day be used as a fuel, because the hydrogen and oxygen which constitute it, used separately or together, will furnish an inexhaustible source of heat and light. I therefore believe that, when coal (oil) deposits are oxidised, we will heat ourselves by means of water. Water is the fuel of the future"

Solar energy is the only renewable energy source that has sufficient capacity for the global energy need; it is the only one that can address the issues of energy crisis and global climate change. A vast amount of solar energy is harvested and stored via photosynthesis in plants, algae, and cyanobacteria since over 3 billion years. Today, it is estimated that photosynthesis produces more than 100 billion tons of dry biomass annually, which would be equivalent to a hundred times the weight of the total human population on our planet at the present time, and equal to a global energy storage rate of about 100 TW.

The solar power is the most abundant source of renewable energy, and oxygenic photosynthesis uses this energy to power the planet using the amazing reaction of water splitting. During water splitting, driven ultimately by sunlight, oxygen is released into the atmosphere, and this, along with food production by photosynthesis, supports life on our

earth. The other product of water oxidation is "hydrogen" (proton and electron). This 'hydrogen' is not normally released into the atmosphere as hydrogen gas but combined with carbon dioxide to make high energy containing organic molecules. When we burn fuels we combine these organic molecules with oxygen. The design of new solar energy systems must adhere to the same principle as that of natural photosynthesis. For us to manipulate it to our benefit, it is imperative that we completely understand the basic processes of natural photosynthesis, and chemical conversion, such as light harvesting, excitation energy transfer, electron transfer, ion transport, and carbon fixation. Equally important, we must exploit application of this knowledge to the development of fully synthetic and/or hybrid devices. Understanding of photosynthetic reactions is not only a satisfying intellectual pursuit, but it is important for improving agricultural yields and for developing new solar technologies. Today, we have considerable knowledge of the working of photosynthesis and its photosystems, including the water oxidation reaction. Recent advances towards the understanding of the structure and the mechanism of the natural photosynthetic systems are being made at the molecular level. To mimic natural photosynthesis, inorganic chemists, organic chemists, electrochemists, material scientists, biochemists, biophysicists, and plant biologists must work together and only then significant progress in harnessing energy via "artificial photosynthesis" will be possible.

This Research Topic provides recent advances of our understanding of photosynthesis, gives to our readers recent information on photosynthesis research, and summarizes the characteristics of the natural system from the standpoint of what we could learn from it to produce an efficient artificial system, i.e., from the natural to the artificial. This topic is intended to include exciting breakthroughs, possible limitations, and open questions in the frontiers in photosynthesis research.

Table of Contents

frontiers in
PLANT SCIENCE

EDITORIAL
published: 28 May 2014
doi: 10.3389/fpls.2014.00232

Current challenges in photosynthesis: from natural to artificial

Harvey J. M. Hou[1]*, Suleyman I. Allakhverdiev[2,3], Mohammad M. Najafpour[4] and Govindjee[5]

[1] Department of Physical Sciences, Alabama State University, Alabama, AL, USA
[2] Institute of Plant Physiology, Russian Academy of Sciences, Moscow, Russia
[3] Institute of Basic Biological Problems, Russian Academy of Sciences, Moscow, Russia
[4] Department of Chemistry, Center of Climate Change and Global Warming, Institute for Advanced Studies in Basic Sciences, Zanjan, Iran
[5] Departments of Biochemistry and Plant Biology, Center of Biophysics and Quantitative Biology, University of Illinois at Urbana-Champaign, Urbana, IL, USA
*Correspondence: hhou@alasu.edu

Edited and reviewed by:
Steven Carl Huber, USDA-ARS, USA

Keywords: photosynthesis, artificial photosynthesis, water oxidation, thylakoid, chlorophyll *f*

Photosynthesis is a process by which plants, algae, cyanobacteria, and anoxygenic photosynthetic bacteria capture and store solar energy on a massive scale, in particular via the water-splitting chemistry (Hoganson and Babcock, 1997; Blankenship, 2002; Ferreira et al., 2004; Loll et al., 2005; Yano et al., 2006; Umena et al., 2011). It is the most important reaction on Earth, estimated to produce more than 100 billion tons of dry biomass annually; this means that photosynthesis is producing biomass equal to two Egyptian pyramids per hour. But, this will not be enough to sustain life on Earth by the year 2050. The global fossil fuels on which we currently depend are derived from millions of years of past photosynthetic activity. The fossil energy fuels are limited and must be replaced by renewable and environment-friendly energy source to support and sustain life on Earth (Lewis and Nocera, 2006; Blankenship et al., 2011). To address this immediate energy crisis, worldwide efforts are being made on artificial photosynthesis using the principles and mechanisms observed in nature (Brimblecombe et al., 2009; McConnell et al., 2010; Kanady et al., 2011; Wiechen et al., 2012; Najafpour et al., 2013). It is not a matter of mimicking natural photosynthesis, but to use its current knowledge to improve photosynthesis itself, as well as to produce biofuels, including hydrogen evolution by artificial means (Barber, 2009; Hou, 2010; Nocera, 2012; He et al., 2013).

This book contains 10 chapters and presents recent advances in photosynthesis and artificial photosynthesis. It starts with two opinion articles on possible strategies to improve photosynthesis in plants and fascinating mechanisms of unidirectional photodamage of pheophytin in photosynthesis. The idea that plant photosynthesis is maximized due to the perfect evolution might be faulty. Leister evaluated and argued the issue openly and proposed that improvement of photosynthesis can be made by synthetic biology including genetic engineering, redesign or de novo creation of entire photosystems as well as conventional breeding (Leister, 2012). Unidirectional photodamage of a pheophytin molecule in photosystem II and purple bacterial reaction centers was observed. The mysterious phenomena were analyzed and discussed in terms of different possible functions of the pheophytin in photosynthesis (Hou, 2014).

The book is followed by four review articles that discuss the current state of research on: photosynthetic water oxidation in natural and artificial photosynthesis, as obtained by mass spectrometry (MS) and Fourier transform infrared spectroscopy (FTIR); functional models of thylakoid lumen; and horizontal gene transfer in photosynthetic eukaryotes. The time-resolved isotope-ratio membrane-inlet mass spectrometry (TR-IR-MIMS) is able to determine the isotopic composition of gaseous products. Shevela et al briefly introduced the key aspects of the methodology, summarized the recent results on the mechanisms and pathways of oxygen formation in PS II using this unique technique and outlined the future perspectives of the application in water splitting chemistry (Shevela and Messinger, 2013) Another unique technique in probing the mechanism of water oxidation in PS II is the light-induced FTIR difference spectroscopy. Chu reviewed the recent fruitful structural data, and believed that the FTIR will continue to provide vital structural and mechanistic insights into the water-splitting process in PS II together with isotopic labeling, site-directed mutagenesis, model compound studies, and computational calculation (Chu, 2013). The thylakoid lumen offers the environment for oxygen evolution, electron transfer, and photoprotection in photosynthesis. Jarvi et al evaluated the recent studies of many lumen proteins and highlighted the importance of the thiol-disulfide modulation in controlling the functions of the thylakoid lumen proteins and their pathways of photosynthesis (Järvi et al., 2013). Qiu et al discussed that importance of the horizontal gene transfer (HGT) in enriching the algal genomes and proposed that the alga endosymbionts may be the HGT vectors in photosynthetic eukaryotes (Qiu et al., 2013).

Finally, the book offers four research articles, which focus on FTIR studies on photosynthetic reaction centers, functions of thylakoid protein kinases STN7 and STN8, photosynthesis acclimation of maize seedlings, and characterization of the newly discovered chlorophyll *f*-containing cyanobacterium *Halomicronema hongdechloris*. The computational calculation (ONIOM) is increasingly critical in interpreting the FTIR data in elucidating the structural and functional relationship in photosynthesis. Zhao et al using ONIOM type calculation to simulate isotope edited FTIR difference spectra for reaction centers with a variety of foreign quinones in the Q_A site and allows a direct assessment of the appropriateness of previous IR assignments and suggestions (Zhao et al., 2013). The protein kinases STN7 and STN8 are predominately responsible for the thylakoid

phosphorylation in PS II. Wunder et al reported the effects of the STN8 expression levels on the formation and modulation of thylakoid proteins and kinases (Wunder et al., 2013). Hirth et al assessed the photosynthetic acclimation responses of the C3 and C4 plants under simulated field light conditions (Hirth et al., 2013). Recently a chlorophyll *f* (Chl *f*) in cyanobacterium *Halomincronema hongdechloris* was identified and has the most red-shifted absorption peak of 707 nm in oxygenic photosynthesis (Chen et al., 2010), which may enhance the potential photosynthesis efficiency for solar fuel production. The *Halomincronema hongdechloris* was characterized upon the exposure to the different light, pH, salinity, temperature, and nutrition to achieve the optimizing growth culture conditions (Li et al., 2014).

Due to the extremely limited time frame for collecting manuscripts and the strict deadline for publishing this book, several planned manuscripts by world leaders, who had agreed to contribute, are unfortunately not included in this book. Thus, the current book provides a snapshot of the latest work in photosynthesis research. To obtain complete information on the current progress in the field of photosynthesis, we highly recommend reviews and research articles, published in 2013, in two volumes of *Photosynthesis Research* (Allakhverdiev et al., 2013a,b)

In conclusion, the book provides readers with some of the most recent and exciting breakthroughs from natural to artificial photosynthesis, discusses the potential limitations of the results, and addresses open questions in photosynthesis and energy research. It is written by 31 young active scientists and established leading experts from Australia, Finland, Germany, Sweden, Taiwan, and the United States. We hope that this book is able to provide novel and insightful information to readers and stimulate the future research endeavors in the photosynthesis community.

ACKNOWLEDGMENTS

We take this opportunity to acknowledge and thank all the authors for writing excellent book chapters, and for being supportive and cooperative when their manuscripts were being reviewed and revised. We also thank the external reviewers for their timely contribution and effort in judging the value of the manuscript and delivering constructive comments, which have undoubtedly improved the quality and readability of the book. We thank the Specialty Chief Editor of *Frontiers in Plant Science*, Steve Huber, for his valuable advice and insightful discussions. We also thank Kennedy Wekesa and Audrey Napier for critical reading of the manuscript. We are very grateful to Amanda Baker, Graeme Moffat, Despoina Evangelakou, and Adriana Timperi of the Frontiers Production Office for their insightful advice and meaningful assistance during the entire book project.

REFERENCES

Allakhverdiev, S. I., Shen, J.-R., and Edwards, G. E. (2013a). Special issues on photosynthesis education honoring govindjee. *Photosynthesis Res.* 116, 1–534.

Allakhverdiev, S. I., Shen, J.-R., and Edwards, G. E. (2013b). Special issues on photosynthesis education honoring govindjee. *Photosynthesis Res.* 117, 1–566.

Barber, J. (2009). Photosynthetic energy conversion: natural and artificial. *Chem. Soc. Rev.* 38, 185–196 doi: 10.1039/b802262n

Blankenship, R. E. (2002). *Molecular Mechanisms of Photosynthesis*. Oxford: Blackwell Science. doi: 10.1002/9780470758472

Blankenship, R. E., Tiede, D. M., Barber, J., Brudvig, G. W., Fleming, G., Ghirardi, M., et al. (2011). Comparing the efficiency of photosynthesis with photovoltaic devices and recognizing opportunities for improvement. *Science* 332, 805–809 doi: 10.1126/science.1200165

Brimblecombe, R., Dismukes, G. C., Swiegers, G. F., and Spiccia, L. (2009). Molecular water-oxidation catalysts for photoelectrochemical cells. *Dalton Trans.* 43, 9374–9384 doi: 10.1039/b912669d

Chen, M., Schliep, M., Willows, R. D., Cai, Z. L., Neilan, B. A., and Scheer, H. (2010). A red-shifted chlorophyll. *Science* 329, 1318–1319. doi: 10.1126/science.1191127e.1

Chu, H.-A. (2013). Fourier transform infrared difference spectroscopy for studying the molecular mechanism of photosynthetic water oxidation. *Front. Plant Sci.* 4:146. doi: 10.3389/fpls.2013.00146

Ferreira, K. N., Iverson, T. M., Maghlaoui, K., Barber, J., and Iwata, S. (2004). Architecture of the photosynthetic oxygen-evolving center. *Science* 303, 1831–1838. doi: 10.1126/science.1093087

He, W., Zhao, K.-H., and Hou, H. J. M. (2013). Toward solar fuel production using manganese/semiconductor systems to mimic photosynthesis. *NanoPhotoBioSciences* 1, 63–78.

Hirth, M., Dietzel, L., Steiner, S., Ludwig, R., Weidenbach, H., Pfalz, J., et al. (2013). Photosynthetic acclimation responses of maize seedlings grown under artificial laboratory light gradients mimicking natural canopy conditions. *Front. Plant Sci.* 4:334. doi: 10.3389/fpls.2013.00334

Hoganson, C. W., and Babcock, G. T. (1997). A metallo radical mechanism for the generation of oxygen from water in photosynthesis. *Science* 277, 1953–1956. doi: 10.1126/science.277.5334.1953

Hou, H. J. M. (2010). Structural and mechanistic aspects of Mn-oxo and Co-based compounds in water oxidation catalysis and potential application in solar fuel production. *J. Integr. Plant Biol.* 52, 704–711 doi: 10.1111/j.1744-7909.2010.00974.x

Hou, H. J. M. (2014). Unidirectional photodamage of pheophytin in photosynthesis. *Front. Plant Sci.* 4:554. doi: 10.3389/fpls.2013.00554

Järvi, S., Gollan, P. J., and Aro, E.-M. (2013). Understanding the roles of the thylakoid lumen in photosynthesis regulation. *Front. Plant Sci.* 4:434. doi: 10.3389/fpls.2013.00434

Kanady, J. S., Tsui, E. Y., Day, M. W., and Agapie, T. (2011). A synthetic model of the Mn_3Ca subsite of the oxygen-evolving complex in photosystem II. *Science* 333, 733–736. doi: 10.1126/science.1206036

Leister, D. (2012). How can the light reactions of photosynthesis be improved in plants? *Front. Plant Sci.* 3:199. doi: 10.3389/fpls.2012.00199

Lewis, N. S., and Nocera, D. G. (2006). Powering the planet: chemical challenges in solar energy utilization. *Proc. Natl. Acad. Sci. U.S.A.* 103, 15729–15735 doi: 10.1073/pnas.0603395103

Li, Y., Lin, Y., Loughlin, P. C., and Chen, M. (2014). Optimization and effects of different culture conditions on growth of *Halomicronema hongdechloris* – a filamentous cyanobacterium containing chlorophyll *f*. *Front. Plant Sci.* 5:67. doi: 10.3389/fpls.2014.00067

Loll, B., Kern, J., Saenger, W., Zouni, A., and Biesiadka, J. (2005). Towards complete cofactor arrangement in the 3.0A resolution structure of photosystem II. *Nature* 438, 1040–1044. doi: 10.1038/nature04224

McConnell, I., Li, G., and Brudvig, G. W. (2010). Energy conversion in natural and artificial photosynthesis. *Chem. Biol.* 17, 434–447. doi: 10.1016/j.chembiol.2010.05.005

Najafpour, M. M., Mahnaz Abasi, M., and Allakhverdiev, S. I. (2013). Recent proposed mechanisms for biological water oxidation. *NanoPhotoBioSciences* 1, 79–92.

Nocera, D. G. (2012). The artificial leaf. *Acc. Chem. Res.* 45, 767–776. doi: 10.1021/ar2003013

Qiu, H., Yoon, H. S., and Bhattacharya, D. (2013). Alga lendosymbionts as vectors of horizontal gene transfer in photosynthetic eukaryotes. *Front. Plant Sci.* 4:366. doi: 10.3389/fpls.2013.00366

Shevela, D., and Messinger, J. (2013). Studying the oxidation of water to molecular oxygen in photosynthetic and artificial systems by time-resolved membrane-inlet mass spectrometry. *Front. Plant Sci.* 4:473. doi: 10.3389/fpls.2013.00473

Umena, Y., Kawakami, K., Shen, J. R., and Kamiya, N. (2011). Crystal structure of oxygen-evolving photosystem II at a resolution of 1.9 A. *Nature* 473, 55–61. doi: 10.1038/nature09913

Wiechen, M., Berends, H.-M., and Kurz, P. (2012). Water oxidation catalysed by manganese compounds: from complexes to "biomimetic rocks." *Dalton Trans.* 41, 21–31. doi: 10.1039/c1dt11537e

Wunder, T., Xu, W., Liu, Q., Wanner, G., Leister, D., and Pribil, M. (2013). The major thylakoid protein kinases STN7 and STN8 revisited: effects of altered STN8 levels and regulatory specificities of the STN kinases. *Front. Plant Sci.* 4:417. doi: 10.3389/fpls.2013.00417

Yano, J., Kern, J., Sauer, K., Latimer, M. J., Pushkar, Y., Biesiadka, J., et al. (2006). Where water is oxidized to dioxygen: structure of the photosynthetic Mn_4Ca cluster. *Science* 314, 821–825. doi: 10.1126/science.1128186

Zhao, N., Lamichhane, H. P., and Hastings, G. (2013). Comparison of calculated and experimental isotope edited FTIR difference spectra for purple bacterial photosynthetic reaction centers with different quinones incorporated into the Q_A binding site. *Front. Plant Sci.* 4:328. doi: 10.3389/fpls.2013.00328

Conflict of Interest Statement: The authors declare that the research was conducted in the absence of any commercial or financial relationships that could be construed as a potential conflict of interest.

Received: 26 March 2014; accepted: 09 May 2014; published online: 28 May 2014.
Citation: Hou HJM, Allakhverdiev SI, Najafpour MM and Govindjee (2014) Current challenges in photosynthesis: from natural to artificial. Front. Plant Sci. ***5****:232. doi: 10.3389/fpls.2014.00232*
This article was submitted to Plant Physiology, a section of the journal Frontiers in Plant Science.

frontiers in
PLANT SCIENCE

OPINION ARTICLE
published: 28 August 2012
doi: 10.3389/fpls.2012.00199

How can the light reactions of photosynthesis be improved in plants?

Dario Leister*

Plant Molecular Biology, Department Biology I, Ludwig-Maximilians-University Munich, Planegg-Martinsried, Germany
**Correspondence: leister@lmu.de*

Edited by:
Suleyman I. Allakhverdiev, Russian Academy of Sciences, Russia

The evolutionary patchwork nature of the light reactions of photosynthesis in plants provides ample scope for their improvement, particularly with respect to its light-harvesting components and the susceptibility of photosystems to photodamage. Such improvements can be achieved by genetic engineering and, more indirectly, by conventional breeding, whereas synthetic biology should allow in the long-term the redesign or de novo creation of entire photosystems that are more efficient because they are less susceptible to photodamage and produce fewer harmful reactive oxygen species. This photosystem redesigning will require novel model organisms in which such concepts can be realized, tested, and reiteratively improved.

HOW "PERFECT" IS PHOTOSYNTHESIS?

The idea that plant photosynthesis cannot be improved, because evolution has already perfected it, is surprisingly widespread. I do not share this notion, for several reasons. (1) Natural selection, which maximizes total fitness rather than (agronomic) yield, has shaped plant photosynthesis for life in environments that differ considerably from the resource-rich settings provided by modern agriculture. (2) Even assuming that plant photosynthesis has been optimized during evolution, major parts of the original "hardware" were obviously sub-optimal, and have been bypassed rather than replaced. This is because plant photosynthesis originated in prokaryotes, and initially evolved in low-light (i.e., marine) conditions in the absence of oxygen. In consequence, plants have to cope with an evolutionary inheritance that includes a photosystem II (PSII), which is damaged by high concentrations of its substrate – light (Nishiyama et al., 2011; Murata et al., 2012). To avoid photodamage, plants have had to develop a whole set of regulatory and protective responses, including processes that dissipate excess excitation energy as heat and allow for rapid repair and turnover of photodamaged PSII subunits. These mechanisms are wasteful under natural conditions and possibly even unnecessary or disadvantageous under the artificial conditions employed in agriculture. Likewise, as an adaptation to the intense irradiation experienced by land plants, the light-harvesting complexes (LHCs) replaced the original cyanobacterial light-harvesting system (phycobilisomes), which was optimized to harvest low levels of light. Ironically, when land plants had to re-adapt to low-light conditions with the advent of woodland and forest canopy, they evolved the capacity to increase light-harvesting by appressing thylakoid membranes into grana stacks (Mullineaux, 2005), but whether grana are as efficient as the original phycobilisomes in harvesting low-light intensities is not at all clear. In the carbon fixation arm of photosynthesis, RuBisCO, the key enzyme of the Calvin-Benson Cycle, is a prominent example for another flawed photosynthetic component. RuBisCO is very inefficient and wastes lots of energy by using O_2 (which was absent from the atmosphere when the enzyme was invented) as well as CO_2 as a substrate.

Thus, the patchwork nature of photosynthesis provides, at least in theory, ample scope for improvement of the light reactions, particularly with respect to its light-harvesting components and the susceptibility of photosystems to photodamage.

POTENTIAL TARGETS FOR CONVENTIONAL BREEDING

Conventional breeding requires intraspecific variation. Given the high degree of conservation of the structural components of the light reactions among land plants, the fact that there is almost no natural variation in basic photosynthetic parameters among different accessions of the model plant *Arabidopsis*, as determined by chlorophyll fluorescence parameters (El-Lithy et al., 2005), comes as no surprise. However, some natural variation has been found in mechanisms of constitutive protection against PSII photodamage (Jansen et al., 2010) and in non-photochemical quenching (NPQ; Jung and Niyogi, 2009). Increased vegetative biomass observed in hybrids between *Arabidopsis* accessions is only indirectly associated with an increase in photosynthesis, because the rate of photosynthesis per unit leaf area in parents and hybrids turns out to be constant (Fujimoto et al., 2012). Instead, heterosis is due to the larger cell size in hybrids, with correspondingly more chloroplasts and more chlorophyll per cell (Fujimoto et al., 2012).

It can therefore be concluded that the structural components of the light reactions of photosynthesis are very probably not susceptible to improvement by breeding, whereas mechanisms involved in the regulation or protection of the photosynthetic light reactions might be amenable to adjustment (**Table 1**).

POTENTIAL TARGETS FOR GENETIC ENGINEERING

One obvious route to the improvement of carbon fixation is the transfer of genes from one species to another. Attempts to introduce C4 photosynthesis or other carbon-concentrating systems into C3 plants, engineer improved versions of RuBisCO, or even replace the entire Calvin-Benson cycle, are ongoing (reviewed in: Blankenship et al., 2011; Langdale, 2011). But how can the light reactions of photosynthesis in plants benefit from replacing components by their counterparts from other species? The most pronounced differences between the light reactions in photoautotrophic oxygen-evolving organisms reside in their light-harvesting antenna systems. For instance, cyanobacteria, glaucophytes, and red algae contain the aforementioned phycobilisomes, whereas land plants use LHCs. To

Table 1 | Overview of approaches to improving photosynthetic light reactions.

Approaches and targets	Reference
BREEDING	
NPQ	Jung and Niyogi (2009)
PSII photoinhibition	Jansen et al. (2010)
Unknown regulators of photosynthesis-associated traits	Fujimoto et al. (2012)
GENETIC ENGINEERING	
Modification/exchange of light-harvesting systems	Reviewed in: Blankenship et al. (2011)
Overexpression of endogenous or heterologous proteins	Chida et al. (2007), Pesaresi et al. (2009)
Inactivation of (wasteful) regulatory processes	Pribil et al. (2010)
SYNTHETIC BIOLOGY	
Redesign of photosensitive photosystem subunits	This study
Novel single-subunit photosystems without assembly	This study
Novel pigments introduced by synthetic amino acids	This study

Whereas breeding and genetic engineering exploit pre-existing intra- and interspecific variation, respectively, entirely novel amino acids, genes, proteins and pigments can be employed in synthetic biology approaches. By some definitions, the exchange of entire light-harvesting systems can be considered to lie within the ambit of synthetic biology.

enhance light-harvesting indirectly, research efforts are underway in crop plants to enable more light to penetrate to lower levels of the canopy. These involve either modifying plant architecture or decreasing chlorophyll content (reviewed in: Blankenship et al., 2011). The introduction of prokaryotic pigments that absorb further into the near-infrared (Blankenship et al., 2011), or even entire prokaryotic light-harvesting systems (to supplement or replace LHCs), into plants might make it possible to expand the absorption spectrum of photosynthesis and thus increase photosynthetic efficiency at low-light levels.

Moreover, the potential of genetic engineering is not restricted to the modification or replacement of LHCs. The removal or overexpression of single components of the photosynthetic light reactions can improve the efficiency of photosynthesis, at least under certain conditions. For instance, overexpression of either plastocyanin, the soluble electron transporter that reduces photosystem I (PSI), or its algal substitute cytochrome c_6, increases biomass in *A. thaliana* (Chida et al., 2007; Pesaresi et al., 2009; **Table 1**). Similarly, increased phosphorylation of thylakoid proteins, achieved by inactivating the thylakoid phosphatase TAP38, improves photosynthetic electron flow under certain light conditions (Pribil et al., 2010). This indicates that simple single-gene genetic engineering of photosynthetic light reaction might have practical applications. Moreover, these findings, together with the observation that manipulation of photosynthetic carbon fixation in *Arabidopsis* (by introducing a prokaryotic glycolate catabolic pathway to bypass photorespiration) also increases biomass accumulation (Kebeish et al., 2007), argue strongly against the idea that plants are limited in their sink, but not in their source, capacity (reviewed in: Kant et al., 2012). Nevertheless, it is clear that neutralization of the feedback mechanisms that down-regulate photosynthesis when sink capacity becomes limiting, and increasing sink capacity *per se*, are both necessary to get the most out of improved photosynthetic light reactions.

Hence, genetic engineering of the light reactions of photosynthesis should focus primarily on modifying light-harvesting and regulators of photosynthetic electron flow, as well as on increasing the sink capacity of plants to cope with an enhanced photosynthetic rate. The resulting plants should exhibit more efficient photosynthesis under controlled conditions, e.g., in greenhouses, or in regions that cannot otherwise be extensively used for agriculture because of their short growing seasons.

POTENTIAL TARGETS FOR SYNTHETIC BIOLOGY

Whereas some of the opportunities for genetic engineering described above might be defined as synthetic biology approaches, a true synthetic biology project would aim to design photosystems that are insensitive to damage by light. This will need novel "hardware" and, therefore, will require the replacement of the light-sensitive subunits, or even the complete remodeling of photosystems, in particular PSII (**Table 1**). Assuming that wholesale remodeling is feasible, the problem arises of what to do when more excitation energy is available than is needed for carbon fixation? In natural photosynthesis, excess excitation energy is dissipated as heat, not only to prevent damage to the photosystems but to also to avoid the generation of reactive oxygen species (ROS). Therefore, a redesigned photosystem must not only be light-stable but also avoid ROS production. The latter attribute might be very difficult to realize, and require the design of additional "devices" that utilize or quench excess excitation energy. Hence, one may hazard the guess that several versions of photosystem cores and light-harvesting antenna will have to be designed and combined to fulfill the needs of different organisms and habitats. Such a redesigned photosystem core will probably not be a multiprotein-pigment complex like the natural photosystems. Instead, the number of proteins in such a redesigned photosystem might have to be dramatically reduced to avoid the complex assembly processes that operate in plants, which require a plethora of assembly factors – not all of which have been identified. Moreover, pigments might be introduced into such a novel photosystem by using synthetic amino acids with novel side-chains that absorb light. Finally, these novel photosystems might be used not only in the classical Z-scheme to produce ATP and NADPH, but also exploit novel ways to convert charge separation into chemical energy.

FINAL REMARKS

The considerations outlined above suggest that the light reactions of photosynthesis can be improved by genetic engineering and, more indirectly, by conventional breeding. The redesign or *de novo* creation of entire photosystems that are less susceptible to photodamage and produce fewer harmful ROS, is a formidable challenge. However, the gain in photosynthetic efficiency when photosystems require less repair and photoprotection will be significant. It is clear that crop plants are the least suited test systems for such approaches, given their long life

cycle and inaccessibility to efficient genetic engineering technologies. Therefore, redesigning photosystems will not only require a very deep understanding of the structure and dynamics of the natural photosynthetic light reactions, but also open-minded and innovative concepts of what a perfect photosystem should look like, as well as novel model organisms in which such concepts can be realized, tested, and reiteratively improved.

REFERENCES

Blankenship, R. E., Tiede, D. M., Barber, J., Brudvig, G. W., Fleming, G., Ghirardi, M., Gunner, M. R., Junge, W., Kramer, D. M., Melis, A., Moore, T. A., Moser, C. C., Nocera, D. G., Nozik, A. J., Ort, D. R., Parson, W. W., Prince, R. C., and Sayre, R. T. (2011). Comparing photosynthetic and photovoltaic efficiencies and recognizing the potential for improvement. *Science* 332, 805–809.

Chida, H., Nakazawa, A., Akazaki, H., Hirano, T., Suruga, K., Ogawa, M., Satoh, T., Kadokura, K., Yamada, S., Hakamata, W., Isobe, K., Ito, T., Ishii, R., Nishio, T., Sonoike, K., and Oku, T. (2007). Expression of the algal cytochrome c6 gene in *Arabidopsis* enhances photosynthesis and growth. *Plant Cell Physiol.* 48, 948–957.

El-Lithy, M. E., Rodrigues, G. C., Van Rensen, J. J., Snel, J. F., Dassen, H. J., Koornneef, M., Jansen, M. A., Aarts, M. G., and Vreugdenhil, D. (2005). Altered photosynthetic performance of a natural *Arabidopsis* accession is associated with atrazine resistance. *J. Exp. Bot.* 56, 1625–1634.

Fujimoto, R., Taylor, J. M., Shirasawa, S., Peacock, W. J., and Dennis, E. S. (2012). Heterosis of *Arabidopsis* hybrids between C24 and Col is associated with increased photosynthesis capacity. *Proc. Natl. Acad. Sci. U.S.A.* 109, 7109–7114.

Jansen, M. A., Martret, B. L., and Koornneef, M. (2010). Variations in constitutive and inducible UV-B tolerance; dissecting photosystem II protection in *Arabidopsis thaliana* accessions. *Physiol Plant* 138, 22–34.

Jung, H. S., and Niyogi, K. K. (2009). Quantitative genetic analysis of thermal dissipation in *Arabidopsis*. *Plant Physiol.* 150, 977–986.

Kant, S., Seneweera, S., Rodin, J., Materne, M., Burch, D., Rothstein, S. J., and Spangenberg, G. (2012). Improving yield potential in crops under elevated CO2: integrating the photosynthetic and nitrogen utilization efficiencies. *Front. Plant Sci.* 3:162. doi: 10.3389/fpls.2012.00162

Kebeish, R., Niessen, M., Thiruveedhi, K., Bari, R., Hirsch, H. J., Rosenkranz, R., Stabler, N., Schonfeld, B., Kreuzaler, F., and Peterhänsel, C. (2007). Chloroplastic photorespiratory bypass increases photosynthesis and biomass production in *Arabidopsis thaliana*. *Nat. Biotechnol.* 25, 593–599.

Langdale, J. A. (2011). C4 cycles: past, present, and future research on C4 photosynthesis. *Plant Cell* 23, 3879–3892.

Mullineaux, C. W. (2005). Function and evolution of grana. *Trends Plant Sci.* 10, 521–525.

Murata, N., Allakhverdiev, S. I., and Nishiyama, Y. (2012). The mechanism of photoinhibition in vivo: Re-evaluation of the roles of catalase, α-tocopherol, non-photochemical quenching, and electron transport. *Biochim. Biophys. Acta* 1817, 1127–1133.

Nishiyama, Y., Allakhverdiev, S. I., and Murata, N. (2011). Protein synthesis is the primary target of reactive oxygen species in the photoinhibition of photosystem II. *Physiol. Plant* 142, 35–46.

Pesaresi, P., Scharfenberg, M., Weigel, M., Granlund, I., Schroder, W. P., Finazzi, G., Rappaport, F., Masiero, S., Furini, A., Jahns, P., and Leister, D. (2009). Mutants, overexpressors, and interactors of *Arabidopsis plastocyanin* isoforms: revised roles of plastocyanin in photosynthetic electron flow and thylakoid redox state. *Mol. Plant* 2, 236–248.

Pribil, M., Pesaresi, P., Hertle, A., Barbato, R., and Leister, D. (2010). Role of plastid protein phosphatase TAP38 in LHCII dephosphorylation and thylakoid electron flow. *PLoS Biol.* 8, e1000288. doi: 10.1371/journal.pbio.1000288

Received: 05 August 2012; accepted: 09 August 2012; published online: 28 August 2012.
*Citation: Leister D (2012) How can the light reactions of photosynthesis be improved in plants? Front. Plant Sci. **3**:199. doi: 10.3389/fpls.2012.00199*
This article was submitted to Frontiers in Plant Physiology, a specialty of Frontiers in Plant Science.

frontiers in
PLANT SCIENCE

OPINION ARTICLE
published: 13 January 2014
doi: 10.3389/fpls.2013.00554

Unidirectional photodamage of pheophytin in photosynthesis

Harvey J. M. Hou*

Department of Physical Sciences, Alabama State University, Montgomery, AL, USA
**Correspondence: hhou@alasu.edu*

Edited by:
Suleyman I. Allakhverdiev, Russian Academy of Sciences, Russia

Reviewed by:
Mohammad M. Najafpour, Institute for Advanced Studies in Basic Sciences, Iran

Keywords: pheophytin, photosystem II, electron transfer, photodamage, photoinhibition

The primary reactions in photosynthesis take place in the reaction centers surrounded by light harvesting complexes (Blankenship, 2002; Diner and Rappaport, 2002; Frank and Brudvig, 2004). There are two types of photosynthetic reaction centers. The type I reaction center has iron-sulfur cluster as stable electron acceptor, such as photosystem I complexes, green bacterial and heliobacterial reaction centers, and the type II uses quinone as stable electron acceptor including photosystem II and purple bacterial reaction centers. The electron transfer in type II reaction center in unidirectional via the L-subunit of the reaction centers (Maroti et al., 1985; Hoerber et al., 1986; Martin et al., 1986; Michel-Beyerle et al., 1988). However, the electron transfer in the type I reaction center is different from that in the type II centers, which is bidirectional (Guergova-Kuras et al., 2001; Li et al., 2006). The three dimensional structures of both types of reaction centers were determined at atomic resolution (Jordan et al., 2001; Ferreira et al., 2004; Loll et al., 2005; Amunts et al., 2007; Umena et al., 2011). The electron transfer pathways in both types of reaction centers are well established (Van Grondelle, 1985; Schatz et al., 1988; Fleming and van Grondelle, 1997; Dekker and Van Grondelle, 2000; Gobets and van Grondelle, 2001; Seibert and Wasielewski, 2003; Van Grondelle and Novoderezhkin, 2006). The primary electron donor in the reaction centers is a pair of chlorophyll molecules, and pheophytin is the primary electron acceptor (Klimov et al., 1977; Holzwarth et al., 2006).

Light is the only source of energy for photosynthesis; it can also be harmful to plants (Powles, 1984). During the recent 10 years the molecular processes of photoinhibition had been intensively studied (Adams and Demmig-Adams, 1993; Aro et al., 1993; Baker and Bowyer, 1994; Anderson et al., 1997; Asada, 1999; Melis, 1999; Niyogi, 1999; Adir et al., 2003; Telfer, 2005; Murata et al., 2007; Tyystjarvi, 2008; Kramer, 2010; Hou and Hou, 2013). The PSII complex is composed of more than 15 polypeptides and 200 pigment molecules. Because there are many pigment and protein molecules not related directly to the photoinhibition reaction, it is difficult to identify which molecule is photodamaged. The preparation of PS II reaction center D1/D2/cytochrome b-559 complex, which contains only a few polypeptides and pigments, can be a good material to meet the difficulty (Nanba and Satoh, 1989).

The PS II reaction center D1/D2/cytochrome b-559 complexes from higher plants contain five polypeptide subunits (Seibert et al., 2004). It contains six chlorophyll a (Chl a), two β-carotene (Telfer et al., 1987; Seibert et al., 1988; Gounaris et al., 1990; Kobayashi et al., 1990; Barbato et al., 1991). The PSII reaction center does not contain the quinone electron acceptors Q_A and Q_B. It photochemical reaction is restricted to radical pair formation and recombination (Takahashi et al., 1987; Crystall et al., 1989; Wasielewski et al., 1989). Addition of exogenous electron donors and acceptors allows secondary electron flow reaction to occur. Therefore the D1/D2/cytochrome b-559 complex constitutes a good simple system for probing on the mechanisms from both acceptor-side and donor-side photoinhibition (Barber and Andersson, 1992; Barber and De Las Rivas, 1993; Yu et al., 1995). It has found that primary electron donor P_{680}, accessary chlorophyll, carotene, amino acid residues such as histidine, and pheophytin are vulnerable to excess light.

The primary electron donor P_{680} of PSII can be damaged easily by exposure of strong light, when no additions are made (Telfer and Barber, 1989). Singlet oxygen is formed as a consequence of radical pair recombination (McTavish et al., 1989; Durrant et al., 1990). The generation of this highly toxic species causes initially a selective and irreversible bleaching of the chlorophylls that constitute P_{680} and a breakdown of the D1 protein to a 23-kDa fragment containing the N terminus of the complete protein (De Las Rivas et al., 1993). In the presence of a suitable electron acceptor such as silicomolybdate or decylplastoquinone, the P_{680}^+ lifetime is increased, and irreversible bleaching of β-carotene and chlorophyll are observed, which are independent of oxygen (Telfer et al., 1991). Under these conditions breakdown of the D1 protein leads to a 24-kDa fragment of C-terminal origin (Shipton and Barber, 1991).

The photobleaching at 680 nm is usually attributed to the photodamage of P_{680} in the PS II reaction center (Telfer et al., 1990). There is the significant overlapping of absorption of P_{680}, accessary chlorophyll, and pheophytin in the PS II reaction center (Diner and Rappaport, 2002). Using high performance liquid chromatography (HPLC) the one pheophytin in PS II reaction center is photo damaged (Hou et al., 1995; Kuang et al., 1995). The time course of pheophytin photodamage showed the content of pheophytin decreases faster than that of chlorophyll, suggesting that

light-induced damage of pheophytin and P_{680} occurred step by step in which pheophytin photodamage first and followed by P_{680} (Hou et al., 1996). The kinetics of the photodamage reaction of P_{680} suggested that the photodegradation product of P_{680} photodamage is possibly a pheophytin-like molecule (Peng et al., 1999).

A photoprotective hypothesis of pheophytin against photoinactivation induced from acceptor-side in PS II was proposed (Hou et al., 1996). When P_{680} bounding to D1 and D2 proteins is excited by light energy, primary charge separation takes place and the radial pair P_{680}^{+} $Pheo^{-}$ is formed, in which the excited state P_{680} ejects and transfers one electron to the primary electron acceptor pheophytin bound to D1 protein. Since primary quinone electron acceptor Q_A is lost in the preparation of PS II reaction center complex, the radical pair may be recombined and the P_{680} triplet is formed. The singlet oxygen generated by the reaction of the triplet P_{680} and oxygen in the solution is a highly toxic species to PS II reaction center. The pheophytin molecule probably bound to D2 protein firstly damaged by the singlet state oxygen. More excitation energy accumulated in PS II may cause the photodestruction of P_{680} and accessary chlorophyll. The photodamage of P_{680} and accessory chlorophyll resulted in the loss of photochemical activity of PS II. The role of the pheophytin molecule bound to D2 subunit is probably to remove the singlet state oxygen as a result protecting P_{680} against the photoinduced damage. A study of photoinhibition *in vitro* and *in vivo* concluded that photoinhibition in intact pea leaves at low temperature is mainly due to the acceptor-side mechanism (Shipton and Barber, 1994). The unidirectional photodamage and photoprotection of pheophytin is probably the important scheme by which the photoinhibitory reaction takes place in green plants *in vivo*.

As we discussed early, the role of the second or inactive electron transfer branch is unclear. Because the pheophytin molecule on D2 protein is the key component of the second electron-transfer branch in the PS II reaction center, the unidirectional photodamage of pheophytin infer that the role of the second branch is to protect the first one. In other words, the function of the second electron-transfer branch is to remove the singlet state oxygen species using the pheophytin molecule on D2 protein.

As PS II and purple bacterial reaction centers are both belong to the type-II reaction centers, the significant similarity in both structure and function are expected. During the early stages of the photoinhibition of isolated spinach PS II reaction center there is a loss of pheophytin (Hou et al., 1995; Kuang et al., 1995). To see if the process of photoinhibition is similar or different between the purple bacterial and plant reaction centers, the photosynthetic pigments and their correlation to the photochemical activity of the isolated reaction centers from *Rb. sphaeroides* were assessed (Hou et al., 2005). The experimental data demonstrated: (1) One bacteriopheophytin molecule associated with photochemical activity of the isolated reaction center from *Rb. sphaeroides* is damaged under strong light illumination; (2) The damaged bacteriopheophytin is likely located in the L subunit of the reaction center; (3) The special pair P_{870} undergoes a two-step photodamage reaction.

Further investigation on the photodamage mechanisms of bacteriopheophytin in the reaction centers from *Rb. sphaeroides* is conducted by using liquid chromatography-mass spectrometry (Hou, 2008). The experimental results show that one of the two bacteriopheophytin molecules in the purple bacterial centers accompanying with the complete loss of photoactivity is damaged under strong illumination due to the destruction of its chemical structure. Three degradation products of the bacteriopheophytin photodamage reactions are identified and probably produced by the hydration, dehydrogen, and de-methylation of bacteriopheophytin molecule under strong light conditions. The main degradation product is probably formed by the demethylation at C-8 in the bacteriopheophytin molecule.

Which pheophytin in PS II is more sensitive to strong light is currently unknown and need further investigation. The pigment analysis using HPLC and UV-vis-NIR spectroscopy indicates that one pheophytin in PS II and purple bacterial reaction center is more photosensitive than the other (Hou et al., 1996, 2005). The damaged pheophytin may be bound to D1 or D2 proteins (**Figure 1**). The HPLC and photochemical activity analysis suggested that the damaged pheophytin is likely in the inactive branch in PS II reaction center complex. However, we cannot exclude that possibility of the alternative option,

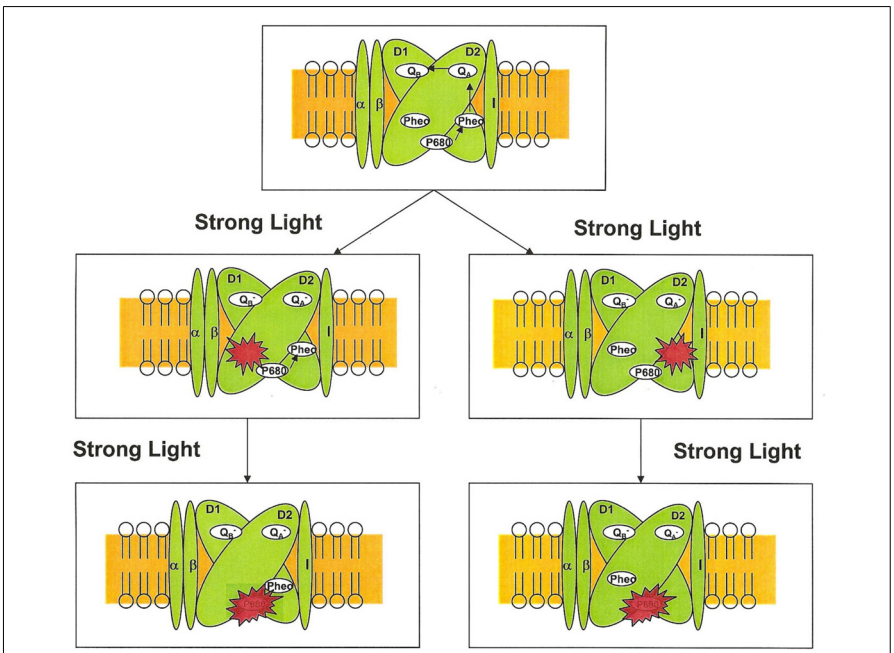

FIGURE 1 | Unidirectional photodamage of pheophytin in PS II reaction centers.

i.e., the damaged pheophytin is located in the active is via D1 protein. This notion is supported by the observation that the photodamage of bacteriopheophytin in purple bacterial reaction center seems to be located in L-subunit.

The pheophytin mutants of *Synechocystis* sp. PCC 6803 might be useful to provide additional evidence on the site of the photosensitive pheophytin in photosynthesis. Two mutants, D1-Leu210His and D2-Leu209His, wherein the pheophytin in D1 and D2 protein is replaced by a chlorophyll, respectively. In these two mutants, there is only one pheophytin per reaction center. In the D1-Leu210His mutant, the only pheophytin in the reaction center is bound to D2 protein. If the photo damaged pheophytin in D2 protein, the photodamage of pheophytin would be expected in the D1-Leu210His mutant. Alternatively, if the pheophytin in D1 protein is more photosensitive, one would observe that photodamage of pheophytin in the D2-Leu209His mutant.

Unidirectionality of pheophytin photodamage might involve electron transfer reaction. For example, upon excitation with blue light (390 nm) a transient B-side charge separated electron transfer was observed in picoseconds at room temperature (Haffa et al., 2003). A series of mutations involving the introduction of potentially negative amino acids in the vicinity of P_{870} were characterized in terms of the nature of this reaction. B-side electron transfer in bacterial reaction center from *Rb. sphaeroides* was proposed to be possible photoprotection via rapidly quenching higher excited states of the reaction center (Lin et al., 2001).

Unidirectional electron transfer and photodamage are also discovered in other cofactors such as carotenoid in PS II. The reaction centers of PS II contain two types of β-carotene with different orientations. The β-carotene (I) absorbing at 470 and 505 nm is roughly parallel to the membrane plane, and β-carotene (II) absorbing at 460 and 490 nm seems to be perpendicular orientation (Breton and Kato, 1987) The linear dichroism signal at 485 nm in the PS II core complex CP47/D1/D2/cytochrome b-559 is decreased upon strong illumination (Hou et al., 2000). The observation may be explained as the conformation changes of β-carotene (II) pool, which tends to more perpendicular orientation respective to the membrane plane.

Multiple photoprotective hypotheses have been established including Mn-mediated UV photoinactivation (Hakala et al., 2005; Ohnishi et al., 2005; Wei et al., 2011; Hou et al., 2013), cytochrome b-559 cyclic electron flow or cytochrome b-559 reversible interconvertion between the two redox forms (Thompson and Brudvig, 1988; Barber and De Las Rivas, 1993; Shinopoulos and Brudvig, 2012), and a β-carotene photooxidation (Telfer et al., 2003; Alric, 2005; Shinopoulos et al., 2014). The unidirectional photodamage of pheophytin in photosynthesis is discovered. However the site of the damage pheophytin is unknown. The possible function of the pheophytin in photosynthesis is complex and likely involves forward electron transfer, photoprotection, structural support, photosynthetic evolution, and alternative electron transfer. Further investigation using biophysical techniques and mutagenic methods is required to approve or exclude these possibilities.

ACKNOWLEDGMENTS

This work is supported by Alabama State University.

REFERENCES

Adams, W. W. 3rd., and Demmig-Adams, B. (1993). Energy dissipation and photoprotection in leaves of higher plants. *Curr. Top. Plant Physiol.* 8, 27–36.

Adir, N., Zer, H., Shochat, S., and Ohad, I. (2003). Photoinhibition - a historical perspective. *Photosyn. Res.* 76, 343–370. doi: 10.1023/A:1024969518145

Alric, J. (2005). *In vivo* carotenoid triplet formation in response to excess light: a supramolecular photoprotection mechanism revisited. *Photosyn. Res.* 83, 335–341. doi: 10.1007/s11120-005-1105-3

Amunts, A., Drory, O., and Nelson, N. (2007). The structure of a plant photosystem I supercomplex at 3.4.ANG. resolution. *Nature* 447, 58–63. doi: 10.1038/nature05687

Anderson, J. M., Park, Y. L., and Chow, W. S. (1997). Photoinactivation and photoprotection of photosystem II in nature. *Physiol. Plant.* 100, 214–223. doi: 10.1111/j.1399-3054.1997.tb04777.x

Aro, E. M., McCaffery, S., and Anderson, J. M. (1993). Photoinhibition and D1 protein degradation in peas acclimated to different growth irradiances. *Plant Physiol.* 103, 835–843.

Asada, K. (1999). The water-water cycle in chloroplasts: scavenging of active oxygens and dissipation of excess photons. *Annu. Rev. Plant Physiol. Plant Mol. Biol.* 50, 601–639. doi: 10.1146/annurev.arplant.50.1.601

Baker, N. R., and Bowyer, J. R. (1994). *Photoinhibition of Photosynthesis: From Molecular Mechanisms to the Field*. Oxford: BIOS Scientific Publishers.

Barbato, R., Race, H. L., Friso, G., and Barber, J. (1991). Chlorophyll levels in the pigment-binding proteins of photosystem II. A study based on the chlorophyll to cytochrome ratio in different photosystem II preparations. *FEBS Lett.* 286, 86–90. doi: 10.1016/0014-5793(91)80947-2

Barber, J., and Andersson, B. (1992). Too much of a good thing: light can be bad for photosynthesis. *Trends Biochem. Sci.* 17, 61–66. doi: 10.1016/0968-0004(92)90503-2

Barber, J., and De Las Rivas, J. (1993). A functional model for the role of cytochrome b559 in the protection against donor and acceptor side photoinhibition. *Proc. Natl. Acad. Sci. U.S.A.* 90, 10942–10946. doi: 10.1073/pnas.90.23.10942

Blankenship, R. E. (2002). *Molecular Mechanisms of Photosynthesis*. Oxford: Blackwell Science.

Breton, J., and Kato, S. (1987). Orientation of the pigments in photosystem II: low-temperature linear-dichroism study of a core particle and of its chlorophyll-protein subunits isolated from *Synechococcus* sp. *Biochim. Biophys. Acta* 892, 99–107. doi: 10.1016/0005-2728(87)90252-0

Crystall, B., Booth, P. J., Klug, D. R., Barber, J., and Porter, G. (1989). Resolution of a long lived fluorescence component from D1/D2/cytochrome b-559 reaction centers. *FEBS Lett.* 249, 75–78. doi: 10.1016/0014-5793(89)80019-5

Dekker, J. P., and Van Grondelle, R. (2000). Primary charge separation in Photosystem II. *Photosyn. Res.* 63, 195–208. doi: 10.1023/A:1006468024245

De Las Rivas, J., Shipton, C. A., Ponticos, M., and Barber, J. (1993). Acceptor side mechanism of photoinduced proteolysis of the D1 protein in photosystem II reaction centers. *Biochemistry* 32, 6944–6950. doi: 10.1021/bi00078a019

Diner, B. A., and Rappaport, F. (2002). Structure, dynamics, and energetics of the primary photochemistry of photosystem II of oxygenic photosynthesis. *Annu. Rev. Plant Biol.* 53, 551–580. doi: 10.1146/annurev.arplant.53.100301.135238

Durrant, J. R., Giorgi, L. B., Barber, J., Klug, D. R., and Porter, G. (1990). Characterization of triplet states in isolated photosystem II reaction centers: oxygen quenching as a mechanism for photodamage. *Biochim. Biophys. Acta* 1017, 167–175. doi: 10.1016/0005-2728(90)90148-W

Ferreira, K. N., Iverson, T. M., Maghlaoui, K., Barber, J., and Iwata, S. (2004). Architecture of the photosynthetic oxygen-evolving center. *Science* 303, 1831–1838. doi: 10.1126/science.1093087

Fleming, G. R., and van Grondelle, R. (1997). Femtosecond spectroscopy of photosynthetic light-harvesting systems. *Curr. Opin. Struct. Biol.* 7, 738–748. doi: 10.1016/S0959-440X(97)80086-3

Frank, H. A., and Brudvig, G. W. (2004). Redox functions of carotenoids in photosynthesis. *Biochemistry* 43, 8607–8615. doi: 10.1021/bi0492096

Gobets, B., and van Grondelle, R. (2001). Energy transfer and trapping in photosystem I. *Biochim. Biophys. Acta* 1507, 80–99. doi: 10.1016/S0005-2728(01)00203-1

Gounaris, K., Chapman, D. J., Booth, P., Crystall, B., Giorgi, L. B., Klug, D. R., et al. (1990). Comparison of the D1/D2/cytochrome b559 reaction centre complex of photosystem two isolated by two different methods. *FEBS Lett.* 265, 88–92. doi: 10.1016/0014-5793(90)80890-U

Guergova-Kuras, M., Boudreaux, B., Joliot, A., Joliot, P., and Redding, K. (2001). Evidence for two active branches for electron transfer in photosystem I. *Proc. Natl. Acad. Sci. U.S.A.* 98, 4437–4442. doi: 10.1073/pnas.081078898

Haffa, A. L. M., Lin, S., Williams, J. C., Taguchi, A. K. W., Allen, J. P., and Woodbury, N. W. (2003). High yield of long-lived B-side charge separation at room temperature in mutant bacterial reaction centers. *J. Phys. Chem. B* 107, 12503–12510. doi: 10.1021/jp034703p

Hakala, M., Tuominen, I., Keranen, M., Tyystjarvi, T., and Tyystjarvi, E. (2005). Evidence for the role of the oxygen-evolving manganese complex in photoinhibition of Photosystem II. *Biochim. Biophys. Acta* 1706, 68–80. doi: 10.1016/j.bbabio.2004.09.001

Hoerber, J. K. H., Goebel, W., Ogrodnik, A., Michel-Beyerle, M. E., and Cogdell, R. J. (1986). Time-resolved measurements of fluorescence from reaction centers of *Rhodopseudomonas viridis* and the effect of menaquinone reduction. *FEBS Lett.* 198, 268–272. doi: 10.1016/0014-5793(86)80418-5

Holzwarth, A. R., Muller, M. G., Reus, M., Nowaczyk, M., Sander, J., and Rogner, M. (2006). Kinetics and mechanism of electron transfer in intact photosystem II and in the isolated reaction center: pheophytin is the primary electron acceptor. *Proc. Natl. Acad. Sci. U.S.A.* 103, 6895–6900. doi: 10.1073/pnas.0505371103

Hou, H. J. M. (2008). "Identification of the degradation products involved in bacteriopheophytin photodamage of the photosynthetic reaction centers from *Rb. sphaeroides* by liquid chromatography-mass spectrometry," in *Photosynthesis: Energy from the Sun*, eds J. P. Allen, B. Osmond, J. H. Golbeck and E. Gantt (Dordrecht: Springer), 1473–1478.

Hou, H. J. M., Zhang, X., Liu, H., Steven, J., Young, E., Lien, T., et al. (2005). "Photodamage of one bacteriopheophytin molecule in the photosynthetic reaction center from *Rb sphaeroides*," in *Photosynthesis: Fundamental Aspects to Global Perspertives*, eds A. Van Der Est and D. Bruce (Lawrence: Allen Press), 501–503.

Hou, J. M., Dejonghe, D., Shan, J. X., Li, L. B., and Kuang T. Y. (2000). Orientation of pigments in the isolated photosystem II sub-core reaction center complex: a linear dichroism study, *J. Integr. Plant Biol.* 42, 1211–1214

Hou, J. M., Kuang, T. Y., Peng, D. C., Tang, C. Q., and Tang, P. (1996). The photodamage and protective role of pheophytin a in the photosystem II reaction center against light-induced damage. *Prog. Nat. Sci.* 6, 489–493.

Hou, J. M., Peng, D. C., Kuang, T. Y., Tang, C. Q., and Tang, P. (1995). Pheophytin A molecule association with primary photochemistry in the isolated photosystem II reaction center D1/D2/Cyt B559 complex. *J. Integr. Plant Biol.* 37, 405–408.

Hou, X., and Hou, H. J. M. (2013). Roles of manganese in photosystem II dynamics to irradiations and temperatures. *Front. Biol.* 8, 312–322. doi: 10.1007/s11515-012-1214-2

Hou, X., Raposo, A., and Hou, H. J. M. (2013). Response of chlorophyll d-containing cyanobacterium *Acaryochloris marina* to UV and visible irradiations. *Photosynth. Res.* 117, 497–507. doi: 10.1007/s11120-013-9946-7

Joliot, P., and Joliot, A. (1999). *In vivo* analysis of the electron transfer within photosystem I: are the two phylloquinones involved? *Biochemistry* 38, 11130–11136.

Jordan, P., Fromme, P., Witt, H. T., Klukas, O., Saenger, W., and Krauss, N. (2001). Three-dimensional structure of cyanobacterial photosystem I at 2.5 A resolution. *Nature* 411, 909–917. doi: 10.1038/35082000

Klimov, V. V., Klevanik, A. V., Shuvalov, V. A., and Kransnovsky, A. A. (1977). Reduction of pheophytin in the primary light reaction of photosystem II. *FEBS Lett.* 82, 183–186. doi: 10.1016/0014-5793(77)80580-2

Kobayashi, M., Maeda, H., Watanabe, T., Nakane, H., and Satoh, K. (1990). Chlorophyll a and β-carotene content in the D1/D2/cytochrome b-559 reaction center complex from spinach. *FEBS Lett.* 260, 138–140. doi: 10.1016/0014-5793(90)80086-X

Kramer, D. M. (2010). The photonic smart grid of the chloroplast in action. *Proc. Natl. Acad. Sci. U.S.A.* 107, 2729–2730. doi: 10.1073/pnas.0914429107

Kuang, T. Y., Hou, J. M., Peng, D. C., Tang, C. Q., and Tang, P. (1995). Light-induced damage of pheophytin a molecule in the isolated photosystem II reaction center D1/D2/Cyt b559 complex. *J. Integr. Plant Biol.* 37, 401–404.

Li, Y., van der Est, A., Lucas, M. G., Ramesh, V. M., Gu, F., Petrenko, A., et al. (2006). Directing electron transfer within Photosystem I by breaking H-bonds in the cofactor branches. *Proc. Natl. Acad. Sci. U.S.A.* 103, 2144–2149. doi: 10.1073/pnas.0506537103

Lin, S., Katilius, E., Haffa, A. L. M., Taguchi, A. K. W., and Woodbury, N. W. (2001). Blue light drives B-side electron transfer in bacterial photosynthetic reaction centers. *Biochemistry* 40, 13767–13773. doi: 10.1021/bi015612q

Loll, B., Kern, J., Saenger, W., Zouni, A., and Biesiadka, J. (2005). Towards complete cofactor arrangement in the 3.0 A resolution structure of photosystem II. *Nature* 438, 1040–1044. doi: 10.1038/nature04224

Maroti, P., Kirmaier, C., Wraight, C., Holten, D., and Pearlstein, R. M. (1985). Photochemistry and electron transfer in borohydride-treated photosynthetic reaction centers. *Biochim. Biophys. Acta.* 810, 132–139. doi: 10.1016/0005-2728(85)90128-8

Martin, J. L., Breton, J., Hoff, A. J., Migus, A., and Antonetti, A. (1986). Femtosecond spectroscopy of electron transfer in the reaction center of the photosynthetic bacterium *Rhodopseudomonas sphaeroides* R-26: direct electron transfer from the dimeric bacteriochlorophyll primary donor to the bacteriopheophytin acceptor with a time constant of 2.8 +- 0.2 psec. *Proc. Natl. Acad. Sci. U.S.A.* 83, 957–961. doi: 10.1073/pnas.83.4.957

McTavish, H., Picorel, R., and Seibert, M. (1989). Stabilization of isolated photosystem II reaction center complex in the dark and in the light using polyethylene glycol and an oxygen-scrubbing system. *Plant Physiol.* 89, 452–456. doi: 10.1104/pp.89.2.452

Melis, A. (1999). Photosystem-II damage and repair cycle in chloroplasts: what modulates the rate of photodamage? *Trends Plant Sci.* 4, 130–135.

Michel-Beyerle, M. E., Plato, M., Deisenhofer, J., Michel, H., Bixon, M., and Jortner, J. (1988). Unidirectionality of charge separation in reaction centers of photosynthetic bacteria. *Biochim. Biophys. Acta* 932, 52–70. doi: 10.1016/0005-2728(88)90139-9

Murata, N., Takahashi, S., Nishiyama, Y., and Allakhverdiev Suleyman, I. (2007). Photoinhibition of photosystem II under environmental stress. *Biochim. Biophys. Acta* 1767, 414–421. doi: 10.1016/j.bbabio.2006.11.019

Nanba, O., and Satoh, K. (1989). Isolation of a photosystem II reaction center consisting of D-1 and D-2 polypeptides and cytochrome b-559. *Proc. Natl. Acad. Sci. U.S.A.* 84, 109–112. doi: 10.1073/pnas.84.1.109

Niyogi, K. K. (1999). Photoprotection revisited: genetic and molecular approaches. *Annu. Rev. Plant Physiol. Plant Mol. Biol.* 50, 333–359

Ohnishi, N., Allakhverdiev, S. I., Takahashi, S., Higashi, S., Watanabe, M., Nishiyama, Y., et al. (2005). Two-step mechanism of photodamage to photosystem II: step 1 occurs at the oxygen-evolving complex and step 2 occurs at the photochemical reaction center. *Biochemistry* 44, 8494–8499

Peng, D. C., Hou, J. M., Kuang, T. Y., Tang, C. Q., and Tang P. (1999). Photoinduced damage of the photosystem II primary electron donor P680: a high performance liquid chromatographic analysis of pigment content in D1/D2/cytochrome b559 complex under photoinhibitory conditions. *J. Integr. Plant Biol.* 41, 1307–1311

Powles, S. B. (1984). Photoinhibition of photosynthesis induced by visible light. *Annu. Rev. Plant Physiol.* 35, 15–44. doi: 10.1146/annurev.pp.35.060184.000311

Schatz, G. H., Brock, H., and Holzwarth, A. R. (1988). Kinetic and energetic model for the primary processes in photosystem II. *Biophys. J.* 54, 397–405. doi: 10.1016/S0006-3495(88)82973-4

Seibert, M., Picorel, R., Rubin, A. B., and Connolly, J. S. (1988). Spectral, photophysical, and stability properties of isolated photosystem II reaction center. *Plant Physiol.* 87, 303–306. doi: 10.1104/pp.87.2.303

Seibert, M., and Wasielewski, M. R. (2003). The isolated Photosystem II reaction center: first attempts to directly measure the kinetics of primary charge separation. *Photosyn. Res.* 76, 263–268. doi: 10.1023/A:1024986307839

Seibert, M., Yruela, I., and Picorel, R. (2004). Isolation of photosystem II reaction center complexes from plants. *Methods Mol. Biol.* 274, 53–62. doi: 10.1007/978-1-60761-925-3_3

Shinopoulos, K. E., and Brudvig, G. W. (2012). Cytochrome b559 and cyclic electron transfer within photosystem II. *Biochim. Biophys. Acta* 1817, 66–75. doi: 10.1016/j.bbabio.2011.08.002

Shinopoulos, K. E., Yu, J., Nixon P. J., and Brudvig, G. W. (2014). Using site-directed mutagenesis to probe the role of the D2 carotenoid in the secondary electron-transfer pathway of photosystem II. *Photosynth Res.* [Epub ahead of print].

Shipton, C. A., and Barber, J. (1991). Photoinduced degradation of the D1 polypeptide in isolated

reaction centers of photosystem II: evidence for an autoproteolytic process triggered by the oxidizing side of the photosystem. *Proc. Natl. Acad. Sci. U.S.A.* 88, 6691–6695. doi: 10.1073/pnas.88.15.6691

Shipton, C. A., and Barber, J. (1994). *In vivo* and *in vitro* photoinhibition reactions generate similar degradation fragments of D1 and D2 photosystem-II reaction-centre proteins. *Eur. J. Biochem.* 220, 801–808. doi: 10.1111/j.1432-1033.1994.tb18682.x

Takahashi, Y., Hansson, O., Mathis, P., and Satoh, K. (1987). Primary radical pair in the photosystem II reaction center. *Biochim. Biophys. Acta* 893, 49–59. doi: 10.1016/0005-2728(87)90147-2

Telfer, A. (2005). Too much light? How β-carotene protects the photosystem II reaction centre. *Photochem. Photobiol. Sci.* 4, 950–956. doi: 10.1039/b507888c

Telfer, A., and Barber, J. (1989). Evidence for the photoinduced oxidation of the primary electron donor P680 in the isolated photosystem II reaction center. *FEBS Lett.* 246, 223–228. doi: 10.1016/0014-5793(89)80287-X

Telfer, A., De las Rivas, J., and Barber, J. (1991). β-carotene within the isolated photosystem II reaction center: photooxidation and irreversible bleaching of this chromophore by oxidized P680. *Biochim. Biophys. Acta* 1060, 106–114. doi: 10.1016/S0005-2728(05)80125-2

Telfer, A., Frolov, D., Barber, J., Robert, B., and Pascal, A. (2003). Oxidation of the two β-carotene molecules in the photosystem IIreaction center. *Biochemistry* 42, 1008–1015. doi: 10.1021/bi026206p

Telfer, A., He, W. Z., and Barber, J. (1990). Spectral resolution of more than one chlorophyll electron donor in the isolated photosystem II reaction center complex. *Biochim. Biophys. Acta* 1017, 143–151. doi: 10.1016/0005-2728(90)90145-T

Telfer, A., Marder, J. B., and Barber, J. (1987). Photosystem II reaction centers isolated from phosphorylated pea thylakoids carry phosphate on the D1 and D2 polypeptide subunits. *Biochim. Biophys. Acta* 893, 557–563. doi: 10.1016/0005-2728(87)90107-1

Thompson, L. K., and Brudvig, G. W. (1988). Cytochrome b-559 may function to protect photosystem II from photoinhibition. *Biochemistry* 27, 6653–6658. doi: 10.1021/bi00418a002

Tyystjarvi, E. (2008). Photoinhibition of Photosystem II and photodamage of the oxygen evolving manganese cluster. *Coord. Chem. Rev.* 252, 361–376. doi: 10.1016/j.ccr.2007.08.021

Umena, Y., Kawakami, K., Shen, J. R., and Kamiya, N. (2011). Crystal structure of oxygen-evolving photosystem II at a resolution of 1.9 A. *Nature* 473, 55–61. doi: 10.1038/nature09913

Van Grondelle, R. (1985). Excitation energy transfer, trapping and annihilation in photosynthetic systems. *Biochim. Biophys. Acta* 811, 147–195. doi: 10.1016/0304-4173(85)90017-5

Van Grondelle, R., and Novoderezhkin, V. I. (2006). Energy transfer in photosynthesis: experimental insights and quantitative models. *Phys. Chem. Chem. Phys.* 8, 793–807. doi: 10.1039/b514032c

Wasielewski, M. R., Johnson, D. G., Seibert, M., and Govindjee. (1989). Determination of the primary charge separation rate in isolated photosystem II reaction centers with 500-fs time resolution. *Proc. Natl. Acad. Sci. U.S.A.* 86, 524–528. doi: 10.1073/pnas.86.2.524

Wei, Z., Cady, C. W., Brudvig, G. W., and Hou, H. J. M. (2011). Photodamage of a Mn(III/IV)-oxo mix valence compound and photosystem II complexes: evidence that high-valent manganese species is responsible for UV-induced photodamage of oxygen evolving complex in photosystem II. *J. Photochem. Photobiol. B* 104, 118–125. doi: 10.1016/j.jphotobiol.2011.01.017

Yu, Z., Kuang, T., Lu, R., Tang, C., and Tang, P. (1995). Light-induced damage of amino acid residues and degradation of polypeptides in D1/D2/cytochrome b559 complex. *J. Integr. Plant Biol.* 37, 267–273.

Received: 19 December 2013; accepted: 26 December 2013; published online: 13 January 2014.

*Citation: Hou HJM (2014) Unidirectional photodamage of pheophytin in photosynthesis. Front. Plant Sci. **4**:554. doi: 10.3389/fpls.2013.00554*

This article was submitted to Plant Physiology, a section of the journal Frontiers in Plant Science.

frontiers in
PLANT SCIENCE

REVIEW ARTICLE
published: 26 November 2013
doi: 10.3389/fpls.2013.00473

Studying the oxidation of water to molecular oxygen in photosynthetic and artificial systems by time-resolved membrane-inlet mass spectrometry

Dmitriy Shevela* and Johannes Messinger*

Department of Chemistry, Chemistry Biology Centre, Umeå University, Umeå, Sweden

Edited by:
Suleyman I. Allakhverdiev, Russian Academy of Sciences, Russia

Reviewed by:
Mohammad M. Najafpour, Institute for Advanced Studies in Basic Sciences, Iran
Harvey J. M. Hou, Alabama State University, USA

****Correspondence:***
Dmitriy Shevela and Johannes Messinger, Department of Chemistry, Chemistry Biology Centre, Umeå University, Linnaeus Väg 6, S-90187 Umeå, Sweden
e-mail: dmitriy.shevela@chem.umu.se; johannes.messinger@chem.umu.se

Monitoring isotopic compositions of gaseous products (e.g., H_2, O_2, and CO_2) by time-resolved isotope-ratio membrane-inlet mass spectrometry (TR-IR-MIMS) is widely used for kinetic and functional analyses in photosynthesis research. In particular, in combination with isotopic labeling, TR-MIMS became an essential and powerful research tool for the study of the mechanism of photosynthetic water-oxidation to molecular oxygen catalyzed by the water-oxidizing complex of photosystem II. Moreover, recently, the TR-MIMS and ^{18}O-labeling approach was successfully applied for testing newly developed catalysts for artificial water-splitting and provided important insight about the mechanism and pathways of O_2 formation. In this mini-review we summarize these results and provide a brief introduction into key aspects of the TR-MIMS technique and its perspectives for future studies of the enigmatic water-splitting chemistry.

Keywords: isotope-ratio membrane-inlet mass spectrometry, isotope labeling, O_2 evolution, photosynthetic and artificial water-splitting, photosystem II, water-oxidizing complex

INTRODUCTION

In nature, the splitting of water to molecular oxygen (O_2) is catalyzed by the membrane-bound pigment-protein photosystem II (PSII) of plants, algae, and cyanobacteria (Vinyard et al., 2013). The catalytic site of the water-splitting reaction is an inorganic tetra-manganese mono-calcium penta-oxygen (Mn_4CaO_5) cluster (**Figure 1**) that forms, together with its protein ligands, the water-oxidizing complex (WOC) of PSII (Yano et al., 2006; Umena et al., 2011). Water-splitting by the Mn_4CaO_5 cluster is energetically driven by the strongest biological oxidant, $P680^+$ (with a midpoint potential of ~1.25 V), generated by the light-induced charge separation within the Chl-containing reaction center (RC) of PSII (Diner and Rappaport, 2002; Ishikita et al., 2005). A redox-active tyrosine residue (Y_Z) is the essential electron transfer intermediate between the photoactive RC and the Mn_4CaO_5 cluster of PSII. Following light absorption, the Mn_4CaO_5 cluster is oxidized step-wise (one electron at a time) and thereby cycles through five redox states, known as S_i states (where *i* reflects the number of oxidizing equivalents stored by the cluster) (**Figure 1**). The four-electron four-proton oxidation chemistry of two water molecules is completed when the four oxidizing equivalents are accumulated within the WOC, and the highly reactive S_4 state relaxes into the most reduced S_0 state with the concomitant O–O bond formation and release of O_2 (Messinger et al., 2012; Cox and Messinger, 2013). This reaction cycle of water oxidation is also known as the Kok cycle (Kok et al., 1970).

Abbreviations: C_i, inorganic carbon (CO_2, H_2CO_3, HCO_3^-, CO_3^{2-}); Chl, chlorophyll; PSII, photosystem II; RC, reaction center; WOC, water-oxidizing complex.

During the last few decades an enormous progress in elucidation of the WOC structure and in understanding the mechanism of the water-splitting became possible due to employment of numerous biophysical techniques (summarized in Aartsma and Matysik, 2008; Messinger et al., 2009a,b; also see refs therein). Among them, *time-resolved isotope-ratio membrane-inlet mass spectrometry* (TR-IR-MIMS) in combination with isotope labeling (Konermann et al., 2008; Beckmann et al., 2009) provided the most direct information on the S_i state dependent substrate water binding to the WOC (Messinger et al., 1995; Wydrzynski et al., 1996). These findings were recently reviewed in detail by Hillier and Wydrzynski (2008), Messinger et al. (2012), and Cox and Messinger (2013) and are, therefore, only briefly discussed here. However, TR-MIMS has also been successfully employed and yielded important data on other structural and mechanistic aspects of the water-splitting chemistry in both natural PSII and in variously designed artificial O_2-evolving catalysts. In this mini-review, we summarize these recent investigations and also provide some comments on perspectives of the TR-MIMS technique for future studies of water-splitting and O_2 evolution.

KEY CONCEPTS OF TR-MIMS

The concept of TR-MIMS was first applied in 1963, when Georg Hoch and Bessel Kok began to use mass spectrometer with a *semipermeable membrane* as inlet system (Hoch and Kok, 1963). This allowed to separate the liquid sample from the high vacuum space of the mass spectrometer, while at the same time it was permeable to the gaseous analytes. This excellent solution allowed continuous *on-line* measurements of dissolved gaseous analytes (either dissolved in solution or directly from the gas phase) with a temporal resolution of a few seconds. Therefore,

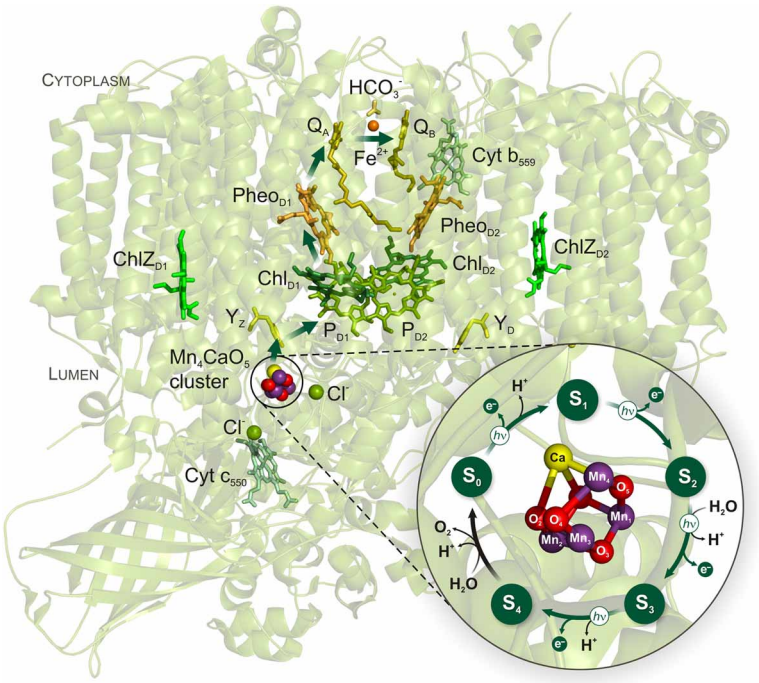

FIGURE 1 | Cyanobacterial PSII structure and Kok cycle of photosynthetic water oxidation by the Mn_4CaO_5 cluster. The arrows within PSII indicate the direction of electron transfer which comprises the following redox-active cofactors: inorganic Mn_4CaO_5 cluster, redox-active tyrosine Z (Y_Z), the primary electron donor P680 that includes a pair of Chls *a* (P_{D1} and P_{D2}) and two accessory Chls (Chl_{D1} and Chl_{D2}), the primary pheophytin ($Pheo_{D1}$) acceptor, the primary (Q_A) and the secondary (Q_B) quinone acceptors. The phytyl tails of the Chl's and Pheo's, and the isoprenyl chains of the quinones have been cut for clarity. The light-induced S state transitions of the Mn_4CaO_5 cluster are indicated by arrows with "*hν*" labels. The PSII structure and the zoomed structural model of the Mn_4CaO_5 cluster in the center of the Kok cycle are based on the recent PSII crystal structure at a resolution of 1.9 Å (PDB entry 3ARC; Umena et al., 2011).

the TR-MIMS technique is ideally suited for investigations of photosynthetic and artificial water-oxidation/O_2 evolution (for instance, see Konermann et al., 2008; Beckmann et al., 2009). For an outline of other TR-MIMS applications in biological and in industrial systems, see reviews by Lauritsen and Kotiaho (1996) and Johnson et al. (2000). Recent technological advances in MIMS instrumentation are summarized in Davey et al. (2011).

A schematic view of a TR-MIMS set-up employing an isotope ratio mass spectrometer is shown in **Figure 2**. This type of mass spectrometers is normally equipped with an electron-impact ion source, magnetic sector field analyzer, and individual detectors (Faraday cups) that provide simultaneous detection of several masses (ions) with high sensitivity and signal stability. For its ability to monitor and to selectively analyze all *isotopologues* (molecules that differ only in their isotopic composition) of gaseous products with one instrument, the TR-MIMS approach in combination with isotope enrichments became indispensable tool for kinetic and functional analyses of photosynthetic enzymes (Konermann et al., 2008; Beckmann et al., 2009). The key part of the TR-MIMS instrument is a gas inlet system that is integrated within a MIMS cell. The design of MIMS cells may vary depending on the measuring purposes (Konermann et al., 2008; Beckmann et al., 2009), but all of them contain a gas-permeable membrane functioning as analyte inlet system into the vacuum of the mass spectrometer. The coupling of such a cell to various light sources (e.g., Xenon lamps or lasers) allows carrying out the measurements of light-induced O_2 evolution in photosynthetic samples or light-driven O_2-evolving artificial catalysts. Before entering the ion source of the mass spectrometer the analytes pass through a cryogenic trap (**Figure 2**), which freezes out water vapor that inadvertently pervaporate through the membrane in trace amounts.

Enrichment of aqueous sample suspension with oxygen's heavy isotope (^{18}O) for isotope ratio measurements of O_2 (and/or CO_2) isotopologues is a powerful and commonly used tool in studies of water-splitting chemistry and/or related reactions. Therefore, most of the experiments are carried out in $H_2^{18}O$-labeled sample suspensions/solutions.

IS WATER THE IMMEDIATE SUBSTRATE OF PHOTOSYNTHETIC O_2 EVOLUTION?

It is widely accepted that water is the immediate substrate for photosynthetic O_2 production. However, Metzner (1978) suggested that instead hydrogen carbonate (bicarbonate; HCO_3^-) is the immediate substrate for O_2 formation that is subsequently replenished by the reaction of CO_2 with H_2O. This hypothesis was discounted for long because the isotopic equilibration between ^{18}O-water and HCO_3^- is too slow to account for early isotope labeling studies (Ruben et al., 1941; Stemler and Radmer, 1975; Stevens et al., 1975; Radmer and Ollinger, 1980). Due to the discovery that a carbonic anhydrase (CA) activity is associated with PSII (Lu and Stemler, 2002; Villarejo et al., 2002; Moskvin et al., 2004) the "bicarbonate-as-substrate hypothesis" needed to be re-investigated with refined expriments. Indeed, due to rapid

exchange of HCO_3^- and CO_2 species by CA, the ^{18}O-label could "escape" from HCO_3^- to water (which has a several orders higher concentration than the added ^{18}O-labeled HCO_3^-), and, thus, lead to the lack of O_2 yield from HCO_3^- (Stemler and Radmer, 1975; Radmer and Ollinger, 1980).

Two different TR-MIMS approaches were taken recently and both exclude that HCO_3^- is a physiologically significant substrate (Clausen et al., 2005a; Hillier et al., 2006). Clausen et al. (2005a) reported that under $H_2^{18}O$-labeled and CO_2/HCO_3^--depleted conditions the typical oscillation pattern of ^{18}O-enriched O_2 evolution is obtained in response to single light flashes, but didn't find any evidence for CO_2 release. The latter would be expected in case the Metzner's hypothesis would be correct. Hillier et al. (2006), in their TR-MIMS study, employed $^{18}O/^{13}C$-labeled HCO_3^- to probe the capability of PSII (from higher plants and cyanobacteria) to oxidize HCO_3^-. The authors were able to detect an extremely small (and, thus, non-physiological) flux of ^{18}O from HCO_3^- into O_2 similar to that observed in an early TR-MIMS study of Radmer and Ollinger (1980). Moreover, no relationship between O_2 evolution and PSII-associated CA activity was found by McConnell et al. (2007) in their TR-MIMS examination of PSII preparations from higher plants.

IS HYDROGEN CARBONATE A LIGAND TO THE WOC?

Hydrogen carbonate had been proposed to bind as integral cofactor to the Mn_4CaO_5 cluster after accumulation of many experimental results indicating: (i) the requirement of HCO_3^- ions for optimal stability and functionality of the WOC (Van Rensen and Klimov, 2005), and (ii) it's important role for the photoassembly reaction of the Mn_4CaO_5 cluster (Dasgupta et al., 2008). Moreover, in the PSII crystal structure from *Thermosynechococcus elongatus* at 3.5 Å resolution, HCO_3^- was modeled as a non-protein ligand bridging Mn and Ca ions within the WOC (Ferreira et al., 2004).

Earlier, interesting TR-MIMS experiments were performed by Stemler (1989) and Govindjee et al. (1991), in which formate

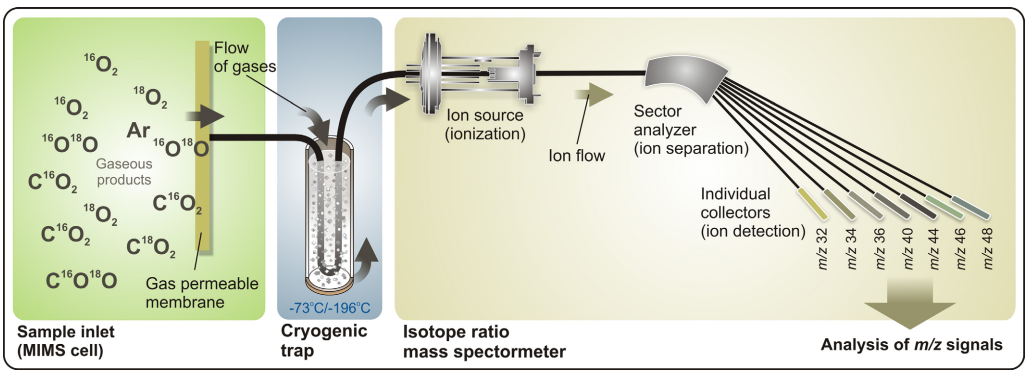

FIGURE 2 | Representation of a TR-IR-MIMS set-up. Gaseous products, produced by sample suspension (for instance, by PSII samples) in the cell, penetrate through a gas-permeable membrane into a high-vacuum space, pass through a cryogenic trap (which removes water vapor from a flow of gaseous analytes), and enter the isotope ratio mass spectrometer. Here, gaseous analytes are first ionized in the ion source by electron impact, and are then separated according to their *m/z* ratios by a magnetic field in the sector analyzer that allows simultaneous online detection by individual collector cups (e.g., a 7-cup Faraday detector array). MS signals are monitored and analyzed using a personal computer. See text for further details.

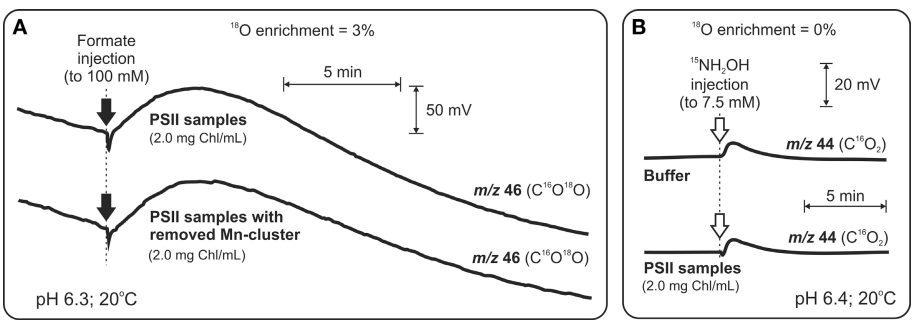

FIGURE 3 | TR-MIMS experiments demonstrating that HCO_3^- is not a tightly bound ligand to the Mn_4CaO_5 cluster in spinach PSII membrane fragments. (A) Amount of released CO_2 upon formate addition (black arrows) to intact PSII membranes is the same as in the case of PSII membranes without the Mn_4CaO_5 cluster (due to 75-min pre-incubation with 80 mM N_2H_4). Due to enrichment of sample suspension with $H_2^{18}O$ (3%) CO_2 was detected as $C^{16}O^{18}O$ at *m/z* 46. **(B)** Addition of the strong reductant NH_2OH (white arrows) at concentrations known to cause rapid reduction of the Mn_4CaO_5 cluster and release of Mn ions as Mn^{II} into the solution didn't lead to a release of CO_2/HCO_3^- above background. In order to avoid the overlay of CO_2 and N_2O signals (the latter is known to be produced during interaction of NH_2OH with the Mn_4CaO_4 cluster), the N_2O signal was shifted from *m/z* 44 to *m/z* 46 by employing the ^{15}N-labeled NH_2OH for these experiments. To facilitate equilibration between CO_2 and HCO_3^- all measurements were performed in the presence of externally added CA (to a final concentration of 3 μg ml^{-1}). Modified from Shevela et al. (2008b).

was tested to induce the release of HCO_3^- (that can be detected by TR-MIMS as CO_2) from PSII. Although Govindjee et al. (1991) provided clear evidence for the formate-induced release of CO_2/HCO_3^-, the HCO_3^- binding site was not specified in this study. Based on numerous previous data indicating that HCO_3^- is a ligand to the non-heme iron (NHI) at the electron acceptor side of PSII, the released CO_2 was suggested to derive from this binding site. However, later formate was shown to bind both at the acceptor and the donor (water-splitting) side of PSII (Feyziev et al., 2000), and therefore, the released CO_2/HCO_3^- could also originate from the water-splitting side.

In order to specifically probe the possible binding of HCO_3^- to the Mn_4CaO_5 cluster at the donor side of PSII, Shevela et al. (2008a,b) re-examined and extended the earlier TR-MIMS investigations. Thus, a comparison of the formate-induced $C^{16}O^{18}O$ yields (**Figure 3A**), under $H_2^{18}O$-enriched conditions, in intact PSII and Mn-depleted PSII was performed. This was complemented by experiments in which the gaseous products produced by a quick reductive destruction of the of the Mn_4CaO_5 cluster by ^{15}N-labeleld NH_2OH (**Figure 3B**) were studied. Both approaches clearly demonstrated that the detected CO_2/HCO_3^- *does not* originate from the inorganic core of the water-splitting site of PSII (Shevela et al., 2008a,b). Independent evidence for absence of HCO_3^- bound to the WOC was provided by FTIR and GS-MS experiments (Aoyama et al., 2008; Ulas et al., 2008). Moreover, in recent x-ray crystallography studies at resolutions of 1.9-3.0 Å no HCO_3^- was found in the vicinity of the Mn_4CaO_5 cluster, while they all clearly show HCO_3^- bound to the NHI on the acceptor side of PSII (Guskov et al., 2010; Umena et al., 2011) (also, see **Figure 1**). Thus, it can be excluded that HCO_3^- is a tightly bound ligand of the Mn_4CaO_5 cluster.

However, none of the mentioned studies negates the option that a mobile, weakly bound, and rapidly exchanging HCO_3^- affects the activity of the WOC. Thus, in case of the TR-MIMS measurements, weakly bound HCO_3^- may have been removed during the required degassing of the MIMS cell prior to formate or NH_2OH additions to PSII samples. Therefore, the possible loss of weakly bound HCO_3^- and the amount of HCO_3^- associated with PSII under air-saturated condition remain to be established in future TR-MIMS experiments.

WHEN AND HOW DOES SUBSTRATE WATER BIND TO THE WOC?

Indisputably, the most significant and unique contribution of the TR-MIMS instrumentation in understanding of water-oxidation mechanism in photosynthesis was its application for studying substrate binding in the different S_i states of the WOC. In these experiments the binding of water to the WOC is probed by the rapid injection of $H_2^{18}O$ into the PSII samples which were preset into the desired S_i state by pre-illumination with 0, 1, 2, or 3 flashes. Then, after desired incubation times, O_2 evolution is induced by a sequence of additional flashes. The exchange rates of the two substrate molecules are then calculated from the change of the $^{16}O^{18}O$ and $^{18}O^{18}O$ yields as a function of incubation time (see **Figure 4A** for protocol of the TR-MIMS measurements of substrate water exchange in the S_3 state). The mixing time of $H_2^{18}O$ with the PSII samples after injection and a very low level of dissolved O_2 in $H_2^{18}O$ are highly important for these experiments

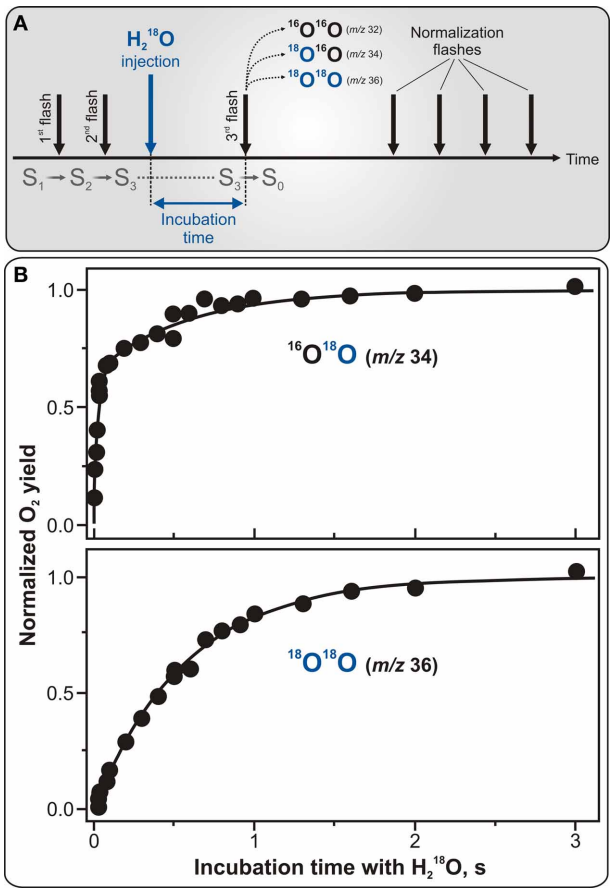

FIGURE 4 | Protocol for TR-MIMS measurements of $H_2^{16}O/H_2^{18}O$ exchange in the S_3 state of PSII (A) and experimentally obtained substrate water exchange rates in spinach thylakoids (B). (A) The S_3 state is populated by two pre-flashes given at 2 Hz (shown by the two first black vertical arrows). This is followed by the rapid injection of $H_2^{18}O$ into the PSII sample (shown by blue vertical arrow) and subsequent fast mixing of the injected $H_2^{18}O$ with the sample. Evolution of O_2 isotopologues is then induced by a 3rd flash, given at varying delay times (from 0 to 10 s) after the $H_2^{18}O$ injection (signified as incubation time). Finally, a series of four flashes is given at 2 Hz to induce O_2 yield used for normalization. **(B)** TR-MIMS measurements of substrate $H_2^{16}O/H_2^{18}O$ exchange kinetics were performed at *m/z* 34 (top plot) for singly-labeled isotopologue $^{16}O^{18}O$, and at *m/z* 36 (bottom plot) for doubly-labeled $^{18}O^{18}O$ in the S_3 state in spinach thylakoids at 10°C and pH 6.8. Symbols in both plots are experimental data, and the lines in the top and bottom plots are biexponential and monoexponential fits, respectively. The biexponential fit yields rate constants of ~40 s^{-1} for the fast phase and ~2 s^{-1} for the slow phase. The slow phase in the $^{16}O^{18}O$ data is matching the rate found in the monoexponential fit of the $^{18}O^{18}O$ data (Messinger et al., 1995; Hillier et al., 1998; Hillier and Wydrzynski, 2000, 2004). Adapted from Cox and Messinger (2013).

since they determine the time resolution of the TR-MIMS measurements. In the first $H_2^{16}O/H_2^{18}O$-exchange TR-MIMS experiments the water exchange kinetics could not be resolved (Radmer and Ollinger, 1986; Bader et al., 1993). The development of the MIMS cell by Messinger et al. (1995), which allowed for fast mixing of $H_2^{18}O$ with the sample and also implemented O_2 removal from the labeled water by the glucose—glucose oxidase—catalase method, greatly improved the time resolution down to the milliseconds scale and allowed measurements of substrate water

exchange in all semistable S_i states (Messinger et al., 1995; Hillier et al., 1998; Hillier and Wydrzynski, 2000).

Figure 4B illustrates characteristic water exchange kinetics in the S_3 state as measured in spinach thylakoids with the time resolution of 8 ms. In this figure, the yields of the singly-labeled ($^{16}O^{18}O$) and doubly-labeled ($^{18}O^{18}O$) isotopologues of molecular oxygen are plotted as a function of $H_2^{18}O$ incubation time in the S_3 state. While the former plot reflects the result when only one of the two possible ^{18}O-water substrates is exchanged, the latter one is for the case when both ^{18}O-waters are exchanged. The biphasic behavior of the $^{16}O^{18}O$ rise (detected at *m/z* 34) (see **Figure 4B**) is known to represent the exchange rates of two independent *slowly* and *fast* exchanging substrate water molecules bound at separate sites within the WOC. In contrast, the $^{18}O^{18}O$ product (monitored at *m/z* 36) exhibits a mono-exponential rise with a rate equal to that of the slow phase kinetic of the $^{16}O^{18}O$ data, thus-reflecting the exchange of the same "slowly" exchanging substrate water as observed at *m/z* 34. This finding clearly confirms that the two phases of the $^{16}O^{18}O$ data are an intrinsic feature of the WOC and do not originate from PSII heterogeneity (Messinger et al., 1995; Hillier et al., 1998).

Further TR-MIMS experiments also revealed that the "slowly" exchanging water is bound to the WOC in all semi-stable S_i states, while the "fast" exchanging water was detected only in the S_2 and S_3 states (Hillier et al., 1998; Hillier and Wydrzynski, 2000, 2004; Hendry and Wydrzynski, 2002). Thus, the TR-MIMS technique provides not only the most direct evidence for independent substrate water binding within the WOC, but also allows to monitor the change in their binding affinities throughout the reaction cycle. For a complete overview of the TR-MIMS findings in this field, we refer the readers to reviews by Hillier and Messinger (2005), Hillier and Wydrzynski (2008), Beckmann et al. (2009), Messinger et al. (2012), and Cox and Messinger (2013).

THE $^{16}O/^{18}O$ ISOTOPE EFFECT AND PHOTOSYNTHETIC WATER-SPLITTING

Up to now there is no final agreement on whether isotopic discrimination during O_2 production by photosynthetic water-splitting in PSII contributes to the so-called *Dole effect*, which describes the finding that the percentage of the ^{18}O isotope in atmosphere is higher (by 23‰) than in oceanic waters (Dole, 1936; Tcherkez and Farquhar, 2007). While many gas isotope ratio studies clearly showed that oxygen produced by O_2-evolving organisms is isotopically identical to the water they are suspended in (Dole and Jenks, 1944; Stevens et al., 1975; Guy et al., 1993; Helman et al., 2005), recent ^{18}O-enriched TR-MIMS experiments indicated that the ^{18}O isotope is favored by the WOC for O_2 production, thus-suggesting a significant $^{16}O/^{18}O$ isotope effect in the photosynthetic water-splitting (Burda et al., 2001, 2003). This finding was challenged by recent theoretical estimations that suggest a very small isotope effect (Tcherkez and Farquhar, 2007). Undoubtedly, a resolution of these conflicting results can be provided by revisiting TR-MIMS studies. These future studies should be designed to account for: (i) technical limitations/drawbacks of the previous TR-MIMS experiments (for instance, the absence of fast $H_2^{18}O$ mixing upon its addition to sample suspension inside the MIMS cuvette Bader et al., 1987; Burda et al., 2003), (ii) possible contribution of isotopic fractionation due to transfer of O_2 isotopologues through the membrane inlet toward the high vacuum of mass spectrometer recently reported by Hillier et al. (2006), and (iii) current knowledge of the S-state dependent substrate water binding and exchange rates as derived from TR-MIMS measurements (for reviews, see Hillier and Wydrzynski, 2008; Cox and Messinger, 2013). However, we note here, that without specific investigations of the ^{18}O isotope effect in photosynthetic water-oxidation, our TR-MIMS studies do not reveal any oxygen isotope discrimination in photosynthetically produced O_2 (for instance, see **Figure 6C** and text below for explanations), indicating that any such effect must be small at best.

IN SEARCH FOR INTERMEDIATES OF WATER SPLITTING BY TR-MIMS APPROACH

While most states of the Kok cycle (S_0, S_1, S_2, S_3) are semistable, the $S_3Y_Z^{\bullet}$ and S_4 state are known to be a highly reactive intermediates that until very recently were not characterized. Clausen and Junge (2004) attempted to stabilize and identify putative intermediate(s) of the S_4 state by applying a high partial O_2 pressure in order to shift the equilibrium of the terminal S_4

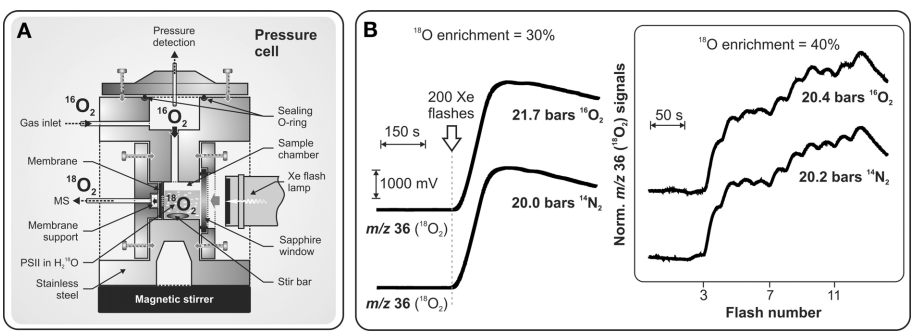

FIGURE 5 | Schematic representation of the pressure cell (A) specially designed for TR-MIMS measurements of light-induced $^{18}O_2$ evolution of PSII under high $^{16}O_2/N_2$ pressures (up to 20 bars). (B) ***MIMS*** **signals in panel (B); Left:** $^{18}O_2$ production of PSII core complexes from *Synechocystis* sp. PCC 6803 induced by a series of 200 saturating Xenon flashes (given at 2 Hz; indicated by arrow) at 21.7 bars O_2, or 20 bars N_2. Other conditions: 30% $H_2^{18}O$ enrichment; [Chl] = 50 μM; 250 μM DCBQ, pH 6.7, 20°C. **Right:** Flash-induced $^{18}O_2$ evolution patterns of PSII membrane fragments from spinach induced by a series of saturating laser flashes (separated by dark times of 25 s) at 20.4 bars O_2, or 20.2 bars N_2. Other conditions: as above, but with 40% $H_2^{18}O$. Adapted from Shevela et al. (2011a).

$\rightarrow S_0 + O_2 + nH^+$ reaction backwards. Based on their UV-absorption transients the authors observed half suppression of Mn oxidation under only 10-fold increase of ambient O_2 pressure (2.3 bar). These results were considered to be the first indication for an intermediate in the $S_3 \rightarrow S_4 \rightarrow S_0$ transition and as a possible route for stabilizing it (Clausen and Junge, 2004). Although a further delayed Chl fluorescence study corroborated these results (Clausen et al., 2005b), experiments by time-resolved X-ray absorption spectroscopy (TR-XAS) (Haumann et al., 2008) and by visible fluorescence study (Kolling et al., 2009) shed doubt on the existence of accessible S_4 intermediate(s) that can be populated by inhibition of the terminal step of O_2 release from the WOC by elevated O_2 concentrations. These controversial studies prompted application of the TR-MIMS technique, which allowed investigation of the effect of elevated O_2 pressure on photosynthetic O_2 release by direct O_2 detection (Shevela et al., 2011a). In these experiments direct monitoring of $^{18}O_2$ evolution from ^{18}O-labeled water against a high level of $^{16}O_2$ in a suspension of PSII complexes became possible due to a specially designed high pressure MIMS cell (for details, see **Figure 5A**). This study demonstrated that neither an inhibition nor altered flash-induced pattern of O_2 evolution take place under up to 50-fold increased concentration of dissolved O_2 around PSII (**Figure 5B**). These findings show that the terminal water-splitting reaction/O_2 release in PSII is highly exothermic, and are in line with the results obtained by TR-XAS (Haumann et al., 2008) and variable fluorescence (Kolling et al., 2009) studies.

APPLICATIONS IN ARTIFICIAL PHOTOSYNTHESIS

One of the central goals of artificial photosynthesis is the development of bio-inspired, efficient and robust catalysts that are able to split water employing the energy of sunlight in a fashion similar to the water-oxidizing Mn_4CaO_5 cluster in PSII (Concepcion et al., 2012; Nocera, 2012; Wiechen et al., 2012). Therefore, data concerning catalytic rates and turnover numbers (stability) of newly synthetized O_2-evolving catalysts are highly important for their further development. In this regard, in addition to traditionally used amperometric methods for O_2 detection (Renger and Hanssum, 2009), TR-MIMS can be applied as a highly sensitive method for studying the O_2-evolving capability of these complexes. However, a major advantage and uniqueness of the TR-MIMS technique in this field is that, in combination with ^{18}O-labeling experiments, it can be employed for studying the pathways of O_2 formation in reactions catalyzed by the 'potential' solar water-oxidation catalysts (Poulsen et al., 2005; Beckmann et al., 2008; Sala et al., 2010; Shevela et al., 2011b; Najafpour et al., 2012; Vigara et al., 2012). Thus, TR-MIMS detection of the isotopologues of O_2 ($^{16}O_2$, $^{16}O^{18}O$, $^{18}O_2$) during catalytic O_2-formation in the ^{18}O-enriched aqueous solutions allows to analyze the ^{18}O-fraction ($^{18}\alpha$) of the evolved O_2 with good time resolution and very high accuracy. A correlation of the ^{18}O-fraction in the substrate water ($^{18}\alpha_{theor}$; reflects the $H_2^{18}O$-enrichment of the solvent water) and in the product O_2 ($^{18}\alpha_{exp}$) gives important information about the origin of the O atoms in the produced molecular oxygen. For instance, the incorporation of exactly half of the possible ^{18}O-fraction into the evolved O_2 may indicate that only one of the two O atoms of the O_2 product originates from the bulk water as it has been monitored by TR-MIMS in the reactions of O_2-evolving catalysts with oxygen-transferring oxidizing agent, oxone (HSO_5^-) (Poulsen et al., 2005; Beckmann et al., 2008; Shevela et al., 2011b) (see **Figure 6A**). In

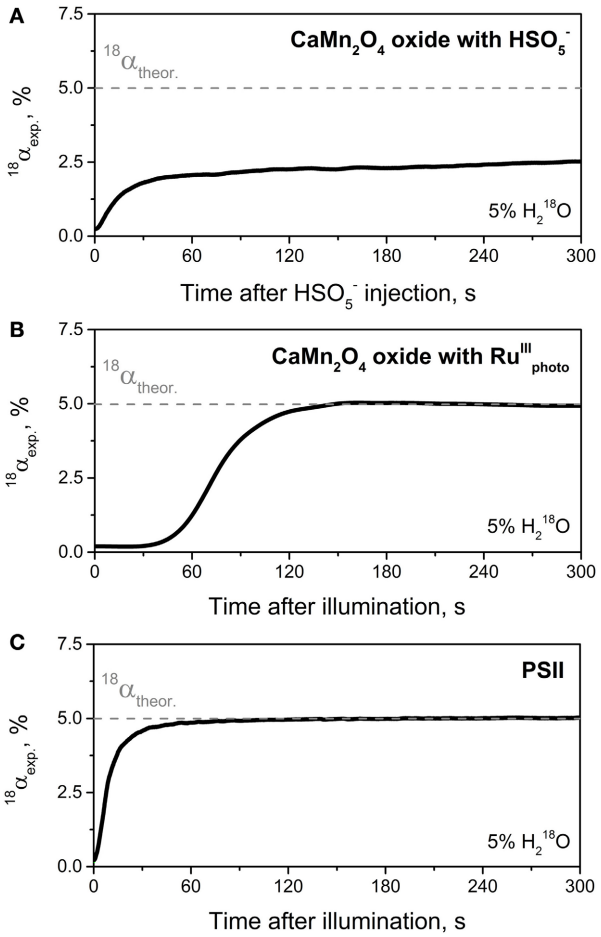

FIGURE 6 | Development of the ^{18}O-isotope fraction ($^{18}\alpha$) over time for the course of the catalytic O_2-formation in reactions catalyzed by synthesized $CaMn_2O_4 \cdot H_2O$ oxide (A,B) and by the WOC of PSII (C). (A) Change in $^{18}\alpha$-value for the reaction of $CaMn_2O_4 \cdot H_2O$ with HSO_5^- (oxone) indicating that only one of the two oxygen atoms of O_2 evolved originates from the bulk water. A solution of HSO_5^- in $H_2^{18}O$-enriched water was injected at $t = 0$ into the MIMS cell filled in with a non-enriched oxide suspension (1 mg ml^{-1}; pH ~4.5) to give a final HSO_5^- concentration of 3.7 mM and an $H_2^{18}O$ enrichment of 5%. Note that the rise of $^{18}\alpha$ to the value of 2.5% corresponds to half the percentage of the ^{18}O-labeled water. **(B)** Change in $^{18}\alpha$-value for the reaction of $CaMn_2O_4 \cdot H_2O$ with photogenerated $[Ru^{III}(bipy)_3]^{3+}$. Shortly before illumination (started at $t = 0$) the reaction mixture ($H_2^{18}O$ (5%), $CaMn_2O_4 \cdot H_2O$ (1 mg ml^{-1}), $[Ru(bipy)_3]^{2+}$ (1.5 mM), and $[Co(NH_3)_5Cl]^{2+}$ (12.5 mM); pH ~4) inside the MIMS cell was purged with N_2 until "zero" O_2 level was reached. **(C)** Change in $^{18}\alpha$-value for O_2 production by PSII membrane fragments isolated from spinach. O_2 evolution was induced by actinic continuous light at $t = 0$. Other conditions: 5% $H_2^{18}O$, [Chl] = 0.03 mg ml^{-1}, 0.6 mM PPBQ, 2 mM $K_3[Fe(CN)_6]$, pH 6.0, and 20°C. Gray dashed lines in all panels indicates the theoretical $^{18}\alpha$ value expected for reaction of the "true" water-splitting, i.e., when both oxygen atoms of formed O_2 originate from water. In all cases O_2 production was detected by TR-MIMS as $^{16}O_2$ (at *m/z* 32), $^{16}O^{18}O$ (*m/z* 34), and $^{18}O_2$ (*m/z* 36), and the $^{18}\alpha$ was calculated according to the following equation: $^{18}\alpha = ([^{18}O_2] + 1/2[^{16}O^{18}O])/[O_2]_{total}$. Adapted from Shevela et al. (2011b).

the case of "true" water-splitting, ^{18}O-fractions in bulk water and in evolved O_2 are expected to be same (i.e., $^{18}\alpha_{theor} = {}^{18}\alpha_{exp}$) as depicted in **Figure 6B** for the reaction of a synthetic catalyst ($CaMn_2O_4 \cdot H_2O$ oxide) with photogenerated oxidizing agent $[Ru^{III}(bipy)_3]^{3+}$ (Ru^{III}_{photo}), and in **Figure 6C** for natural light-induced water-splitting reaction performed by PSII. It's worth mentioning here, that the initial phase of the presented traces until stable $^{18}\alpha$ values (**Figure 6**) is a technical artefact, merely caused by the response time of the membrane-inlet system of the mass spectrometer which seems to be related to the overall O_2 concentration. However, the difference in time needed to reach final $^{18}\alpha$ value in two water-splitting reactions shown in **Figure 6** also reflects a much slower reaction rate for the reaction of the oxide with Ru^{III}_{photo}. Thus, O_2 evolution for this reaction was detected only after 1 min of illumination since this time is required to build up a sufficient concentration of photosensitizer Ru^{III}_{photo} (data not shown here; for details, see Shevela et al., 2011b). We note that one of the attractive extensions to the described TR-MIMS approach for the characterization of water-splitting catalysts is the coupling of the TR-MIMS instrument to an electrochemical cell (for further details, see Konermann et al., 2008 and refs therein).

CONCLUSIONS AND FUTURE PERSPECTIVES

Application of the TR-MIMS technique and isotope labeling for studies of various biophysical aspects of photosynthetic water-splitting and O_2 production is continuously growing. It provides not only insightful and unique information (which is sometimes not accessible by other methods) about this fundamental biological process, but also becomes an essential and highly precise tool for testing artificial water-oxidizing catalysts. Future applications of TR-MIMS for studies of water-splitting chemistry and O_2 production could follow from advances in membrane materials, different designs of the membrane-inlet systems, coupling with electrochemistry and spectroscopy, and technological developments of the mass spectrometers.

ACKNOWLEDGMENTS

The authors acknowledge financial support by the Kempe Foundation, the Swedish Research Council, the Energimyndigheten, the Strong Research Environment Solar Fuels (Umeå University), and the Artificial Leaf Project (K&A Wallenberg Foundation).

REFERENCES

Aartsma, T. J., and Matysik, J. (eds.). (2008). *Biophysical Techniques in Photosynthesis.* Dordrecht: Springer. doi: 10.1007/978-1-4020-8250-4

Aoyama, C., Suzuki, H., Sugiura, M., and Noguchi, T. (2008). Flash-induced FTIR difference spectroscopy shows no evidence for the structural coupling of bicarbonate to the oxygen-evolving Mn cluster in photosystem II. *Biochemistry* 47, 2760–2765. doi: 10.1021/bi702241t

Bader, K. P., Renger, G., and Schmid, G. H. (1993). A mass-spectrometric analysis of the water splitting reaction. *Photosynth. Res.* 38, 355–361. doi: 10.1007/BF00046761

Bader, K. P., Thibault, P., and Schmid, G. H. (1987). Study on the properties of the S_3 state by mass-spectrometry in the filamentous cyanobacterium *Oscillatoria chalybea*. *Biochim. Biophys. Acta* 893, 564–571. doi: 10.1016/0005-2728(87)90108-3

Beckmann, K., Messinger, J., Badger, M. R., Wydrzynski, T., and Hillier, W. (2009). On-line mass spectrometry: membrane inlet sampling. *Photosynth. Res.* 102, 511–522. doi: 10.1007/s11120-009-9474-7

Beckmann, K., Uchtenhagen, H., Berggren, G., Anderlund, M. F., Thapper, A., Messinger, J., et al. (2008). Formation of stoichiometrically ^{18}O-labelled oxygen from the oxidation of ^{18}O-enriched water mediated by a dinuclear manganese complex-a mass spectrometry and EPR study. *Energy Environ. Sci.* 1, 668–676. doi: 10.1039/b811806j

Burda, K., Bader, K. P., and Schmid, G. H. (2001). An estimation of the size of the water cluster present at the cleavage site of the water splitting enzyme. *FEBS Lett.* 491, 81–84. doi: 10.1016/S0014-5793(01)02175-5

Burda, K., Bader, K. P., and Schmid, G. H. (2003). ^{18}O isotope effect in the photosynthetic water splitting process. *Biochim. Biophys. Acta* 1557, 77–82. doi: 10.1016/S0005-2728(02)00395-X

Clausen, J., Beckmann, K., Junge, W., and Messinger, J. (2005a). Evidence that bicarbonate is not the substrate in photosynthetic oxygen evolution. *Plant Physiol.* 139, 1444–1450. doi: 10.1104/pp.105.068437

Clausen, J., Junge, W., Dau, H., and Haumann, M. (2005b). Photosynthetic water oxidation at high O_2 backpressure monitored by delayed chlorophyll fluorescence. *Biochemistry* 44, 12775–12779. doi: 10.1021/bi051183a

Clausen, J., and Junge, W. (2004). Detection of an intermediate of photosynthetic water oxidation. *Nature* 430, 480–483. doi: 10.1038/nature02676

Concepcion, J. J., House, R. L., Papanikolas, J. M., and Meyer, T. J. (2012). Chemical approaches to artificial photosynthesis. *Proc. Natl. Acad. Sci. U.S.A.* 109, 15560–15564. doi: 10.1073/pnas.1212254109

Cox, N., and Messinger, J. (2013). Reflections on substrate water and dioxygen formation. *Biochim. Biophys. Acta* 1827, 1020–1030. doi: 10.1016/j.bbabio.2013.01.013

Dasgupta, J., Ananyev, G. M., and Dismukes, G. C. (2008). Photoassembly of the water-oxidizing complex in photosystem II. *Coord. Chem. Rev.* 252, 347–360. doi: 10.1016/j.ccr.2007.08.022

Davey, N. G., Krogh, E. T., and Gill, C. G. (2011). Membrane-introduction mass spectrometry (MIMS). *Trends Anal. Chem.* 30, 1477–1485. doi: 10.1016/j.trac.2011.05.003

Diner, B. A., and Rappaport, F. (2002). Structure, dynamics, and energetics of the primary photochemistry of photosystem II of oxygenic photosynthesis. *Annu. Rev. Plant Biol.* 53, 551–580. doi: 10.1146/annurev.arplant.53.100301.135238

Dole, M. (1936). The relative atomic weight of oxygen in water and in air. *J. Chem. Phys.* 4, 268–275. doi: 10.1063/1.1749834

Dole, M., and Jenks, G. (1944). Isotopic composition of photosynthetic oxygen. *Science* 3, 409. doi: 10.1126/science.100.2601.409

Ferreira, K. N., Iverson, T. M., Maghlaoui, K., Barber, J., and Iwata, S. (2004). Architecture of the photosynthetic oxygen-evolving center. *Science* 303, 1831–1838. doi: 10.1126/science.1093087

Feyziev, Y. M., Yoneda, D., Yoshii, T., Katsuta, N., Kawamori, A., and Watanabe, Y. (2000). Formate-induced inhibition of the water-oxidizing complex of photosystem II studied by EPR. *Biochemistry* 39, 3848–3855. doi: 10.1021/bi992479h

Govindjee, Weger, H. G., Turpin, D. H., Van Rensen, J. J. S., Devos, O. J., and Snel, J. F. H. (1991). Formate releases carbon dioxide/bicarbonate from thylakoid membranes - measurements by mass spectroscopy and infrared gas analyzer. *Naturwissenschaften* 78, 168–170. doi: 10.1007/BF01136204

Guskov, A., Gabdulkhakov, A., Broser, M., Glöckner, C., Hellmich, J., Kern, J., et al. (2010). Recent progress in the crystallographic studies of photosystem II. *ChemPhysChem* 11, 1160–1171. doi: 10.1002/cphc.200900901

Guy, R. D., Fogel, M. L., and Berry, J. A. (1993). Photosynthetic fractionation of the stable isotopes of oxygen and carbon. *Plant Physiol.* 101, 37–47.

Haumann, M., Grundmeier, A., Zaharieva, I., and Dau, H. (2008). Photosynthetic water oxidation at elevated dioxygen partial pressure monitored by time-resolved X-ray absorption measurements. *Proc. Natl. Acad. Sci. U.S.A.* 105, 17384–17389. doi: 10.1073/pnas.0802596105

Helman, Y., Barkan, E., Eisenstadt, D., Luz, B., and Kaplan, A. (2005). Fractionation of the three stable oxygen isotopes by oxygen-producing and oxygen-consuming reactions in photosynthetic organisms. *Plant Physiol.* 138, 2292–2298. doi: 10.1104/pp.105.063768

Hendry, G., and Wydrzynski, T. (2002). The two substrate water molecules are already bound to the oxygen evolving complex in the S_2 state of photosystem II. *Biochemistry* 41, 13328–13334. doi: 10.1021/bi026246t

Hillier, W., McConnell, I., Badger, M. R., Boussac, A., Klimov, V. V., Dismukes, G. C., et al. (2006). Quantitative assessment of intrinsic carbonic anhydrase activity

and the capacity for bicarbonate oxidation in photosystem II. *Biochemistry* 45, 2094–2102. doi: 10.1021/bi051892o

Hillier, W., Messinger, J., and Wydrzynski, T. (1998). Kinetic determination of the fast exchanging substrate water molecule in the S_3 state of photosystem II. *Biochemistry* 37, 16908–16914. doi: 10.1021/bi980756z

Hillier, W., and Messinger, J. (2005). "Mechanism of photosynthetic oxygen production," in *Photosystem II. The Light-Driven Water:Plastoquinone Oxidoredutase*, eds T. Wydrzynski and K. Satoh (Dordrecht: Springer), 567–608.

Hillier, W., and Wydrzynski, T. (2000). The affinities for the two substrate water binding sites in the O_2 evolving complex of photosystem II vary independently during S-state turnover. *Biochemistry* 39, 4399–4405. doi: 10.1021/bi992318d

Hillier, W., and Wydrzynski, T. (2004). Substrate water interactions within the photosystem II oxygen evolving complex. *Phys. Chem. Chem. Phys.* 6, 4882–4889. doi: 10.1039/b407269c

Hillier, W., and Wydrzynski, T. (2008). ^{18}O-Water exchange in photosystem II: Substrate binding and intermediates of the water splitting cycle. *Coord. Chem. Rev*. 252, 306–317. doi: 10.1016/j.ccr.2007.09.004

Hoch, G., and Kok, B. (1963). A mass spectrometer inlet system for sampling gases dissolved in liquid phases. *Arch. Biochem. Biophys*. 101, 160–170. doi: 10.1016/0003-9861(63)90546-0

Ishikita, H., Loll, B., Biesiadka, J., Saenger, W., and Knapp, E.-W. (2005). Redox potentials of chlorophylls in the photosystem II reaction center. *Biochemistry* 44, 4118–4124. doi: 10.1021/bi047922p

Johnson, R. C., Cooks, R. G., Allen, T. M., Cisper, M. E., and Hemberger, P. H. (2000). Membrane introduction mass spectrometry: Trends and applications. *Mass Spectrom. Rev*. 19, 1–37. doi: 10.1002/(SICI)1098-2787(2000)19:1<1::AID-MAS1>3.0.CO;2-Y

Kok, B., Forbush, B., and McGloin, M. (1970). Cooperation of charges in photosynthetic O_2 evolution. *Photochem. Photobiol*. 11, 457–476. doi: 10.1111/j.1751-1097.1970.tb06017.x

Kolling, D. R. J., Brown, T. S., Ananyev, G., and Dismukes, G. C. (2009). Photosynthetic oxygen evolution is not reversed at high oxygen pressures: mechanistic consequences for the water-oxidizing complex. *Biochemistry* 48, 1381–1389. doi: 10.1021/bi801774f

Konermann, L., Messinger, J., and Hillier, W. (2008). "Mass spectrometry based methods for studying kinetics and dynamics in biological systems," in *Biophysical Techniques in Photosynthesis*, eds J. Amesz and A. J. Hoff (Dordrecht: Springer), 167–190. doi: 10.1007/978-1-4020-8250-4_9

Lauritsen, F. R., and Kotiaho, T. (1996). Advances in membrane inlet mass spectrometry (MIMS). *Rev. Anal. Chem*. 15, 237–264. doi: 10.1515/REVAC.1996.15.4.237

Lu, Y. K., and Stemler, A. J. (2002). Extrinsic photosystem II carbonic anhydrase in maize mesophyll chloroplasts. *Plant Physiol*. 128, 643–649. doi: 10.1104/pp.010643

McConnell, I. L., Badger, M. R., Wydrzynski, T., and Hillier, W. (2007). A quantitative assessment of the carbonic anhydrase activity in photosystem II. *Biochim. Biophys. Acta* 1767, 639–647. doi: 10.1016/j.bbabio.2007.01.019

Messinger, J., Alia, A., and Govindjee, (2009a). Special educational issue on "Basics and application of biophysical techniques in photosynthesis and related processes." *Photosynth. Res*. 101, 89–92. doi: 10.1007/s11120-009-9471-x

Messinger, J., Alia, A., and Govindjee, (2009b). Special educational issue on "Basics and application of biophysical techniques in photosynthesis and related processes"—Part B. *Photosynth. Res*. 102, 103–106. doi: 10.1007/s11120-009-9494-3

Messinger, J., Badger, M. R., and Wydrzynski, T. (1995). Detection of one slowly exchanging substrate water molecule in the S_3 state of photosystem II. *Proc. Natl. Acad. Sci. U.S.A*. 92, 3209–3213. doi: 10.1073/pnas.92.8.3209

Messinger, J., Noguchi, T., and Yano, J. (2012). "Photosynthetic O2 evolution," in *Molecular Solar Fuels*, eds T. Wydrzynski and W. Hillier (Cambridge: RSC Publishing), 163–207.

Metzner, H. (1978). *Photosynthetic Oxygen Evolution*. London: Academic Press.

Moskvin, O. V., Shutova, T. V., Khristin, M. S., Ignatova, L. K., Villarejo, A., Samuelsson, G., et al. (2004). Carbonic anhydrase activities in pea thylakoids—A photosystem II core complex-associated carbonic anhydrase. *Photosynth. Res*. 79, 93–100. doi: 10.1023/B:PRES.0000011925.93313.db

Najafpour, M. M., Hillier, W., Shamkhali, A. N., Amini, M., Beckmann, K., Jaglicic, Z., et al. (2012). Synthesis, characterization, DFT studies and catalytic activities of manganese(ii) complex with 1,4-bis(2,2′:6,2″-terpyridin-4′-yl) benzene. *Dalton Trans*. 41, 12282–12288. doi: 10.1039/c2dt31544k

Nocera, D. G. (2012). The artificial leaf. *Acc. Chem. Res*. 45, 767–776. doi: 10.1021/ar2003013

Poulsen, A. K., Rompel, A., and McKenzie, C. J. (2005). Water oxidation catalyzed by a dinuclear Mn complex: a functional model for the oxygen-evolving center of photosystem II. *Angew. Chem. Int. Ed*. 44, 6916–6920. doi: 10.1002/anie.200502114

Radmer, R., and Ollinger, O. (1980). Isotopic composition of photosynthetic O_2 flash yields in the presence of $H_2^{18}O$ and $HC^{18}O_3^-$. *FEBS Lett*. 110, 57–61. doi: 10.1016/0014-5793(80)80022-6

Radmer, R., and Ollinger, O. (1986). Do the higher oxidation states of the photosynthetic O_2 evolving system contain bound water? *FEBS Lett*. 195, 285–289. doi: 10.1016/0014-5793(86)80178-8

Renger, G., and Hanssum, B. (2009). Oxygen detection in biological systems. *Photosynth. Res*. 102, 487–498. doi: 10.1007/s11120-009-9434-2

Ruben, S., Randall, M., Kamen, M., and Hyde, J. L. (1941). Heavy oxygen (O^{18}) as a tracer in the study of photosynthesis. *J. Am. Chem. Soc*. 63, 877–879. doi: 10.1021/ja01848a512

Sala, X., Ertem, M. Z., Vigara, L., Todorova, T. K., Chen, W., Rocha, R. C., et al. (2010). The *cis*-$[RuII(bpy)_2(H_2O)_2]^{2+}$ water-oxidation catalyst revisited. *Angew. Chem. Int. Ed*. 49, 7745–7747. doi: 10.1002/anie.201002398

Shevela, D., Beckmann, K., Clausen, J., Junge, W., and Messinger, J. (2011a). Membrane-inlet mass spectrometry reveals a high driving force for oxygen production by photosystem II. *Proc. Natl. Acad. Sci. U.S.A*. 108, 3602–3607. doi: 10.1073/pnas.1014249108

Shevela, D., Koroidov, S., Najafpour, M. M., Messinger, J., and Kurz, P. (2011b). Calcium manganese oxides as oxygen evolution catalysts: O_2 formation pathways indicated by ^{18}O-labelling studies. *Chem. Eur. J*. 17, 5415–5423. doi: 10.1002/chem.201002548

Shevela, D., Klimov, V., and Messinger, J. (2008a). "Formate-induced release of carbon dioxide/hydrogencarbonate from photosystem II," in *Photosynthesis. Energy From the Sun*, eds J. F. Allen, E. Gantt, J. H. Golbeck, and B. Osmond (Glasgow: Springer), 497–501.

Shevela, D., Su, J. H., Klimov, V., and Messinger, J. (2008b). Hydrogencarbonate is not a tightly bound constituent of the water-oxidizing complex in photosystem II. *Biochim. Biophys. Acta* 1777, 532–539. doi: 10.1016/j.bbabio.2008.03.031

Stemler, A. (1989). Absence of a formate-induced release of bicarbonate from photosystem 2. *Plant Physiol*. 91, 287–290. doi: 10.1104/pp.91.1.287

Stemler, A., and Radmer, R. (1975). Source of photosynthetic oxygen in bicarbonate-stimulated Hill reaction. *Science* 190, 457–458. doi: 10.1126/science.190.4213.457

Stevens, C. L. R., Schultz, D., Van Baalen, C., and Parker, P. L. (1975). Oxygen isotope fractionation during photosynthesis in a blue-green and a green alga. *Plant Physiol*. 56, 126–129. doi: 10.1104/pp.56.1.126

Tcherkez, G., and Farquhar, G. D. (2007). On the ^{16}O/^{18}O isotope effect associated with photosynthetic O_2 production. *Funct. Plant Biol*. 34, 1049–1052. doi: 10.1071/FP07168

Ulas, G., Olack, G., and Brudvig, G. W. (2008). Evidence against bicarbonate bound in the O_2-evolving complex of photosystem II. *Biochemistry* 47, 3073–3075. doi: 10.1021/bi8000424

Umena, Y., Kawakami, K., Shen, J.-R., and Kamiya, N. (2011). Crystal structure of oxygen-evolving photosystem II at a resolution of 1.9 Å. *Nature* 473, 55–60. doi: 10.1038/nature09913

Van Rensen, J. J. S., and Klimov, V. V. (2005). "Bicarbonate interactions," in *Photosystem II. The Light-Driven Water:Plastoquinone Oxidoreductase*, eds T. Wydrzynski and K. Satoh (Dordrecht: Springer), 329–346.

Vigara, L., Ertem, M. Z., Planas, N., Bozoglian, F., Leidel, N., Dau, H., et al. (2012). Experimental and quantum chemical characteriazation of the water oxidation cycle catalysed by $[Ru^{II}(damp)(bpy)(H_2O)]^{2+}$. *Chem. Sci.* 3, 2576–2586. doi: 10.1039/c2sc20399e

Villarejo, A., Shutova, T., Moskvin, O., Forssen, M., Klimov, V. V., and Samuelsson, G. (2002). A photosystem II-associated carbonic anhydrase regulates the efficiency of photosynthetic oxygen evolution. *EMBO J*. 21, 1930–1938. doi: 10.1093/emboj/21.8.1930

Vinyard, D. J., Ananyev, G. M., and Dismukes, G. C. (2013). Photosystem II: the reaction center of oxygenic photosynthesis*. *Annu. Rev. Biochem*. 82, 577–606. doi: 10.1146/annurev-biochem-070511-100425

Wiechen, M., Berends, H.-M., and Kurz, P. (2012). Water oxidation catalysed by manganese compounds: from complexes to 'biomimetic rocks'. *Dalton Trans*. 41, 21–31. doi: 10.1039/c1dt11537e

Wydrzynski, T., Hillier, W., and Messinger, J. (1996). On the functional significance of substrate accessibility in the photosynthetic water oxidation mechanism. *Physiol. Plant*. 96, 342–350. doi: 10.1111/j.1399-3054.1996.tb00224.x

Yano, J., Kern, J., Sauer, K., Latimer, M. J., Pushkar, Y., Biesiadka, J., et al. (2006). Where water is oxidized to dioxygen: structure of the photosynthetic Mn_4Ca cluster. *Science* 314, 821–825. doi: 10.1126/science.1128186

Conflict of Interest Statement: The authors declare that the research was conducted in the absence of any commercial or financial relationships that could be construed as a potential conflict of interest.

Received: 04 October 2013; accepted: 01 November 2013; published online: 26 November 2013.

*Citation: Shevela D and Messinger J (2013) Studying the oxidation of water to molecular oxygen in photosynthetic and artificial systems by time-resolved membrane-inlet mass spectrometry. Front. Plant Sci. **4**:473. doi: 10.3389/fpls.2013.00473*

This article was submitted to Plant Physiology, a section of the journal Frontiers in Plant Science.

frontiers in
PLANT SCIENCE

MINI REVIEW ARTICLE
published: 21 May 2013
doi: 10.3389/fpls.2013.00146

Fourier transform infrared difference spectroscopy for studying the molecular mechanism of photosynthetic water oxidation

Hsiu-An Chu*

Institute of Plant and Microbial Biology, Academia Sinica, Taipei, Taiwan

Edited by:
Harvey J. M. Hou, Alabama State University, USA

Reviewed by:
Takumi Noguchi, Nagoya University, Japan
Richard Debus, University of California at Riverside, USA

****Correspondence:***
Hsiu-An Chu, Institute of Plant and Microbial Biology, Academia Sinica, Taipei 11529, Taiwan.
e-mail: chuha@gate.sinica.edu.tw

The photosystem II reaction center mediates the light-induced transfer of electrons from water to plastoquinone, with concomitant production of O_2. Water oxidation chemistry occurs in the oxygen-evolving complex (OEC), which consists of an inorganic Mn_4CaO_5 cluster and its surrounding protein matrix. Light-induced Fourier transform infrared (FTIR) difference spectroscopy has been successfully used to study the molecular mechanism of photosynthetic water oxidation. This powerful technique has enabled the characterization of the dynamic structural changes in active water molecules, the Mn_4CaO_5 cluster, and its surrounding protein matrix during the catalytic cycle. This mini-review presents an overview of recent important progress in FTIR studies of the OEC and implications for revealing the molecular mechanism of photosynthetic water oxidation.

Keywords: photosystem II, oxygen evolution, FTIR, manganese cluster, infrared spectroscopy

INTRODUCTION

Photosynthetic water oxidation is catalyzed by a Mn_4Ca cluster and its surrounding protein matrix in photosystem II (PSII; Ferreira et al., 2004; Loll et al., 2005; Yano et al., 2006; Umena et al., 2011). The oxygen-evolving complex (OEC) accumulates oxidizing equivalents from the photochemical reactions within PSII and cycles through five oxidation states, termed S_n ($n = 0$–4, n representing the storage of oxidizing equivalents in the OEC; Kok et al., 1970; **Figure 1A**). The molecule O_2 is produced in the transition of S_3-(S_4)-S_0. One of the recent major breakthroughs in PSII research was the report of the crystal structure of oxygen-evolving PSII at 1.9 Å resolution (Umena et al., 2011). The structure of the Mn_4CaO_5 cluster is shown in **Figure 1B**. Three Mn, one Ca, and four oxygen atoms form a cubane-like structure; the fourth Mn connects to the cubic structure by two μ-oxo-bridges. The Mn_4CaO_5 cluster is connected with four water molecules: two are ligated to Ca and two to Mn_4 (Umena et al., 2011; **Figure 1B**). These water molecules are candidates for substrates in photosynthetic water oxidation. Another distinct feature in the structure is the apparently longer bond distances between the O_5-bridging oxygen atom and neighboring metal ions, which indicates weak bonding of this oxygen atom in the cluster. O_5 was proposed as a candidate for one of the substrates in dioxygen formation (Umena et al., 2011). More recent studies have suggested that the structure of the X-ray diffraction (XRD) model of PSII is modified by radiation-induced reduction of the Mn cluster (Luber et al., 2011; Grundmeier and Dau, 2012). Despite this problem, the 1.9 Å XRD structure is the crucial foundation for spectroscopic and mechanistic studies of photosynthetic water oxidation.

Abbreviations: EPR, electron paramagnetic resonance; FTIR, Fourier transform infrared; OEC, oxygen-evolving complex; OTG, octyl-β-D-thioglucopyranoside; PSII, photosystem II; Q_A, primary quinone electron acceptor in PSII; XRD, X-ray diffraction.

Several structural models of photosynthetic water oxidation have been proposed (Hoganson and Babcock, 1997; Pecoraro et al., 1998; McEvoy and Brudvig, 2006; Kusunoki, 2007; Pushkar et al., 2008; Siegbahn, 2009; Grundmeier and Dau, 2012), with differing locations and molecular structures of S-state intermediates (i.e., terminal water molecules or water-derived metal ligands). Several molecular spectroscopic techniques, including advanced electron paramagnetic resonance (EPR) spectroscopy (Britt et al., 2004; McConnell et al., 2011; Rapatskiy et al., 2012) and light-induced Fourier transform infrared (FTIR) difference spectroscopy (see below) have been extensively used to resolve this issue.

Fourier transform infrared difference spectroscopy has been widely used to study the structural changes in the OEC during the S-state catalytic cycle. The S_2-minus-S_1 mid-frequency (1800–1000 cm^{-1}) FTIR difference spectrum was first reported in 1992 (Noguchi et al., 1992). The S_3-minus-S_2 spectrum of the PSII/OEC was reported in 2000 (Chu et al., 2000b), and spectra of flash-induced S-state transitions ($S_1 \rightarrow S_2$, $S_2 \rightarrow S_3$, $S_3 \rightarrow S_0$, and $S_0 \rightarrow S_1$) during the complete S-state cycle were reported 1 year later (Hillier and Babcock, 2001; Noguchi and Sugiura, 2001). Many FTIR studies of the OEC focused on the mid-frequency region (1800–1000 cm^{-1}) of the IR spectrum, which contains information on structural changes of protein backbones and amino acid side-chains associated with S-state transitions of the OEC. One very important development in FTIR studies of the OEC were reports of high-frequency spectra (3700–3500 cm^{-1}) of the OEC, which contain information on structural changes of the weakly H-bonded OH-stretching of active water molecules during S-state transitions of the OEC (Noguchi and Sugiura, 2000, 2002a,b). The other important developments were reports of low-frequency spectra (<1000 cm^{-1}), which contain information on metal-ligand and manganese-substrate vibration modes

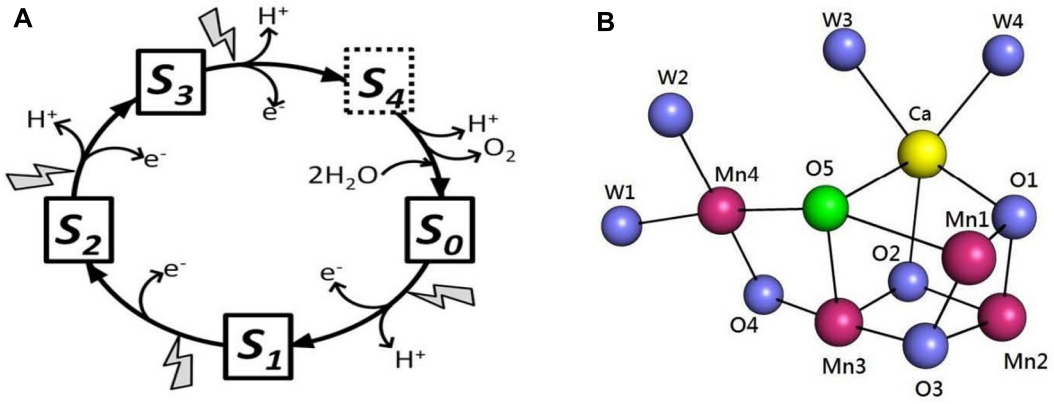

FIGURE 1 | (A) S-state cycle of photosynthetic water oxidation. **(B)** Structure of the Mn_4CaO_5 cluster as revealed by the 1.9 Å XRD study (Umena et al., 2011). Images generated in the PyMOL program using Protein Data Bank entry 3ARC.

of the OEC (Chu et al., 1999, 2000a,c; Yamanari et al., 2004; Kimura et al., 2005b).

This mini-review gives an overview of recent important progress in FTIR studies of the OEC, combined with new spectroscopic and XRD structural information, to understand the chemical mechanism of photosynthetic water oxidation. More comprehensive reviews on FTIR studies of the OEC are available (Noguchi, 2007, 2008a,b; Debus, 2008).

OH-STRETCHING VIBRATIONAL MODES OF ACTIVE WATER MOLECULES IN THE HIGH-FREQUENCY REGION (3700–3500 cm^{-1}) OF THE OEC

The reactions of substrate water during the S-state catalytic cycle of the OEC are of paramount importance to understand the chemical mechanism of photosynthetic water oxidation. In the new XRD structure of the Mn_4CaO_5 cluster, the four water molecules connected to the OEC are involved in a hydrogen-bonded network linking the Mn_4CaO_5-cluster and Y_Z (Umena et al., 2011). The bond distances (2.8–3.3 Å) between oxygen atoms of coordinated water molecules and their neighboring water molecules indicate that most of the O–H groups of the water molecules are weakly hydrogen bonded and will appear in the weakly hydrogen-bonded OH-stretch (3750–3500 cm^{-1}) region of the FTIR spectra. Noguchi and colleagues reported flash-induced difference spectra of S-state transitions in the weakly H-bonded OH-stretching region (Noguchi and Sugiura, 2000, 2002a,b). One active water molecule on the OEC, which gave rise to the S_1 band at ~3585 cm^{-1} and the S_2 band at ~3618 cm^{-1}, was identified at 250 K in light-induced S_2/S_1 FTIR difference spectrum (Noguchi and Sugiura, 2000) and during the S-state cycle at 10°C (Noguchi and Sugiura, 2002a,b) in PSII core complexes from *Thermosynechococcus elongatus*. The results indicated a weakened hydrogen bond of the OH group for one water molecule connected to the OEC during the $S_1 \rightarrow S_2$ transition. In contrast to the $S_1 \rightarrow S_2$ transition, the $S_2 \rightarrow S_3$, $S_3 \rightarrow S_0$, and $S_0 \rightarrow S_1$ transitions all showed a negative OH-stretching mode at different frequencies, which indicates that these water (or hydroxide) molecules were involved in proton release reactions of the OEC or formed strong hydrogen-bonding interactions during these transitions (Noguchi and Sugiura, 2002a,b). In addition, these observations are consistent with a recent FTIR study which concluded that the proton release pattern from the substrate water on the OEC is in 1:0:1:2 stoichiometry for the $S_0 \rightarrow S_1 \rightarrow S_2 \rightarrow S_3 \rightarrow S_0$ transition (Suzuki et al., 2009). One of the important issues is the exact location of these active water molecules detected by FTIR difference spectra on the OEC (e.g., associated with Mn or Ca) in the new XRD structure.

Mn-LIGAND AND Mn-SUBSTRATE VIBRATION MODES IN THE LOW-FREQUENCY REGION (<1000 cm^{-1}) OF THE OEC

From studies of Mn model compound, Mn-ligand and Mn-substrate vibration modes of the PSII/OEC are expected to show up in the low-frequency region (<1000 cm^{-1}) of the IR spectrum (Chu et al., 2001c). In low-frequency S_2/S_1 FTIR difference spectra of octyl-β-D-thioglucopyranoside (OTG) PSII core preparations of spinach, a positive mode at 606 cm^{-1} in ^{16}O water clearly downshifted to 596 cm^{-1} in ^{18}O water (Chu et al., 2000c; **Figure 2A**). With double-difference (S_2/S_1 and ^{16}O minus ^{18}O) spectra, the 606 cm^{-1} mode was assigned to an S_2 mode, and a corresponding S_1 mode at about 625 cm^{-1} was identified (Chu et al., 2000c). In addition, this 606-cm^{-1} mode was up-shifted to about 618 cm^{-1} with Sr^{2+} substitution but not significantly affected by ^{44}Ca isotope substitution (Chu et al., 2000c; Kimura et al., 2005a; **Figure 2B**). From these results and studies of Mn model compounds, this vibrational mode at 606 cm^{-1} in the S_2 state was assigned to a Mn–O–Mn cluster vibration in the OEC (Chu et al., 2000c). The structure of this Mn–O–Mn cluster very likely includes additional oxo and carboxylate bridges(s). IR modes for υ(Mn=O) and υ_{asy}(Mn–O–Mn) for a singly oxo-bridged Mn cluster usually occur at >700 cm^{-1} and typically have a 30–40 cm^{-1} downshift (Chu et al., 2001c). They are unlikely to be the origin of the 606-cm^{-1} mode. Furthermore, this 606-cm^{-1} mode was altered in S_2/S_1 FTIR difference spectra of Ala344D1Gly, Glu189Gln, and Asp170HisD1 *Synechocystis* mutant PSII particles (Chu et al., 2001a; Mizusawa et al., 2004; Kimura et al., 2005c). All the above amino acid residues are direct ligands for the Mn_4Ca

cluster. Therefore, the structure of the Mn–O–Mn cluster is structurally coupled to its surrounding ligand environment.

Low-frequency S_3/S_2 spectra were reported in OTG PSII core preparations of spinach, in which intense bands at 604(−) and 621 (+) cm^{-1} were sensitive to ^{18}O water exchange (Chu et al., 2001b). The S_3 mode at ~621 cm^{-1} was attributed to the Mn–O–Mn cluster mode of the S_3 state. Kimura et al. (2005b) reported on $^{16}O/^{18}O$- and/or H/D water-sensitive low-frequency vibrations of the OEC during the complete S-state cycle in PSII core particles from *T. elongatus*. The S_2 mode at ~606 cm^{-1} changed their sign and intensity during S-state cycling, which indicates S-state-dependent changes in the core structure of the Mn_4CaO_5 cluster. In addition, several IR bands sensitive to both $^{16}O/^{18}O$ and H/D exchanges were attributed to S-state intermediates during the S-state cycling (Kimura et al., 2005b). Furthermore, an intense 577(−) cm^{-1} band in the S_2/S_1 spectra was found insensitive to universal ^{15}N- and ^{13}C-isotope labeling and assigned to the skeletal vibration of the Mn cluster or stretching vibrational modes of the Mn ligand (Kimura et al., 2003).

Low-frequency FTIR results demonstrate that one bridged oxygen atom in the Mn–O–Mn cluster of the OEC is accessible to and can be exchanged with bulky-phase water. This exchange occurs within minutes or faster because it is complete within 30 min (Chu et al., 2000c). A recent study involving W-band ^{17}O electron–electron double resonance-detected nuclear magnetic resonance (NMR) spectroscopy reported that one μ-oxo bridge of the OEC can exchange with $H_2{}^{17}O$ on a time scale (≤15 s) similar to that of substrate water on the OEC (Rapatskiy et al., 2012). This study also suggested that the exchangeable μ-oxo bridge links the outer Mn to the Mn_3O_3Ca open-cuboidal unit (O_4 and O_5 in **Figure 1**). The authors of this study favored the Ca-linked O_5 oxygen assignment (Rapatskiy et al., 2012). Low-frequency FTIR results showed that the Mn–O–Mn cluster mode at 606 cm^{-1} is sensitive to Sr^{2+} substitution but not ^{44}Ca substitution (Chu et al., 2000c; Kimura et al., 2005a). Considering the structure of O_5 in the Mn_4CaO_5 cluster (Umena et al., 2011; **Figure 1B**), the ^{44}Ca-induced isotopic shift of the Mn–O–Mn cluster mode may have been too small to be detected by previous FTIR studies. Thus, the O_5-bridging oxygen atom is a good candidate for the exchangeable-bridged oxygen atom in the Mn–O–Mn cluster identified by FTIR. A recent continue-wave Q-band electron nuclear double resonance (ENDOR) study reported a much slower ^{17}O exchange rate (on the time scale of hours) with ^{17}O-labeled water into the μ-oxo bridge of the OEC (McConnell et al., 2011). Future study is required to resolve this discrepancy.

EFFECT OF AMMONIA ON THE OEC

Because of the structural similarity between NH_3 and H_2O and the ability of NH_3 to inhibit photosynthetic water oxidation, the NH_3 binding site on the OEC might occur at the substrate water-binding site. Previous EPR studies of NH_3-treated PSII samples demonstrated that the S_2-state multiline EPR signal is altered when samples illuminated at 200 K are subsequently "annealed" above 250 K (Beck et al., 1986; Britt et al., 1989). FTIR studies showed that NH_3 induced characteristic spectral changes in the S_2/S_1 spectra at 250 K (Chu et al., 2004a; Fang et al., 2005). Among them, the S_2-state symmetric carboxylate stretching mode at 1365 cm^{-1} in

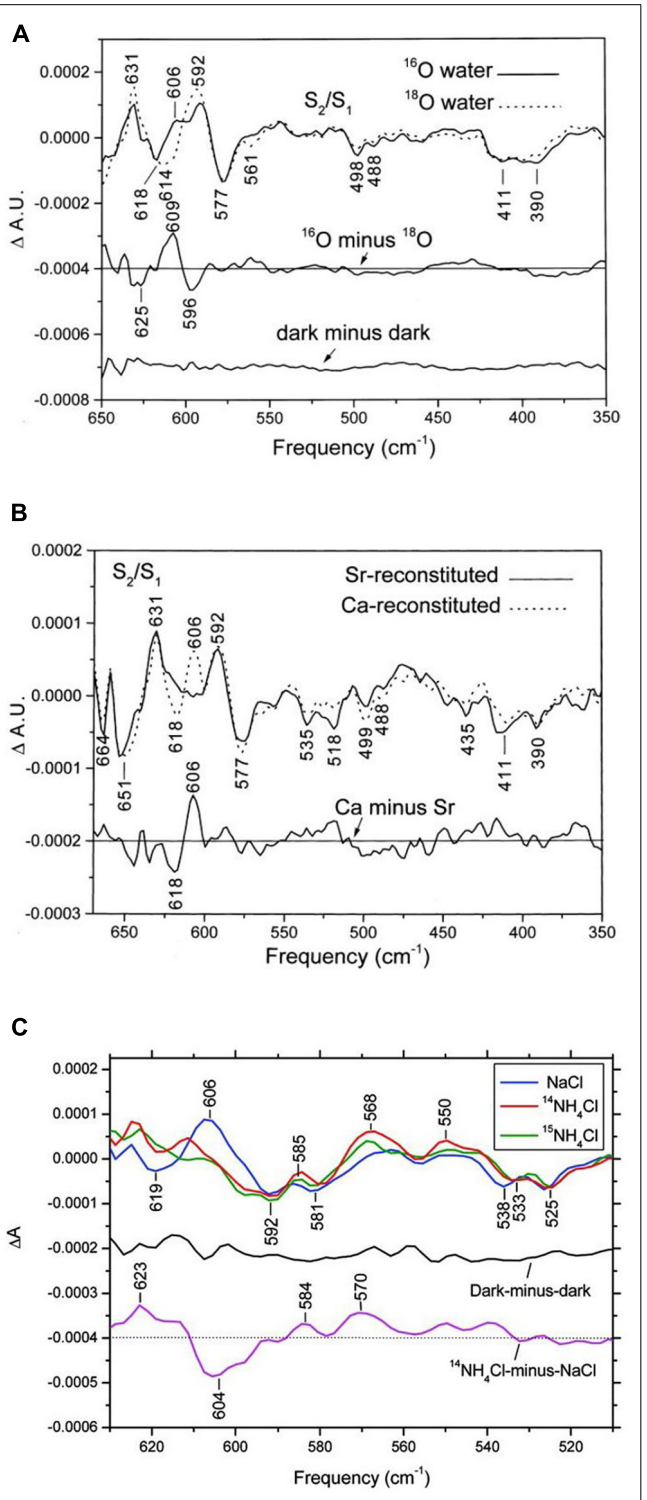

FIGURE 2 | Comparison of the low-frequency S_2/S_1 FTIR difference spectra of spinach PSII core complexes (A) in buffered $H_2{}^{16}O$ (solid line) or $H_2{}^{18}O$ (dotted line), (B) with Sr^{2+}-reconstitution (solid line) or Ca^{2+}-reconstitution (dashed line), and (C) $S_2Q_A^-/S_1Q_A$ FTIR difference spectra with 50 mM NaCl (blue line), 50 mM $^{14}NH_4Cl$ (red line), or 50 mM $^{15}NH_4Cl$ (green line). The sample temperature was 250 K (reprinted with permission from Chu et al., 2000c, copyright 2000 and 2011, by the American Chemical Society).

the S_2/S_1 spectrum of control samples up-shifted to ∼1379 cm^{-1} in NH_3-treated samples. This carboxylate mode was also altered by Sr^{2+} substitution (Strickler et al., 2005; Suzuki et al., 2006), which indicates that the action site of NH_3 on the OEC is near the Ca^{2+} site. In addition, the conditions that give rise to the NH_3-induced up-shift of this S_2-state carboxylate stretching mode at 1365 cm^{-1} are strongly correlated with those producing the modified S_2-state multiline EPR signal (Chu et al., 2004a; Fang et al., 2005). Furthermore, a recent FTIR result showed that NH_3 did not replace the active water molecule connected to the OEC during the S_1-to-S_2 transition at 250 K, whereas the Mn–O–Mn cluster vibrational mode at 606 cm^{-1} was diminished or underwent a large shift (Hou et al., 2011; **Figure 2C**). The above results are consistent with the proposal that NH_3 may replace one of the bridging oxygen atoms, presumably O_5, in the Mn_4CaO_5 cluster during the S_1-to-S_2 transition (Britt et al., 1989).

The other intriguing FTIR finding is that the effect of NH_3-induced up-shift of 1365 cm^{-1} mode in the S_2/S_1 spectrum was diminished at temperatures above 0°C (Huang et al., 2008). The results indicate that the interaction of NH_3 with the OEC is attenuated at temperatures above 0°C (Huang et al., 2008). In addition, a recent FTIR study reported an inhibitory effect of the ammonium cation on the PSII/OEC at 283 K (Tsuno et al., 2011). The results suggested that the ammonium cation perturbs some carboxylate residues coupled to the Mn cluster during the S_1-to-S_2 transition and inhibits the oxygen evolution reaction at 283 K (Tsuno et al., 2011).

FTIR RESULTS FOR PROTEIN LIGANDS OF THE OEC

Fourier transform infrared studies involving isotopic labeling and site-directed mutagenesis have provided a wealth of information on dynamic structural changes of the protein backbones and amino acid side-chains during the S-state transitions of the OEC (Debus, 2008; Noguchi, 2008a; Shimada et al., 2011). An isotope-edited FTIR study identified the L-[1-^{13}C]alanine-sensitive symmetric carboxylate stretching modes in S_2/S_1 difference spectra to the α-COO^- group of D1-Ala344 (Chu et al., 2004b). This mode appears at ∼1356 cm^{-1} in the S_1 state and at ∼1339 or ∼1320 cm^{-1} in the S_2 state in unlabeled wild-type PSII particles but not in D1-Ala344Gly and D1-Ala344Ser mutant PSII particles. These frequencies are consistent with unidentate ligation of the α-COO^- group of D1-Ala344 to the Mn_4Ca cluster in both the S_1 and S_2 state (Chu et al., 2004b; Strickler et al., 2005). In addition, substituting Sr for Ca did not alter the symmetric carboxylate stretching modes of D1-Ala344 (Strickler et al., 2005). The results suggested that the α-COO^- group of D1-Ala344 did not ligate Ca. In the 1.9 Å XRD structure, the α-COO^- group of D1-Ala344 shows very asymmetrical bridging between Mn_2 and Ca in the cluster, with the Mn–O distance 2.0 Å and Ca–O distance 2.6 Å (Kawakami et al., 2011). In addition, the isotopic bands for the α-COO^- group of D1-Ala344 showed characteristic changes during S-state cycling (Kimura et al., 2005d). These results indicated that the C-terminal Ala 344D1 is structurally coupled, presumably directly ligated, to the Mn ion that undergoes oxidation of Mn(III) to Mn(IV) during the S_1-to-S_2 transition and is reduced in reverse with the S_3-to-S_0 transition (Chu et al., 2004b; Kimura et al., 2005d). In contrast, mutations of D1-Asp170, D1-Glu189, and D1-Asp342 did not eliminate any carboxylate vibrational stretching modes during S-state cycling of the OEC (Debus et al., 2005; Strickler et al., 2006, 2007). Recent computational studies suggested that vibrations of carboxylate ligands can be quite insensitive to Mn oxidation, if they are not coordinated along the Jahn–Teller axis (Sproviero et al., 2008). In their model, the only amino acid residue that is ligated along the Jahn–Teller axis of a Mn^{III} ion is CP43-E354.

Of note, CP43-E354Q mutant PSII particles gave rise to characteristic spectral changes in the amide and carboxylate stretch regions of FTIR difference spectra during S-state transitions (Strickler et al., 2008; Shimada et al., 2009; Service et al., 2010). In addition, the weakly H-bonded O–H stretching modes of the active water molecule associated with the OEC were significantly altered in S_2/S_1 FTIR difference spectra of CP43-E354Q mutant PSII particles (Shimada et al., 2009). Furthermore, $H_2{}^{18}O$ exchange mass spectrometry experiments showed that the CP43-E354Q mutation weakened the binding of both substrate-water molecules (or water-derived ligands), particularly affecting the one with faster exchange in the S_3 state (Service et al., 2010). The XRD structure of the OEC showed that coordinated water molecules were on Ca^{2+} and Mn_4, which were both not ligated by CP43-E354 (Umena et al., 2011). Presumably, CP43-E354Q mutation may induce significant structural changes to the Mn_4CaO_5 core that affects associated active water molecule(s) on the OEC during the S_1-to-S_2 transition.

A recent time-resolved infrared study revealed the proton and protein dynamics associated with the OEC during the S-state transitions (Noguchi et al., 2012). The results suggest that during the S_3-to-S_0 transition, protons are greatly rearranged to form a transient state before the oxidation of the Mn_4CaO_5 cluster that leads to O_2 formation. In addition, an early proton movement was detected during the $S_2 \rightarrow S_3$ transition, indicating a proton release coupled with the electron transfer reaction. Furthermore, a relatively slow carboxylate movement occurred in the $S_0 \rightarrow S_1$ transition, which might reflect the protein relaxation process to stabilize the S_1 state (Noguchi et al., 2012). This study demonstrates that time-resolved infrared technique is extremely useful to monitor proton and protein dynamics of the OEC during photosynthetic oxygen evolution.

BIOINORGANIC MODELS FOR FTIR SPECTRAL INTERPRETATION

Vibrational data from model compounds relevant to the OEC is crucial to interpret FTIR data of the OEC during S-state cycling. However, vibrational data for synthetic multinuclear Mn complexes are still limited (Cua et al., 2003; Berggren et al., 2012). Particularly, vibrational data are needed for the Ca–Mn multinuclear cluster that models the Mn_4CaO_5 cluster (Kanady et al., 2011; Mukherjee et al., 2012). One previous study reported IR spectra and normal mode analysis of the adamantine-like complex $[Mn_4O_6(bpea)_4]^{n+}$ (Visser et al., 2002). By using the electrochemical method to record the difference IR spectrum and ^{18}O isotopic labeling, the authors identified Mn–O vibrational modes for $[Mn^{IV}{}_4]$ and $[Mn^{IV}{}_3Mn^{III}]$. Comparison with OEC data ruled out the adamantine-like complex as the possible structure

intermediate. Nevertheless, this approach is very powerful for interpreting FTIR data for the OEC during S-state cycling.

CONCLUSIONS AND PERSPECTIVES

Light-induced FTIR difference spectroscopy has become a fruitful structural technique to study the molecular mechanism of photosynthetic water oxidation. The new high-resolution XRD structure of the OEC has served as a crucial foundation for designing FTIR experiments and interpreting FTIR data. Combined with isotopic labeling, site-directed mutagenesis, model compound studies, and normal mode analysis, FTIR difference spectroscopy will continue to provide important structural and mechanistic insights into the water-splitting process in PSII.

ACKNOWLEDGMENTS

The author is grateful to Prof. Richard J. Debus for helpful suggestions on the manuscript. This work was supported by National Science Council in Taiwan (NSC 101-2627-M-001-001) and by Academia Sinica.

REFERENCES

Beck, W. F., De Paula, J. C., and Brudvig, G. W. (1986). Ammonia binds to the manganese site of the oxygen-evolving complex of photosystem II in the S2 state. *J. Am. Chem. Soc.* 108, 4018–4022.

Berggren, G., Anderlund, M. F., Styring, S., and Thapper, A. (2012). FTIR study of manganese dimers with carboxylate donors as model complexes for the water oxidation complex in photosystem II. *Inorg. Chem.* 51, 2332–2337.

Britt, R. D., Campbell, K. A., Peloquin, J. M., Gilchrist, M. L., Aznar, C. P., Dicus, M. M., et al. (2004). Recent pulsed EPR studies of the photosystem II oxygen-evolving complex: implications as to water oxidation mechanisms. *Biochim. Biophys. Acta* 1655, 158–171.

Britt, R. D., Zimmermann, J. L., Sauer, K., and Klein, M. P. (1989). Ammonia binds to the catalytic manganese of the oxygen-evolving complex of photosystem II. Evidence by electron spin-echo envelope modulation spectroscopy. *J. Am. Chem. Soc.* 111, 3522–3532.

Chu, H.-A., Debus, R. J., and Babcock, G. T. (2001a). D1-Asp170 is structurally coupled to the oxygen evolving complex in photosystem II as revealed by light-induced Fourier transform infrared difference spectroscopy. *Biochemistry* 40, 2312–2316.

Chu, H.-A., Hillier, W., Law, N. A., and Babcock, G. T. (2001b). "Identification of a possible Mn–O–Mn cluster vibrational mode of the S3 state in the oxygen-evolving complex of photosystem II by the low-frequency FTIR spectroscopy," in *PS2001 proceedings: 12th Intenational Congress on Photosynthesis, S13-027*, CSIRO Publishing, Collingwood, Australia.

Chu, H.-A., Hillier, W., Law, N. A., and Babcock, G. T. (2001c). Vibrational spectroscopy of the oxygen-evolving complex and of manganese model compounds. *Biochim. Biophys. Acta* 1503, 69–82.

Chu, H.-A., Feng, Y.-W., Wang, C.-M., Chiang, K.-A., and Ke, S.-C. (2004a). Ammonia-induced structural changes of the oxygen-evolving complex in photosystem II as revealed by light-induced FTIR difference spectroscopy. *Biochemistry* 43, 10877–10885.

Chu, H.-A., Hillier, W., and Debus, R. J. (2004b). Evidence that the C-terminus of the D1 polypeptide of photosystem II is ligated to the manganese ion that undergoes oxidation during the S1 to S2 transition: an isotope-edited FTIR study. *Biochemistry* 43, 3152–3166.

Chu, H.-A., Gardner, M., Hillier, W., and Babcock, G. (2000a). Low-frequency Fourier transform infrared spectroscopy of the oxygen-evolving complex in photosystem II. *Photosynth. Res.* 66, 57–63.

Chu, H.-A., Hillier, W., Law, N. A., Sackett, H., Haymond, S., and Babcock, G. T. (2000b). Light-induced FTIR difference spectroscopy of the S2-to-S3 state transition of the oxygen-evolving complex in photosystem II. *Biochim. Biophys. Acta* 1459, 528–532.

Chu, H.-A., Sackett, H., and Babcock, G. T. (2000c). Identification of a Mn–O–Mn cluster vibrational mode of the oxygen-evolving complex in photosystem II by low-frequency FTIR spectroscopy. *Biochemistry* 39, 14371–14376.

Chu, H.-A., Gardner, M. T., O'Brie, J. P., and Babcock, G. T. (1999). Low-frequency Fourier transform infrared spectroscopy of the oxygen-evolving and quinone acceptor complexes in photosystem II. *Biochemistry* 38, 4533–4541.

Cua, A., Vrettos, J., Paula, J., Brudvig, G., and Bocian, D. (2003). Raman spectra and normal coordinate analyses of low-frequency vibrations of oxo-bridged manganese complexes. *J. Biol. Inorg. Chem.* 8, 439–451.

Debus, R. J. (2008). Protein ligation of the photosynthetic oxygen-evolving center. *Coord. Chem. Rev.* 252, 244–258.

Debus, R. J., Strickler, M. A., Walker, L. M., and Hillier, W. (2005). No evidence from FTIR difference spectroscopy that aspartate-170 of the D1 polypeptide ligates a manganese ion that undergoes oxidation during the S0 to S1, S1 to S2, or S2 to S3 transitions in photosystem II. *Biochemistry* 44, 1367–1374.

Fang, C.-H., Chiang, K.-A., Hung, C.-H., Chang, K., Ke, S.-C., and Chu, H.-A. (2005). Effects of ethylene glycol and methanol on ammonia-induced structural changes of the oxygen-evolving complex in photosystem II. *Biochemistry* 44, 9758–9765.

Ferreira, K. N., Iverson, T. M., Maghlaoui, K., Barber, J., and Iwata, S. (2004). Architecture of the photosynthetic oxygen-evolving center. *Science* 303, 1831–1838.

Grundmeier, A., and Dau, H. (2012). Structural models of the manganese complex of photosystem II and mechanistic implications. *Biochim. Biophys. Acta* 1817, 88–105.

Hillier, W., and Babcock, G. T. (2001). S-state dependent Fourier transform infrared difference spectra for the photosystem II oxygen evolving complex. *Biochemistry* 40, 1503–1509.

Hoganson, C. W., and Babcock, G. T. (1997). A metalloradical mechanism for the generation of oxygen from water in photosynthesis. *Science* 277, 1953–1956.

Hou, L.-H., Wu, C.-M., Huang, H.-H., and Chu, H.-A. (2011). Effects of ammonia on the structure of the oxygen-evolving complex in photosystem II as revealed by light-induced FTIR difference spectroscopy. *Biochemistry* 50, 9248–9254.

Huang, H.-H., Wang, T.-H., and Chu, H.-A. (2008). "Ammonia-induced structural changes of the oxygen-evolving complex in photosystem II diminished at 277 K as revealed by light-induced FTIR difference Spectroscopy," in *Photosynthesis. Energy from the Sun*, eds J. Allen, E. Gantt, J. Golbeck, and B. Osmond (Dordrecht: Springer), 389–391.

Kanady, J. S., Tsui, E. Y., Day, M. W., and Agapie, T. (2011). A synthetic model of the Mn_3Ca subsite of the oxygen-evolving complex in photosystem II. *Science* 333, 733–736.

Kawakami, K., Umena, Y., Kamiya, N., and Shen, J.-R. (2011). Structure of the catalytic, inorganic core of oxygen-evolving photosystem II at 1.9 Å resolution. *J. Photochem. Photobiol. B Biol.* 104, 9–18.

Kimura, Y., Hasegawa, K., Yamanari, T., and Ono, T.-A. (2005a). Studies on photosynthetic oxygen-evolving complex by means of Fourier transform infrared spectroscopy: calcium and chloride cofactors. *Photosynth. Res.* 84, 245–250.

Kimura, Y., Ishii, A., Yamanari, T., and Ono, T.-A. (2005b). Water-sensitive Low-frequency vibrations of reaction intermediates during S-state cycling in photosynthetic water oxidation. *Biochemistry* 44, 7613–7622.

Kimura, Y., Mizusawa, N., Ishii, A., Nakazawa, S., and Ono, T. A. (2005c). Changes in structural and functional properties of oxygen-evolving complex induced by replacement of D1-glutamate 189 with glutamine in photosystem II: ligation of glutamate 189 carboxylate to the manganese cluster. *J. Biol. Chem.* 280, 37895–37900.

Kimura, Y., Mizusawa, N., Yamanari, T., Ishii, A., and Ono, T. A. (2005d). Structural changes of D1 C-terminal alpha-carboxylate during S-state cycling in photosynthetic oxygen evolution. *J. Biol. Chem.* 280, 2078–2083.

Kimura, Y., Mizusawa, N., Ishii, A., Yamanari, T., and Ono, T.-A. (2003). Changes of low-frequency vibrational modes induced by universal ^{15}N- and ^{13}C-isotope labeling in S2/S1 FTIR difference spectrum of oxygen-evolving complex. *Biochemistry* 42, 13170–13177.

Kok, B., Forbush, B., and McGloin, M. (1970). Cooperation of charges in photosynthetic O_2 evolution-I. A linear four step mechanism. *Photochem. Photobiol.* 11, 457–475.

Kusunoki, M. (2007). Mono-manganese mechanism of the photosystem II water splitting reaction by a unique Mn_4Ca cluster. *Biochim. Biophys. Acta* 1767, 484–492.

Loll, B., Kern, J., Saenger, W., Zouni, A., and Biesiadka, J. (2005). Towards complete cofactor arrangement in the 3.0 Å resolution structure of photosystem II. *Nature* 438, 1040–1044.

Luber, S., Rivalta, I., Umena, Y., Kawakami, K., Shen, J.-R., Kamiya, N., et al. (2011). S1-state model of the O_2-evolving complex of photosystem II. *Biochemistry* 50, 6308–6311.

McConnell, I. L., Grigoryants, V. M., Scholes, C. P., Myers, W. K., Chen, P.-Y., Whittaker, J. W., et al. (2011). EPR–ENDOR characterization of (^{17}O, ^{1}H, ^{2}H) water in manganese catalase and its relevance to the oxygen-evolving complex of photosystem II. *J. Am. Chem. Soc.* 134, 1504–1512.

McEvoy, J. P., and Brudvig, G. W. (2006). Water-splitting chemistry of photosystem II. *Chem. Rev.* 106, 4455–4483.

Mizusawa, N., Kimura, Y., Ishii, A., Yamanari, T., Nakazawa, S., Teramoto, H., et al. (2004). Impact of replacement of D1 C-terminal alanine with glycine on structure and function of photosynthetic oxygen-evolving complex. *J. Biol. Chem.* 279, 29622–29627.

Mukherjee, S., Stull, J. A., Yano, J., Stamatatos, T. C., Pringouri, K., Stich, T. A., et al. (2012). Synthetic model of the asymmetric $[Mn_3CaO_4]$ cubane core of the oxygen-evolving complex of photosystem II. *Proc. Natl. Acad. Sci. U.S.A.* 109, 2257–2262.

Noguchi, T. (2007). Light-induced FTIR difference spectroscopy as a powerful tool toward understanding the molecular mechanism of photosynthetic oxygen evolution. *Photosynth. Res.* 91, 59–69.

Noguchi, T. (2008a). Fourier transform infrared analysis of the photosynthetic oxygen-evolving center. *Coord. Chem. Rev.* 252, 336–346.

Noguchi, T. (2008b). FTIR detection of water reactions in the oxygen-evolving centre of photosystem II. *Philos. Trans. R. Soc. Lond. B Biol. Sci.* 363, 1189–1194.

Noguchi, T., Ono, T., and Inoue, Y. (1992). Detection of structural changes upon S1-to-S2 transition in the oxygen-evolving manganese cluster in photosystem II by light-induced Fourier transform infrared difference spectroscopy. *Biochemistry* 31, 5953–5956.

Noguchi, T., and Sugiura, M. (2000). Structure of an active water molecule in the water-oxidizing complex of photosystem II as studied by FTIR spectroscopy. *Biochemistry* 39, 10943–10949.

Noguchi, T., and Sugiura, M. (2001). Flash-induced Fourier transform infrared detection of the structural changes during the S-state cycle of the oxygen-evolving complex in photosystem II. *Biochemistry* 40, 1497–1502.

Noguchi, T., and Sugiura, M. (2002a). Flash-induced FTIR difference spectra of the water oxidizing complex in moderately hydrated photosystem II core films: effect of hydration extent on S-state transitions. *Biochemistry* 41, 2322–2330.

Noguchi, T., and Sugiura, M. (2002b). FTIR detection of water reactions during the flash-induced S-state cycle of the photosynthetic water-oxidizing complex. *Biochemistry* 41, 15706–15712.

Noguchi, T., Suzuki, H., Tsuno, M., Sugiura, M., and Kato, C. (2012). Time-resolved infrared detection of the proton and protein dynamics during photosynthetic oxygen evolution. *Biochemistry* 51, 3205–3214.

Pecoraro, V., Baldwin, M., Caudle, M., Hsieh, W.-Y., and Law, N. (1998). A proposal for water oxidation in photosystem II. *Pure Appl. Chem.* 70, 925–930.

Pushkar, Y., Yano, J., Sauer, K., Boussac, A., and Yachandra, V. K. (2008). Structural changes in the Mn_4Ca cluster and the mechanism of photosynthetic water splitting. *Proc. Natl. Acad. Sci. U.S.A.* 105, 1879–1884.

Rapatskiy, L., Cox, N., Savitsky, A., Ames, W. M., Sander, J., Nowaczyk, M. M., et al. (2012). Detection of the water-binding sites of the oxygen-evolving complex of photosystem II using W-band ^{17}O electron–electron double resonance-detected NMR spectroscopy. *J. Am. Chem. Soc.* 134, 16619–16634.

Service, R., Yano, J., McConnell, I., Hwang, H. J., Niks, D., Hille, R., et al. (2010). Participation of glutamate-354 of the CP43 polypeptide in the ligation of Mn and the binding of substrate water in photosystem II. *Biochemistry* 50, 63–81.

Shimada, Y., Suzuki, H., Tsuchiya, T., Mimuro, M., and Noguchi, T. (2011). Structural coupling of an arginine side chain with the oxygen-evolving Mn_4Ca cluster in photosystem II as revealed by isotope-edited Fourier transform infrared spectroscopy. *J. Am. Chem. Soc.* 133, 3808–3811.

Shimada, Y., Suzuki, H., Tsuchiya, T., Tomo, T., Noguchi, T., and Mimuro, M. (2009). Effect of a single-amino acid substitution of the 43 kDa chlorophyll protein on the oxygen-evolving reaction of the cyanobacterium *Synechocystis* sp. PCC 6803: analysis of the Glu354Gln mutation. *Biochemistry* 48, 6095–6103.

Siegbahn, P. E. M. (2009). Structures and energetics for O_2 formation in photosystem II. *Acc. Chem. Res.* 42, 1871–1880.

Sproviero, E. M., Gascón, J. A., Mcevoy, J. P., Brudvig, G. W., and Batista, V. S. (2008). Computational studies of the O_2-evolving complex of photosystem II and biomimetic oxomanganese complexes. *Coord. Chem. Rev.* 252, 395–415.

Strickler, M. A., Hillier, W., and Debus, R. J. (2006). No evidence from FTIR difference spectroscopy that glutamate-189 of the D1 polypeptide ligates a Mn ion that undergoes oxidation during the S0 to S1, S1 to S2, or S2 to S3 transitions in photosystem II. *Biochemistry* 45, 8801–8811.

Strickler, M. A., Hwang, H. J., Burnap, R. L., Yano, J., Walker, L. M., Service, R. J., et al. (2008). Glutamate-354 of the CP43 polypeptide interacts with the oxygen-evolving Mn_4Ca cluster of photosystem II: a preliminary characterization of the Glu354Gln mutant. *Philos. Trans. R. Soc. Lond. B Biol. Sci.* 363, 1179–1187.

Strickler, M. A., Walker, L. M., Hillier, W., Britt, R. D., and Debus, R. J. (2007). No evidence from FTIR difference spectroscopy that aspartate-342 of the D1 polypeptide ligates a Mn ion that undergoes oxidation during the S0 to S1, S1 to S2, or S2 to S3 transitions in photosystem II. *Biochemistry* 46, 3151–3160.

Strickler, M. A., Walker, L. M., Hillier, W., and Debus, R. J. (2005). Evidence from biosynthetically incorporated strontium and FTIR difference spectroscopy that the C-terminus of the D1 polypeptide of photosystem II does not ligate calcium. *Biochemistry* 44, 8571–8577.

Suzuki, H., Sugiura, M., and Noguchi, T. (2009). Monitoring proton release during photosynthetic water oxidation in photosystem II by means of isotope-edited infrared spectroscopy. *J. Am. Chem. Soc.* 131, 7849–7857.

Suzuki, H., Taguchi, Y., Sugiura, M., Boussac, A., and Noguchi, T. (2006). Structural perturbation of the carboxylate ligands to the manganese cluster upon Ca^{2+}/Sr^{2+} exchange in the S-state cycle of photosynthetic oxygen evolution as studied by flash-induced FTIR difference spectroscopy. *Biochemistry* 45, 13454–13464.

Tsuno, M., Suzuki, H., Kondo, T., Mino, H., and Noguchi, T. (2011). Interaction and inhibitory effect of ammonium cation in the oxygen evolving center of photosystem II. *Biochemistry* 50, 2506–2514.

Umena, Y., Kawakami, K., Shen, J. R., and Kamiya, N. (2011). Crystal structure of oxygen-evolving photosystem II at a resolution of 1.9 Å. *Nature* 473, 55–60.

Visser, H., Dubé, C. E., Armstrong, W. H., Sauer, K., and Yachandra, V. K. (2002). FTIR spectra and normal-mode analysis of a tetranuclear manganese adamantane-like complex in two electrochemically prepared oxidation states: relevance to the oxygen-evolving complex of photosystem II. *J. Am. Chem. Soc.* 124, 11008–11017.

Yamanari, T., Kimura, Y., Mizusawa, N., Ishii, A., and Ono, T.-A. (2004). Mid-to low-frequency Fourier transform infrared spectra of S-state cycle for photosynthetic water oxidation in *Synechocystis* sp. PCC 6803. *Biochemistry* 43, 7479–7490.

Yano, J., Kern, J., Sauer, K., Latimer, M. J., Pushkar, Y., Biesiadka, J., et al. (2006). Where water is oxidized to dioxygen: structure of the photosynthetic Mn_4Ca cluster. *Science* 314, 821–825.

Conflict of Interest Statement: The author declares that the research was conducted in the absence of any commercial or financial relationships that could be construed as a potential conflict of interest.

Received: 31 March 2013; paper pending published: 26 April 2013; accepted: 29 April 2013; published online: 21 May 2013.

Citation: Chu H-A (2013) Fourier transform infrared difference spectroscopy for studying the molecular mechanism of photosynthetic water oxidation. Front. Plant Sci. ***4****:146. doi: 10.3389/fpls.2013.00146*

This article was submitted to Frontiers in Plant Physiology, a specialty of Frontiers in Plant Science.

frontiers in
PLANT SCIENCE

REVIEW ARTICLE
published: 31 October 2013
doi: 10.3389/fpls.2013.00434

Understanding the roles of the thylakoid lumen in photosynthesis regulation

Sari Järvi*†, *Peter J. Gollan*† *and Eva-Mari Aro*

Molecular Plant Biology, Department of Biochemistry, University of Turku, Turku, Finland

Edited by:
Suleyman I. Allakhverdiev, Russian Academy of Sciences, Russia

Reviewed by:
Suleyman I. Allakhverdiev, Russian Academy of Sciences, Russia
Peter Horton, University of Sheffield, UK

***Correspondence:**
Eva-Mari Aro, Molecular Plant Biology, Department of Biochemistry, University of Turku, FIN-20014 Turku, Finland
e-mail: evaaro@utu.fi

†*Sari Järvi and Peter J. Gollan have contributed equally to this work.*

It has been known for a long time that the thylakoid lumen provides the environment for oxygen evolution, plastocyanin-mediated electron transfer, and photoprotection. More recently lumenal proteins have been revealed to play roles in numerous processes, most often linked with regulating thylakoid biogenesis and the activity and turnover of photosynthetic protein complexes, especially the photosystem II and NAD(P)H dehydrogenase-like complexes. Still, the functions of the majority of lumenal proteins in *Arabidopsis thaliana* are unknown. Interestingly, while the thylakoid lumen proteome of at least 80 proteins contains several large protein families, individual members of many protein families have highly divergent roles. This is indicative of evolutionary pressure leading to neofunctionalization of lumenal proteins, emphasizing the important role of the thylakoid lumen for photosynthetic electron transfer and ultimately for plant fitness. Furthermore, the involvement of anterograde and retrograde signaling networks that regulate the expression and activity of lumen proteins is increasingly pertinent. Recent studies have also highlighted the importance of thiol/disulfide modulation in controlling the functions of many lumenal proteins and photosynthetic regulation pathways.

Keywords: NAD(P)H dehydrogenase, photosystem, proteome, thioredoxin, thylakoid lumen

INTRODUCTION

Photosystem (PS)I, PSII, and the light harvesting complexes (LHCI and LHCII), in concert with the cytochrome (cyt) b_6f, ATP synthase, and the NAD(P)H dehydrogenase-like (NDH) are responsible for light harvesting and transduction of solar energy into chemical energy via photosynthetic electron transport (PET). These multi-subunit pigment–protein complexes are embedded in the highly folded thylakoid membrane, which encloses a continuous internal compartment known as the thylakoid lumen. The linear electron transport (LET) chain represents the predominant pathway of PET. Three major thylakoid membrane protein complexes – PSII, cyt b_6f, and PSI – cooperate in LET in order to transport electrons from water molecules to oxidized nicotinamide adenine dinucleotide phosphate ($NADP^+$). Photosynthetic water-splitting occurs at the lumenal side of PSII at the oxygen-evolving complex (OEC). Hydrogen ions accumulating in the lumen as a result of water-splitting and cyt b_6f activity generate the proton motive force (*pmf*) that drives ATP synthesis. Lumenal proton concentration is also an important regulator of PET, triggering non-photochemical quenching (NPQ) of harvested energy and slowing down electron transfer in the cyt b_6f complex under acidic lumenal conditions. While LET generates both NADPH and ATP, cyclic electron transport (CET) around PSI produces *pmf* and thus ATP without reducing $NADP^+$ (Heber and Walker, 1992). To that end, the main role of PSI CET is to balance the production of ATP and NADPH according to metabolic needs and to alleviate stromal over-reduction (Shikanai, 2007).

Although the photosynthetic apparatus and light-driven electron transport have been studied extensively, there remains a great deal to learn about factors that regulate PET according to the energy requirements of metabolic pathways and environmental cues. Recent characterizations of thylakoid lumen proteomes and analyses of the component proteins have revealed a range of novel proteins and protein families. Furthermore, the details of recent studies show that the lumen holds key factors for regulation and repair of the photosynthetic membrane, facilitating PET flexibility that is vital for efficient energy conversion. Here we review the current understanding of the functions of thylakoid lumen proteins in LET, CET, and PSII repair, and explore factors that regulate their expression, translocation, and activity (**Figure 1**; **Table 1**). Although uncharacterized lumen proteins have mainly been excluded from this review, their roles in PET regulation, retrograde signaling and/or acclimation are also likely to be vital for plant growth and development.

DISTINCTIVE FEATURES OF THYLAKOID LUMEN

A decade ago, the thylakoid lumen was believed to be largely devoid of proteins, containing only the OEC proteins, the electron carrier plastocyanin (PC) and violaxanthin de-epoxidase (VDE). Proteomic and genomic studies have now revealed up to 80 proteins in *Arabidopsis thaliana* (*Arabidopsis*) to be localized in this compartment (Peltier et al., 2002; Schubert et al., 2002; Kieselbach and Schroder, 2003). All characterized lumenal proteins in *Arabidopsis* (**Table 1**) are nuclear-encoded and post-translationally transported into the chloroplast by the TOC/TIC (translocon at the outer/inner envelope of chloroplasts) system (Soll and Schleiff, 2004), while the secretory (Sec) and twin-arginine translocation (Tat) pathways import proteins into the lumen (discussed below; Albiniak et al., 2012). The thylakoid lumen is a constricted and crowded environment in which protein mobility is largely

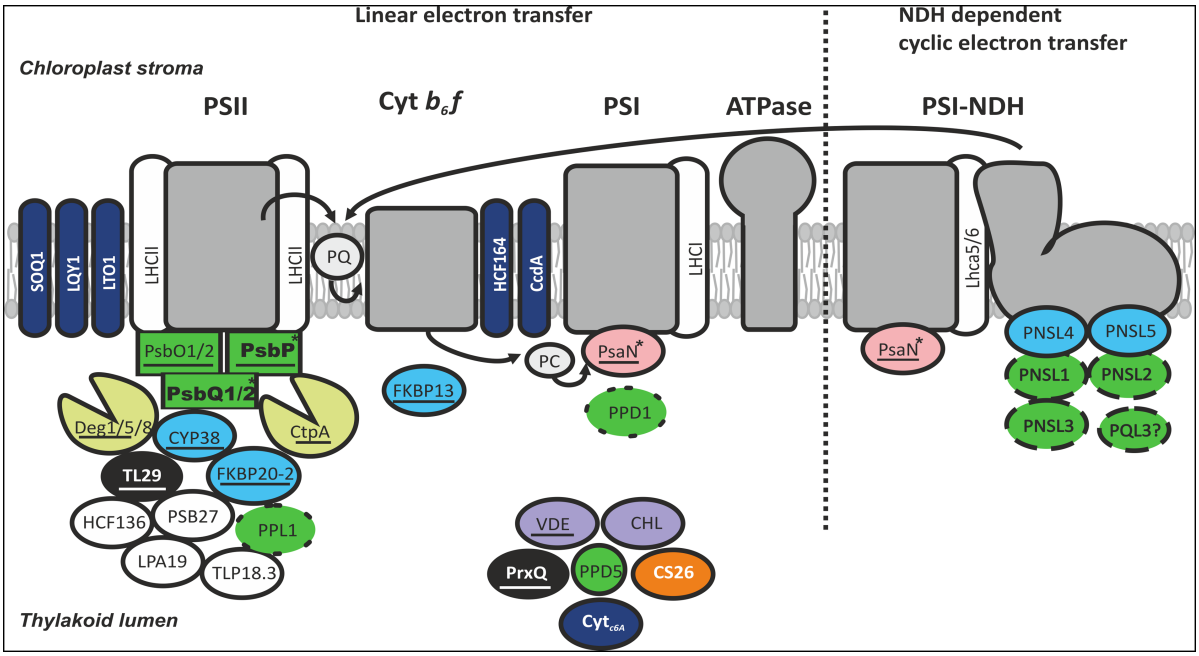

FIGURE 1 | The majority of thylakoid lumen proteins with experimentally verified roles are involved in the function of either the PSII complex or the PSI–NDH supercomplex. The most abundant protein families in the thylakoid lumen are the OEC and OEC-like proteins (green), the immunophilins (blue), and proteases (yellow). In addition, the lumen proteome comprises peroxidases (black), photoprotective enzymes (purple), and several auxiliary proteins. The OEC proteins are proposed to function in water oxidation (square boxes), granal stacking (bolded), photosystem assembly (dotted outline), strigolactone biosynthesis (circle box), and NDH-dependent cyclic electron transfer (dashed outline). A high proportion of lumen proteins are thioredoxin targets (underlined). Regulation of thylakoid redox reactions involves membrane-embedded and soluble proteins (dark blue), and other lumen proteins are also implicated (white typeface). Lumen proteins with phosphorylation sites (asterisked) may be regulated by TLP18.3 phosphatase. Based on current knowledge, verified components of lumenal NDH subcomplex are not under post-translational regulation. No characterized lumenal proteins have so far been linked to the function of ATP synthase.

restricted; however, the dimensions of the thylakoid lumen are quite flexible (Mullineaux, 2008). Expansion of the lumenal space occurring in high light is linked to light-induced decrease in pH from around 7.0 in darkness to 5.8 and 6.5 in the light (Kramer et al., 1999; Cruz et al., 2001; Tikhonov, 2013) due the concomitant influx of anions upon acidification (Kirchhoff et al., 2011). The increase in lumenal space under light conditions is thought to allow protein diffusion that is important for PSII maintenance during photosynthetic activity (Kirchhoff et al., 2011). The lumenal pH controls the activities of many lumenal proteins, effectively functioning as a light-sensing on/off switch (discussed below).

PHOTOSYNTHETIC ELECTRON TRANSFER FROM A LUMENAL PERSPECTIVE

WATER-SPLITTING

The OEC contains a Mn_4O_5Ca cluster that operates in water oxidation at the lumenal side of PSII. After storing four positive charges as a result of four successive electron transfer steps, the OEC oxidizes two water molecules and releases one oxygen molecule and four protons to the thylakoid lumen. Hence the OEC both liberates electrons for the electron transport chain and participates in acidification of the lumen. The OEC is supported by an extrinsic lumen protein complex, which reversibly associates with intrinsic PSII proteins. The OEC proteins are PsbO (also called OEC33), which is located proximal to the Mn_4O_5Ca cluster, PsbP (OEC23) and PsbQ (OEC17; Bricker et al., 2012). In *Arabidopsis* each OEC protein is encoded by two duplicate genes. The PsbO1 isoform exhibits higher oxygen-evolving activity than PsbO2 and accounts for around 90% of the total PsbO in WT plants (Murakami et al., 2005). PsbQ1 differs from PsbQ2 in a phosphorylatable serine residue that occurs in the latter (Reiland et al., 2009), while the PsbP1 is the major isoform of PsbP in the Columbia-0 ecotype since the *PSBP2* gene contains a frameshift that leads to truncated PsbP2 protein that is probably excluded from the thylakoids (Ifuku et al., 2008).

All three OEC proteins are required for maximal oxygen evolution, most likely because they sequester Cl^- and Ca^{2+} ions required for water-splitting (Miqyass et al., 2007; Popelkova and Yocum, 2007). Additionally, each of the OEC proteins appears to have a unique role in the integrity of PSII complexes. PsbQ is important for PSII stability, particularly under low light (Yi et al., 2006), while PsbP is required for assembly and/or stability of PSII and formation of PSII–LHCII supercomplexes (Yi et al., 2007; Ido et al., 2009). PsbQ stabilizes the interaction between PsbP and the membrane-bound PSII subunit PsbR (Suorsa et al., 2006; Allahverdiyeva et al., 2013). These results suggest that PsbP and PsbQ may coordinate the removal and/or reintegration of the Mn_4O_5Ca cluster with the disassembly and/or reassembly of PSII complexes during the PSII repair cycle (De Las Rivas et al., 2007).

Table 1 | Summary of characterized thylakoid lumen proteins in *Arabidopsis*.

Name	Gene code	Protein family/domain	Function/pathway	Signal peptide	Network	TRX target	Phosphorylation site	Reference
PSII								
PsbO1	At5g66570	OEC	Subunit of PSII OEC	Sec	C	Yes	–	Murakami et al. (2005)
PsbO2	At3g50820	OEC	Subunit of PSII OEC	Sec	C	Yes	–	Murakami et al. (2005)
PsbP1	At1g06680	OEC	Subunit of PSII OEC	Tat	C	Yes	Yes	Yi et al. (2007), Ifuku et al. (2008)
PsbQ1	At4g21280	OEC	Subunit of PSII OEC	Tat	C	–	–	Yi et al. (2006)
PsbQ2	At4g05180	OEC	Subunit of PSII OEC	Tat	C	–	Yes	Yi et al. (2006)
PSB27	At1g03600	PSB27	D1 processing	Tat	C	–	–	Chen et al. (2006)
LPA19	At1g05385	PSB27	D1 processing	Tat	–	–	–	Wei et al. (2010)
TLP18.3	At1g54780	Acid phosphatase	Degradation of D1, dimerization of PSII	Sec	C	–	–	Sirpio et al. (2007), Wu et al. (2011)
TL29/APX4	At4g09010	Peroxidase-like	Associated with PSII	Tat	C	Yes	–	Granlund et al. (2009b), Lundberg et al. (2011)
HCF136	At5g23120	–	Assembly of PSII	Tat	R	–	–	Meurer et al. (1998), Plucken et al. (2002)
CYP38	At3g01480	PPIase	Assembly of PSII	Sec	R	Yes	–	Fu et al. (2007), Sirpio et al. (2008), Vasudevan et al. (2012)
FKBP20-2	At3g60370	PPIase	Assembly of PSII	Tat	R	Yes	–	Lima et al. (2006)
PPL1	At3g55330	OEC, PsbP-like	Assembly of OEC	Tat	R	–	–	Ishihara et al. (2007)
CtpA	At5g46390	Peptidase	Processing of D1	Sec	R	Yes	–	Anbudurai et al. (1994)
CtpA	At4g17740	Peptidase	Processing of D1	Sec	R	Yes	–	Anbudurai et al. (1994)
CtpA	At3g57680	Peptidase	Processing of D1	No	–	–	–	Yin et al. (2008)
Deg1	At3g27925	Protease	Degradation of D1	Sec	R	Yes	–	Kapri-Pardes et al. (2007), Sun et al. (2007), Kley et al. (2011)
Deg5	At4g18370	Protease	Degradation of D1	Tat	–	Yes	–	Sun et al. (2007)
Deg8	At5g39830	Protease	Degradation of D1	Tat	R	–	–	Sun et al. (2007)
PSI								
PsaN	At5g64040	PSI	Subunit of PSI	Tat	C	Yes	Yes	Haldrup et al. (1999)
PPD1	At4g15510	OEC, PsbP-like	Assembly of PSI	Tat	R	–	–	Liu et al. (2012)

(Continued)

Table 1 | Continued

Name	Gene code	Protein family/domain	Function/pathway	Signal peptide	Network	TRX target	Phosphorylation site	Reference
Cyt b6f								
FKBP13	At5g45680	PPIase	Assembly of cyt b6f	Tat	R	Yes	–	Gupta et al. (2002a), Gollan et al. (2011)
NDH								
PNSL1/PPL2	At2g39470	OEC, PsbP-like	Subunit of NDH	Tat	R	–	–	Ishihara et al. (2007)
PNSL2	At1g14150	OEC, PsbQ-like	Subunit of NDH	Tat	R	–	–	Suorsa et al. (2010), Yabuta et al. (2010)
PNSL3	At3g01440	OEC, PsbQ-like	Subunit of NDH	Tat	R	–	–	Suorsa et al. (2010), Yabuta et al. (2010)
PNSL4/FKBP16-2	At4g39710	PPIase	Subunit of NDH	Tat	R	–	–	Peng et al. (2009)
PNSL5/CYP20-2	At5g13120	PPIase	Subunit of NDH	Sec	–	–	–	Romano et al. (2004a), Shapiguzov et al. (2006), Peng et al. (2009), Sirpio et al. (2009)
PQL3	At2g01918	OEC, PsbQ-like	Subunit of NDH	Tat	–	–	–	Yabuta et al. (2010)
Photoprotection								
VDE	At1g08550	VDE, lipocalin	Xanthophyll cycle enzyme	Sec	–	Yes	–	Niyogi et al. (1998), Arnoux et al. (2009)
CHL	At3g47860	Lipocalin	Prevent lipid peroxidation	Sec	–	–	–	Levesque-Tremblay et al. (2009)
Others								
PETE2	At1g20340	Plastocyanin	Electron transport	Sec	C	–	–	Weigel et al. (2003), Pesaresi et al. (2009b)
PETE1	At1g76100	Plastocyanin	Electron transport	Sec	C	–	–	Weigel et al. (2003), Pesaresi et al. (2009b)
PRXQ	At3g26060	PRXQ-like	Antioxidant? Signaling?	No	–	Yes	–	Petersson et al. (2006)
PPD5	At5g11450	OEC, PsbP-like	Strigolactone biosynthesis	Tat	R	–	–	Roose et al. (2011)
Cyt c_{6A}	At5g45040	Dithio-cytochrome	Oxidizing lumenal proteins	Sec	–	–	–	Gupta et al. (2002b), Weigel et al. (2003), Pesaresi et al. (2009b)
CS26	At3g03630	Cysteine synthase	*S*-sulfocysteine synthase	No	–	–	–	Bermudez et al. (2010), Bermudez et al. (2012)

Thylakoid lumen proteome in Arabidopsis comprises of about 80 proteins of which half has a functionally verified role. Network based on Ifuku et al. (2010). R, regulatory protein; C, constitutively expressed protein. TRX target proteins based on Lindahl and Kieselbach (2009) and Hall et al. (2010).

In addition, PsbP and PsbQ are linked to granal stacking (Dekker and Boekema, 2005), but evidence regarding the specific role of PsbQ in thylakoid architecture is contradictory (Yi et al., 2009). PsbO has been described as a GTPase that regulates PSII repair (Spetea et al., 2004; Lundin et al., 2007) and as a carbonic anhydrase (Lu et al., 2005), and has also demonstrated Ca^{2+} ion-binding activity (Heredia and De Las Rivas, 2003; Murray and Barber, 2006), although all of these features of PsbO are somewhat contentious and remain to be unequivocally demonstrated.

THE Q CYCLE AND cyt b_6f

Part of electrons from PSII is shuttled to cyt b_6f via the so-called "Q cycle," which involves successive reduction and oxidation of the membrane-soluble electron- and proton-carrier plastoquinone (PQ). Each Q cycle pumps two protons from the stroma to the lumen, coupling the pH of the lumen to PET activity (Tikhonov, 2013). A subunit of the cyt b_6f complex known as the Rieske protein has a lumenal [2Fe-2S] cluster-binding domain that operates in electron transfer between cyt b_6 and cyt *f*. Rieske interacts with the lumenal immunophilin FKBP13 (Gupta et al., 2002a; Gollan et al., 2011), which was thought to regulate the assembly of the cyt b_6f complex from the stromal side (Gupta et al., 2002a), although recent results suggest that the FKBP13–Rieske interaction occurs in the thylakoid lumen (Gollan et al., 2011). The chaperone activity of FKBP13 is sensitive to redox regulation, as discussed below.

PLASTOCYANIN AND PSI

Electron transfer from cyt b_6f to PSI takes place in the lumen, and yet few lumen proteins appear to be directly involved. The major lumenal electron carrier is the copper-containing protein PC, comprising two isoforms in *Arabidopsis* that are encoded by the *PETE1* and *PETE2* genes, of which the latter is more highly expressed (Pesaresi et al., 2009b). A cyt *c* protein that operates as an alternative electron donor for PSI in cyanobacteria and green algae also occurs in the *Arabidopsis* thylakoid lumen (cyt c_{6A}), where it has been suggested to have a similar function (Gupta et al., 2002b); however, strong evidence suggests this is not the case in *Arabidopsis* (Weigel et al., 2003; Pesaresi et al., 2009b). PsaN is the only lumenal subunit of PSI (Kieselbach and Schroder, 2003). Mutants lacking PsaN are capable of assembling functional PSI complexes and growing photoautotrophically; however, restricted electron flow between PSII and PSI in mutant plants show that PsaN is necessary for efficient interaction between PSI and PC (Haldrup et al., 1999).

CYCLIC ELECTRON TRANSFER

In PSI CET, electrons are directed from ferredoxin (Fd) back into the Q cycle rather than to $NADP^+$. The commonly accepted role of CET is in adjusting stromal ATP:NADPH ratios in response to metabolic requirements; however, CET also operates to maintain the low lumenal pH required for NPQ and photosynthetic control of cyt b_6f to protect both PSII and PSI, particularly under conditions where PSII is disengaged or inhibited (Kramer et al., 2004; Munekage et al., 2004; Joliot and Johnson, 2011). PSI CET proceeds by two partially redundant pathways; the major route is dependent on proton gradient regulation (PGR) proteins (Munekage et al., 2002; Okegawa et al., 2007) and the formation of a multi-protein CET supercomplex (DalCorso et al., 2008; Iwai et al., 2010), although some of the components remain to be discovered.

The second, minor route for PSI CET involves the membrane-intrinsic NADPH dehydrogenase-like (NDH) complex, which also forms a CET-specific supercomplex through association with PSI (Rumeau et al., 2007; Peng et al., 2009). Based on the structural similarities with mitochondrial complex I of the respiratory chain (Friedrich and Weiss, 1997), which oxidizes NADH and reduces ubiquinone in a process that is coupled to proton translocation across the mitochondrial inner membrane, the NDH-like complex is proposed to play a similar role in the thylakoid membrane. However, the physiological relevance, functional mechanism, and regulation of the chloroplast NDH-like complex have not been fully elucidated (Shikanai, 2007; Yamamoto et al., 2011), partly due to the fact that the abundance of NDH-like complexes in the thylakoid membrane is very low (Sazanov et al., 1998). Nevertheless, the complex is known to be stable only when associated with at least two copies of PSI, and the role of NDH in PSI CET and chlororespiration has been established (Peng and Shikanai, 2011).

The NDH-like complex is composed of at least 30 subunits and auxiliary proteins (Ifuku et al., 2011), and thus the PSI–NDH supercomplex is among the largest protein complexes in the thylakoid membrane. The subunits of NDH include both nuclear-encoded and plastid-encoded proteins, indicating strict control of expression, protein import and assembly processes. Based on characterization of *ndh* mutant *Arabidopsis* lines, the chloroplast NDH is postulated to comprise four subcomplexes, known as "A," "B," "membrane," and "lumen" subcomplexes (Ifuku et al., 2011), although detailed structural data for any of these is currently missing. The higher plant NDH is closely related to its cyanobacterial counterpart, with the major differences being the lumenal subcomplex and some auxiliary proteins that are characteristic to plant NDH (Peng et al., 2009; Battchikova et al., 2011).

The lumenal subcomplex, which is vital for stability of subcomplex A, comprises a PsbP homolog (PPL2, also called PNSL1), a PsbQ homolog (PNSL2), and immunophilins FKBP16-2 (PNSL4) and CYP20-2 (PNSL5; Peng et al., 2009; Sirpio et al., 2009; Suorsa et al., 2010; Yabuta et al., 2010). Of these PNSL5/CYP20-2 is the sole contributor to cyclophilins (CYP)-mediated lumenal PPIase activity (Shapiguzov et al., 2006) and was initially found to co-migrate with LHCII (Romano et al., 2004a). Incorporation of subcomplex A into the thylakoid membrane is one of the final steps in formation of functional NDH, and it may be a reversible one that can disengage CET or accommodate NDH repair (Peng and Shikanai, 2011). It seems plausible that the lumenal subcomplex could regulate the assembly and/or (more likely) disassembly of NDH according to the conditions in the thylakoid lumen.

THE PSII ASSEMBLY AND REPAIR INVOLVE A LARGE ARRAY OF LUMENAL PROTEINS

Photosystem II biogenesis shares many components with the repair cycle occurring after photoinhibition of PSII. The D1 protein in the PSII reaction center is the major target of irreversible photodamage during photosynthesis under high light, leading to NPQ by photoinhibition-related quenching (qI); however, balanced damage and repair of PSII have been shown to occur

at all light intensities (Tyystjärvi and Aro, 1996). Replacement of damaged D1 requires disassembly of PSII–LHCII complexes, PSII migration from crowded grana thylakoids to the stromal lamellae, D1 removal and replacement, reassembly and finally relocation of functional PSII (Baena-González and Aro, 2002). The lumenal components of PSII biogenesis/repair cycle are discussed below.

Degradation of the damaged D1 protein, carried out primarily by thylakoid-associated FtsH proteases, occurs in cooperation with the lumenal Deg1, Deg5, and Deg8 proteases (Kato et al., 2012). Deg1 is activated by homo-hexamerization in response to pH changes in the lumen (Kley et al., 2011), and interaction between Deg5 and Deg8 to form an active protease complex may also be pH-dependent (Sun et al., 2007). While activated, Deg proteases specifically degrade lumen-exposed loops of D1 (Kapri-Pardes et al., 2007; Sun et al., 2007). Deg1 has proteolytic activity against other lumenal proteins *in vitro*, including PC and PsbO, suggesting it may operate as a general protease in the thylakoid lumen (Chassin et al., 2002). In addition to proteolytic activity, Deg1 assists PSII assembly through interaction with the reaction center protein D2 (Sun et al., 2010b). Interestingly, the thylakoid lumen acidic phosphatase TLP18.3 is also involved in the degradation of D1 protein, but also in dimerization of PSII (Sirpio et al., 2007; Wu et al., 2011). Interaction between TLP18.3 and Deg1 (Zienkiewicz et al., 2012) might regulate the protease through dephosphorylation (Spetea and Lundin, 2012). The D1 protein is the primary target of photodamage, but other PSII core proteins are also damaged and degraded, particularly in response to environmental stresses. Stromal Deg7 has been shown to be involved in the proteolysis of photodamaged D1, D2, CP47, and CP43 (Sun et al., 2010a), while stromal FtsH proteases and lumenal Deg1 mediate the degradation of LHCII proteins (Zienkiewicz et al., 2012; Luciński and Jackowski, 2013).

Newly synthesized D1 protein is co-translationally inserted into the thylakoid membrane and the core complex. The latter step is assisted by two lumenal proteins, immunophilin CYP38 and "high chlorophyll fluorescence 136" (HCF136), both of which are present already in the proteome of pre-chloroplastic etioplasts, presumably for prompt D1 assembly during thylakoid biogenesis (Meurer et al., 1998; Kanervo et al., 2008). The HCF136 protein is a prerequisite for the assembly of PSII reaction centers during complex biogenesis, while CYP38 assists the assembly of PSII core complexes during both biogenesis and repair (Meurer et al., 1998; Plucken et al., 2002; Fu et al., 2007; Sirpio et al., 2008). The C-terminal CYP-like domain of CYP38 interacts with the PSII apoprotein, CP47 (Vasudevan et al., 2012). Thus, CYP38 might assist the correct folding and integration of CP47 into the PSII core. An additional role for CYP38 may lie in the regulation of correct conformation of D1 and possibly also CP43 during PSII biogenesis and/or repair and as a negative regulator of the thylakoid protein phosphatase that dephosphorylates PSII core proteins (Fulgosi et al., 1998; Vener et al., 1999; Rokka et al., 2000; Fu et al., 2007; Sirpio et al., 2008). The lumenal immunophilin FKBP20-2 also has a role in PSII complex assembly by a yet unknown mechanism (Lima et al., 2006).

Processing of precursor D1 protein to the mature form by the C-terminal processing protease CtpA (Anbudurai et al., 1994; Yamamoto et al., 2001) is required for integration of the OEC complex to PSII (Roose and Pakrasi, 2004). The lumen proteome of *Arabidopsis* includes three CtpA homologs. Mutation in one of these genes (At3g57680) does not affect accumulation of the D1 precursor suggesting that there may be functional redundancy between the CtpA homologs (Yin et al., 2008). The lumenal homologs Psb27 and "low PSII accumulation 19" (LPA19) interact with the newly inserted D1 precursor and are involved in processing of nascent D1 during PSII biogenesis in *Arabidopsis* (Chen et al., 2006; Wei et al., 2010). The Psb27 homolog in cyanobacteria interacts with PSII to prevent premature assembly of the Mn_4O_5Ca cluster at the lumenal side of PSII (Roose and Pakrasi, 2008), suggesting that the timing of D1 maturation is important in the PSII assembly. The importance of a PsbP homolog PPL1 for the PSII repair cycle was shown by the slow recovery of PSII from photoinhibition in *ppl1* plants (Ishihara et al., 2007). Finally, the lumenal ascorbate peroxidase APX4/TL29 has been described as a lumen-located component and/or auxiliary protein of PSII (Granlund et al., 2009b), although according to its crystal structure its function is unlikely to involve peroxidase activity (Lundberg et al., 2011).

PSI ASSEMBLY IS DEPENDENT ON LUMENAL PsbP-LIKE PROTEIN PPD1

Compared to PSII, PSI is much more tolerant to, and/or very well protected from photoinhibition, as PSI photodamage exists *in vivo* only under specific conditions such as chilling temperature (Zhang and Scheller, 2004) or in the deficiency of PGR-dependent CET (Suorsa et al., 2012a,b). So far only one lumenal protein assisting PSI biogenesis, namely the PsbP-like protein PPD1, has been identified. PPD1 interacts directly with PSI reaction center proteins PsaA and PsaB and assists the folding and insertion of these two proteins into the thylakoid membrane (Liu et al., 2012). A lack of PPD1 leads to the loss of PSI and an inability to grow photoautotrophically (Liu et al., 2012).

PHOTOPROTECTION COMPONENTS IN THE THYLAKOID LUMEN

In naturally fluctuating light conditions, the energy harvested by LHCII can become unbalanced in relation to the capacity of stromal acceptors, thus saturating the electron transport chain and generating reactive oxygen species (ROS) that cause photodamage of membrane proteins (Nishiyama et al., 2006; Murata et al., 2007). In order to protect the photosynthetic machinery amidst natural light conditions, plants use energy dissipation mechanisms (NPQ) that are partially located in the thylakoid lumen (Niyogi et al., 1998).

NON-PHOTOCHEMICAL QUENCHING

The major NPQ mechanism (qE) is rapid and reversible, involving dissipation of absorbed light energy as heat. This is predominantly achieved through production of the carotenoid zeaxanthin and reorganization of LHCII, both processes that are triggered by acidification of the thylakoid lumen. Upon protonation, lumenal VDE converts from a monomer to a dimer, opening access to the active site that facilitates the conversion of violaxanthin to zeaxanthin (Arnoux et al., 2009). Protonation of the PSII protein PsbS causes a structural rearrangement of PSII–LHCII supercomplexes

(Li et al., 2000, 2004; Kereïche et al., 2010), although the exact role of PsbS in qE remains to be defined (Johnson and Ruban, 2011).

LUMEN RESPONSE TO OXIDATIVE STRESS

Cysteine synthesis 26 (CS26) is an *S*-sulfocysteine synthase and occurs in low abundance in the thylakoid lumen, but it has a vital role in detection of lumenal redox conditions, particularly in long photoperiods (Pesaresi et al., 2009a; Bermudez et al., 2010, 2012). A lack of CS26 led to strong photoinhibition and a systemic ROS response that was accompanied by reduced levels of OEC proteins and PSII assembly factors (Bermudez et al., 2012). CS26 was recently proposed as a ROS sensor through its sensitivity to thiosulfate accumulation in the lumen (Gotor and Romero, 2013). The "chloroplastic lipocalin" (CHL) is involved in photoprotection of thylakoid membrane lipids. CHL accumulates in the thylakoid lumen during environmental stress conditions such as drought and high light, as well as in paraquat and abscisic acid treatments, to protect the thylakoid membrane from peroxidation (Levesque-Tremblay et al., 2009).

LUMEN PROTEIN FAMILIES

DIVERSE ROLES OF THE PsbP-LIKE AND PsbQ-LIKE PROTEINS

The PsbP family has at least ten members in the *Arabidopsis* thylakoid lumen (Hall et al., 2010; Sato, 2010). Aside from the OEC protein PsbP, these are PPL1 and PPL2, involved in PSII repair and NDH stability, respectively (discussed above), and at least seven "PsbP domain" proteins (PPD1–7). An eighth (PPD8) is encoded, but has not been detected at the protein level. The role of PPD1 in PSI assembly has been discussed above, but the specific activities of other PPDs in the lumen remain a mystery in many respects. A homolog of PPD2 in the green alga *Chlamydomonas reinhardtii* is implicated in the generation of singlet oxygen signals (Brzezowski et al., 2012) and PPD5 knockout in *Arabidopsis* led to a reduction in NDH activity and is linked to production of the carotenoid-derived hormone strigolactone (Roose et al., 2011).

Similarly, multiple PsbQ-like proteins occur in the *Arabidopsis* lumen. PQL1 and PQL2 are lumenal subunits of NDH (see above), while a third (PQL3) is also required for NDH function, but has not been found in the proteome (Yabuta et al., 2010). The cyanobacterial ancestors of plant PsbP and PsbQ domains, called "cyanoP" and "cyanoQ," respectively, are involved in PSII oxygen evolution, but may have more of an auxiliary role in regulation of OEC structure and assembly. Notably, cyanoP is considerably more closely related, at least in sequence and structure, to PPL1 than to PsbP in plants (Sato, 2010; Jackson et al., 2012). Considering the few details about the PsbP- and PsbQ-like proteins known so far, it is tempting to speculate that expansion of these families in the lumen has provided opportunities for regulating the lumen-exposed parts of various photosynthetic complexes.

LUMENAL IMMUNOPHILINS REGULATE THE ASSEMBLY, MAINTENANCE, AND TURNOVER OF THYLAKOID MEMBRANE PROTEIN COMPLEXES

The immunophilins include two unrelated protein families, the CYP and the FK506-binding proteins (FKBP), both of which are abundant in the thylakoid lumen proteome (He et al., 2004). Immunophilins are well known for their ability to rotate the peptide bond of a proline residue, known as PPIase activity, which has been linked to protein folding; however, a majority of the lumenal immunophilins does not show PPIase activity against synthetic peptides (Shapiguzov et al., 2006; Edvardsson et al., 2007). The best characterized of the lumen immunophilins is CYP38, which has an atypical CYP domain in the C-terminus and an N-terminal helical bundle, possibly for autoinhibition (Vasudevan et al., 2012). CYP38 does not show PPIase activity, but has a vital role in the assembly of PSII (Fu et al., 2007; Sirpio et al., 2008). Contrary to earlier observations (He et al., 2004; Romano et al., 2004b; Sirpio et al., 2008), CYP38 in *Arabidopsis* lacks a leucine zipper domain due to a frameshift in the coding sequence. The spinach ortholog of CYP38, called "thylakoid lumen PPIase of 40 kDa" (TLP40; 82% sequence identity to CYP38) is likely to possess a similar functional role to CYP38, but appears to behave differently to its *Arabidopsis* counterpart in that TLP40 has PPIase activity *in vitro* (Fulgosi et al., 1998; Vener et al., 1999). FKBP20-2 was also implicated in PSII assembly based on the observed increase of unassembled PSII monomers and dimers in the *fkbp20-2* knockout, suggesting a role in formation of PSII supercomplexes (Lima et al., 2006). As discussed earlier, FKBP16-2 and CYP20-2 take part in the lumenal NDH subcomplex (Peng et al., 2009), while another immunophilin, FKBP13, is linked to cyt b_6f regulation through interaction with Rieske (Gupta et al., 2002a; Gollan et al., 2011). In wheat, FKBP16-1 and FKBP16-3 may have a role in development of photosynthetic membranes through their interaction partners, the PsaL subunit of PSI and "thylakoid formation-1" (THF1, also called PSB29), respectively (Gollan et al., 2011).

The roles of most lumenal immunophilins remain unclear, although accumulating evidence indicates a primary role in the assembly and/or turnover of photosynthetic complexes. FKBP16-2, FKBP16-4, and CYP37 have been found both in the membrane-bound and lumen-soluble thylakoid proteomes (Peltier et al., 2002; Friso et al., 2004), suggesting that they may be involved in recruitment of lumen proteins to the membrane.

PENTAPEPTIDE REPEAT PROTEINS IN THYLAKOID LUMEN HAVE UNKNOWN FUNCTION

A lumenal pentapeptide repeat-containing (PPR) family has three members; TL15, TL17, and TL20.3 (Schubert et al., 2002; Hall et al., 2010). The lumenal pentapeptide proteins TL15 and TL17 in *Arabidopsis* increase in abundance upon light adaptation (Granlund et al., 2009a) and are, together with TL20.3, putative targets of thioredoxin (TRX) reduction (Hall et al., 2010). In line with this, the crystal structure of TL15 has revealed an internal disulfide bridge (Ni et al., 2011). Cyanobacterial PPRs have diverse roles, two of which may be relevant in the thylakoid lumen; regulation of light-induced manganese ion import (Chandler et al., 2003) and galactolipid translocation (Black et al., 1995).

POST-TRANSLATIONAL MODIFICATIONS OF LUMEN PROTEINS

REGULATION OF LUMEN PROTEINS BY REVERSIBLE PHOSPHORYLATION

Phosphoproteomics studies have identified several phosphorylated proteins in the thylakoid lumen (**Table 1**), including the

OEC proteins PsbP and PsbQ (Reiland et al., 2009) and lumen-exposed regions of the PSII subunits PsbR and CP47 (Reiland et al., 2009) and the PSI subunits PsaF (Sugiyama et al., 2008) and PsaN (Stael et al., 2012). Phosphorylation of photosynthetic proteins is thought to regulate assembly of the photosynthetic machinery in response to environmental conditions (Reiland et al., 2009). The recent discovery that PsaN phosphorylation is calcium-dependent may link PSI maintenance with dark-induced stromal Ca^{2+} flux (Stael et al., 2012). Despite these results, neither lumenal kinases, nor the physiological significance of phosphorylation events in the lumen have been found, while a single candidate for dephosphorylation activity is the membrane anchored TLP18.3 (Sirpio et al., 2007; Wu et al., 2011), although its substrates are unknown. The existence of any nucleotide-dependent processes in the lumen is contentious (Kieselbach and Schroder, 2003), although accumulating evidence suggests that ATP can be imported to the lumen by a membrane-embedded thylakoid ADP/ATP carrier (TAAC; Thuswaldner et al., 2007), where it is presumed to be available for protein phosphorylation. Recently TAAC was also described as a phosphosulfate channel in the plastid envelope (Gigolashvili et al., 2012). A nucleoside diphosphate kinase 3 (NDK3) found both in the thylakoid lumen and in mitochondria is capable of hydrolyzing ATP to generate GTP thought to be the substrate for GTPase activity of PsbO that is implicated in OEC dissociation for PSII repair cycle (Spetea and Lundin, 2012).

REDOX REGULATION THROUGH DISULFIDE BRIDGE MODULATION

According to current knowledge, more than 40% of the lumen proteome may be regulated by redox reactions through modulation of disulfide bonds that control protein translocation and folding and/or enzyme activation (Hall et al., 2010). This observation places lumenal redox enzymes as powerful regulators of numerous processes. In comparison, less than 10% of stromal proteins are regulated by TRX, although at least 10 TRX isoforms exist in the stroma. Chloroplast redox enzymes have recently been thoroughly reviewed (Lindahl and Kieselbach, 2009; Hall et al., 2010), and will be discussed here only briefly.

The leading candidate for the source of disulfide reduction in the lumen is HCF164, an integral membrane enzyme with a lumenal TRX domain, thought to accept reducing equivalents from stromal TRX via the membrane-localized "cyt *c* defective A" (CcdA; Motohashi and Hisabori, 2006, 2010). HCF164 interacts with cyt *f* and the Rieske iron–sulfur protein and is required for assembly of the cyt b_6f complex (Lennartz et al., 2001), and is also capable of reducing PsaN (Motohashi and Hisabori, 2006). A similarly membrane-embedded TRX-like protein is the "suppressor of quenching 1" (SOQ1), thought to regulate NPQ through a previously uncharacterized pathway (Brooks et al., 2013). "Low quantum yield of photosystem II" (LQY1) is a thylakoid membrane-bound Zn finger protein with protein disulfide isomerase activity that interacts with PSII core complexes to modulate disulfide bond formation in PSII subunits during the PSII repair cycle (Lu et al., 2011). "Peroxiredoxin Q" (PRXQ) generally transfers reductants from TRX to hydrogen peroxide for detoxification; however, lumenal PRXQ does not appear to reduce hydrogen peroxide (Petersson et al., 2006).

Disulfide bond formation in the lumen requires an electron acceptor to oxidize thiol groups, although the mechanism for this is not clear. One prospect is lumenal oxygen that is released by water-splitting reactions (Buchanan and Luan, 2005). In an interesting development of this idea, CS26 was proposed to regulate thiol oxidation by production of *S*-sulfocysteine in the lumen (Bermudez et al., 2012). Another candidate thiol oxidase is the lumenal cyt c_{6A}, which is proposed to shuttle reducing equivalents between thiols and PC (Schlarb-Ridley et al., 2006). Recently the "lumen thiol oxidoreductase 1" (LTO1) protein was found to be a thylakoid membrane-localized enzyme with a lumenal TRX domain that was recently shown to catalyze disulfide bond formation in PsbO *in vitro* (Karamoko et al., 2011).

Although the mechanisms of thiol/disulfide modulation in the lumen remain unclear, important photosynthetic processes are redox-regulated. Disulfide bond formation is important for folding of PsbO1 and PsbO2, which are susceptible to proteolysis in their unfolded state (Hashimoto et al., 1997; Hall et al., 2010; Karamoko et al., 2011). VDE contains disulfides that are vital for its activity in NPQ (Hall et al., 2010). The substrate-binding/PPIase activity of FKBP13 is controlled by two disulfide bridges that can be reduced and oxidized *in vitro* by TRX (Gopalan et al., 2004, 2006) and LTO1 (Lu et al., 2013), respectively. This suggests that the interaction between FKBP13 and the Rieske iron–sulfur protein may be linked to redox state of the thylakoid (Gollan et al., 2011). Furthermore, homology between FKBP13 and FKBP16-2 infers similar redox sensitivity for the assembly of the lumenal NDH subcomplex (Gollan et al., 2012), although these possibilities have not been tested experimentally. The activity of lumen immunophilins FKBP20-2 and CYP38 may also be regulated by disulfide bond modulation (Lima et al., 2006; Fu et al., 2007; Sirpio et al., 2008). Identification of lumen TRX targets indicates that the PSII repair cycle and OEC assembly are under redox control (Hall et al., 2010). Finally, a lumen-exposed disulfide bridge is thought to regulate the activity of the membrane-bound LHCII kinase STN7 (Lemeille et al., 2009), although the redox factors responsible have not been found.

PROTEIN TRANSLOCATION INTO THYLAKOID LUMEN

Four separate methods of protein import into thylakoids are established; the "signal recognition particle-dependent" (SRP) method and the "spontaneous" method insert integral membrane proteins into the thylakoid membrane and are employed by many photosynthetic subunits (Michl et al., 1994; Kim et al., 1999). Lumen proteins are translocated from the chloroplast stroma by either the Sec pathway or the Tat pathway, depending on the signal peptide in the precursor of the passenger protein (Albiniak et al., 2012; **Table 1**).

The Sec system comprises three components; SecA binds the signal peptide in the passenger protein, hydrolyses ATP and threads the unfolded precursor through a fixed channel in the thylakoid membrane comprising SecE and SecY subunits (Yuan et al., 1994; Laidler et al., 1995; Schuenemann et al., 1999). Sec substrates include PsbO, PC, and VDE (Mori et al., 1999).

Unlike the Sec pathway, the Tat pathway operates independently of ATP hydrolysis, instead deriving energy from the *pmf* across the thylakoid membrane. The Tat system comprises three integral

membrane subunits; "high chlorophyll fluorescence 106" (Hcf106) and cpTatC associate together to form a large, hetero-oligomeric complex in the thylakoid membrane, while Tha4 occurs in separate homo-oligomeric complexes. The signal peptides of Tat passengers conserve a central, basic "Arg-Arg" motif that is recognized by the Hcf106–cpTatC receptor complex which, in the presence of suitable *pmf*, then transiently associates with Tha4, which, according to the current model, forms the translocation pore to conduct the passenger protein through a membrane (Albiniak et al., 2012). According to their signal peptides, all PsbP and PsbQ proteins and their homologs in *Arabidopsis* are Tat substrates, as are all lumenal FKBPs (including FKBP16-2; Gollan et al., 2012). A compelling feature of the Tat pathway is its capacity to transport folded proteins and protein–cofactor complexes. In the homologous bacterial Tat system, this is a "quality control" mechanism that ensures proper protein folding and cofactor integration prior to protein export (Hynds et al., 1998; Berks et al., 2000). In plants the Tat pathway could similarly facilitate folding and assembly in the relatively stable environment of the chloroplast stroma to underwrite protein and cofactor integrity in the fluctuating conditions of the lumen (Muller and Klosgen, 2005). Furthermore, thylakoid import of folded proteins could abrogate the need for post-translational modifications such as phosphorylation in the lumen. It should be noted that important details of the Tat pathway in plants remain unclear, including (i) the physical mechanism of translocation, (ii) contributions of the *pmf* components, (iii) involvement of stromal chaperones, and (iv) the conformations, post-translational modifications and complex states of Tat passengers.

RESPONSE OF THE LUMEN PROTEOME TO ENVIRONMENTAL CUES

TRANSCRIPTION REGULATION

The importance of retrograde signals emitted from the chloroplast, and from other sites in the plant cell, in regulating the nuclear expression of photosynthetic proteins is becoming clear (Foyer et al., 2012; Queval and Foyer, 2012). Similar signaling factors are likely to regulate expression of lumenal proteins, which are all encoded in the nucleus (**Table 1**), and yet elucidation of these signals has received little attention. A recent analysis of the expression profiles divided lumen proteins into two networks; a "constitutive factor" group that included predominantly PSI and PSII subunits and few PSII auxiliary proteins, and a "regulatory factor" group containing NDH subunits, as well as several proteins involved in PSII regulation (Ifuku et al., 2010).

ACCLIMATIONS OF THE LUMEN PROTEOME TO LIGHT AND TEMPERATURE

Fifteen thylakoid lumen proteins displayed increased abundance in light-adapted *Arabidopsis* compared to dark-adapted plants indicating that their roles are related to photosynthetic activity (Granlund et al., 2009a). These include OEC proteins PsbP1 and PsbQ2, PSII auxiliary proteins HCF136 and PPL1 as well as major PC (PETE2). Additionally PPD5, two pentapeptide proteins and a group of other functionally uncharacterized thylakoid lumen proteins are up-regulated at the protein level in light compared to darkness (Granlund et al., 2009a). Notably, a majority of the proteins found in higher abundance in the light-adapted lumen are Tat substrates, suggesting that the Tat system may regulate the lumen proteome in response to prevailing light (and other stress) conditions according to the *pmf* that is generated.

Acclimation to low temperature affects the accumulation of eight thylakoid lumen proteins in *Arabidopsis* (Goulas et al., 2006). These include PsbO1/2, PsbP1/2 proteins, HCF136, NDH related immunophilin PNSL5/CYP20-2, and two FKBP proteins. The drastic increase in accumulation of PNSL5/CYP20-2, which occurs concomitantly with down-regulation of the Calvin–Benson cycle enzymes during cold acclimation, might be linked to the activation of NDH-dependent CET under such conditions. However, it should be noted that *Arabidopsis* is a cold-tolerant plant and a different response, e.g., in the accumulation of the NDH-like complex, could be present in rice or other cold-sensitive plant species.

THE IMPORTANCE OF pH AS A REGULATOR OF LUMEN PROTEIN ACTIVITY

Light-induced protonation of the thylakoid lumen contributes the major portion of the *pmf* that drives ATP production; however, the acidic lumen is an important factor in many other processes, as reviewed above (**Figure 2**). Low pH is required to regulate electron transport, through qE activation and photosynthetic control of cyt b_6f (Bratt et al., 1995; Kramer et al., 2004; Li et al., 2004; Joliot and Johnson, 2011). pH-dependent oligomerization of Deg proteases connects thylakoid lumen pH to photoinhibition, recovery and the proteolytic breakdown of other lumenal proteins (Hall et al., 2010). Likewise, OEC is known to become inactivated by pH below 6.0 (Commet et al., 2012). Finally, the light- and dark-induced changes in thylakoid membrane architecture, and the internal dimensions of the thylakoids, are also linked to thylakoid lumen pH (Kirchhoff et al., 2011). The pH of the lumen is determined by the respective rates of electron transfer and ATP synthase activity, and regulation of these processes is used to maintain stromal homeostasis (Kramer et al., 2004; Joliot and Johnson, 2011). It stands to reason that other lumenal activities may also be regulated according to metabolic requirements through controlled changes in thylakoid lumen pH.

CONCLUDING REMARKS

The thylakoid lumen not only provides the environment for oxygen evolution, PC-mediated electron transfer and zeaxanthin formation, but also houses factors that are important for the biogenesis, maintenance and turnover of photosynthetic protein complexes, activity of the NDH-like complex and, based on recent findings, even various signaling cascades. Indeed, most characterized lumenal proteins are linked to the PSII and NDH-like complexes, while only few are associated with PSI or cyt b_6f complexes and none have functions related to ATP synthase (**Figure 1**). A striking feature of the thylakoid lumen proteome is the presence of large protein families such as the OEC-like proteins and immunophilins, suggesting that neofunctionalization of lumenal protein homologs in regulation of photosynthetic complexes has driven the evolution of the lumen proteome. It is evident that lumenal proteins

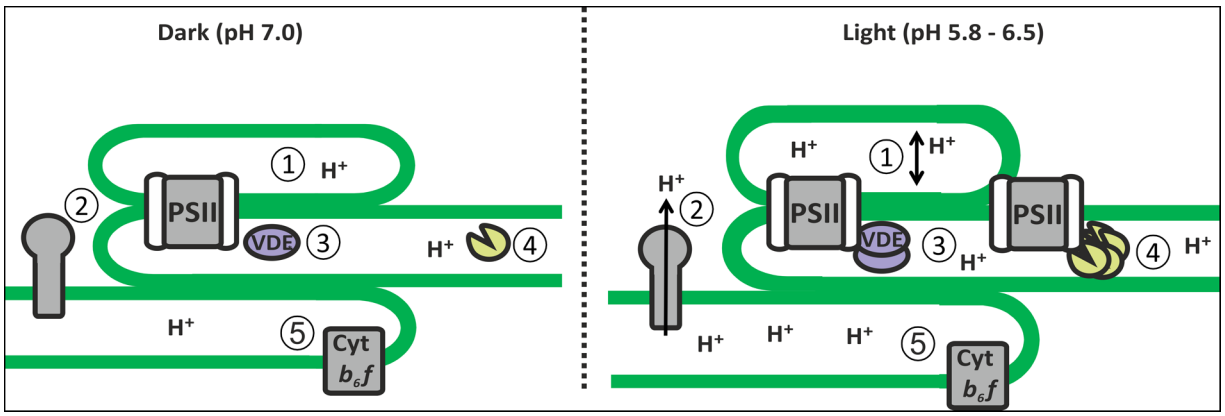

FIGURE 2 | Lumenal processes under pH regulation. (1) Light-induced expansion of the lumen volume facilitating plastocyanin migration and (2) enhancement of ATP synthase activity; (3) Light-induced activation of VDE and PsbS by protonation for photoprotection; (4) Deg oligomerization for PSII repair; and (5) induction of photosynthetic control via cyt b_6f.

are imported, regulated and degraded directly by changes in the lumenal conditions that reflect the metabolic requirements of the plant. Several novel retrograde and anterograde signaling networks regulating expression and activity of lumen proteins according to environmental cues are likely to be revealed during forthcoming years. To that end, the multitude of photosynthetic regulatory proteins located in the thylakoid lumen should be carefully considered when identifying targets for improving photosynthetic reactions through genetic modifications and/or selection.

ACKNOWLEDGMENT

This research was supported by the Academy of Finland project 118637.

REFERENCES

Albiniak, A. M., Baglieri, J., and Robinson, C. (2012). Targeting of lumenal proteins across the thylakoid membrane. *J. Exp. Bot.* 63, 1689–1698. doi: 10.1093/jxb/err444

Allahverdiyeva, Y., Suorsa, M., Rossi, F., Pavesi, A., Kater, M. M., Antonacci, A., et al. (2013). *Arabidopsis* plants lacking PsbQ and PsbR subunits of the oxygen-evolving complex show altered PSII super-complex organization and short-term adaptive mechanisms. *Plant J.* 75, 671–684. doi: 10.1111/tpj.12230

Anbudurai, P. R., Mor, T. S., Ohad, I., Shestakov, S. V., and Pakrasi, H. B. (1994). The ctpA gene encodes the C-terminal processing protease for the D1 protein of the photosystem II reaction center complex. *Proc. Natl. Acad. Sci. U.S.A.* 91, 8082–8086. doi: 10.1073/pnas.91.17.8082

Arnoux, P., Morosinotto, T., Saga, G., Bassi, R., and Pignol, D. (2009). A structural basis for the pH-dependent xanthophyll cycle in *Arabidopsis thaliana*. *Plant Cell* 21, 2036–2044. doi: 10.1105/tpc.109.068007

Baena-González, E., and Aro, E. M. (2002). Biogenesis, assembly and turnover of photosystem II units. *Philos. Trans. R. Soc. Lond. B Biol. Sci.* 357, 1451–1460. doi: 10.1098/rstb.2002.1141

Battchikova, N., Eisenhut, M., and Aro, E. M. (2011). Cyanobacterial NDH-1 complexes: novel insights and remaining puzzles. *Biochim. Biophys. Acta* 1807, 935–944. doi: 10.1016/j.bbabio.2010.10.017

Berks, B. C., Sargent, F., and Palmer, T. (2000). The Tat protein export pathway. *Mol. Microbiol.* 35, 260–274. doi: 10.1046/j.1365-2958.2000.01719.x

Bermudez, M. A., Galmes, J., Moreno, I., Mullineaux, P. M., Gotor, C., and Romero, L. C. (2012). Photosynthetic adaptation to length of day is dependent on *S*-sulfocysteine synthase activity in the thylakoid lumen. *Plant Physiol.* 160, 274–288. doi: 10.1104/pp.112.201491

Bermudez, M. A., Paez-Ochoa, M. A., Gotor, C., and Romero, L. C. (2010). *Arabidopsis S*-sulfocysteine synthase activity is essential for chloroplast function and long-day light-dependent redox control. *Plant Cell* 22, 403–416. doi: 10.1105/tpc.109.071985

Black, K., Buikema, W. J., and Haselkorn, R. (1995). The hglK gene is required for localization of heterocyst-specific glycolipids in the cyanobacterium *Anabaena* sp. strain PCC 7120. *J. Bacteriol.* 177, 6440–6448.

Bratt, C. E., Arvidsson, P., Carlsson, M., and Åkerlund, H. (1995). Regulation of violaxanthin de-epoxidase activity by pH and ascorbate concentration. *Photosynth. Res.* 45, 169–175. doi: 10.1007/BF00032588

Bricker, T. M., Roose, J. L., Fagerlund, R. D., Frankel, L. K., and Eaton-Rye, J. J. (2012). The extrinsic proteins of Photosystem II. *Biochim. Biophys. Acta* 1817, 121–142. doi: 10.1016/j.bbabio.2011.07.006

Brooks, M. D., Sylak-Glassman, E. J., Fleming, G. R., and Niyogi, K. K. (2013). A thioredoxin-like/beta-propeller protein maintains the efficiency of light harvesting in *Arabidopsis*. *Proc. Natl. Acad. Sci. U.S.A.* 110, E2733–E2740. doi: 10.1073/pnas.1305443110

Brzezowski, P., Wilson, K. E., and Gray, G. R. (2012). The PSBP2 protein of *Chlamydomonas reinhardtii* is required for singlet oxygen-dependent signaling. *Planta* 236, 1289–1303. doi: 10.1007/s00425-012-1683-1

Buchanan, B. B., and Luan, S. (2005). Redox regulation in the chloroplast thylakoid lumen: a new frontier in photosynthesis research. *J. Exp. Bot.* 56, 1439–1447. doi: 10.1093/jxb/eri158

Chandler, L. E., Bartsevich, V. V., and Pakrasi, H. B. (2003). Regulation of manganese uptake in *Synechocystis* 6803 by RfrA, a member of a novel family of proteins containing a repeated five-residues domain. *Biochemistry* 42, 5508–5514. doi: 10.1021/bi027113a

Chassin, Y., Kapri-Pardes, E., Sinvany, G., Arad, T., and Adam, Z. (2002). Expression and characterization of the thylakoid lumen protease DegP1 from *Arabidopsis*. *Plant Physiol.* 130, 857–864. doi: 10.1104/pp.007922

Chen, H., Zhang, D., Guo, J., Wu, H., Jin, M., Lu, Q., et al. (2006). A Psb27 homologue in *Arabidopsis thaliana* is required for efficient repair of photodamaged photosystem II. *Plant Mol. Biol.* 61, 567–575. doi: 10.1007/s11103-006-0031-x

Commet, A., Boswell, N., Yocum, C. F., and Popelka, H. (2012). pH optimum of the photosystem II H_2O oxidation reaction: effects of PsbO, the manganese-stabilizing protein, Cl^- retention, and deprotonation of a component required for O_2 evolution activity. *Biochemistry* 51, 3808–3818. doi: 10.1021/bi201678m

Cruz, J. A., Sacksteder, C. A., Kanazawa, A., and Kramer, D. M. (2001). Contribution of electric field ($\Delta\psi$) to steady-state transthylakoid proton motive force (pmf) in vitro and in vivo. Control of pmf parsing into $\Delta\psi$ and ΔpH by ionic strength. *Biochemistry* 40, 1226–1237. doi: 10.1021/bi0018741

DalCorso, G., Pesaresi, P., Masiero, S., Aseeva, E., Schunemann, D., Finazzi, G., et al. (2008). A complex containing PGRL1 and PGR5 is involved in the switch

between linear and cyclic electron flow in *Arabidopsis*. *Cell* 132, 273–285. doi: 10.1016/j.cell.2007.12.028

Dekker, J. P., and Boekema, E. J. (2005). Supramolecular organization of thylakoid membrane proteins in green plants. *Biochim. Biophys. Acta* 1706, 12–39. doi: 10.1016/j.bbabio.2004.09.009

De Las Rivas, J., Heredia, P., and Roman, A. (2007). Oxygen-evolving extrinsic proteins (PsbO, P, Q, R): bioinformatic and functional analysis. *Biochim. Biophys. Acta* 1767, 575–582. doi: 10.1016/j.bbabio.2007.01.018

Edvardsson, A., Shapiguzov, A., Petersson, U. A., Schroder, W. P., and Vener, A. V. (2007). Immunophilin AtFKBP13 sustains all peptidyl-prolyl isomerase activity in the thylakoid lumen from *Arabidopsis thaliana* deficient in AtCYP20-2. *Biochemistry* 46, 9432–9442. doi: 10.1021/bi700426q

Foyer, C. H., Neukermans, J., Queval, G., Noctor, G., and Harbinson, J. (2012). Photosynthetic control of electron transport and the regulation of gene expression. *J. Exp. Bot.* 63, 1637–1661. doi: 10.1093/jxb/ers013

Friedrich, T., and Weiss, H. (1997). Modular evolution of the respiratory NADH:ubiquinone oxidoreductase and the origin of its modules. *J. Theor. Biol.* 187, 529–540. doi: 10.1006/jtbi.1996.0387

Friso, G., Giacomelli, L., Ytterberg, A. J., Peltier, J. B., Rudella, A. Sun, Q., et al. (2004). In-depth analysis of the thylakoid membrane proteome of *Arabidopsis thaliana* chloroplasts: new proteins, new functions, and a plastid proteome database. *Plant Cell* 16, 478–499. doi: 10.1105/tpc.017814

Fu, A., He, Z., Cho, H. S., Lima, A., Buchanan, B. B., and Luan, S. (2007). A chloroplast cyclophilin functions in the assembly and maintenance of photosystem II in *Arabidopsis thaliana*. *Proc. Natl. Acad. Sci. U.S.A.* 104, 15947–15952. doi: 10.1073/pnas.0707851104

Fulgosi, H., Vener, A. V., Altschmied, L., Herrmann, R. G., and Andersson, B. (1998). A novel multi-functional chloroplast protein: identification of a 40 kDa immunophilin-like protein located in the thylakoid lumen. *EMBO J.* 17, 1577–1587. doi: 10.1093/emboj/17.6.1577

Gigolashvili, T., Geier, M., Ashykhmina, N., Frerigmann, H., Wulfert, S., Krueger, S., et al. (2012). The *Arabidopsis* thylakoid ADP/ATP carrier TAAC has an additional role in supplying plastidic phosphoadenosine 5′-phosphosulfate to the cytosol. *Plant Cell* 24, 4187–4204. doi: 10.1105/tpc.112.101964

Gollan, P. J., Bhave, M., and Aro, E. M. (2012). The FKBP families of higher plants: exploring the structures and functions of protein interaction specialists. *FEBS Lett.* 586, 3539–3547. doi: 10.1016/j.febslet.2012.09.002

Gollan, P. J., Ziemann, M., and Bhave, M. (2011). PPIase activities and interaction partners of FK506-binding proteins in the wheat thylakoid. *Physiol. Plant.* 143, 385–395. doi: 10.1111/j.1399-3054.2011.01503.x

Gopalan, G., He, Z., Balmer, Y., Romano, P., Gupta, R., Heroux, A., et al. (2004). Structural analysis uncovers a role for redox in regulating FKBP13, an immunophilin of the chloroplast thylakoid lumen. *Proc. Natl. Acad. Sci. U.S.A.* 101, 13945–13950. doi: 10.1073/pnas.0405240101

Gopalan, G., He, Z., Battaile, K. P., Luan, S., and Swaminathan, K. (2006). Structural comparison of oxidized and reduced FKBP13 from *Arabidopsis thaliana*. *Proteins* 65, 789–795. doi: 10.1002/prot.21108

Gotor, C., and Romero, L. C. (2013). *S*-sulfocysteine synthase function in sensing chloroplast redox status. *Plant Signal. Behav.* 8, e23313. doi: 10.4161/psb.23313

Goulas, E., Schubert, M., Kieselbach, T., Kleczkowski, L. A., Gardestrom, P., Schroder, W., et al. (2006). The chloroplast lumen and stromal proteomes of *Arabidopsis thaliana* show differential sensitivity to short- and long-term exposure to low temperature. *Plant J.* 47, 720–734. doi: 10.1111/j.1365-313X.2006.02821.x

Granlund, I., Hall, M., Kieselbach, T., and Schroder, W. P. (2009a). Light induced changes in protein expression and uniform regulation of transcription in the thylakoid lumen of *Arabidopsis thaliana*. *PLoS ONE* 4:e5649. doi: 10.1371/journal.pone.0005649.

Granlund, I., Storm, P., Schubert, M., Garcia-Cerdan, J. G., Funk, C., and Schroder, W. P. (2009b). The TL29 protein is lumen located, associated with PSII and not an ascorbate peroxidase. *Plant Cell Physiol.* 50, 1898–1910. doi: 10.1093/pcp/pcp134

Gupta, R., Mould, R. M., He, Z., and Luan, S. (2002a). A chloroplast FKBP interacts with and affects the accumulation of Rieske subunit of cytochrome bf complex. *Proc. Natl. Acad. Sci. U.S.A.* 99, 15806–15811. doi: 10.1073/pnas.222550399

Gupta, R., He, Z., and Luan, S. (2002b). Functional relationship of cytochrome c6 and plastocyanin in *Arabidopsis*. *Nature* 417, 567–571. doi: 10.1038/417567a

Haldrup, A., Naver, H., and Scheller, H. V. (1999). The interaction between plastocyanin and photosystem I is inefficient in transgenic *Arabidopsis* plants lacking the PSI-N subunit of photosystem I. *Plant J.* 17, 689–698. doi: 10.1046/j.1365-313X.1999.00419.x

Hall, M., Mata-Cabana, A., Akerlund, H. E., Florencio, F. J., Schroder, W. P., Lindahl, M., et al. (2010). Thioredoxin targets of the plant chloroplast lumen and their implications for plastid function. *Proteomics* 10, 987–1001.

Hashimoto, A., Ettinger, W. F., Yamamoto, Y., and Theg, S. M. (1997). Assembly of newly imported oxygen-evolving complex subunits in isolated chloroplasts: sites of assembly and mechanism of binding. *Plant Cell* 9, 441–452.

He, Z., Li, L., and Luan, S. (2004). Immunophilins and parvulins. Superfamily of peptidyl prolyl isomerases in *Arabidopsis*. *Plant Physiol.* 134, 1248–1267. doi: 10.1104/pp.103.031005

Heber, U., and Walker, D. (1992). Concerning a dual function of coupled cyclic electron transport in leaves. *Plant Physiol.* 100, 1621–1626. doi: 10.1104/pp.100.4.1621

Heredia, P., and De Las Rivas, J. (2003). Calcium-dependent conformational change and thermal stability of the isolated PsbO protein detected by FTIR spectroscopy. *Biochemistry* 42, 11831–11838. doi: 10.1021/bi034582j

Hynds, P. J., Robinson, D., and Robinson, C. (1998). The sec-independent twin-arginine translocation system can transport both tightly folded and malfolded proteins across the thylakoid membrane. *J. Biol. Chem.* 273, 34868–34874. doi: 10.1074/jbc.273.52.34868

Ido, K., Ifuku, K., Yamamoto, Y., Ishihara, S., Murakami, A., Takabe, K., et al. (2009). Knockdown of the PsbP protein does not prevent assembly of the dimeric PSII core complex but impairs accumulation of photosystem II supercomplexes in tobacco. *Biochim. Biophys. Acta* 1787, 873–881. doi: 10.1016/j.bbabio.2009.03.004

Ifuku, K., Endo, T., Shikanai, T., and Aro, E. M. (2011). Structure of the chloroplast NADH dehydrogenase-like complex: nomenclature for nuclear-encoded subunits. *Plant Cell Physiol.* 52, 1560–1568. doi: 10.1093/pcp/pcr098

Ifuku, K., Ishihara, S., and Sato, F. (2010). Molecular functions of oxygen-evolving complex family proteins in photosynthetic electron flow. *J. Integr. Plant. Biol.* 52, 723–734. doi: 10.1111/j.1744-7909.2010.00976.x

Ifuku, K., Ishihara, S., Shimamoto, R., Ido, K., and Sato, F. (2008). Structure, function, and evolution of the PsbP protein family in higher plants. *Photosynth. Res.* 98, 427–437. doi: 10.1007/s11120-008-9359-1

Ishihara, S., Takabayashi, A., Ido, K., Endo, T., Ifuku, K., and Sato, F. (2007). Distinct functions for the two PsbP-like proteins PPL1 and PPL2 in the chloroplast thylakoid lumen of *Arabidopsis*. *Plant Physiol.* 145, 668–679. doi: 10.1104/pp.107.105866

Iwai, M., Takizawa, K., Tokutsu, R., Okamuro, A., Takahashi, Y., and Minagawa, J. (2010). Isolation of the elusive supercomplex that drives cyclic electron flow in photosynthesis. *Nature* 464, 1210–1213. doi: 10.1038/nature08885

Jackson, S. A., Hinds, M. G., and Eaton-Rye, J. J. (2012). Solution structure of CyanoP from *Synechocystis* sp. PCC 6803: new insights on the structural basis for functional specialization amongst PsbP family proteins. *Biochim. Biophys. Acta* 1817, 1331–1338. doi: 10.1016/j.bbabio.2012.02.032

Johnson, M. P., and Ruban, A. V. (2011). Restoration of rapidly reversible photoprotective energy dissipation in the absence of PsbS protein by enhanced ΔpH. *J. Biol. Chem.* 286, 19973–19981. doi: 10.1074/jbc.M111.237255

Joliot, P., and Johnson, G. N. (2011). Regulation of cyclic and linear electron flow in higher plants. *Proc. Natl. Acad. Sci. U.S.A.* 108, 13317–13322. doi: 10.1073/pnas.1110189108

Kanervo, E., Singh, M., Suorsa, M., Paakkarinen, V., Aro, E., Battchikova, N., et al. (2008). Expression of protein complexes and individual proteins upon transition of etioplasts to chloroplasts in pea (*Pisum sativum*). *Plant Cell Physiol.* 49, 396–410. doi: 10.1093/pcp/pcn016

Kapri-Pardes, E., Naveh, L., and Adam, Z. (2007). The thylakoid lumen protease Deg1 is involved in the repair of photosystem II from photoinhibition in *Arabidopsis*. *Plant Cell* 19, 1039–1047. doi: 10.1105/tpc.106.046573

Karamoko, M., Cline, S., Redding, K., Ruiz, N., and Hamel, P. P. (2011). Lumen thiol oxidoreductase1, a disulfide bond-forming catalyst, is required for the assembly of photosystem II in *Arabidopsis*. *Plant Cell* 23, 4462–4475. doi: 10.1105/tpc.111.089680

Kato, Y., Sun, X., Zhang, L., and Sakamoto, W. (2012). Cooperative D1 degradation in the photosystem II repair mediated by chloroplastic proteases in *Arabidopsis*. *Plant Physiol.* 159, 1428–1439. doi: 10.1104/pp.112.199042

Kereïche, S., Kiss, A. Z., Kouøil, R., Boekema, E. J., and Horton, P. (2010). The PsbS protein controls the macro-organisation of photosystem II complexes in

the grana membranes of higher plant chloroplasts. *FEBS Lett.* 584, 759–764. doi: 10.1016/j.febslet.2009.12.031

Kieselbach, T., and Schroder, W. P. (2003). The proteome of the chloroplast lumen of higher plants. *Photosynth. Res.* 78, 249–264. doi: 10.1023/B:PRES.0000006913.86689.f1

Kim, S. J., Jansson, S., Hoffman, N. E., Robinson, C., and Mant, A. (1999). Distinct "assisted" and "spontaneous" mechanisms for the insertion of polytopic chlorophyll-binding proteins into the thylakoid membrane. *J. Biol. Chem.* 274, 4715–4721. doi: 10.1074/jbc.274.8.4715

Kirchhoff, H., Hall, C., Wood, M., Herbstova, M., Tsabari, O., Nevo, R., et al. (2011). Dynamic control of protein diffusion within the granal thylakoid lumen. *Proc. Natl. Acad. Sci. U.S.A.* 108, 20248–20253. doi: 10.1073/pnas.1104141109

Kley, J., Schmidt, B., Boyanov, B., Stolt-Bergner, P. C., Kirk, R., Ehrmann, M., et al. (2011). Structural adaptation of the plant protease Deg1 to repair photosystem II during light exposure. *Nat. Struct. Mol. Biol.* 18, 728–731. doi: 10.1038/nsmb.2055

Kramer, D., Sacksteder, C., and Cruz, J. (1999). How acidic is the lumen. *Photosynth. Res.* 60, 151–163. doi: 10.1023/A:1006212014787

Kramer, D. M., Avenson, T. J., and Edwards, G. E. (2004). Dynamic flexibility in the light reactions of photosynthesis governed by both electron and proton transfer reactions. *Trends Plant Sci.* 9, 349–357. doi: 10.1016/j.tplants.2004.05.001

Laidler, V., Chaddock, A. M., Knott, T. G., Walker, D., and Robinson, C. (1995). A SecY homolog in *Arabidopsis thaliana.* Sequence of a full-length cDNA clone and import of the precursor protein into chloroplasts. *J. Biol. Chem.* 270, 17664–17667.

Lemeille, S., Willig, A., Depege-Fargeix, N., Delessert, C., Bassi, R., and Rochaix, J. D. (2009). Analysis of the chloroplast protein kinase Stt7 during state transitions. *PLoS Biol.* 7:e1000045. doi: 10.1371/journal.pbio.1000045.

Lennartz, K., Plucken, H., Seidler, A., Westhoff, P., Bechtold, N., and Meierhoff, K. (2001). HCF164 encodes a thioredoxin-like protein involved in the biogenesis of the cytochrome b(6)f complex in *Arabidopsis. Plant Cell* 13, 2539–2551.

Levesque-Tremblay, G., Havaux, M., and Ouellet, F. (2009). The chloroplastic lipocalin AtCHL prevents lipid peroxidation and protects *Arabidopsis* against oxidative stress. *Plant J.* 60, 691–702. doi: 10.1111/j.1365-313X.2009.03991.x

Li, X.-P., Björkman, O., Shih, C., Grossman, A. R., Rosenquist, M., Jansson, S., et al. (2000). A pigment-binding protein essential for regulation of photosynthetic light harvesting. *Nature* 403, 391–395. doi: 10.1038/35000131

Li, X. P., Gilmore, A. M., Caffarri, S., Bassi, R., Golan, T., Kramer, D., et al. (2004). Regulation of photosynthetic light harvesting involves intrathylakoid lumen pH sensing by the PsbS protein. *J. Biol. Chem.* 279, 22866–22874. doi: 10.1074/jbc.M402461200

Lima, A., Lima, S., Wong, J. H., Phillips, R. S., Buchanan, B. B., and Luan, S. (2006). A redox-active FKBP-type immunophilin functions in accumulation of the photosystem II supercomplex in *Arabidopsis thaliana. Proc. Natl. Acad. Sci. U.S.A.* 103, 12631–12636. doi: 10.1073/pnas.0605452103

Lindahl, M., and Kieselbach, T. (2009). Disulphide proteomes and interactions with thioredoxin on the track towards understanding redox regulation in chloroplasts and cyanobacteria. *J. Proteomics* 72, 416–438. doi: 10.1016/j.jprot.2009.01.003

Liu, J., Yang, H., Lu, Q., Wen, X., Chen, F., Peng, L., et al. (2012). PsbP-domain protein1, a nuclear-encoded thylakoid lumenal protein, is essential for photosystem I assembly in *Arabidopsis. Plant Cell* 24, 4992–5006. doi: 10.1105/tpc.112.106542

Lu, Y., Hall, D. A., and Last, R. L. (2011). A small zinc finger thylakoid protein plays a role in maintenance of photosystem II in *Arabidopsis thaliana. Plant Cell* 23, 1861–1875. doi: 10.1105/tpc.111.085456

Lu, Y., Wang, H. R., Li, H., Cui, H. R., Feng, Y. G., and Wang, X. Y. (2013). A chloroplast membrane protein LTO1/AtVKOR involving in redox regulation and ROS homeostasis. *Plant Cell Rep.* 32, 1427–1440. doi: 10.1007/s00299-013-1455-9

Lu, Y. K., Theg, S. M., and Stemler, A. J. (2005). Carbonic anhydrase activity of the photosystem II OEC33 protein from pea. *Plant Cell Physiol.* 46, 1944–1953. doi: 10.1093/pcp/pci209

Luciński, R., and Jackowski, G. (2013). AtFtsH heterocomplex-mediated degradation of apoproteins of the major light harvesting complex of photosystem II (LHCII) in response to stresses. *J. Plant Physiol.* 170, 1082–1089. doi: 10.1016/j.jplph.2013.03.008

Lundberg, E., Storm, P., Schroder, W. P., and Funk, C. (2011). Crystal structure of the TL29 protein from *Arabidopsis thaliana*: an APX homolog without peroxidase activity. *J. Struct. Biol.* 176, 24–31. doi: 10.1016/j.jsb.2011.07.004

Lundin, B., Hansson, M., Schoefs, B., Vener, A. V., and Spetea, C. (2007). The *Arabidopsis* PsbO2 protein regulates dephosphorylation and turnover of the photosystem II reaction centre D1 protein. *Plant J.* 49, 528–539. doi: 10.1111/j.1365-313X.2006.02976.x

Meurer, J., Plucken, H., Kowallik, K. V., and Westhoff, P. (1998). A nuclear-encoded protein of prokaryotic origin is essential for the stability of photosystem II in *Arabidopsis thaliana. EMBO J.* 17, 5286–5297. doi: 10.1093/emboj/17.18.5286

Michl, D., Robinson, C., Shackleton, J. B., Herrmann, R. G., and Klosgen, R. B. (1994). Targeting of proteins to the thylakoids by bipartite presequences: CFoII is imported by a novel, third pathway. *EMBO J.* 13, 1310–1317.

Miqyass, M., van Gorkom, H. J., and Yocum, C. F. (2007). The PSII calcium site revisited. *Photosynth Res.* 92, 275–287. doi: 10.1007/s11120-006-9124-2

Mori, H., Summer, E. J., Ma, X., and Cline, K. (1999). Component specificity for the thylakoidal Sec and delta pH-dependent protein transport pathways. *J. Cell Biol.* 146, 45–56.

Motohashi, K., and Hisabori, T. (2006). HCF164 receives reducing equivalents from stromal thioredoxin across the thylakoid membrane and mediates reduction of target proteins in the thylakoid lumen. *J. Biol. Chem.* 281, 35039–35047. doi: 10.1074/jbc.M605938200

Motohashi, K., and Hisabori, T. (2010). CcdA is a thylakoid membrane protein required for the transfer of reducing equivalents from stroma to thylakoid lumen in the higher plant chloroplast. *Antioxid. Redox Signal.* 13, 1169–1176. doi: 10.1089/ars.2010.3138

Muller, M., and Klosgen, R. B. (2005). The Tat pathway in bacteria and chloroplasts (review). *Mol. Membr. Biol.* 22, 113–121. doi: 10.1080/09687860500041809

Mullineaux, C. W. (2008). Factors controlling the mobility of photosynthetic proteins. *Photochem. Photobiol.* 84, 1310–1316. doi: 10.1111/j.1751-1097.2008.00420.x

Munekage, Y., Hashimoto, M., Miyake, C., Tomizawa, K., Endo, T., Tasaka, M., et al. (2004). Cyclic electron flow around photosystem I is essential for photosynthesis. *Nature* 429, 579–582. doi: 10.1038/nature02598

Munekage, Y., Hojo, M., Meurer, J., Endo, T., Tasaka, M., and Shikanai, T. (2002). PGR5 is involved in cyclic electron flow around photosystem I and is essential for photoprotection in *Arabidopsis. Cell* 110, 361–371. doi: 10.1016/S0092-8674(02)00867-X

Murakami, R., Ifuku, K., Takabayashi, A., Shikanai, T., Endo, T., and Sato, F. (2005). Functional dissection of two *Arabidopsis* PsbO proteins: PsbO1 and PsbO2. *FEBS J.* 272, 2165–2175. doi: 10.1111/j.1742-4658.2005.04636.x

Murata, N., Takahashi, S., Nishiyama, Y., and Allakhverdiev, S. I. (2007). Photoinhibition of photosystem II under environmental stress. *Biochim. Biophys. Acta* 1767, 414–421. doi: 10.1016/j.bbabio.2006.11.019

Murray, J. W., and Barber, J. (2006). Identification of a calcium-binding site in the PsbO protein of photosystem II. *Biochemistry* 45, 4128–4130. doi: 10.1021/bi052503t

Ni, S., McGookey, M. E., Tinch, S. L., Jones, A. N., Jayaraman, S., Tong, L., et al. (2011). The 1.7 A resolution structure of At2g44920, a pentapeptide-repeat protein in the thylakoid lumen of *Arabidopsis thaliana. Acta Crystallogr. Sect. F Struct. Biol. Cryst. Commun.* 67, 1480–1484. doi: 10.1107/S1744309111037432

Nishiyama, Y., Allakhverdiev, S. I., and Murata, N. (2006). A new paradigm for the action of reactive oxygen species in the photoinhibition of photosystem II. *Biochim. Biophys. Acta* 1757, 742–749. doi: 10.1016/j.bbabio.2006.05.013

Niyogi, K. K., Grossman, A. R., and Bjorkman, O. (1998). *Arabidopsis* mutants define a central role for the xanthophyll cycle in the regulation of photosynthetic energy conversion. *Plant Cell* 10, 1121–1134.

Okegawa, Y., Long, T. A., Iwano, M., Takayama, S., Kobayashi, Y., Covert, S. F., et al. (2007). A balanced PGR5 level is required for chloroplast development and optimum operation of cyclic electron transport around photosystem I. *Plant Cell Physiol.* 48, 1462–1471. doi: 10.1093/pcp/pcm116

Peltier, J. B., Emanuelsson, O., Kalume, D. E., Ytterberg, J., Friso, G., Rudella, A., et al. (2002). Central functions of the lumenal and peripheral thylakoid proteome of *Arabidopsis* determined by experimentation and genome-wide prediction. *Plant Cell* 14, 211–236. doi: 10.1105/tpc.010304

Peng, L., Fukao, Y., Fujiwara, M., Takami, T., and Shikanai, T. (2009). Efficient operation of NAD(P)H dehydrogenase requires supercomplex formation with photosystem I via minor LHCI in *Arabidopsis. Plant Cell* 21, 3623–3640. doi: 10.1105/tpc.109.068791

Peng, L., and Shikanai, T. (2011). Supercomplex formation with photosystem I is required for the stabilization of the chloroplast NADH dehydrogenase-like complex in *Arabidopsis*. *Plant Physiol.* 155, 1629–1639. doi: 10.1104/pp.110.171264

Pesaresi, P., Hertle, A., Pribil, M., Kleine, T., Wagner, R., Strissel, H., et al. (2009a). *Arabidopsis* STN7 kinase provides a link between short- and long-term photosynthetic acclimation. *Plant Cell* 21, 2402–2423. doi: 10.1105/tpc.108.064964

Pesaresi, P., Scharfenberg, M., Weigel, M., Granlund, I., Schroder, W. P., Finazzi, G., et al. (2009b). Mutants, overexpressors, and interactors of *Arabidopsis* plastocyanin isoforms: revised roles of plastocyanin in photosynthetic electron flow and thylakoid redox state. *Mol. Plant.* 2, 236–248. doi: 10.1093/mp/ssn041

Petersson, U. A., Kieselbach, T., Garcia-Cerdan, J. G., and Schroder, W. P. (2006). The Prx Q protein of *Arabidopsis thaliana* is a member of the luminal chloroplast proteome. *FEBS Lett.* 580, 6055–6061. doi: 10.1016/j.febslet.2006.10.001

Plucken, H., Muller, B., Grohmann, D., Westhoff, P., and Eichacker, L. A. (2002). The HCF136 protein is essential for assembly of the photosystem II reaction center in *Arabidopsis thaliana*. *FEBS Lett.* 532, 85–90. doi: 10.1016/S0014-5793(02)03634-7

Popelkova, H., and Yocum, C. F. (2007). Current status of the role of Cl(−) ion in the oxygen-evolving complex. *Photosynth. Res.* 93, 111–121. doi: 10.1007/s11120-006-9121-5

Queval, G., and Foyer, C. H. (2012). Redox regulation of photosynthetic gene expression. *Philos. Trans. R. Soc. Lond. B Biol. Sci.* 367, 3475–3485. doi: 10.1098/rstb.2012.0068

Reiland, S., Messerli, G., Baerenfaller, K., Gerrits, B., Endler, A., Grossmann, J., et al. (2009). Large-scale *Arabidopsis* phosphoproteome profiling reveals novel chloroplast kinase substrates and phosphorylation networks. *Plant Physiol.* 150, 889–903. doi: 10.1104/pp.109.138677

Rokka, A., Aro, E. M., Herrmann, R. G., Andersson, B., and Vener, A. V. (2000). Dephosphorylation of photosystem II reaction center proteins in plant photosynthetic membranes as an immediate response to abrupt elevation of temperature. *Plant Physiol.* 123, 1525–1536. doi: 10.1104/pp.123.4.1525

Romano, P. G., Edvardsson, A., Ruban, A. V., Andersson, B., Vener, A. V., Gray, J. E., et al. (2004a). *Arabidopsis* AtCYP20-2 is a light-regulated cyclophilin-type peptidyl-prolyl *cis–trans* isomerase associated with the photosynthetic membranes. *Plant Physiol.* 134, 1244–1247. doi: 10.1104/pp.104.041186

Romano, P. G., Horton, P., and Gray, J. E. (2004b). The *Arabidopsis* cyclophilin gene family. *Plant Physiol.* 134, 1268–1282. doi: 10.1104/pp.103.022160

Roose, J. L., Frankel, L. K., and Bricker, T. M. (2011). Developmental defects in mutants of the PsbP domain protein 5 in *Arabidopsis thaliana*. *PLoS ONE* 6:e28624. doi: 10.1371/journal.pone.0028624

Roose, J. L., and Pakrasi, H. B. (2004). Evidence that D1 processing is required for manganese binding and extrinsic protein assembly into photosystem II. *J. Biol. Chem.* 279, 45417–45422. doi: 10.1074/jbc.M408458200

Roose, J. L., and Pakrasi, H. B. (2008). The Psb27 protein facilitates manganese cluster assembly in photosystem II. *J. Biol. Chem.* 283, 4044–4050. doi: 10.1074/jbc.M708960200

Rumeau, D., Peltier, G., and Cournac, L. (2007). Chlororespiration and cyclic electron flow around PSI during photosynthesis and plant stress response. *Plant Cell Environ.* 30, 1041–1051. doi: 10.1111/j.1365-3040.2007.01675.x

Sato, N. (2010). Phylogenomic and structural modeling analyses of the PsbP superfamily reveal multiple small segment additions in the evolution of photosystem II-associated PsbP protein in green plants. *Mol. Phylogenet. Evol.* 56, 176–186. doi: 10.1016/j.ympev.2009.11.021

Sazanov, L. A., Burrows, P. A., and Nixon, P. J. (1998). The plastid ndh genes code for an NADH-specific dehydrogenase: isolation of a complex I analogue from pea thylakoid membranes. *Proc. Natl. Acad. Sci. U.S.A.* 95, 1319–1324. doi: 10.1073/pnas.95.3.1319

Schlarb-Ridley, B. G., Nimmo, R. H., Purton, S., Howe, C. J., and Bendall, D. S. (2006). Cytochrome c(6A) is a funnel for thiol oxidation in the thylakoid lumen. *FEBS Lett.* 580, 2166–2169. doi: 10.1016/j.febslet.2006.03.052

Schubert, M., Petersson, U. A., Haas, B. J., Funk, C., Schroder, W. P., and Kieselbach, T. (2002). Proteome map of the chloroplast lumen of *Arabidopsis thaliana*. *J. Biol. Chem.* 277, 8354–8365. doi: 10.1074/jbc.M108575200

Schuenemann, D., Amin, P., Hartmann, E., and Hoffman, N. E. (1999). Chloroplast SecY is complexed to SecE and involved in the translocation of the 33-kDa but not the 23-kDa subunit of the oxygen-evolving complex. *J. Biol. Chem.* 274, 12177–12182. doi: 10.1074/jbc.274.17.12177

Shapiguzov, A., Edvardsson, A., and Vener, A. V. (2006). Profound redox sensitivity of peptidyl-prolyl isomerase activity in *Arabidopsis* thylakoid lumen. *FEBS Lett.* 580, 3671–3676. doi: 10.1016/j.febslet.2006.05.054

Shikanai, T. (2007). Cyclic electron transport around photosystem I: genetic approaches. *Annu. Rev. Plant. Biol.* 58, 199–217. doi: 10.1146/annurev.arplant.58.091406.110525

Sirpio, S., Allahverdiyeva, Y., Suorsa, M., Paakkarinen, V., Vainonen, J., Battchikova, N., et al. (2007). TLP18.3, a novel thylakoid lumen protein regulating photosystem II repair cycle. *Biochem. J.* 406, 415–425. doi: 10.1042/BJ20070460

Sirpio, S., Holmstrom, M., Battchikova, N., and Aro, E. M. (2009). AtCYP20-2 is an auxiliary protein of the chloroplast NAD(P)H dehydrogenase complex. *FEBS Lett.* 583, 2355–2358. doi: 10.1016/j.febslet.2009.06.031

Sirpio, S., Khrouchtchova, A., Allahverdiyeva, Y., Hansson, M., Fristedt, R., Vener, A. V., et al. (2008). AtCYP38 ensures early biogenesis, correct assembly and sustenance of photosystem II. *Plant J.* 55, 639–651. doi: 10.1111/j.1365-313X.2008.03532.x

Soll, J., and Schleiff, E. (2004). Protein import into chloroplasts. *Nat. Rev.* 5, 198–208. doi: 10.1038/nrm1333

Spetea, C., Hundal, T., Lundin, B., Heddad, M., Adamska, I., and Andersson, B. (2004). Multiple evidence for nucleotide metabolism in the chloroplast thylakoid lumen. *Proc. Natl. Acad. Sci. U.S.A.* 101, 1409–1414. doi: 10.1073/pnas.0308164100

Spetea, C., and Lundin, B. (2012). Evidence for nucleotide-dependent processes in the thylakoid lumen of plant chloroplasts – an update. *FEBS Lett.* 586, 2946–2954. doi: 10.1016/j.febslet.2012.07.005

Stael, S., Rocha, A. G., Wimberger, T., Anrather, D., Vothknecht, U. C., and Teige, M. (2012). Cross-talk between calcium signalling and protein phosphorylation at the thylakoid. *J. Exp. Bot.* 63, 1725–1733. doi: 10.1093/jxb/err403

Sugiyama, N., Nakagami, H., Mochida, K., Daudi, A., Tomita, M., Shirasu, K., et al. (2008). Large-scale phosphorylation mapping reveals the extent of tyrosine phosphorylation in *Arabidopsis*. *Mol. Syst. Biol.* 4, 193. doi: 10.1038/msb.2008.32

Sun, X., Fu, T., Chen, N., Guo, J., Ma, J., Zou, M., et al. (2010a). The stromal chloroplast Deg7 protease participates in the repair of photosystem II after photoinhibition in *Arabidopsis*. *Plant Physiol.* 152, 1263–1273. doi: 10.1104/pp.109.150722

Sun, X., Ouyang, M., Guo, J., Ma, J., Lu, C., Adam, Z., et al. (2010b). The thylakoid protease Deg1 is involved in photosystem-II assembly in *Arabidopsis thaliana*. *Plant J.* 62, 240–249. doi: 10.1111/j.1365-313X.2010.04140.x

Sun, X., Peng, L., Guo, J., Chi, W., Ma, J., Lu, C., et al. (2007). Formation of DEG5 and DEG8 complexes and their involvement in the degradation of photodamaged photosystem II reaction center D1 protein in *Arabidopsis*. *Plant Cell* 19, 1347–1361. doi: 10.1105/tpc.106.049510

Suorsa, M., Grieco, M., Jarvi, S., Gollan, P. J., Kangasjarvi, S., Tikkanen, M., et al. (2012a). PGR5 ensures photosynthetic control to safeguard photosystem I under fluctuating light conditions. *Plant Signal. Behav.* 8, e22741. doi: 10.4161/psb.22741

Suorsa, M., Jarvi, S., Grieco, M., Nurmi, M., Pietrzykowska, M., Rantala, M., et al. (2012b). PROTON GRADIENT REGULATION5 is essential for proper acclimation of *Arabidopsis* photosystem I to naturally and artificially fluctuating light conditions. *Plant Cell* 24, 2934–2948. doi: 10.1105/tpc.112.097162

Suorsa, M., Sirpio, S., Allahverdiyeva, Y., Paakkarinen, V., Mamedov, F., Styring, S., et al. (2006). PsbR, a missing link in the assembly of the oxygen-evolving complex of plant photosystem II. *J. Biol. Chem.* 281, 145–150. doi: 10.1074/jbc.M510600200

Suorsa, M., Sirpio, S., Paakkarinen, V., Kumari, N., Holmstrom, M., and Aro, E. M. (2010). Two proteins homologous to PsbQ are novel subunits of the chloroplast NAD(P)H dehydrogenase. *Plant Cell Physiol.* 51, 877–883. doi: 10.1093/pcp/pcq070

Thuswaldner, S., Lagerstedt, J. O., Rojas-Stutz, M., Bouhidel, K., Der, C., Leborgne-Castel, N., et al. (2007). Identification, expression, and functional analyses of a thylakoid ATP/ADP carrier from *Arabidopsis*. *J. Biol. Chem.* 282, 8848–8859. doi: 10.1074/jbc.M609130200

Tikhonov, A. N. (2013). pH-dependent regulation of electron transport and ATP synthesis in chloroplasts. *Photosynth. Res.* doi: 10.1007/s11120-013-9845-y

Tyystjärvi, E., and Aro, E. M. (1996). The rate constant of photoinhibition, measured in lincomycin-treated leaves, is directly proportional to light intensity. *Proc. Natl. Acad. Sci. U.S.A.* 93, 2213–2218. doi: 10.1073/pnas.93.5.2213

Vasudevan, D., Fu, A., Luan, S., and Swaminathan, K. (2012). Crystal structure of *Arabidopsis* cyclophilin38 reveals a previously uncharacterized immunophilin fold and a possible autoinhibitory mechanism. *Plant Cell* 24, 2666–2674. doi: 10.1105/tpc.111.093781

Vener, A. V., Rokka, A., Fulgosi, H., Andersson, B., and Herrmann, R. G. (1999). A cyclophilin-regulated PP2A-like protein phosphatase in thylakoid membranes of plant chloroplasts. *Biochemistry* 38, 14955–14965. doi: 10.1021/bi990971v

Wei, L., Guo, J., Ouyang, M., Sun, X., Ma, J., Chi, W., et al. (2010). LPA19, a Psb27 homolog in *Arabidopsis thaliana*, facilitates D1 protein precursor processing during PSII biogenesis. *J. Biol. Chem.* 285, 21391–21398. doi: 10.1074/jbc.M110.105064

Weigel, M., Varotto, C., Pesaresi, P., Finazzi, G., Rappaport, F., Salamini, F., et al. (2003). Plastocyanin is indispensable for photosynthetic electron flow in *Arabidopsis thaliana*. *J. Biol. Chem.* 278, 31286–31289. doi: 10.1074/jbc.M302876200

Wu, H. Y., Liu, M. S., Lin, T. P., and Cheng, Y. S. (2011). Structural and functional assays of AtTLP18.3 identify its novel acid phosphatase activity in thylakoid lumen. *Plant Physiol.* 157, 1015–1025. doi: 10.1104/pp.111.184739

Yabuta, S., Ifuku, K., Takabayashi, A., Ishihara, S., Ido, K., Ishikawa, N., et al. (2010). Three PsbQ-like proteins are required for the function of the chloroplast NAD(P)H dehydrogenase complex in *Arabidopsis*. *Plant Cell Physiol.* 51, 866–876. doi: 10.1093/pcp/pcq060

Yamamoto, H., Peng, L., Fukao, Y., and Shikanai, T. (2011). An Src homology 3 domain-like fold protein forms a ferredoxin binding site for the chloroplast NADH dehydrogenase-like complex in *Arabidopsis*. *Plant Cell* 23, 1480–1493. doi: 10.1105/tpc.110.080291

Yamamoto, Y., Inagaki, N., and Satoh, K. (2001). Overexpression and characterization of carboxyl-terminal processing protease for precursor D1 protein: regulation of enzyme-substrate interaction by molecular environments. *J. Biol. Chem.* 276, 7518–7525. doi: 10.1074/jbc.M008877200

Yi, X., Hargett, S. R., Frankel, L. K., and Bricker, T. M. (2006). The PsbQ protein is required in *Arabidopsis* for photosystem II assembly/stability and photoautotrophy under low light conditions. *J. Biol. Chem.* 281, 26260–26267. doi: 10.1074/jbc.M603582200

Yi, X., Hargett, S. R., Frankel, L. K., and Bricker, T. M. (2009). The PsbP protein, but not the PsbQ protein, is required for normal thylakoid architecture in *Arabidopsis thaliana*. *FEBS Lett.* 583, 2142–2147. doi: 10.1016/j.febslet.2009.05.048

Yi, X., Hargett, S. R., Liu, H., Frankel, L. K., and Bricker, T. M. (2007). The PsbP protein is required for photosystem II complex assembly/stability and photoautotrophy in *Arabidopsis thaliana*. *J. Biol. Chem.* 282, 24833–24841. doi: 10.1074/jbc.M705011200

Yin, S., Sun, X., and Zhang, L. (2008). An *Arabidopsis* ctpA homologue is involved in the repair of photosystem II under high light. *Chin. Sci. Bull.* 53, 1021–1026. doi: 10.1007/s11434-008-0153-4

Yuan, J., Henry, R., McCaffery, M., and Cline, K. (1994). SecA homolog in protein transport within chloroplasts: evidence for endosymbiont-derived sorting. *Science* 266, 796–798. doi: 10.1126/science.7973633

Zhang, S., and Scheller, H. V. (2004). Photoinhibition of photosystem I at chilling temperature and subsequent recovery in *Arabidopsis thaliana*. *Plant Cell Physiol.* 45, 1595–1602. doi: 10.1093/pcp/pch180

Zienkiewicz, M., Ferenc, A., Wasilewska, W., and Romanowska, E. (2012). High light stimulates Deg1-dependent cleavage of the minor LHCII antenna proteins CP26 and CP29 and the PsbS protein in *Arabidopsis thaliana*. *Planta* 235, 279–288. doi: 10.1007/s00425-011-1505-x

Conflict of Interest Statement: The authors declare that the research was conducted in the absence of any commercial or financial relationships that could be construed as a potential conflict of interest.

Received: 17 July 2013; accepted: 12 October 2013; published online: 31 October 2013.

*Citation: Järvi S, Gollan PJ and Aro E-M (2013) Understanding the roles of the thylakoid lumen in photosynthesis regulation. Front. Plant Sci. **4**:434. doi: 10.3389/fpls.2013.00434*

This article was submitted to Plant Physiology, a section of the journal Frontiers in Plant Science.

frontiers in
PLANT SCIENCE

REVIEW ARTICLE
published: 19 September 2013
doi: 10.3389/fpls.2013.00366

Algal endosymbionts as vectors of horizontal gene transfer in photosynthetic eukaryotes

Huan Qiu[1], Hwan Su Yoon[2] and Debashish Bhattacharya[1]*

[1] *Department of Ecology, Evolution, and Natural Resources, Institute of Marine and Coastal Science, Rutgers University, New Brunswick, NJ, USA*
[2] *Department of Biological Sciences, Sungkyunkwan University, Suwon, South Korea*

Edited by:
Mohammad Mahdi Najafpour, Institute for Advanced Studies in Basic Sciences, Iran

Reviewed by:
Suleyman I. Allakhverdiev, Russian Academy of Sciences, Russia
Shan Lu, Nanjing University, China

***Correspondence:**
Debashish Bhattacharya, Department of Ecology, Evolution, and Natural Resources, Institute of Marine and Coastal Science, Rutgers University, 59 Dudley Road, Foran Hall 102, New Brunswick, NJ 08901, USA
e-mail: debash.bhattacharya@gmail.com

Photosynthesis in eukaryotes occurs in the plastid, an organelle that is derived from a single cyanobacterial primary endosymbiosis in the common ancestor of the supergroup Plantae (or Archaeplastida) that includes green, red, and glaucophyte algae and plants. However a variety of other phytoplankton such as the chlorophyll *c*-containing diatoms, dinoflagellates, and haptophytes contain a red alga-derived plastid that traces its origin to secondary or tertiary (eukaryote engulfs eukaryote) endosymbiosis. The hypothesis of Plantae monophyly has only recently been substantiated, however the extent and role of endosymbiotic and horizontal gene transfer (EGT and HGT) in algal genome evolution still remain to be fully understood. What is becoming clear from analysis of complete genome data is that algal gene complements can no longer be considered essentially eukaryotic in provenance; i.e., with the expected addition of several hundred cyanobacterial genes derived from EGT and a similar number derived from the mitochondrial ancestor. For example, we now know that foreign cells such as Chlamydiae and other prokaryotes have made significant contributions to plastid functions in Plantae. Perhaps more surprising is the recent finding of extensive bacterium-derived HGT in the nuclear genome of the unicellular red alga *Porphyridium purpureum* that does not relate to plastid functions. These non-endosymbiont gene transfers not only shaped the evolutionary history of Plantae but also were propagated *via* secondary endosymbiosis to a multitude of other phytoplankton. Here we discuss the idea that Plantae (in particular red algae) are one of the major players in eukaryote genome evolution by virtue of their ability to act as "sinks" and "sources" of foreign genes through HGT and endosymbiosis, respectively. This hypothesis recognizes the often under-appreciated Rhodophyta as major sources of genetic novelty among photosynthetic eukaryotes.

Keywords: algal evolution, Plantae plastid origin, primary endosymbiosis, chromalveolates, EGT, HGT

INTRODUCTION

Photosynthetic eukaryotes (i.e., algae and plants) are a taxonomically diverse group with a wide variety of cell morphologies (e.g., diatoms, dinoflagellates, coccolithophores) and lifestyles that are key primary producers (Field et al., 1998). All eukaryotic photosynthesis relies on the intracellular organelle, the plastid (chloroplast in plants and green algae) that was derived over one billion years ago from a cyanobacterial primary endosymbiosis. In this process, a once free-living cyanobacterium capable of oxygenic photosynthesis was engulfed and retained in a heterotrophic protist, and over time evolved into the intracellular organelle (Section I in **Figure 1**; Cavalier-Smith, 1999; Bhattacharya et al., 2004). The resulting plastid-harboring protist ancestor gave rise to three lineages of Plantae (or Archaeplastida); i.e., Glaucophyta, Rhodophyta (red algae), and Viridiplantae (green algae and land plants; Section II in **Figure 1**; Adl et al., 2005). The establishment of Plantae plastid monophyly (e.g., Rodriguez-Ezpeleta et al., 2005) and, only recently, the monophyly of Plantae hosts (Chan et al., 2011; Price et al., 2012) provides strong support for the idea that the Plantae primary endosymbiosis occurred once in evolution. Despite its groundbreaking impact on eukaryote evolution and overall, the trajectory of life on Earth, primary endosymbiosis appears to be exceedingly rare. The only other known case of plastid primary endosymbiosis is provided by a single lineage of Rhizaria, *Paulinella* (Lauterborn, 1895; Yoon et al., 2006), which acquired a *Synechococcus*-like alpha-cyanobacterium ~65 million years ago (Nowack et al., 2008). The rarity of primary endosymbiosis is ascribed to difficulties in the initial "domestication" of the wild-type cyanobacterium and its integration into host cell metabolism. It is believed that primary endosymbiosis in the Plantae ancestor was made possible by the concomitant infection by parasitic Chlamydiae (Huang and Gogarten, 2007). Recent work suggests that effector proteins secreted by Chlamydiae might have facilitated the integration of carbon metabolism between the cyanobacterial endosymbiont and the host (Ball et al., 2013; Baum, 2013).

Whereas eukaryotic photosynthesis commenced with primary endosymbiosis, its greatest impact was achieved through additional rounds of secondary and tertiary endosymbiosis, whereby the cyanobacterium-derived organelle was transferred to a myriad of other protist hosts (e.g., red algal endosymbiosis; Section III in **Figure 1**; Keeling, 2010; Dorrell and Smith, 2011). Green algae

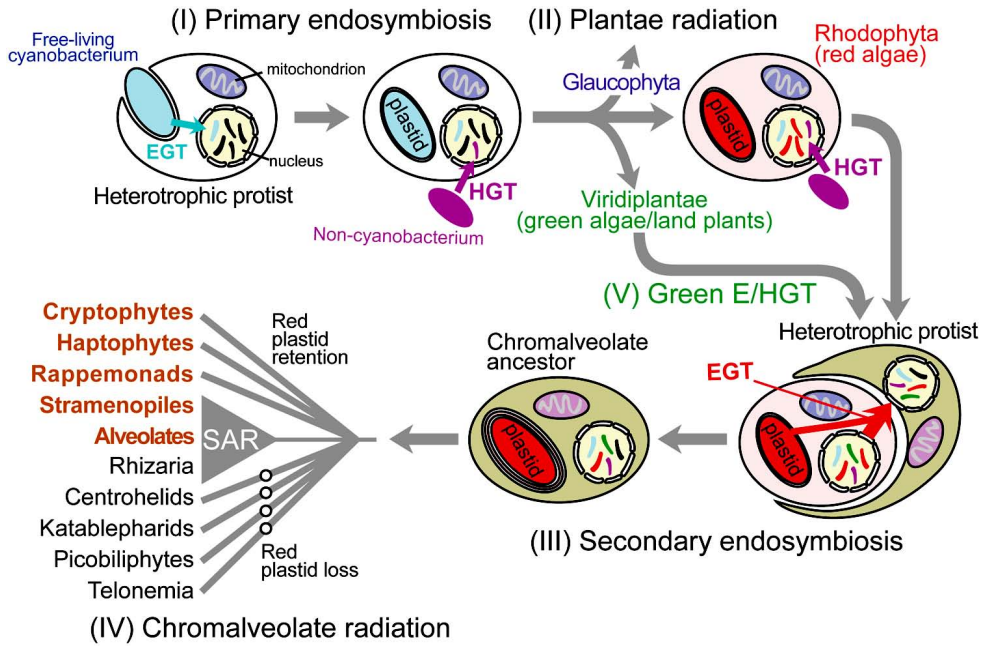

FIGURE 1 | Schematic illustration of cyanobacterial primary endosymbiosis and red algal secondary endosymbiosis that gave rise to the plastid in the vast majority of photosynthetic eukaryotes. Gene movement *via* endosymbiotic gene transfer (EGT) and horizontal gene transfer (HGT) is indicated with the arrows. Important intracellular organelles (i.e., nucleus, mitochondrion, and plastid) are shown. Genetic material of non-lineal evolutionary origin in the nucleus is presented as stripes of different colors with the color indicating the source of the gene.

were taken up at least three times by the ancestors of chlorarachniophytes, euglenids, and some "green" dinoflagellates (Archibald and Keeling, 2002; Rogers et al., 2007; Dorrell and Smith, 2011). The red algal plastid is found in diverse taxa such as cryptomonads, haptophytes, heterokonts, dinoflagellates, and apicomplexans, which collectively are often referred to as "chromalveolates" due to the presence of chlorophyll *c* in many of their plastids (Cavalier-Smith, 1999). Whether chromalveolates constitute a monophyletic group (Lane and Archibald, 2008; Keeling, 2009), however, clearly not under the scheme envisioned by (Cavalier-Smith, 1999), and whether the red alga-derived plastid found in many of its constituent taxa are derived from a single red algal endosymbiosis event (Section IV in **Figure 1**; Keeling, 2010) remain subjects of active debate. Even more complicated is tertiary endosymbiosis, in which secondary plastid-containing algae were engulfed and reduced to endosymbionts. This process has occurred multiple times in dinoflagellate lineages (Keeling, 2010) as evidenced by the haptophyte-derived plastid in *Karenia* and *Karlodinium* spp. (Hansen et al., 2000), the diatom-derived plastid in taxa such as *Kryptoperidinium foliaceum* (Chesnick et al., 1997), and the cryptophyte-derived plastid in *Dinophysis* spp. (Chesnick et al., 1996; Park et al., 2010; Kim et al., 2012).

In addition to the clear instances of plastid endosymbiosis described above in which the organelle is retained in the cell and identifies the donor, are the other more intriguing cases of plastid replacement. When these events are recent and the ancestral plastid source is unambiguous, then the inference is trivial even when both plastid sources are ultimately of the same origin (e.g., dinoflagellate peridinin-containing "red" plastid is replaced by a haptophyte "red" plastid; Ishida and Green, 2002). Apart from phylogenetic signal embedded in the organelle genome, "footprints" of the two endosymbionts can also be found in the nuclear genome in the form of transferred genes associated with each event (Nosenko et al., 2006). However if the cryptic endosymbiosis occurred in deep time (e.g., hundreds of millions of years ago), then such a hypothesis is exceedingly difficult to test if the plastid donors derive from the same ancestral lineage; i.e., making it intractable to discriminate between genes associated with each event. However if the plastid donors are phylogenetically distantly related then it may be possible to identify cases of cryptic endosymbiosis. We proposed such a case involving a cryptic green algal endosymbiosis, initially described in diatom genomes, and then more broadly applied to chromalveolates (Section V in **Figure 1**; Moustafa et al., 2009). Under this scenario, the cryptic green alga-derived plastid was presumably replaced by the canonical red algal endosymbiont in these taxa. An opposite case is found in the chlorarachniophyte *Bigelowiella natans*, which contains a green alga-derived secondary plastid but encodes a large number of nuclear-encoded genes of red algal origin (Curtis et al., 2012), potentially derived from the ancient red algal endosymbiont shared by the common ancestor of rhizarians and chromalveolates. Regardless of their mechanism of origin, it is now clear that chromalveolates and rhizarians share a large number of genes of both red and green algal origin. Compared to primary endosymbiosis, once "eukaryotization" of a plastid endosymbiont has occurred then its transfer is more likely. This sort of eukaryote-to-eukaryote plastid transfer resulted in a great deal of plastid diversity and to a large assemblage of taxa with significant ecological, economic, and health

significance than the Plantae lineages alone (Simon et al., 2009; Keeling, 2010).

All photosynthetic eukaryotes have undergone extensive foreign gene transfer (Keeling and Palmer, 2008), particularly from the plastid donor *via* endosymbiotic gene transfer (EGT; **Figure 1**; Timmis et al., 2004). In addition to receiving genes from the endosymbiont, algae and plants also acquire foreign genes from non-cyanobacterial prokaryotes *via* horizontal gene transfer (HGT; **Figure 1**). In contrast to vertical genetic inheritance from parent to offspring, HGT is the genetic movement across species without the involvement of reproduction (Doolittle, 1999). Whereas HGT has long been known as a major force in prokaryote evolution (Gogarten et al., 2002; Boucher et al., 2003), its significance to eukaryote evolution has only recently been appreciated (Keeling and Palmer, 2008; Andersson, 2009; Dunning Hotopp, 2011; Bhattacharya et al., 2013; Wijayawardena et al., 2013). At the broadest level, endosymbiotic (E)/HGT can be thought of as a pipeline that allows the flow of genetic information across branches in the tree of life. Below we summarize recent studies of E/HGT in algae and plants. In particular we focus on complete genome data that was recently generated from the mesophilic, unicellular red alga *Porphyridium purpureum* (Bhattacharya et al., 2013). We determine the significance of E/HGT in this species from prokaryote sources, and elucidate the role of red algae as mediators of prokaryotic gene spread among taxa that contain a red alga-derived plastid.

ENDOSYMBIOTIC/HORIZONTAL GENE TRANSFER OF PROKARYOTIC GENES IN PLANTAE

In the process of plastid origin, the endosymbiont undergoes dramatic genome reduction leading to highly reduced modern-day plastid genomes encoding <250 genes. This genome reduction is explained in part by the movement of hundreds of cyanobacterium-derived genes to the host nuclear genome *via* EGT (**Figure 1**). Many of the protein products of the EGT-derived genes are subsequently synthesized in the cytosol and retargeted to the plastid (Martin et al., 2002; Reyes-Prieto et al., 2006) *via* a sophisticated trafficking system (Li and Chiu, 2010). Some of the cyanobacterial genes also take on functions unrelated to the plastid (Timmis et al., 2004; Kleine et al., 2009). This massive gene relocation process has resulted in mosaic algal nuclear genomes with the cyanobacterium-derived EGT set accounting for 6–20% of the total gene repertoire in Plantae; e.g., glaucophyte *Cyanophora paradoxa* (Reyes-Prieto et al., 2006; Price et al., 2012), extremophilic red alga *Cyanidioschyzon merolae* (Sato et al., 2005; Deusch et al., 2008; Dagan et al., 2013), unicellular green alga *Chlamydomonas reinhardtii* (Deusch et al., 2008; Moustafa and Bhattacharya, 2008), picoplanktonic green alga *Ostreococcus tauri* (Dagan et al., 2013), *Oryza sativa* (Deusch et al., 2008), *Arabidopsis thaliana*, and other land plants (Martin et al., 2002; Deusch et al., 2008; Dagan et al., 2013).

Another source of evolutionary novelty in Plantae is non-cyanobacterial (i.e., Archaea and other bacteria) prokaryote-derived HGT that occurred throughout the history of this supergroup (**Figure 1**). HGT appears to be widespread and is found in all three Plantae phyla; e.g., *Cyanophora paradoxa* (Price et al., 2012), the extremophilic red alga *Galdieria sulphuraria* (Schoenknecht et al., 2013), the mesophilic red alga *Porphyridium purpureum* (Bhattacharya et al., 2013), the red seaweed *Chondrus crispus* (Collen et al., 2013), the green picoprasinophytes *Ostreococcus tauri* (Derelle et al., 2006) and *Micromonas* spp. (Worden et al., 2009), the green algae *Chlorella variabilis NC64A* (Blanc et al., 2010), *Coccomyxa subellipsoidea* (Blanc et al., 2012), *Bathycoccus prasinos* (Moreau et al., 2012), and land plants [e.g., the moss *Physcomitrella patens* (Yue et al., 2012)]. HGT-derived genes have enabled adaptation of red algae to extreme environments (Schoenknecht et al., 2013). A recent genome-wide analysis of *Porphyridium purpureum* showed that ∼5% of the gene repertoire in this mesophile was derived from non-cyanobacterial prokaryotes, which is comparable to the number of cyanobacterium-derived EGTs in this genome (Bhattacharya et al., 2013).

A significant source of non-cyanobacterial genes in algal genomes is from the intracellular parasitic bacteria, Chlamydiae (Huang and Gogarten, 2007; Becker et al., 2008; Moustafa et al., 2008; Ball et al., 2013). Many Chlamydiae-derived genes encode proteins with putative plastid functions (Horn, 2008; Moustafa et al., 2008). The results of a recent study suggest that Chlamydiae may once have existed as symbionts in the Plantae ancestor and aided in the harnessing of the cyanobacterial primary endosymbiont (Ball et al., 2013; Baum, 2013). If this hypothesis is true, then many Chlamydiae-derived algal genes could also be considered as examples of EGT from a long-term (now absent) symbiont.

ENDOSYMBIOTIC GENE TRANSFER OF PLANTAE GENES INTO CHROMALVEOLATES

As described above, like primary endosymbiosis, secondary and tertiary endosymbiosis also led to large-scale gene transfer to the host nuclear genome *via* EGT (**Figure 1**; Lane and Archibald, 2008). This process allows the retention of genes critical for plastid functions because the nucleus of the endosymbiont (e.g., engulfed alga) either shrinks dramatically in size to a nucleomorph (i.e., 500–700 Kbp in cryptophytes; Douglas et al., 2001; Lane et al., 2007; Tanifuji et al., 2011; Moore et al., 2012) and 400 Kbp in *Bigelowiella natans*; Gilson et al., 2006) or is lost outright (Moore and Archibald, 2009; Keeling, 2010). Alga-derived EGT genes have been described in detail from a variety of photosynthetic taxa, including "chromists" (Frommolt et al., 2008), dinoflagellates (Chan et al., 2012b) and *Bigelowiella natans* (Archibald et al., 2003), as well as from ciliates that may once have contained a plastid (Reyes-Prieto et al., 2008).

Whole-genome sequences of photosynthetic chromalveolates and rhizarians provide a global picture of the footprints of algal endosymbiosis. For example, 171 genes with red or/and green algal provenance were identified in the genome of the diatoms *Phaeodactylum tricornutum* (Bowler et al., 2008) and *Thalassiosira pseudonana* (Armbrust et al., 2004). Using more comprehensive methods, thousands of green algal-derived genes were later found in the genomes of these diatoms, which outnumber the contribution from red algae. As described above, this was interpreted as potentially deriving from a cryptic green algal secondary endosymbiosis (added to by independent HGTs) in chromalveolates (Moustafa et al., 2009). Analysis of the genome from the brown, filamentous seaweed *Ectocarpus siliculosus* also revealed a substantial number of green algal-derived (>2000) and red

algal-derived (∼500) genes (Cock et al., 2010). More than 800 genes with a red algal or cyanobacterial provenance were identified in the genomes of the non-photosynthetic plant pathogens *Phytophthora sojae* and *Phytophthora ramorum* (Tyler et al., 2006), suggesting a photosynthetic past for these taxa [but see (Stiller et al., 2009)]. Recent analyses of complete genome data from the nucleomorph-containing taxa *Guillardia theta* (cryptophyte) and *Bigelowiella natans* (rhizarian), turned up 508 and 353 algal-derived genes, respectively, which account for 7 and 6% of all genes analyzed in these two taxa (Curtis et al., 2012).

From the perspective of algal endosymbiosis, analysis of *Porphyridium purpureum* complete genome data shows that ∼40% of its genes are shared with at least one chromalveolate taxon (Bhattacharya et al., 2013). This passage of red algal genes into chromalveolates appears to be very broad in terms of gene function (Bhattacharya et al., 2013). Due to the possible mixotrophic lifestyle of photosynthetic lineages such as *Bigelowiella natans* (Moestrup and Sengco, 2001), the relationship between algal-derived EGT and prey-derived HGT is hard to disentangle. Regardless of the underlying mechanism, Plantae contribution to host genomes of secondary or tertiary endosymbiont-containing algae is significant. These numbers are expected to increase as more Plantae and chromalveolate complete genomes are analyzed.

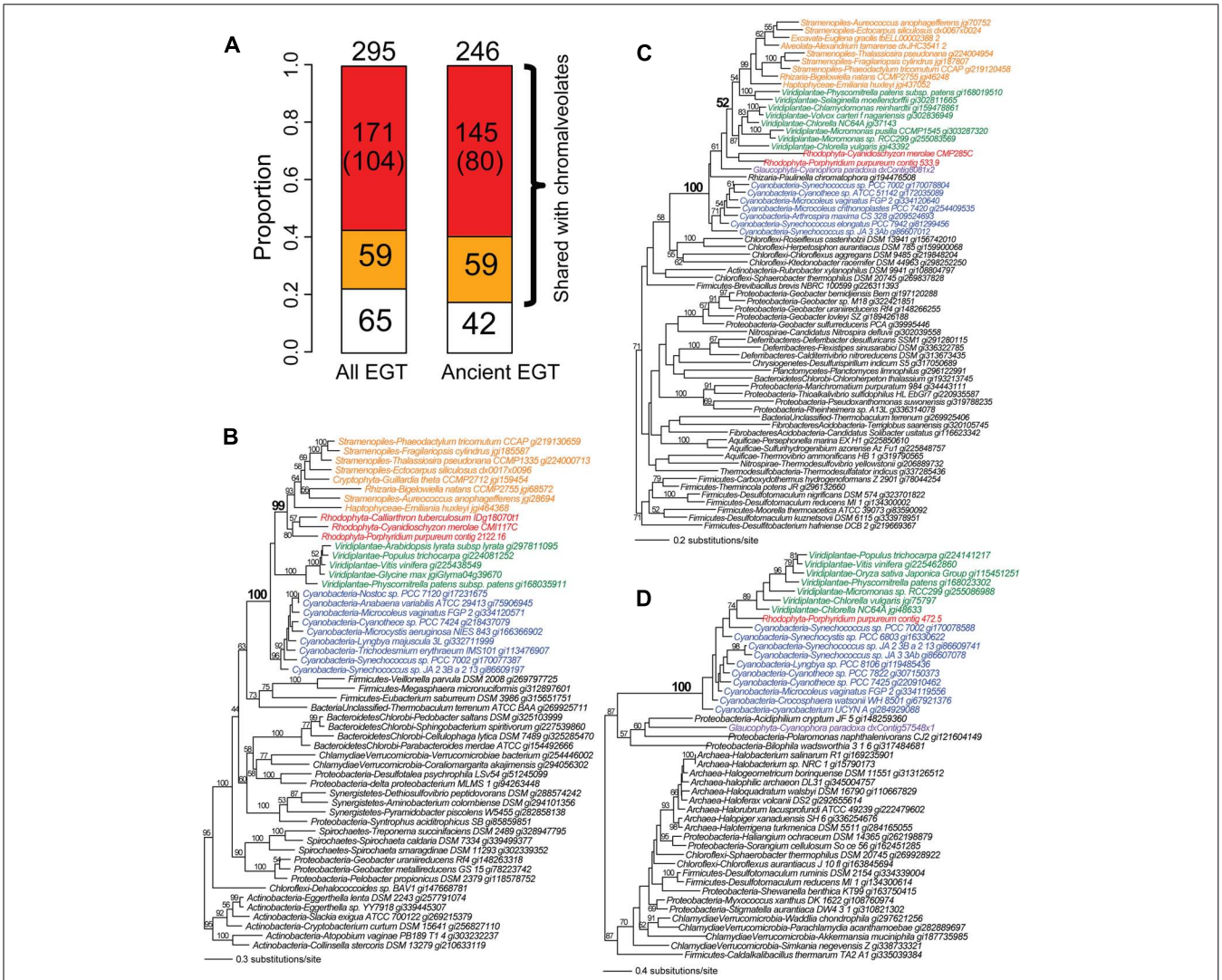

FIGURE 2 | The fate of cyanobacterium derived EGTs in the red alga *Porphyridium purpureum*. (A) Proportion of *Porphyridium purpureum* genes shared with chromalveolates. The red color indicates red algal secondary endosymbiotic gene transfer (EGT) reflected by *Porphyridium purpureum*-chromalveolate monophyly. The number in the parenthesis indicates *Porphyridium purpureum*-chromalveolate monophyly with ≥ 60% bootstrap value (e.g., **Figure 2B**). The orange color indicates other scenarios of red/green algal EGT into chromalveolates (e.g., **Figure 2C**). The white color indicates red algal EGT that have no apparent homologs in chromalveolates (e.g., **Figure 2D**). Ancient EGTs refer to genes shared by red algae and glaucophytes or green alga/plants and excludes red algal-specific EGTs. **(B)** Maximum likelihood phylogeny of an ABC transporter. **(C)** Maximum likelihood phylogeny of an acetyl ornithine aminotransferase. **(D)** Maximum likelihood phylogeny of a prenyltransferase. All RAxML bootstrap values were determined using 100 replicates and only bootstrap values ≥50% are shown.

RED ALGAE MEDIATE CYANOBACTERIAL GENE TRANSFER INTO CHROMALVEOLATES

Given the evidence for massive prokaryote-to-eukaryote gene transfer *via* primary endosymbiosis and eukaryote-to-eukaryote gene transfer *via* secondary and tertiary endosymbiosis, we hypothesize that primary plastid-containing algae (red or green algae) have played a central role as mediators of the spread of prokaryotic genes into eukaryotes. We used the phylogenomic results from the recently generated *Porphyridium purpureum* genome (Bhattacharya et al., 2013) to test this idea. Using a cutoff of ≥60% bootstrap support for *Porphyridium purpureum*-cyanobacterium gene monophyly (followed by manual inspection), we identified 295 cyanobacterium-derived (i.e., *via* EGT) genes in the red alga. Of these, 78% (230/295) were shared with chromalveolates (**Figure 2A**) and among these proteins, 74% (171/230) likely owe their origin to red algal secondary endosymbiosis. The latter value was determined by counting all cases of *Porphyridium purpureum*-chromalveolate monophyly, regardless of bootstrap value. When the bootstrap cutoff ≥60% was applied to *Porphyridium purpureum*-chromalveolate monophyly, the number was 45% (104/230). A typical example of this class is an ABC transporter that is shared exclusively by cyanobacteria, red/green algae, and chromalveolates (100% bootstrap value). Among this group, the red alga (including *Porphyridium purpureum*) sequences are monophyletic with chromalveolates (99% bootstrap value, **Figure 2B**). The remaining 59 cases of EGT shared with chromalveolates represent putative outcomes of a cryptic green algal endosymbiosis or have ambiguous evolutionary histories (**Figures 2A,C**, which is a tree of an acetyl ornithine aminotransferase). A total of 22% (65/295) of the 295 EGT-derived genes have no identifiable homologs in chromalveolates (e.g., a prenyltransferase gene tree shown in **Figure 2D**). Because much of EGT presumably took place early in Plantae evolution, similar results are obtained when the analysis is limited to ancient

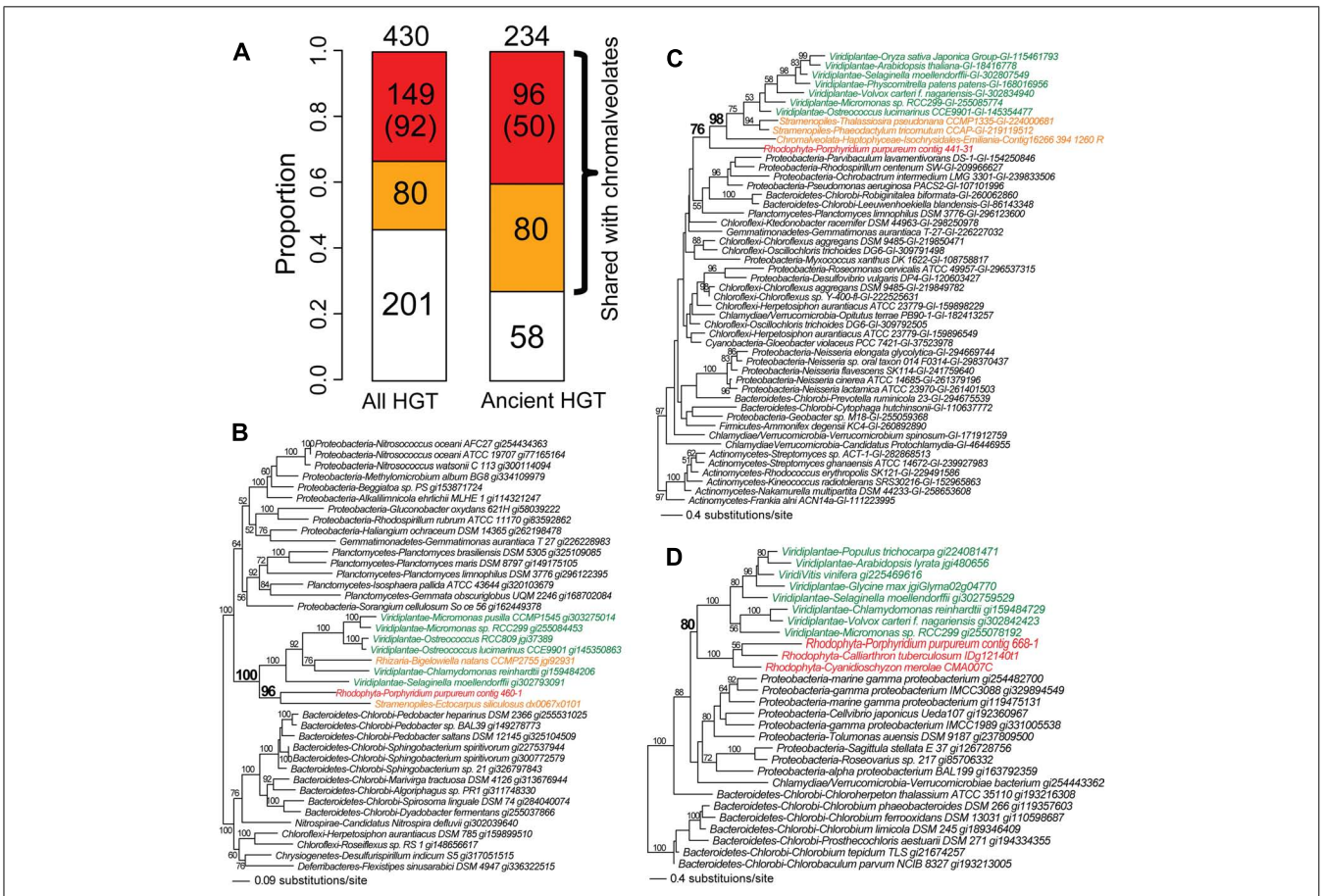

FIGURE 3 | Fate of non-cyanobacterium derived HGTs in the red alga *Porphyridium purpureum*. (A) The proportion of *Porphyridium purpureum* HGTs shared with chromalveolates. The red color indicates secondary EGT of HGT-derived genes in red algae based on *Porphyridium purpureum*-chromalveolate monophyly. The number in parenthesis indicates *Porphyridium purpureum*-chromalveolate monophyly with ≥ 60% bootstrap value (e.g., **Figure 3B**). The orange color indicates other scenarios of red/green algal HGTs into chromalveolates (e.g., **Figure 3C**). The white color indicates red algal HGTs that have no homologs in chromalveolates (e.g., **Figure 3D**). Ancient HGTs refer to genes shared by red algae and glaucophytes or green algae/plants, with exclusion of red algal-specific HGTs. **(B)** Maximum likelihood phylogeny of an ABC transporter. **(C)** Maximum likelihood phylogeny of a transmembrane transport protein. **(D)** Maximum likelihood phylogeny of a serine acetyltransferase. All RAxML bootstrap values were determined using 100 replicates and only bootstrap values ≥50% are shown.

cases of EGT; i.e., genes are counted when shared by *Porphyridium purpureum*, glaucophytes, and/or green algae and land plants (**Figure 2A**).

RED ALGAE MEDIATE NON-CYANOBACTERIAL GENE TRANSFER INTO CHROMALVEOLATES

We identified the instances of non-cyanobacterium-derived HGT in *Porphyridium purpureum*. This number (following manual inspection) was 430 genes at a bootstrap cutoff ≥60%. Of these, 53% (229/430) is shared with chromalveolates, of which 65% (149/229) is likely derived from red algal secondary endosymbiosis, reflecting *Porphyridium purpureum*-chromalveolate monophyly regardless of bootstrap support (**Figure 3A**). This proportion reduces to 40% (92/229) when the bootstrap cutoff ≥60% is applied to *Porphyridium purpureum*-chromalveolate monophyly (**Figure 3A**). One example is an ABC transporter phylogeny (**Figure 3B**) that includes only bacterial and algal sequences. In this tree, *Porphyridium purpureum* forms a monophyletic group with the brown alga *E. siliculosus* (98% bootstrap value) and is sister to a group of green algae and land plant sequences. The *Bigelowiella natans* sequence is nested within green algae, consistent with a secondary endosymbiotic origin of this gene (**Figure 3B**). The remaining 80 HGT-derived genes shared with chromalveolates represent either cryptic green algal endosymbiosis or ambiguous evolutionary histories (**Figure 3A**). An example is a transmembrane transport protein phylogeny that includes only bacterial and algal sequences. In this tree, green algae and land plants form a monophyletic group with chromalveolates (98% bootstrap value) with the exclusion of *Porphyridium purpureum* (**Figure 3C**). The remainder of non-cyanobacterial HGTs (47%, 201/430) is not shared with chromalveolates (e.g., serine acetyltransferase phylogeny, **Figure 3D**).

Among the 430 cases of non-cyanobacterium HGTs in *Porphyridium purpureum*, 234 are shared with glaucophytes or green algae/land plants and likely represent ancient HGT events, consistent with the prevalence of ancient HGT in Plantae (Huang and Yue, 2013). This is comparable to the number of ancient EGTs (246, **Figure 2A**) derived from the cyanobacterial endosymbiont that are shared by the three Plantae lineages. Because independent HGTs are less likely to result in a large number of shared genes among taxa, the extensive shared footprint of ancient non-cyanobacterial HGT provides additional support for the monophyly of Plantae (Price et al., 2012; Spiegel, 2012). Finally, if we limit our analysis to the 234 cases of ancient HGT (**Figure 3A**), then the proportion of *Porphyridium purpureum* genes shared with chromalveolates increases to 75% (176/234; **Figure 3A**). This approaches the number (83%, 204/246) of ancient EGTs that we identified in our study. These results underline the significance of ancient non-cyanobacterial HGT in enriching red algal genomes and the subsequent movement of these genes *via* secondary endosymbiosis to chromalveolates.

CONCLUSION

Ancient red algae (e.g., the ancestor of taxa such as *Porphyridium purpureum*) appear to have mediated transfers of ∼300 prokaryotic genes into chromalveolates. In addition to the expected transfer of cyanobacterium-derived genes *via* EGT, a comparable number of non-cyanobacterium-derived genes, particularly those acquired early in Plantae evolution, appear to have undergone inter-phylum gene transfer. This role of red algae as mediators of gene transfer (exemplified by *Porphyridium purpureum*) is applicable to endosymbionts of other secondary and tertiary endosymbiosis (e.g., green algae). These data suggest a previously under-appreciated source of reticulate gene ancestry among photosynthetic eukaryotes that has great implications for the origin of novel gene functions in algae and for inference of ancient phylogenetic relationships in the tree of life (Lane and Archibald, 2008; Chan et al., 2012a).

ACKNOWLEDGMENTS

This research was supported by a grant from the National Science Foundation awarded to Debashish Bhattacharya (0936884) and Hwan Su Yoon (1317114) and a Korean RDA grant (SSAC PJ009525) awarded to Hwan Su Yoon. We thank Dr. Eun Chan Yang (Korea Institute of Ocean Science and Technology) for assistance in the preparation of **Figure 1**.

REFERENCES

Adl, S. M., Simpson, A. G., Farmer, M. A., Andersen, R. A., Anderson, O. R., Barta, J. R., et al. (2005). The new higher level classification of eukaryotes with emphasis on the taxonomy of protists. *J Eukaryot. Microbiol.* 52, 399–451. doi: 10.1111/j.1550-7408.2005.00053.x

Andersson, J. O. (2009). Gene transfer and diversification of microbial eukaryotes. *Annu. Rev. Microbiol.* 63, 177–193. doi: 10.1146/annurev.micro.091208.073203

Archibald, J. M., and Keeling, P. J. (2002). Recycled plastids: a "green movement" in eukaryotic evolution. *Trends Genet.* 18, 577–584. doi: 10.1016/S0168-9525(02)02777-4

Archibald, J. M., Rogers, M. B., Toop, M., Ishida, K., and Keeling, P. J. (2003). Lateral gene transfer and the evolution of plastid-targeted proteins in the secondary plastid-containing alga *Bigelowiella natans*. *Proc. Natl. Acad. Sci. U.S.A.* 100, 7678–7683. doi: 10.1073/pnas.1230951100

Armbrust, E. V., Berges, J. A., Bowler, C., Green, B. R., Martinez, D., Putnam, N. H., et al. (2004). The genome of the diatom *Thalassiosira pseudonana*: ecology, evolution, and metabolism. *Science* 306, 79–86. doi: 10.1126/science.1101156

Ball, S. G., Subtil, A., Bhattacharya, D., Moustafa, A., Weber, A. P., Gehre, L., et al. (2013). Metabolic effectors secreted by bacterial pathogens: essential facilitators of plastid endosymbiosis? *Plant Cell* 25, 7–21. doi: 10.1105/tpc.112.101329

Baum, D. (2013). The origin of primary plastids: a pas de deux or a menage a trois? *Plant Cell* 25, 4–6. doi: 10.1105/tpc.113.109496

Becker, B., Hoef-Emden, K., and Melkonian, M. (2008). Chlamydial genes shed light on the evolution of photoautotrophic eukaryotes. *BMC Evol. Biol.* 8:203. doi: 10.1186/1471-2148-8-203

Bhattacharya, D., Price, D., Chan, C. X., Qiu, H., Rose, N., Ball, S., et al. (2013). Genome of the red alga *Porphyridium purpureum*. *Nat. Commun.* 4, 1941. doi: 10.1038/ncomms2931

Bhattacharya, D., Yoon, H. S., and Hackett, J. D. (2004). Photosynthetic eukaryotes unite: endosymbiosis connects the dots. *Bioessays* 26, 50–60. doi: 10.1002/bies.10376

Blanc, G., Agarkova, I., Grimwood, J., Kuo, A., Brueggeman, A., Dunigan, D. D., et al. (2012). The genome of the polar eukaryotic microalga *Coccomyxa subellipsoidea* reveals traits of cold adaptation. *Genome Biol.* 13, R39. doi: 10.1186/gb-2012-13-5-r39

Blanc, G., Duncan, G., Agarkova, I., Borodovsky, M., Gurnon, J., Kuo, A., et al. (2010). The *Chlorella variabilis* NC64A genome reveals adaptation to photosymbiosis, coevolution with viruses, and cryptic sex. *Plant Cell* 22, 2943–2955. doi: 10.1105/tpc.110.076406

Boucher, Y., Douady, C. J., Papke, R. T., Walsh, D. A., Boudreau, M. E., Nesbo, C. L., et al. (2003). Lateral gene transfer and the origins of prokaryotic groups. *Annu. Rev. Genet.* 37, 283–328. doi: 10.1146/annurev.genet.37.050503.084247

Bowler, C., Allen, A. E., Badger, J. H., Grimwood, J., Jabbari, K., Kuo, A., et al. (2008). The *Phaeodactylum*

genome reveals the evolutionary history of diatom genomes. *Nature* 456, 239–244. doi: 10.1038/nature07410

Cavalier-Smith, T. (1999). Principles of protein and lipid targeting in secondary symbiogenesis: euglenoid, dinoflagellate, and sporozoan plastid origins and the eukaryote family tree. *J. Eukaryot. Microbiol.* 46, 347–366. doi: 10.1111/j.1550-7408.1999.tb04614.x

Chan, C. X., Bhattacharya, D., and Reyes-Prieto, A. (2012a). Endosymbiotic and horizontal gene transfer in microbial eukaryotes: impacts on cell evolution and the tree of life. *Mob. Genet. Elements* 2, 101–105. doi: 10.4161/mge.20110

Chan, C. X., Soares, M. B., Bonaldo, M. F., Wisecaver, J. H., Hackett, J. D., Anderson, D. M., et al. (2012b). Analysis of *Alexandrium tamarense* (Dinophyceae) genes reveals the complex evolutionary history of a microbial eukaryote. *J. Phycol.* 48, 1130–1142. doi: 10.1111/j.1529-8817.2012.01194.x

Chan, C. X., Yang, E. C., Banerjee, T., Yoon, H. S., Martone, P. T., Estevez, J. M., et al. (2011). Red and green algal monophyly and extensive gene sharing found in a rich repertoire of red algal genes. *Curr. Biol.* 21, 328–333. doi: 10.1016/j.cub.2011.01.037

Chesnick, J. M., Kooistra, W. H., Wellbrock, U., and Medlin, L. K. (1997). Ribosomal RNA analysis indicates a benthic pennate diatom ancestry for the endosymbionts of the dinoflagellates *Peridinium foliaceum* and *Peridinium balticum* (Pyrrhophyta). *J. Eukaryot. Microbiol.* 44, 314–320. doi: 10.1111/j.1550-7408.1997.tb05672.x

Chesnick, J. M., Morden, C. W., and Schmieg, A. M. (1996). Identity of the endosymbiont of *Peridinium foliaceum* (Pyrrophyta): analysis of the rbcLS operon. *J. Phycol.* 32, 850–857. doi: 10.1111/j.0022-3646.1996.00850.x

Cock, J. M., Sterck, L., Rouze, P., Scornet, D., Allen, A. E., Amoutzias, G., et al. (2010). The *Ectocarpus* genome and the independent evolution of multicellularity in brown algae. *Nature* 465, 617–621. doi: 10.1038/nature09016

Collen, J., Porcel, B., Carre, W., Ball, S. G., Chaparro, C., Tonon, T., et al. (2013). Genome structure and metabolic features in the red seaweed *Chondrus crispus* shed light on evolution of the Archaeplastida. *Proc. Natl. Acad. Sci. U.S.A.* 110, 5247–5252. doi: 10.1073/pnas.1221259110

Curtis, B. A., Tanifuji, G., Burki, F., Gruber, A., Irimia, M., Maruyama, S., et al. (2012). Algal genomes reveal evolutionary mosaicism and the fate of nucleomorphs. *Nature* 492, 59–65. doi: 10.1038/nature11681

Dagan, T., Roettger, M., Stucken, K., Landan, G., Koch, R., Major, P., et al. (2013). Genomes of Stigonematalean cyanobacteria (subsection V) and the evolution of oxygenic photosynthesis from prokaryotes to plastids. *Genome Biol. Evol.* 5, 31–44. doi: 10.1093/gbe/evs117

Derelle, E., Ferraz, C., Rombauts, S., Rouze, P., Worden, A. Z., Robbens, S., et al. (2006). Genome analysis of the smallest free-living eukaryote *Ostreococcus tauri* unveils many unique features. *Proc. Natl. Acad. Sci. U.S.A.* 103, 11647–11652. doi: 10.1073/pnas.0604795103

Deusch, O., Landan, G., Roettger, M., Gruenheit, N., Kowallik, K. V., Allen, J. F., et al. (2008). Genes of cyanobacterial origin in plant nuclear genomes point to a heterocyst-forming plastid ancestor. *Mol. Biol. Evol.* 25, 748–761. doi: 10.1093/molbev/msn022

Doolittle, W. F. (1999). Lateral genomics. *Trends Cell Biol.* 9, M5–M8. doi: 10.1016/S0962-8924(99)01664-5

Dorrell, R. G., and Smith, A. G. (2011). Do red and green make brown?: perspectives on plastid acquisitions within chromalveolates. *Eukaryot. Cell* 10, 856–868. doi: 10.1128/EC.00326-10

Douglas, S., Zauner, S., Fraunholz, M., Beaton, M., Penny, S., Deng, L. T., et al. (2001). The highly reduced genome of an enslaved algal nucleus. *Nature* 410, 1091–1096. doi: 10.1038/35074092

Dunning Hotopp, J. C. (2011). Horizontal gene transfer between bacteria and animals. *Trends Genet.* 27, 157–163. doi: 10.1016/j.tig.2011.01.005

Field, C. B., Behrenfeld, M. J., Randerson, J. T., and Falkowski, P. (1998). Primary production of the biosphere: integrating terrestrial and oceanic components. *Science* 281, 237–240. doi: 10.1126/science.281.5374.237

Frommolt, R., Werner, S., Paulsen, H., Goss, R., Wilhelm, C., Zauner, S., et al. (2008). Ancient recruitment by chromists of green algal genes encoding enzymes for carotenoid biosynthesis. *Mol. Biol. Evol.* 25, 2653–2667. doi: 10.1093/molbev/msn206

Gogarten, J. P., Doolittle, W. F., and Lawrence, J. G. (2002). Prokaryotic evolution in light of gene transfer. *Mol. Biol. Evol.* 19, 2226–2238. doi: 10.1093/oxfordjournals.molbev.a004046

Gilson, P. R., Su, V., Slamovits, C. H., Reith, M. E., Keeling, P. J., and McFadden, G. I. (2006). Complete nucleotide sequence of the chlorarachniophyte nucleomorph: nature's smallest nucleus. *Proc. Natl. Acad. Sci. U.S.A.* 103, 9566–9571. doi: 10.1073/pnas.0600707103

Hansen, G., Daugbjerg, N., and Henriksen, P. (2000). Comparative study of *Gymnodinium mikimotoi* and *Gymnodinium aureolum*, comb. nov. (= *Gyrodinium aureolum*) based on morphology, pigment composition, and molecular data. *J. Phycol.* 36, 394–410. doi: 10.1046/j.1529-8817.2000.99172.x

Horn, M. (2008). Chlamydiae as symbionts in eukaryotes. *Annu. Rev. Microbiol.* 62, 113–131. doi: 10.1146/annurev.micro.62.081307.162818

Huang, J., and Gogarten, J. P. (2007). Did an ancient chlamydial endosymbiosis facilitate the establishment of primary plastids? *Genome Biol.* 8, R99. doi: 10.1186/gb-2007-8-6-r99

Huang, J., and Yue, J. (2013). Horizontal gene transfer in the evolution of photosynthetic eukaryotes. *J. Syst. Evol.* 51, 13–29. doi: 10.1111/j.1759-6831.2012.00237.x

Ishida, K., and Green, B. R. (2002). Second- and third-hand chloroplasts in dinoflagellates: phylogeny of oxygen-evolving enhancer 1 (PsbO) protein reveals replacement of a nuclear-encoded plastid gene by that of a haptophyte tertiary endosymbiont. *Proc. Natl. Acad. Sci. U.S.A.* 99, 9294–9299. doi: 10.1073/pnas.142091799

Keeling, P. J. (2009). Chromalveolates and the evolution of plastids by secondary endosymbiosis. *J. Eukaryot. Microbiol.* 56, 1–8. doi: 10.1111/j.1550-7408.2008.00371.x

Keeling, P. J. (2010). The endosymbiotic origin, diversification, and fate of plastids. *Philos. Trans. R. Soc. Lond. B Biol. Sci.* 365, 729–748. doi: 10.1098/rstb.2009.0103

Keeling, P. J., and Palmer, J. D. (2008). Horizontal gene transfer in eukaryotic evolution. *Nat. Rev. Genet.* 9, 605–618. doi: 10.1038/nrg2386

Kim, M., Nam, S. W., Shin, W., Coats, D. W., and Park, M. G. (2012). *Dinophysis caudata* (Dinophyceae) sequesters and retains plastids from the mixotrophic ciliate prey *Mesodinium rubrum*. *J. Phycol.* 48, 569–579. doi: 10.1111/j.1529-8817.2012.01150.x

Kleine, T., Maier, U. G., and Leister, D. (2009). DNA transfer from organelles to the nucleus: the idiosyncratic genetics of endosymbiosis. *Annu. Rev. Plant Biol.* 60, 115–138. doi: 10.1146/annurev.arplant.043008.092119

Lane, C. E., and Archibald, J. M. (2008). The eukaryotic tree of life: endosymbiosis takes its TOL. *Trends Ecol. Evol.* 23, 268–275. doi: 10.1016/j.tree.2008.02.004

Lane, C. E., van den Heuvel, K., Kozera, C., Curtis, B. A., Parsons, B. J., Bowman, S., et al. (2007). Nucleomorph genome of *Hemiselmis andersenii* reveals complete intron loss and compaction as a driver of protein structure and function. *Proc. Natl. Acad. Sci. U.S.A.* 104, 19908–19913. doi: 10.1073/pnas.0707419104

Lauterborn, R. (1895). Protozoenstudien II. *Paulinella chromatophora* nov. gen., nov. spec., ein beschalter Rhizopode des Susswassers mit blaugrunen chromatophorenartigen Einschlussen. *Z. Wiss. Zool.* 59, 537–544.

Li, H. M., and Chiu, C. C. (2010). Protein transport into chloroplasts. *Annu. Rev. Plant Biol.* 61, 157–180. doi: 10.1146/annurev-arplant-042809-112222

Martin, W., Rujan, T., Richly, E., Hansen, A., Cornelsen, S., Lins, T., et al. (2002). Evolutionary analysis of *Arabidopsis*, cyanobacterial, and chloroplast genomes reveals plastid phylogeny and thousands of cyanobacterial genes in the nucleus. *Proc. Natl. Acad. Sci. U.S.A.* 99, 12246–12251. doi: 10.1073/pnas.182432999

Moestrup, O., and Sengco, M. (2001). Ultrastructural studies on *Bigelowiella natans*, gen. et sp. nov., a chlorarachniophyte flagellate. *J. Phycol.* 37, 624–646. doi: 10.1046/j.1529-8817.2001.037004624.x

Moore, C. E., and Archibald, J. M. (2009). Nucleomorph genomes. *Annu. Rev. Genet.* 43, 251–264. doi: 10.1146/annurev-genet-102108-134809

Moore, C. E., Curtis, B., Mills, T., Tanifuji, G., and Archibald, J. M. (2012). Nucleomorph genome sequence of the cryptophyte alga *Chroomonas mesostigmatica* CCMP1168 reveals lineage-specific gene loss and genome complexity. *Genome Biol. Evol.* 4, 1162–1175. doi: 10.1093/gbe/evs090

Moreau, H., Verhelst, B., Couloux, A., Derelle, E., Rombauts, S., Grimsley, N., et al. (2012). Gene functionalities and genome structure in *Bathycoccus prasinos* reflect cellular specializations at the base of the green lineage. *Genome Biol.* 13, R74. doi: 10.1186/gb-2012-13-8-r74

Moustafa, A., Beszteri, B., Maier, U. G., Bowler, C., Valentin, K., and Bhattacharya, D. (2009). Genomic footprints of a cryptic plastid endosymbiosis in diatoms. *Science* 324, 1724–1726. doi: 10.1126/science.1172983

Moustafa, A., and Bhattacharya, D. (2008). PhyloSort: a user-friendly phylogenetic sorting tool and its application to estimating the cyanobacterial contribution to the nuclear genome of *Chlamydomonas*. *BMC Evol. Biol.* 8:6. doi: 10.1186/1471-2148-8-6

Moustafa, A., Reyes-Prieto, A., and Bhattacharya, D. (2008). Chlamydiae has contributed at least 55 genes to Plantae with predominantly plastid functions. *PLoS ONE* 3:e2205. doi: 10.1371/journal.pone.0002205

Nosenko, T., Lidie, K. L., Van Dolah, F. M., Lindquist, E., Cheng, J. F., and Bhattacharya, D. (2006). Chimeric plastid proteome in the Florida "red tide" dinoflagellate *Karenia brevis*. *Mol. Biol. Evol.* 23, 2026–2038. doi: 10.1093/molbev/msl074

Nowack, E. C., Melkonian, M., and Glockner, G. (2008). Chromatophore genome sequence of *Paulinella* sheds light on acquisition of photosynthesis by eukaryotes. *Curr. Biol.* 18, 410–418. doi: 10.1016/j.cub.2008.02.051

Park, M. G., Kim, M., Kim, S., and Yih, W. (2010). Does *Dinophysis caudata* (Dinophyceae) have permanent plastids? *J. Phycol.* 46, 236–242. doi: 10.1111/j.1529-8817.2009.00777.x

Price, D. C., Chan, C. X., Yoon, H. S., Yang, E. C., Qiu, H., Weber, A. P., et al. (2012). *Cyanophora paradoxa* genome elucidates origin of photosynthesis in algae and plants. *Science* 335, 843–847. doi: 10.1126/science.1213561

Reyes-Prieto, A., Hackett, J. D., Soares, M. B., Bonaldo, M. F., and Bhattacharya, D. (2006). Cyanobacterial contribution to algal nuclear genomes is primarily limited to plastid functions. *Curr. Biol.* 16, 2320–2325. doi: 10.1016/j.cub.2006.09.063

Reyes-Prieto, A., Moustafa, A., and Bhattacharya, D. (2008). Multiple genes of apparent algal origin suggest ciliates may once have been photosynthetic. *Curr. Biol.* 18, 956–962. doi: 10.1016/j.cub.2008.05.042

Rodriguez-Ezpeleta, N., Brinkmann, H., Burey, S. C., Roure, B., Burger, G., Loffelhardt, W., et al. (2005). Monophyly of primary photosynthetic eukaryotes: green plants, red algae, and glaucophytes. *Curr. Biol.* 15, 1325–1330. doi: 10.1016/j.cub.2005.06.040

Rogers, M. B., Gilson, P. R., Su, V., McFadden, G. I., and Keeling, P. J. (2007). The complete chloroplast genome of the chlorarachniophyte *Bigelowiella natans*: evidence for independent origins of chlorarachniophyte and euglenid secondary endosymbionts. *Mol. Biol. Evol.* 24, 54–62. doi: 10.1093/molbev/msl129

Sato, N., Ishikawa, M., Fujiwara, M., and Sonoike, K. (2005). Mass identification of chloroplast proteins of endosymbiont origin by phylogenetic profiling based on organism-optimized homologous protein groups. *Genome Inform.* 16, 56–68.

Schoenknecht, G., Chen, W. H., Ternes, C. M., Barbier, G. G., Shrestha, R. P., Stanke, M., et al. (2013). Gene transfer from bacteria and archaea facilitated evolution of an extremophilic eukaryote. *Science* 339, 1207–1210. doi: 10.1126/science.1231707

Simon, N., Cras, A. L., Foulon, E., and Lemee, R. (2009). Diversity and evolution of marine phytoplankton. *C. R. Biol.* 332, 159–170. doi: 10.1016/j.crvi.2008.09.009

Spiegel, F. W. (2012). Contemplating the first Plantae. *Science* 335, 809–810. doi: 10.1126/science.1218515

Stiller, J. W., Huang, J., Ding, Q., Tian, J., and Goodwillie, C. (2009). Are algal genes in nonphotosynthetic protists evidence of historical plastid endosymbioses? *BMC Genomics* 10:484. doi: 10.1186/1471-2164-10-484

Tanifuji, G., Onodera, N. T., Wheeler, T. J., Dlutek, M., Donaher, N., and Archibald, J. M. (2011). Complete nucleomorph genome sequence of the non-photosynthetic alga *Cryptomonas paramecium* reveals a core nucleomorph gene set. *Genome Biol. Evol.* 3, 44–54. doi: 10.1093/gbe/evq082

Timmis, J. N., Ayliffe, M. A., Huang, C. Y., and Martin, W. (2004). Endosymbiotic gene transfer: organelle genomes forge eukaryotic chromosomes. *Nat. Rev. Genet.* 5, 123–135. doi: 10.1038/nrg1271

Tyler, B. M., Tripathy, S., Zhang, X., Dehal, P., Jiang, R. H., Aerts, A., et al. (2006). *Phytophthora* genome sequences uncover evolutionary origins and mechanisms of pathogenesis. *Science* 313, 1261–1266. doi: 10.1126/science.1128796

Wijayawardena, B. K., Minchella, D. J., and DeWoody, J. A. (2013). Hosts, parasites, and horizontal gene transfer. *Trends Parasitol.* 29, 329–338. doi: 10.1016/j.pt.2013.05.001

Worden, A. Z., Lee, J. H., Mock, T., Rouze, P., Simmons, M. P., Aerts, A. L., et al. (2009). Green evolution and dynamic adaptations revealed by genomes of the marine picoeukaryotes *Micromonas*. *Science* 324, 268–272. doi: 10.1126/science.1167222

Yoon, H. S., Reyes-Prieto, A., Melkonian, M., and Bhattacharya, D. (2006). Minimal plastid genome evolution in the *Paulinella* endosymbiont. *Curr. Biol.* 16, R670–R672. doi: 10.1016/j.cub.2006.08.018

Yue, J., Hu, X., Sun, H., Yang, Y., and Huang, J. (2012). Widespread impact of horizontal gene transfer on plant colonization of land. *Nat. Commun.* 3, 1152. doi: 10.1038/ncomms2148

Conflict of Interest Statement: The authors declare that the research was conducted in the absence of any commercial or financial relationships that could be construed as a potential conflict of interest.

Received: 04 July 2013; paper pending published: 01 August 2013; accepted: 28 August 2013; published online: 19 September 2013.

*Citation: Qiu H, Yoon HS and Bhattacharya D (2013) Algal endosymbionts as vectors of horizontal gene transfer in photosynthetic eukaryotes. Front. Plant Sci. **4**:366. doi: 10.3389/fpls.2013.00366*

This article was submitted to Plant Physiology, a section of the journal Frontiers in Plant Science.

frontiers in
PLANT SCIENCE

ORIGINAL RESEARCH ARTICLE
published: 30 August 2013
doi: 10.3389/fpls.2013.00328

Comparison of calculated and experimental isotope edited FTIR difference spectra for purple bacterial photosynthetic reaction centers with different quinones incorporated into the Q_A binding site

Nan Zhao, Hari P. Lamichhane and Gary Hastings*

Department of Physics and Astronomy, Georgia State University, Atlanta, GA, USA

Edited by:
Harvey J. M. Hou, Alabama State University, USA

Reviewed by:
Suleyman I. Allakhverdiev, Russian Academy of Sciences, Russia
Art Van Der Est, Brock University, Canada

***Correspondence:**
Gary Hastings, Department of Physics and Astronomy, Georgia State University, 26 Park Place, Suite 605., Atlanta, GA 30303, USA
e-mail: ghastings@gsu.edu

Previously we have shown that ONIOM type (QM/MM) calculations can be used to simulate isotope edited FTIR difference spectra for neutral ubiquinone in the Q_A binding site in *Rhodobacter sphaeroides* photosynthetic reaction centers. Here we considerably extend upon this previous work by calculating isotope edited FTIR difference spectra for reaction centers with a variety of unlabeled and ^{18}O labeled foreign quinones incorporated into the Q_A binding site. Isotope edited spectra were calculated for reaction centers with 2,3-dimethoxy-5,6-dimethyl-1,4-benzoquinone (MQ_0), 2,3,5,6-tetramethyl-1,4-benzoquinone (duroquinone, DQ), and 2,3-dimethyl-l,4-naphthoquinone (DMNQ) incorporated, and compared to corresponding experimental spectra. The calculated and experimental spectra agree well, further demonstrating the utility and applicability of our ONIOM approach for calculating the vibrational properties of pigments in protein binding sites. The normal modes that contribute to the bands in the calculated spectra, their composition, frequency, and intensity, and how these quantities are modified upon ^{18}O labeling, are presented. This computed information leads to a new and more detailed understanding/interpretation of the experimental FTIR difference spectra. Hydrogen bonding to the carbonyl groups of the incorporated quinones is shown to be relatively weak. It is also shown that there is some asymmetry in hydrogen bonding, accounting for 10–13 cm^{-1} separation in the frequencies of the carbonyl vibrational modes of the incorporated quinones. The extent of asymmetry in H-bonding could only be established by considering the spectra for various types of quinones incorporated into the Q_A binding site. The quinones listed above are "tail-less." Spectra were also calculated for reaction centers with corresponding "tail" containing quinones incorporated, and it is found that replacement of the quinone methyl group by a phytyl or prenyl chain does not alter ONIOM calculated spectra.

Keywords: ONIOM, FTIR, QA, quinone, reaction center, density functional theory (DFT) calculations

INTRODUCTION

Quinones play an important role in biological proton and electron transfer processes that occur in both respiration and photosynthesis (Trumpower, 1982). In type II photosynthetic reaction centers two quinone molecules act as terminal electron acceptors (Ke, 2001a,b). The two quinones are often termed Q_A and Q_B. In this manuscript we will refer to the quinone binding site as Q_A and Q_B, however. The quinones that occupy the Q_A and Q_B binding sites have very different functions. The Q_A quinone is an intermediary cofactor involved in transferring electrons from (bacterio) pheophytin to Q_B, while the Q_B quinone couples proton and electron transfer processes (Ke, 2001b,c,d).

In this manuscript we focus on the Q_A binding site. The quinone occupying the Q_A binding site is species dependent. In *Rhodobacter (Rb.) sphaeroides* purple bacterial reaction centers (PBRCs) a ubiquinone (UQ) molecule occupies the Q_A binding site. In PBRCs from *Blastochloris viridis* (Shopes and Wraight, 1985) and *Chloroflexus aurantiacus* (Hale et al., 1983) a menaquinone occupies the Q_A binding site. In photosystem II reaction centers from oxygen evolving organisms, a plastoquinone (PQ) molecule occupies the Q_A binding site. In photosystem I the secondary electron acceptor, termed A_1, is a vitamin K_1 (VK) molecule (also called phylloquinone). Menaquinone and VK are both naphthoquinone (NQ) moieties that differ only in the degree of saturation of the tail at C_6.

Abbreviations: Ala, alanine; DS, difference spectra/spectrum spectroscopy or spectroscopic; C=O, carbonyl; DQ, duroquinone or 2,3,5,6-tetramethyl-1,4-benzoquinone; DFT, density functional theory; DMNQ, dimethyl naphthoquinone; ET, electron transfer; FTIR, Fourier Transform Infra-red; H-bond, hydrogen bond; His, histidine; MQ_0, 2,3-dimethoxy-5,6-dimethyl-1,4-benzoquinone; MM, molecular mechanics; NQ, naphthoquinone; PQ, plastoquinone; PBRC, purple bacterial reaction center; PED, potential energy distribution; *Rb.*, *Rhodobacter*; QM, quantum mechanics; UQ_n, ubiquinone-n; VK, vitamin K_1 (phylloquinone).

Figure 1 shows the structure, numbering and abbreviations we will use for the various quinones discussed in this manuscript. MQ_0 and DMNQ are UQ and VK analogues, respectively, in which the hydrocarbon tail has been replaced with a methyl group. DQ is a PQ analogue in which the hydrocarbon chain at C_6 is replaced with a methyl group.

It has been suggested, at least for the UQ that occupies the Q_A site in PBRCs, that the role of the hydrocarbon chain at C_6 is to anchor and orient the quinone head-group in a specific way (Warncke et al., 1994). Data is available that may argue against this proposal, however, (McComb et al., 1990; Srinivasan and Golbeck, 2009; Wraight and Gunner, 2009).

Comparison of the properties of PBRCs with MQ_0 and UQ_n, or VK and DMNQ, incorporated into the Q_A binding site will allow one to assess how or if the hydrocarbon chain at C_6 modifies the quinones functional properties. Similarly, comparison of the properties of PBRCs with MQ_0 and DQ incorporated into the Q_A binding site will allow one to assess how or if the methoxy groups at C_2 and C_3 modifies the quinones functional properties. Calculated spectra for *Rb. sphaeroides* PBRCs with VK in the Q_A binding site can be compared to experimental spectra. These calculated spectra may also serve as a useful model for *B. viridis* PBRCs that naturally have VK incorporated into the Q_A binding site.

Fourier transform infrared (FTIR) difference spectroscopy (DS) is a sensitive molecular-level probe of pigment-protein interactions, and it is widely used to study both the neutral and reduced states of quinones in PBRCs (Breton and Nabedryk, 1996) and in photosystem II (Noguchi and Berthomieu, 2005). In this manuscript we focus on Q_A^-/Q_A FTIR DS. Many molecular species contribute to Q_A^-/Q_A FTIR DS, and in the past it has been difficult to identify which bands are associated specifically with UQ in the Q_A site. However, fully functional quinones can be incorporated into Q_A depleted PBRCs, and by collecting Q_A^-/Q_A FTIR DS using PBRCs with unlabeled and isotopically labeled quinones incorporated, so called isotope edited FTIR difference spectra can be constructed, and from these spectra it has proven possible to separate contributions of the quinones from those of the protein in Q_A^-/Q_A FTIR DS (Breton and Nabedryk, 1996). Previously, a variety of unlabeled and ^{18}O labeled quinones have been incorporated into the Q_A binding site in PBRC's, and ^{18}O isotope edited FTIR DS have been obtained (Breton et al., 1994a). The goal in this manuscript is the simulation of these experimental ^{18}O isotope edited FTIR DS associated with the neutral state of the quinone in the Q_A binding site. Calculated IR spectra associated with the quinone anion state are considerably more complicated (Lamichhane and Hastings, 2013) and are currently being undertaken.

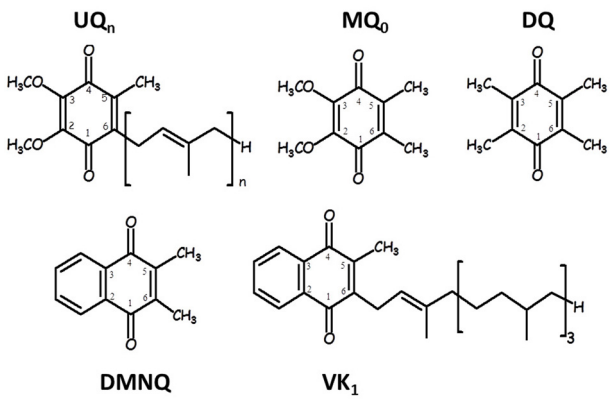

FIGURE 1 | Structure and numbering of ubiquinone (2,3-dimethoxy, 5-methyl,6-prenyl benzoquinone) (UQ_n), 2,3-dimethoxy, 5,6-methyl benzoquinone (MQ_0), 2,3,5,6-methyl benzoquinone (duroquinone, DQ), 2,3-dimethyl, 1,4-naphthoquinone (DMNQ) and 2-methyl, 3-phytyl 1,4-naphthoquinone (VK). The numbering scheme employed here for the naphthoquinone structures is nonstandard, and was chosen to facilitate comparison between naphthoquinone and ubiquinone structures.

Although experimental Q_A^-/Q_A FTIR DS have been obtained using PBRCs with various unlabeled and isotope labeled quinones incorporated, virtually no computational work aimed at modeling the experimental FTIR DS have been undertaken. Calculations aimed at modeling the vibrational properties of quinones in the Q_A binding site must account for the protein environment. Quantum mechanical (QM) calculations of such a large molecular system (pigment plus protein environment) are unfeasible. To circumnavigate this problem methods have been developed that allow one to separate the molecular system into distinct layers that can be treated at different levels of theory. In one layer the chemical properties of the principle species of interest (the pigment) can be calculated using "high-level" QM methods. The surrounding protein environment is included in the calculation but it is treated using computationally less expensive molecular mechanics (MM) methods.

Recently, we have undertaken QM:MM calculations for UQ in the Q_A binding site using the ONIOM method (Vreven et al., 2006). ONIOM is an acronym for: our Own N-layered Integrated molecular Orbital + Molecular mechanics package. In these calculations we showed that we could simulate experimental isotope edited FTIR difference spectra obtained using PBRCs with neutral UQ in the Q_A binding site. Here we extend upon these previous studies by attempting to simulate experimental isotope edited FTIR difference spectra obtained using PBRCs with symmetric tail-less and corresponding tail containing quinones incorporated into the Q_A binding site. We show that the calculated spectra agree well with the experimental spectra, further supporting the notion that the ONIOM method is a useful approach for understanding complex FTIR difference spectra associated with pigments in protein binding sites. We are also able to assess to what extent the quinone hydrocarbon chain may influence the calculated spectra.

MATERIALS AND METHODS

STRUCTURAL MODEL USED IN CALCULATIONS

The molecular model used in ONIOM calculations was generated from the crystal structure of *Rb. sphaeroides* PBRCs at 2.2 Å resolution (Stowell et al., 1997) (PDB file 1AIJ). From the PDB file all atoms within 10 Å of either carbonyl oxygen atom of UQ were selected. This subset of atoms formed the basis of the Q_A binding site structural model. Hydrogen atoms (not included in the PDB file) were added to the model using the software Gaussview4, resulting in a final structural model consisting of

1024 atoms. Following the addition of hydrogen atoms the structural model was optimized (energy minimized) using ONIOM methods with all atoms associated with the protein backbone, and the non-heme iron atom, being held fixed. All atoms of the amino acid side chains and the incorporated quinone are unconstrained. For calculations of UQ/VK the hydrocarbon tail was modeled as a single prenyl/phytyl unit, respectively. Inclusion of further prenyl/phytyl units did not alter the calculated spectra (not shown).

The structural models for the different incorporated quinones are initially set up by simply replacing the molecular substituents of the originally incorporated UQ species. So, the C=O groups of the different quinones incorporated will initially have the same orientation and position to that found for UQ in the Q_A binding site. DMNQ and VK structures were constructed starting from the UQ structure, by replacing the methoxy groups with the NQ aromatic ring, without alteration of the quinone ring (**Figure 2F**). This orientation of the NQ ring (of DMNQ and VK) was chosen as previous docking calculations have suggested it is the most favorable (Hucke et al., 2002).

CALCULATIONS

All calculations were undertaken using Gaussian 03 (Frisch et al., 2004) software. For calculation of UQ molecules in the gas phase, and for the QM part of ONIOM calculations, molecular geometry optimizations and harmonic vibrational frequency calculations were undertaken using hybrid DFT methods, employing the B3LYP functional and the 6–31+G(d) basis set. This choice of functional and basis set are appropriate for calculation of the vibrational properties of quinones (Wheeler, 2001; Bandaranayake et al., 2006). The MM part of the ONIOM calculation is undertaken using the AMBER force field (Case et al., 2005). Following ONIOM geometry optimization of the structural model, the optimized quinone molecule from the model is considered separately for vibrational frequency calculations.

NORMAL MODE ASSESSMENT

Assignment of calculated vibrational frequencies to molecular groups is based on a consideration of the calculated atomic displacements (in Cartesian coordinates) associated with the normal modes. These atomic displacements can be animated using software (GaussView4), and the molecular groups that most prominently contribute to the normal modes can be assessed visually [see **Figure 2** in Bandaranayake et al. (2006)]. In addition, potential energy distributions (PEDs) of the normal modes are calculated using the freeware GAR2PED (Martin and Van Alsenoy, 1995). For the various quinones in the Q_A binding site we calculate both vibrational mode frequencies and intensities. With both the frequency and intensity information "stick spectra" can be constructed. These stick spectra are representative of IR absorption spectra, as described previously (Bandaranayake et al., 2006; Parameswaran et al., 2008; Lamichhane et al., 2010). The calculated stick spectra are convolved with a Gaussian function with half-width of 4 cm^{-1} to produce more realistic looking IR absorption spectra (Bandaranayake et al., 2006; Parameswaran et al., 2008; Lamichhane et al., 2010).

RESULTS

UQ STRUCTURE AND NUMBERING

Figure 1 shows the structure and numbering scheme used here for UQ_n, MQ_0, DQ, DMNQ, and VK. NQ's generally have a different numbering scheme. We have applied the UQ numbering scheme to DMNQ and VK for the sake of easy comparison. **Figure 2** shows a picture of (**A**) DMNQ, (**B**) VK, (**C**) MQ_0, and (**D**) UQ_1 in the Q_A binding site along with the two H-bonding amino acids. The structures shown are after geometry optimization using ONIOM methods. Possible hydrogen bonds (or ligand to the non-heme iron atom) are indicated by dotted lines.

To gain a better sense of the relative orientation of the different quinones in the Q_A binding site **Figure 2** also shows the (**E**) DMNQ/DQ and (**F**) DMNQ/UQ structures from two ONIOM calculations overlapped. These overlapped structures are created by considering the (fixed) atoms of the protein backbone. **Figures 2E,F** indicates that the side chains of HisM219 and AlaM260 are unaltered when a different quinone is incorporated into the binding site.

Table 1 lists several bond lengths and bond angles derived from our ONIOM calculated optimized geometries of the various quinones in the Q_A binding site. For comparison, **Table 1** also lists corresponding bond lengths and angles derived from our DFT calculated optimized geometries of the various quinones in the gas phase. **Table 1** also list results obtained from previous QM/MM calculations (Sinnecker et al., 2006), and data taken from the 1AIJ crystal structure (Stowell et al., 1997).

Table 1 list the three distances associated with the peptide or imidazole H-bond to the carbonyl oxygen atoms of the quinone (N-H, NH–O and N–O distances). These distances completely determine the N-H–O H-bond geometry. Associated angles are also listed in **Table 1**.

For UQ_{10} in the Q_A site the 1AIJ crystal structure (Stowell et al., 1997) indicates that the C_1=O bond is marginally longer than the C_4=O bond. (1.234 vs. 1.232 Å). In contrast, from ONIOM calculations of all the quinones listed in **Table 1** the C_1=O bond is shorter than the C_4=O bond.

In gas phase calculations the C_1=O and C_4=O bond lengths are shorter than that found in ONIOM calculations (except the C_1=O of DQ). This lengthening of the C=O bonds of the quinones in the Q_A binding site is related to hydrogen bonding and other electrostatic interactions of the pigment with the protein environment.

For UQ_1 and MQ_0 the C_1=O bond is shorter than the C_4=O bond in both ONIOM and gas phase calculations. In gas phase calculations this difference in C_1=O and C_4=O bond lengths of UQ_1 and MQ_0 must relate to the differing orientations of the C_2 and C_3 methoxy groups. The ONIOM calculated C_2 and C_3 methoxy group dihedral angles for UQ_1 are −25.3 and 150.5° (**Table 1**). Similar angles are calculated for MQ_0. The calculated dihedral angles for UQ_1 in the gas phase, and the observed angles for UQ_{10} in the Q_A binding site (from the crystal structure) are within 32° of that calculated for UQ_1 using ONIOM methods.

For UQ_{10} in the Q_A site the crystal structure indicates that the C_2=C_3 bond is shorter than the C_5=C_6 bond. (1.404 vs. 1.419 Å). In contrast, for all quinones except DQ, in both ONIOM and gas phase calculations the C_2=C_3 bond is longer than the C_5=C_6

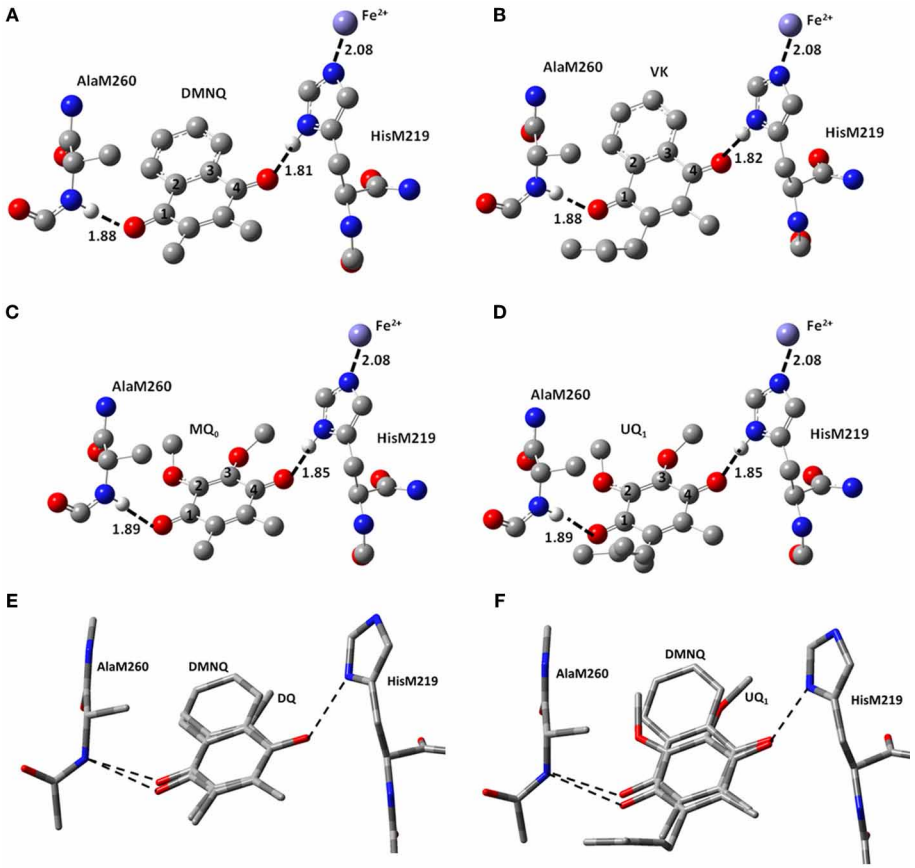

FIGURE 2 | Ball and stick representation of the calculated structure of (A) DMNQ, (B) VK, (C) MQ_0 and (D) UQ_1 in the Q_A binding site in PBRCs from *Rb. sphaeroides*. Structure shown is after geometry optimization using ONIOM methods. Possible H-bonds are shown (dotted). Hydrogen atoms, except the ones involved in H-bonding, have been omitted. Distances quoted are in Å. **(E,F)** Overlap of structures obtained from ONIOM calculations for **(E)** DMNQ and DQ and **(F)** DMNQ and UQ_1. Overlap is based on using the (fixed) backbone atoms of HisM219 and AlaM260. The amino acid side chains are virtually unaltered in the structures shown.

bond. For VK and DMNQ the calculated $C_2{=}C_3$ and $C_5{=}C_6$ bond lengths are considerably different.

For UQ_1 and VK the hydrocarbon chain attached at C_6 makes a distinct "kink" after the first carbon atom (**Figures 2B,D**). The C-C-C bond angle is 112–115° for both quinones in both the ONIOM and gas phase calculations. The calculated angles are virtually the same as that found in the crystal structure. Given these similarities (between the ONIOM and gas phase calculations for both UQ_1 and VK, as well as between calculation and experiment) the suggestion is that the protein environment does not constrain the orientation of the quinone ring relative to the C_6 hydrocarbon chain.

Figure 3A shows ONIOM calculated ^{18}O isotope edited difference spectra for neutral VK and DMNQ. **Figure 3D** shows corresponding DFT calculated spectra for VK and DMNQ in the gas phase. Experimental spectra are also shown (**Figures 3B,C**) for comparison. Positive/negative bands in the isotope edited spectra are due to the unlabeled/^{18}O labeled quinone species, respectively. The ONIOM calculated spectra clearly better describe the experimental spectra. Calculations including the protein environment appear to be necessary in order to adequately simulate the experimental spectra.

In the DFT calculated ^{18}O isotope edited spectrum for DMNQ/VK in the gas phase (**Figure 3D**) the antisymmetric vibration of both C=O groups gives rise to the band at $\sim$1654 cm^{-1} (**Figure 3D**), which downshifts 30 cm^{-1} upon ^{18}O labeling (Bandaranayake et al., 2006). The calculated isotope-edited gas phase spectrum is in excellent agreement with the experimental spectrum for DMNQ in solution (Breton et al., 1994a).

Figure 3 shows that except for a small frequency shift in some of the modes, the calculated spectra for DMNQ and VK are virtually the same. Replacement of the methyl group at C_6 with an isoprene unit therefore, has no influence on the calculated spectra.

The normal modes (frequencies and intensities) that give rise to the various bands in the ONIOM calculated ^{18}O isotope edited spectra of DMNQ and VK are listed in **Table 2**. The PEDs, which quantify to what extent various internal coordinates contribute to the normal modes, are also listed in **Table 2**. Results for DMNQ

Table 1 | Comparison of bond lengths and angles derived from the ONIOM calculated (O) and gas phase calculated (GP) optimized geometry of neutral UQ_1, MQ_0, DQ, VK, and DMNQ.

	x-ray	UQ1		MQo		DQ		VK_1		DMNQ		Ref
		O	GP	O	GP	O	GP	O	GP	O	GP	UQ1
C_1=O	1.234	1.227	1.223	1.227	1.223	1.232	1.230	1.233	1.229	1.232	1.229	1.235
C_4=O	1.232	1.238	1.231	1.238	1.231	1.236	1.231	1.236	1.229	1.236	1.229	1.237
C_2=C_3	1.404	1.366	1.364	1.367	1.364	1.355	1.355	1.405	1.405	1.406	1.405	
C_5=C_6	1.419	1.354	1.354	1.354	1.354	1.357	1.355	1.363	1.361	1.362	1.360	
AlaM260 H-BOND												
N–O	2.837	2.837		2.846		2.895		2.856		2.878		
N-H	1.014	1.014		1.014		1.013		1.013		1.013		1.014
N-H–O	1.912	1.894		1.886		1.907		1.883		1.883		1.94 ± 0.11
∠ N-H-O	150.2	153.3		156.7		164.4		159.9		166.7		147 ± 7
∠ C-O–N	131.5	127.0		125.9		127.4		125.7		124.1		
∠ C-O-H	133.4	128.7		128.3		132.6		128.0		128.1		
HisM219 H-BOND												
N–O	2.788	2.868		2.865		2.829		2.832		2.831		
N-H	1.020	1.020		1.020		1.019		1.020		1.020		1.017
N-H–O	1.788	1.849		1.845		1.810		1.815		1.812		1.79 ± 0.14
∠-N-H–O	166.2	175.8		177.7		178.8		174.3		178.2		170 ± 6
∠ C-O–N	138.4	140.1		139.7		137.4		138.4		137.8		
∠ C-O–H	140.6	139.4		139.2		137.4		137.5		137.3		
C_4=O − Fe	6.832	6.744		6.715		6.627		6.692		6.637		
∠ Tail	113.0	114.9	111.7					114.7	111.6			
C_2-dihedral	−57.1	−25.3	−8.9	−26.5	−10.1							
C_3-dihedral	109.5	150.5	123.6	150.6	123.1							

Bond lengths and angles from the 1AIJ crystal structure (Stowell et al., 1997) are also listed. Distances are in Å and angles are in degrees. The C_2 and C_3 methoxy group dihedral angles are defined as the C_3-C_2-O-CH_3 and C_2-C_3-O-CH_3 dihedral angles from Sinnecker et al. (2006).

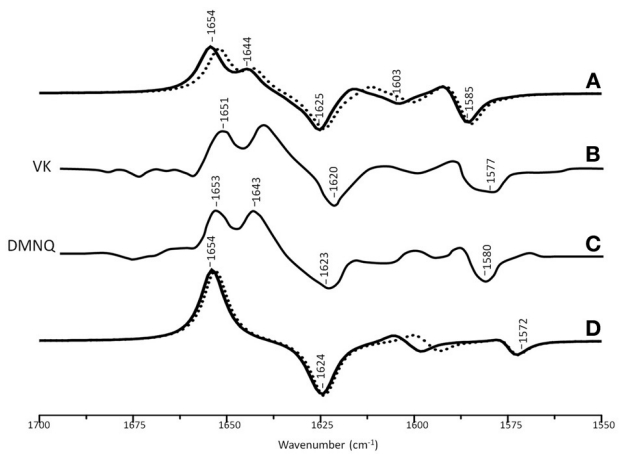

FIGURE 3 | (A) ONIOM calculated ^{18}O isotope edited DDS for neutral VK (dotted) and DMNQ (solid) in the Q_A binding site. Experimental spectra for VK **(B)** and DMNQ **(C)** are also shown, and were taken from Breton et al. (1994a), with permission. **(D)** DFT calculated ^{18}O isotope edited DDS for neutral VK (dotted) and DMNQ (solid) are also shown. ONIOM/gas phase calculated spectra were scaled by 0.9718/0.9608, respectively.

and VK are very similar. Below we will discuss calculated data obtained for DMNQ with the recognition that very similar results and conclusions also apply to VK.

In the ONIOM calculated ^{18}O isotope edited spectra for DMNQ the two bands at 1654 and 1644 cm^{-1} are due to C_1=O and C_4=O stretching vibrations, respectively (**Table 2**). These bands almost certainly correspond to the at 1653 and 1643 cm^{-1} bands in the experimental spectrum (**Figure 3C**). So our calculations *predict* that the 1653 and 1643 cm^{-1} bands in the experimental spectrum are due to C_1=O and C_4=O stretching vibrations, respectively. This is in fact the first direct evidence that the 1653 and 1643 cm^{-1} bands in the experimental spectrum are due to C_1=O and C_4=O stretching vibrations. A direct assignment has never been made because specific $^{13}C_1$ and $^{13}C_4$ isotopic labeled VK or DMNQ has never been incorporated into the Q_A binding site in PBRCs.

In contrast to the observation of two separate C=O modes in ONIOM calculations, in gas phase calculations the two C=O modes of DMNQ are anti-symmetrically coupled (Bandaranayake et al., 2006), giving rise to a single intense band at 1654 cm^{-1} (**Figure 3D**).

In ONIOM calculations it is found that upon ^{18}O labeling the C_1=O and C_4=O modes of DMNQ downshift 23 and 19 cm^{-1},

Table 2 | Normal mode frequencies (in cm^{-1}), intensities (in km/mol) and PEDs (in %) calculated using ONIOM methods for unlabeled and ^{18}O labeled neutral DMNQ, VK, DQ, MQ_0, and UQ_1.

	Unlabeled			^{18}O labeled			
	ν	*I*	**Potential energy distribution**	*ν*	*I*	Δ*ν*	**Potential energy distribution**
DMNQ	1654	235	C_1=O (71)	1631	32	23	C_1=O (28), C_5=C_6 (22), C_2=C_3 (10)
VK	1652	224	C_1=O (69)	1628	29	24	C_1=O (32), C_5 =C_6 (16), C_2=C_3 (6)
DQ	1646	254	C_1=O (83)	1613	264	33	C_1=O (80)
MQ_0	1666	209	C_1=O (81)	1631	211	35	C_1=O (83)
UQ_1	1663	185	C_1=O (80)	1629	187	34	C_1=O (82)
DMNQ	1644	108	C_4=O (60)	1625	199	19	C_4=O (26), −C_1=O (21),C_5 = C6 (8), −C_3 = C_7 (7)
VK	1642	107	C_4=O (60)	1624	188	18	C_4=O (29), −C_1=O (15), C_5=C_6 (8), −C_3 = C_7 (7)
DQ	1632	181	C_4=O (83)	1599	144	33	C_1=O (81)
MQ_0	1627	270	C_4=O (70), −C_2=C_3 (8)	1587	265	40	C_4=O (63), C_2=C_3 (9), −C_5=C_6 (5)
UQ_1	1626	305	C_4=O (68), −C_2=C_3 (9)	1586	249	40	C_4=O (65), C2 = C3 (7),−C_5=C_6 (6)
DMNQ	1617	59	C_5=C_6 (61), −C_4=O (8)	1604	54	13	C_5=C_6 (37), −C_4=O (25), −C_1=O (14)
VK	1611	54	C_5=C_6 (60), −C_4=O (8)	1600	52	11	C_5=C_6 (42), −C_4=O (20), −C_1=O (14)
DQ	1660	1	C_2=C_3 (32), C_5=C_6 (28)	1660	0	0	C_5=C_6 (29), C_2=C_3 (33)
MQ_0	1657	20	C_5=C_6 (52), C_2=C_3 (15)	1657	8	0	C_5=C_6 (49), C_2=C_3 (13)
UQ_1	1653	26	C_5=C_6 (45), C_2=C_3 (19)	1654	18	−8	C_5=C_6 (44), C_2=C_3 (17)
DMNQ	1591	93	C=C_{arom} (55)	1586	181	5	C=C_{arom} (43),−C_4=O (13), C_1=O (10)
VK	1591	96	C=C_{arom} (54),−C_4=O (5)	1585	186	6	C=C_{arom} (40), −C_4=O (14), C_1=O (11)
DQ	1620	55	C5 = C6 (38), −C_2=C_3 (33)	1620	56	0	C_5=C_6 (37), −C_2=C_3 (34)
MQ_0	1601	293	C_2=C_3 (39), −C_5=C_6 (15), C_4=O (12), −C_2 =O (7)	1609	273	−7	C_2=C_3 (40), −C_4=O (15), −C_5=C_6 (12), −C_2 =O (11)
UQ_1	1601	275	C_2=C_3 (35), −C_5=C_6 (18), C_4 =O (14), −C_2 =O (6)	1609	308	−8	C_2=C_3 (37), −C_4=O (13), −C_5=C_6 (15), −C_2–O (10)

Frequency shifts upon ^{18}O labeling are also listed. Negative signs in the PEDs refer to the relative phase of vibration of the internal coordinates. Only internal coordinates that contribute at least 5 % are shown. Mode frequencies were scaled by 0.9718.

to 1631 and 1625 cm^{-1}, respectively (**Table 2**). Upon ^{18}O labeling the 1625 cm^{-1} mode is more than six times more intense than the 1631 cm^{-1} mode. The 1625 cm^{-1} mode in ^{18}O labeled DMNQ is due mainly to the antisymmetric coupled vibration of both C=O groups. That is, two separate C=O modes of unlabeled DMNQ couple upon ^{18}O labeling. This behavior is not predicted based upon consideration of the experimental spectra, where it is "assumed" that the two C=O modes remain separate upon ^{18}O labeling (Breton et al., 1994b; Breton, 1997).

A C=C mode of the quinone ring of DMNQ is found at 1617 cm^{-1}. This quinonic C=C mode downshifts 13 cm^{-1}, to 1604 cm^{-1}, upon ^{18}O labeling, with little change in intensity. The 1604 cm^{-1} mode composition in ^{18}O labeled DMNQ displays considerable mixing of the C=O and C=C modes (the C=O modes account for 39% of the PED). This behavior might be expected given that the C=O and C=C modes are closer in frequency upon ^{18}O labeling.

A C=C mode of the aromatic ring of DMNQ occurs at 1591 cm^{-1}. This aromatic C=C mode downshifts 5 cm^{-1} to 1586 cm^{-1} upon ^{18}O labeling. The 1586 cm^{-1} mode in ^{18}O labeled DMNQ displays some mixing with C=O modes (23%), and the intensity of the aromatic C=C mode nearly doubles upon ^{18}O labeling. The calculated C=C normal modes and their interpretation in terms of internal coordinates, as well as the calculated ^{18}O induced frequency shifts are similar to that suggested on the basis of the experimental spectra (Breton et al., 1994a).

Figure 4A shows ONIOM calculated ^{18}O isotope edited IR difference spectra for neutral DQ in the Q_A binding site. **Figure 4C** shows the corresponding DFT calculated spectrum for DQ in the gas phase. The experimental spectrum is shown in **Figure 4B**. Again, the ONIOM calculated spectrum agrees well with the experimental spectrum while the calculated gas phase spectrum does not. The ONIOM calculated normal modes (frequencies and intensities) that give rise to the bands in the ^{18}O isotope edited spectrum for DQ, as well as the PEDs, are listed in **Table 2**.

In the ONIOM calculated ^{18}O isotope edited spectrum for DQ the two bands at 1646 and 1632 cm^{-1} are due to C_1=O and C_4=O stretching vibrations, respectively (**Table 2**). Upon ^{18}O labeling the C_4=O and C_1=O modes both downshift 33 cm^{-1} with little change in mode intensities (**Table 2**). This 33 cm^{-1}

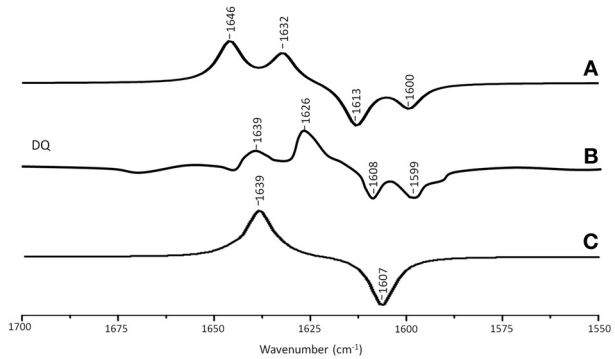

FIGURE 4 | (A) ONIOM calculated ^{18}O isotope edited DDS for neutral DQ in the Q_A binding site. Experimental spectra are shown in **(B)**, and were taken from Breton et al. (1994a) with permission. **(C)** DFT calculated ^{18}O isotope edited DDS for neutral DQ. ONIOM and gas phase calculated spectra were scaled by 0.9718 and 0.9608, respectively.

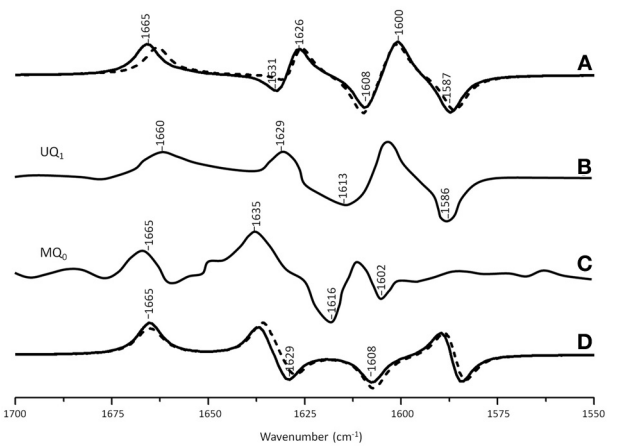

FIGURE 5 | (A) ONIOM calculated ^{18}O isotope edited DDS for neutral MQ_0 (solid) and UQ_1 (dotted) in the Q_A binding site. Experimental spectrum for **(B)** MQ_0 and **(C)** UQ_1 are also shown, and were taken from Breton et al. (1994a) with permission. **(D)** DFT calculated ^{18}O isotope edited DDS for neutral MQ_0 (solid) and UQ_1 (dotted). ONIOM and gas phase calculated spectra were scaled by 0.9718 and 0.9608, respectively.

downshift is large compared to that calculated for DMNQ (19–23 cm^{-1}). For DQ, the ONIOM calculated mode composition is virtually unchanged upon ^{18}O labeling. This is also markedly different to that calculated for DMNQ. The normal modes that give rise to the isotope edited spectra of DQ and DMNQ in the gas phase are very similar, so replacing the methyl groups of DQ with the aromatic ring of DMNQ in the Q_A binding site leads to an alteration in the electronic structure of the quinone ring. This modification is not obvious given the similar orientation of DQ and DMNQ in the Q_A binding site (**Figure 2E**).

In the DFT calculated ^{18}O isotope edited spectrum for DQ in the gas phase, the two C=O modes are strongly coupled, and give rise to the band at 1639 cm^{-1} in **Figure 4C**. The calculated gas phase spectrum is in line with the experimental FTIR spectrum for DQ in solution (Breton et al., 1994a).

From ONIOM calculations for DQ, C=C modes do not couple with the C=O modes. The C_2=C_3 and C_5=C_6 groups couple to produce in phase and out of phase vibrational modes. The in phase mode has negligible IR intensity. The out of phase C=C mode is calculated to be at 1620 cm^{-1}. This C=C mode is virtually unaltered in frequency, intensity, and mode composition upon ^{18}O labeling (**Table 2**).

Figure 5A shows ONIOM calculated ^{18}O isotope edited IR spectra for neutral MQ_0 (solid) and UQ_1 (dotted) in the Q_A binding site. **Figure 5D** shows DFT calculated spectra for MQ_0 and UQ_1 in the gas phase. The experimental spectra for UQ_1 and MQ_0 are shown in **Figures 5B,C,** respectively. The normal modes (frequencies and intensities) that give rise to the various bands in the ONIOM calculated spectra, as well as the PEDs, are listed in **Table 2**. The data for UQ_1 has been presented previously (Lamichhane and Hastings, 2011), and we show here that very similar spectra are calculated for both MQ_0 and UQ_1. Replacement of an isoprene unit at C_6 with a methyl group does not greatly alter the calculated spectra.

In the ONIOM calculated ^{18}O isotope edited spectra for neutral MQ_0 the two bands at 1666 and 1627 cm^{-1} (**Figure 5C**) are due to C_1=O and C_4=O stretching vibrations, respectively (**Table 2**). Upon ^{18}O labeling the C_1=O and C_4=O modes downshift 35 and 40 cm^{-1}, respectively (**Table 2**). The mode intensities and composition are little altered by ^{18}O labeling. The C=C mode of MQ_0/UQ_1 at 1601 cm^{-1} up-shifts 8/7 cm^{-1} upon ^{18}O labeling (**Table 2**). An explanation for this ^{18}O induced frequency upshift has been presented (Lamichhane and Hastings, 2011).

In the DFT calculated ^{18}O isotope edited spectra for UQ_1/MQ_0 in the gas phase, the two C=O modes are well separated, and give rise to bands at ∼1665 and ∼1635 cm^{-1} (**Figure 5D**), which downshift 36 and 27 cm^{-1}, respectively, upon ^{18}O labeling, as described previously (Lamichhane et al., 2011).

DISCUSSION

Previously we have shown that ONIOM methods can be used to calculate isotope edited difference spectra for UQ_1 in the Q_A binding site, and that these calculated spectra model very well the corresponding experimental spectra (Lamichhane and Hastings, 2011). Here we considerably extend these studies, and show that ONIOM calculated isotope edited spectra for different quinones in the Q_A binding site model very well the corresponding experimental spectra. We further show that the calculated spectra for quinones in the gas phase are totally inappropriate for modeling the vibrational properties of quinones in the Q_A binding site. This is also very likely to be the case for modeling the properties of any protein bound pigment.

Without normal mode vibrational frequency calculations interpretation of experimental spectra is limited, and here we clearly show that our computational methods lead to a greatly increased understanding of the normal modes that contribute to the bands in the experimental spectra.

In our ONIOM calculations for neutral UQ_1 in the Q_A binding site we considered all amino acids included in the model only at the molecular mechanics level of computation. Previously,

ONIOM calculations have been undertaken in order to model EPR data associated with the UQ anion in the Q_A binding site (Lin and O'Malley, 2008). In these calculations key amino acids, such as HisM219 and AlaM260, were considered at the higher quantum mechanical level of calculation. Taken together these results may indicate differences in the nature of H-bonding for the neutral and anion UQ species. Changes in H-bonding upon radical formation may be a mechanism for (de)stabilizing cofactors to fine-tune electron transfer processes in biological systems. Clearly it will be useful to undertake calculations similar to that presented here (modeling isotope edited FTIR difference spectra) for the UQ anion in the Q_A binding site, and such calculations are underway in our lab. Based on the above one could argue that the methods used here, with only the quinone treated at the QM level, will be inadequate to simulate the experimental spectra associated with quinone anions in the Q_A binding site. Or, for simulating the vibrational properties of quinone anions in the Q_A binding site it will be necessary to treat key amino acids at a quantum mechanical level. Again, calculations are underway in our lab to test this proposal.

For the neutral state of quinones occupying the Q_A binding site, calculations with the H-bonding amino acids treated at the MM level lead to calculated spectra that are in excellent agreement with experimental spectra (**Figures 3–5**). Clearly, treating H-bonding amino acids quantum mechanically will not lead to improved modeling of the experimental spectra. We have in fact undertaken calculations in which neutral UQ and the H-bonding amino acids are treated using QM, and we have found that the calculated spectra are very similar to that obtained when only neutral UQ is treated using QM (and the surrounding amino acids are treated using MM) (Zhao et al., J. Phys. Chem. B in press). Thus, it is very clear that, at least for the case of neutral quinones occupying the Q_A binding site, and as far as modeling isotope edited FTIR spectra is concerned, QM/MM calculations with only the quinone treated at the QM level need to be considered.

An experimental ^{18}O isotope edited FTIR difference spectrum for UQ in the Q_A binding site is shown in **Figure 5B**. Three positive bands at 1660, 1629, and 1601 cm^{-1} are observed. By considering FTIR difference spectra obtained using PBRCs with unlabeled and specifically $^{13}C_1$ and $^{13}C_4$ labeled UQ occupying the Q_A binding site, it was concluded that the 1660 and 1601 cm^{-1} bands are due to the C_1=O and C_4=O vibrations of unlabeled neutral UQ, respectively. It was also concluded that the 1628 cm^{-1} band is due to a UQ C=C vibration (Breton et al., 1994c). Since the C_4=O mode was so massively downshifted (from ∼1660 cm^{-1} for UQ in solvent to 1601 cm^{-1} for UQ in the Q_A binding site) it was suggested that this group must be engaged in very strong hydrogen bonding, presumably with HisM219 (**Figure 2**) (Breton et al., 1994c). This conclusion is difficult to rationalize based on the crystal structural data and other experimental data [see Wraight and Gunner (2009) for a review]. Such a conclusion is also not supported by the data presented here. Specifically, the C_1=O and C_4=O modes of DMNQ and VK are found at 1653 and 1643 cm^{-1} (**Table 2**), respectively, compared to ∼1662 cm^{-1} for the coupled C=O vibration in solution (Bandaranayake et al., 2006). Thus, the C_1=O/C_4= O mode of DMNQ or VK in the Q_A site is downshifted 9/19 cm^{-1}, respectively, compared to that found in solution. Such shifts suggest that both C=O modes of DMNQ or VK are H-bonded in the Q_A site, albeit quite weakly.

From the experimental spectrum of VK (or DMNQ) in **Figure 3B** two positive bands are observed at 1651 and 1640 cm^{-1} and one negative band at 1620 cm^{-1}. The two C=O modes of unlabeled VK give rise to the positive bands at 1651 and 1640 cm^{-1}, but only a single band is observed at 1620 cm^{-1} upon ^{18}O labeling. Two interpretations for these observations have been proposed (Breton et al., 1994b). One suggestion is that upon ^{18}O labeling the 1640 cm^{-1} band downshifts to ∼1620 cm^{-1}, while the 1651 cm^{-1} band downshifts to near 1640 cm^{-1} and decreases in intensity. The negative band near 1640 cm^{-1} due to a C = ^{18}O group of VK is then masked by the positive band (also at 1640 cm^{-1}) due to the unlabeled C=O group. A second hypothesis is that the two C=O modes of unlabeled VK (at 1651 and 1640 cm^{-1}) both downshift to ∼1620 cm^{-1} upon ^{18}O labeling. The different ^{18}O induced shifts of the two C=O modes results from differential coupling to C=C modes.

The calculated data presented here allow us to address which of these interpretations could be appropriate, or if either is appropriate. The ONIOM calculations show that the C_1=O and C_4=O modes of unlabeled VK occur at 1652 and 1642 cm^{-1}, and that neither of these modes are coupled to C=C modes (**Table 2**). Upon ^{18}O labeling the C_1=O/C_4=O mode downshifts 24/18 cm^{-1}, respectively. The modes of ^{18}O labeled VK also display considerable coupling with C=C modes. Upon ^{18}O labeling the C_1=O/C_4=O group couples with C=C_{ring} in-phase/out-of-phase vibrations, respectively. Coupling of the C_4=O group to the out of phase C=C vibration leads to a large intensity enhancement, while coupling of the C_1=O group to the in-phase C=C vibration leads to a large intensity decrease (**Table 2**). So, the calculations indicate that two separate uncoupled C=O modes in unlabeled VK give rise to predominantly a single mixed mode (that carries most of the intensity) in ^{18}O labeled VK. These calculated results indicate that neither of the two previously proposed interpretations of the experimental spectra is correct. Clearly, the calculations presented here allow a more detailed insight into the nature of the bands in the experimental isotope edited FTIR difference spectra.

Experimentally, the vibrational modes of DMNQ are at a slightly higher frequency (∼3 cm^{-1}) than corresponding modes of VK. Presumably replacing the C_6 methyl group with a phytyl unit causes this difference. Interestingly, this small frequency difference in the modes of DMNQ and VK is also found in our ONIOM calculated spectra (compare spectra in **Figures 5C,B**). This result is not entirely specific to the ONIOM method, however, as a small shift is also found in the gas phase calculations (**Figure 3D**).

The C_1=O and C_4=O modes of DMNQ and VK are calculated to be separated by 10 cm^{-1}. This separation cannot be due to differences in the molecular group attached at C_6. It must be due to differences in how the two C=O groups interact with the protein. Similarly, the two C=O modes of DQ are calculated to be separated by 13 cm^{-1}, and this separation is also likely due to differences in how the two C=O groups of DQ interact with the protein.

For UQ_1 (and MQ_0) the separation of the C=O modes is $\sim$32 cm^{-1} (1660–1628). Some of the differences in frequency of the C=O modes of UQ are due to the different orientation of the methoxy groups. If we assume that protein interactions with the C=O groups gives rise to a 13 cm^{-1} separation in the frequencies of the two C=O modes then this would indicate that the difference in the orientation of the methoxy groups of UQ (or MQ_0) gives rise to a frequency difference of 19 cm^{-1} for the two C=O groups. This result is in quite good agreement with results from experimental spectra of UQ in solution, which show that the two C=O modes are separated by $\sim$16 cm^{-1} (Breton et al., 1994c; Brudler et al., 1994).

Normal mode vibrational frequencies are governed by molecular bonding force constants. These force constants relate to the electronic structure of the molecule. Since the calculated and experimental spectra for DMNQ and VK are virtually the same it is concluded that the replacing the phytyl unit at C_6 of VK with a methyl group does not appreciably perturb the electronic structure of the NQ ring. In addition, the tail does not perturb the protein in a way that significantly modifies any pigment protein interactions.

In VK and UQ_1, the "kink" in the hydrocarbon chain after the first carbon atom is 3.1–3.2° higher in ONIOM calculations compared to gas phase calculations. It seems therefore, that the hydrocarbon chain is somewhat constrained relative to the quinone ring when incorporated into the Q_A binding site. It is not clear if this is a significant constraint, however. The C_1=O and C_4=O bonds of MQ_0 and UQ_1 (and of DMNQ and VK) are virtually unaltered in ONIOM calculations (**Table 1**). The hydrogen bond lengths for the C=O groups are also little altered (**Table 1**). The distance of the C_4=O oxygen to the non heme iron atom is 0.029/0.055 Å longer for UQ_1/VK compared to MQ_0/DMNQ, respectively, suggesting a very small change in orientation of the UQ_1/VK head-group (since the iron atom is fixed) compared to MQ_0/DMNQ in the Q_A binding site. The hydrocarbon chain may therefore, lead to a very slight change in the orientation of the quinone ring in the Q_A binding site. **Figure 2F** shows that there is only a very small difference in the orientation of DMNQ relative to UQ_1.

The experimental ^{18}O isotope edited spectra for MQ_0 and UQ_1 are quite different (compare **Figures 5B,C**). This difference cannot be modeled computationally (**Figure 5A**). The experimental isotope edited spectrum for MQ_0 is considerably noisier than the spectrum for UQ (Breton et al., 1994a). As far as we are aware the Q_A^-/Q_A FTIR difference spectrum for RCs with MQ_0 in the binding site have never been reproduced, so the accuracy of the spectrum may be somewhat questionable. On the other hand MQ_0 may be able to incorporate into the Q_A binding site with the methoxy groups oriented in several different ways. As described previously, each of these methoxy group conformers will have slightly different spectra (Lamichhane et al., 2010). This heterogeneity in orientation of MQ_0 in the Q_A binding site may be a factor that contributes to differences in the experimental spectra for MQ_0 and UQ, as demonstrated in **Figures 5B,C**. In spite of this, there are some overall similarities in the MQ_0 and UQ_1 experimental spectra in **Figures 5B,C**. For the MQ_0 spectrum positive bands are found at 1665, 1631, and 1608 cm^{-1}. For UQ_1 the bands are at 1660, 1628, and 1601 cm^{-1}. For the MQ_0 spectrum negative bands are found at 1616 and 1602 cm^{-1}. For UQ the bands are at 1613 and 1586 cm^{-1}.

The ONIOM calculated and experimental isotope edited spectra for VK are very similar, although the intensity ratios of the different bands do not appear to match well. For example, the intensity ratio of 1652 and 1644 cm^{-1} bands in the calculated spectrum (**Figure 3A**, dotted) is $\sim$2.1, compared to a ratio of $\sim$0.95 in the experimental spectrum. To investigate this further we have also calculated the ^{13}C isotope edited spectrum for VK in the Q_A binding site (**Figure 6A**) (global ^{13}C labeling of VK), and compared it to the corresponding experimental spectrum (**Figure 6B**). For completeness the calculated ^{13}C isotope edited spectrum for VK in the gas phase is shown in **Figure 6C**. Again, it is evident that the calculated gas phase spectrum in no way resembles the experimental spectrum (compare **Figures 6B,C**). The normal modes (frequencies, intensities, and PEDs) that give rise to the various bands in the ONIOM calculated ^{13}C isotope edited spectra of VK in **Figure 6A** are listed in **Table 3**.

Notice that the ONIOM calculation predicts that the two C=O modes remain completely separate (do not mix) upon ^{13}C labeling (**Table 3**), which is unlike the behavior observed for the C=O modes upon ^{18}O labeling (see above). Also notice that in the experimental isotope edited spectrum (**Figure 6B**) the 1640 cm^{-1} band is now considerably more intense than the 1651 cm^{-1} band, whereas in the calculated spectrum the higher frequency band is considerably more intense. The origin of these mode intensity differences are not entirely clear and are currently being investigated by considering calculations associated with VK in the presence of various types of H-bonding molecules.

CONCLUSIONS

We have shown that ONIOM type QM/MM calculations can be used to model experimental isotope edited FTIR difference

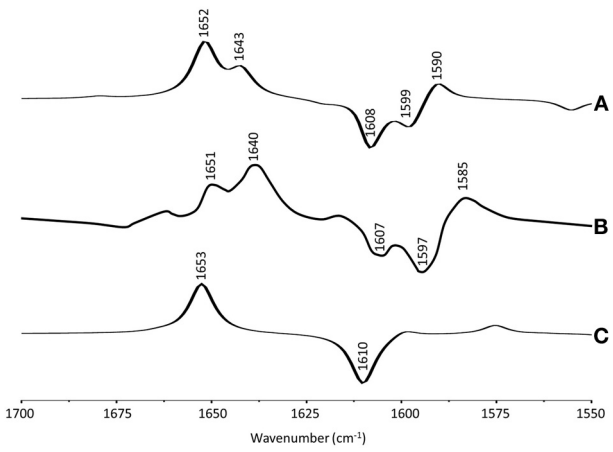

FIGURE 6 | (A) ONIOM calculated ^{13}C isotope edited DDS for neutral VK in the Q_A binding site. Experimental spectrum is also shown **(B)**, taken from Breton (1997) (with permission). **(C)** DFT calculated ^{13}C isotope edited DDS for neutral VK in the gas phase. ONIOM and gas phase calculated spectra were scaled by 0.9718 and 0.9608, respectively.

Table 3 | Normal mode frequencies (in cm^{-1}), intensities (in km/mol) and PEDs (in %) calculated using ONIOM methods for unlabeled and ^{13}C labeled neutral VK.

	Unlabeled			^{13}C labeled			
	ν	*I*	Potential energy distribution	*ν*	*I*	Δ*ν*	Potential energy distribution
VK	1652	224	C_1=O (69)	1609	227	43	C1=O (73)
	1642	107	C_4=O (60)	1598	116	44	C4=O (70)
	1611	54	C_5=C_6 = (60), −C_4=O (8)	1555	43	56	C_5=C_6 (57)
	1591	96	C=C_{arom} (54), −C_4=O (5)	1537	67	54	C=C_{arom} (55)

Frequency shifts upon ^{13}C labeling are also listed. Negative signs in the PEDs refer to the relative phase of vibration of the internal coordinates. Only internal coordinates that contribute at least 5% are shown. Mode frequencies were scaled by 0.9718.

spectra obtained using PBRCs that have had several different quinones incorporated into the Q_A binding site. The fact that the many different spectra can all be modeled is a clear indicator of the appropriateness of the approach.

The calculated spectra appear not to depend on whether the quinone incorporated has a prenyl/phytyl unit or a methyl group attached at C_6. The electronic structure of the quinone ring is therefore, not sensitive to the presence or absence of a hydrocarbon side chain at C_6. This suggests that the hydrocarbon side chain does not significantly constrain the quinone ring in the Q_A binding site.

Comparison of the calculated and experimental spectra, in combination with a consideration of the calculated PEDs of the normal modes, allows a direct assessment of the appropriateness of previous suggestions as to the origin of the bands in the experimental spectra.

ACKNOWLEDGMENTS

This work was supported in part by a grant from the Qatar National Research Fund to Gary Hastings (grant # NPRP 4-183-1-034). Nan Zhao acknowledges support from a fellowship from the Molecular Basis of Disease program at GSU. Calculations were undertaken using the IBM System p7 supercomputer (called CARINA) at GSU. This computer was acquired through a partnership of the Southeastern Universities Research Association and IBM, with additional support from the Georgia Research Alliance.

REFERENCES

Bandaranayake, K., Sivakumar, V., Wang, R., and Hastings, G. (2006). Modeling the A_1 binding site in photosystem I. Density functional theory for the calculation of "Anion – Neutral" FTIR difference spectra of phylloquinone. *Vib. Spectrosc.* 42, 78–87. doi: 10.1016/j.vibspec.2006.01.003

Breton, J. (1997). Efficient exchange of the primary quinone acceptor Q_A in isolated reaction centers of Rhodopseudomonas viridis. *Proc. Natl. Acad. Sci. U.S.A.* 94, 11318–11323. doi: 10.1073/pnas.94.21.11318

Breton, J., Burie J. R., Boullais, C., Berger, G., and Nabedryk, E. (1994a). Binding sites of quinones in photosynthetic bacterial reaction centers investigated by light-induced FTIR difference spectroscopy: binding of chainless symmetrical quinones to the Q_A site of Rhodobacter sphaeroides. *Biochemistry* 33, 12405–12415. doi: 10.1021/bi00207a007

Breton, J., Burie, J. R., Berthomieu, C., Berger, G., and Nabedryk, E. (1994b). The binding sites of quinones in photosynthetic bacterial reaction centers investigated by light-induced FTIR difference spectroscopy: assignment of the Q_A vibrations in Rhodobacter sphaeroides using ^{18}O- or ^{13}C-labeled ubiquinone and vitamin K_1. *Biochemistry* 33, 4953–4965. doi: 10.1021/bi00182a026

Breton, J., Boullais, C., Burie, J. R., Nabedryk, E., and Mioskowski, C. (1994c). Binding sites of quinones in photosynthetic bacterial reaction centers investigated by light-induced FTIR difference spectroscopy: assignment of the interactions of each carbonyl of Q_A in Rhodobacter sphaeroides using site-specific ^{13}C-labeled ubiquinone. *Biochemistry* 33, 14378–14386. doi: 10.1021/bi00252a002

Breton, J., and Nabedryk, E. (1996). Protein-quinone interactions in the bacterial photosynthetic reaction center: light-induced FTIR difference spectroscopy of the quinone vibrations. *Biochim. Biophys. Acta.* 1275, 84–90. doi: 10.1016/0005-2728(96)00054-0

Brudler, R., de Groot, H. J., van Liemt, W. B., Steggerda, W. F., Esmeijer, R., Gast, P., et al. (1994). Asymmetric binding of the 1- and 4-C=O groups of QA in Rhodobacter sphaeroides R26 reaction centres monitored by Fourier transform infra-red spectroscopy using site-specific isotopically labelled ubiquinone-10. *EMBO J.* 13, 5523–5530.

Case, D. A., Cheatham, T. E., Darden, T., Gohlke, H., Luo, R., Merz, K. M., et al. (2005). The Amber biomolecular simulation programs. *J. Comput. Chem.* 26, 1668–1688. doi: 10.1002/jcc.20290

Frisch, M. J., Trucks, G. W., Schlegel, H. B., Scuseria, G. E., Robb, M. A., Cheeseman, J. R., et al. (2004). *Gaussian 03, Revision C.02.* Gaussian 03, Revision D.01.

Hale, M. B., Blankenship, R. E., and Fuller, R. C. (1983). Menaquinone is the sole quinone in the facultatively aerobic green photosynthetic bacterium *Chloroflexus aurantiacus*. *Biochim. Biophys. Acta* 723, 376–382. doi: 10.1016/0005-2728(83)90044-0

Hucke, O., Schmid, R., and Labahn, A. (2002). Exploring the primary electron acceptor (QA)-site of the bacterial reaction center from Rhodobacter sphaeroides. Binding mode of vitamin K derivatives. *Eur. J. Biochem.* 269, 1096–1108. doi: 10.1046/j.0014-2956.2001.02699.x

Ke, B. (2001a). "The bacterial photosynthetic reaction center: chemical composition and crystal structure," in *Photosynthesis: Photobiochemistry and Photobiophysics*, (Dordrecht; Boston: Kluwer Academic Publishers), 47–62.

Ke, B. (2001b). "The stable primary acceptor QA and the secondary electron acceptor QB," in *Photosynthesis: Photobiochemistry and Photobiophysics*, (Dordrecht; Boston: Kluwer Academic Publishers), 289–304.

Ke, B. (2001c). "The "Stable" primary electron acceptor (QA) of photosynthetic bacteria," in *Photosynthesis: Photobiochemistry and Photobiophysics*, (Dordrecht; Boston: Kluwer Academic Publishers), 101–110.

Ke, B. B. (2001d). "The secondary electron acceptor (QB) of photosynthetic bacteria," in *Photobiochemistry and Photobiophysics*, (Dordrecht; Boston: Kluwer Academic Publishers), 111–128.

Lamichhane, H. P., and Hastings, G. (2011). Calculated vibrational properties of pigments in protein binding sites. *Proc. Natl. Acad. Sci. U.S.A.* 108, 10526–10531. doi: 10.1073/pnas.1104046108

Lamichhane, H. P., and Hastings, G. (2013). Calculated vibrational properties of ubisemiquinones. *Comput.*

Biol. J. 2013:11. doi: 10.1155/2013/807592

Lamichhane, H., Wang, R., and Hastings, G. (2010). Comparison of calculated and experimental FTIR spectra of specifically labeled ubiquinones. *Vib. Spectrosc.* 55, 279–286. doi: 10.1016/j.vibspec.2010.12.008

Lamichhane, H., Wang, R. L., and Hastings, G. (2011). Comparison of calculated and experimental FTIR spectra of specifically labeled ubiquinones. *Vib. Spectrosc.* 55, 279–286. doi: 10.1016/j.vibspec.2010.12.008

Lin, T., and O'Malley, P. (2008). An ONIOM study of the Q(A) site semiquinone in the Rhodobacter sphaeroides photosynthetic reaction centre. *J. Mol. Struct. Theochem.* 870, 31–35. doi: 10.1016/j.theochem.2008.08.034

Martin, J. M. L., and Van Alsenoy, C. (1995). *GAR2PED.* Antwerp: University of Antwerp.

McComb, J. C., Stein, R. R., and Wraight, C. A. (1990). Investigations on the influence of headgroup substitution and isoprene side-chain length in the function of primary and secondary quinones of bacterial reaction centers. *Biochim. Biophys. Acta* 1015, 156–171. doi: 10.1016/0005-2728(90)90227-U

Noguchi, T., and Berthomieu, C. (2005). "Molecular analysis by vibrational spectroscopy," in *Photosystem II The Light Driven Water:Plastoquinone Oxidoreductase*, eds T. Wydrzynski and K. Satoh (Dordrecht: Springer), 367–387.

Parameswaran, S., Wang, R., and Hastings, G. (2008). Calculation of the vibrational properties of chlorophyll a in solution. *J. Phys. Chem. B* 112, 14056–14062. doi: 10.1021/jp806115q

Shopes, R. J., and Wraight, C. A. (1985). The acceptor quinone complex of Rhodopseudomonas viridis reaction centers. *Biochim. Biophys. Acta* 806, 348–356. doi: 10.1016/0005-2728(85)90242-7

Sinnecker, S., Flores, M., and Lubitz, W. (2006). Protein-cofactor interactions in bacterial reaction centers from Rhodobacter sphaeroides R-26: effect of hydrogen bonding on the electronic and geometric structure of the primary quinone. A density functional theory study. *Phys. Chem. Chem. Phys.* 8, 5659–5670. doi: 10.1039/b612568a

Srinivasan, N., and Golbeck, J. H. (2009). Protein-cofactor interactions in bioenergetic complexes: the role of the A1A and A1B phylloquinones in Photosystem I. *Biochim. Biophys. Acta* 1787, 1057–1088. doi: 10.1016/j.bbabio.2009.04.010

Stowell, M. H., McPhillips, T. M., Rees, D. C., Soltis, S. M., Abresch, E., and Feher, G. (1997). Light-induced structural changes in photosynthetic reaction center: implications for mechanism of electron-proton transfer. *Science* 276, 812–816. doi: 10.1126/science.276.5313.812

Trumpower, B. (1982). *Function of Quinones in Energy Conserving Systems*. New York, NY: Academic Press.

Vreven, T., Byun, K. S., Komaromi, I., Dapprich, S., Montgomery, J. A., Morokuma, K., et al. (2006). Combining quantum mechanics methods with molecular mechanics methods in ONIOM. *J. Chem. Theory Comput.* 2, 815–826. doi: 10.1021/ct050289g

Warncke, K., Gunner, M. R., Braun, B. S., Gu, L. Q., Yu, C. A., Bruce, J. M., et al. (1994). Influence of hydrocarbon tail structure on quinone binding and electron-transfer performance at the Q(a) and Q(B) sites of the photosynthetic reaction-center protein. *Biochemistry* 33, 7830–7841. doi: 10.1021/bi00191a010

Wheeler, R. A. (2001). "Quinones and quinoidal radicals in photosynthesis," in *Theoretical Biochemistry-Processes and Properties of Biological Systems*, ed L. A. Eriksson (Amsterdam: Elsevier), 655–690. doi: 10.1016/S1380-7323(01)80016-9

Wraight, C. A., and Gunner, M. R. (2009). "The acceptor quinones of purple photosynthetic bacteria—structure and spectroscopy," in *The Purple Photosynthetic Bacteria*, eds C. Hunter, F. Daldal, M. Thurnauer, and T. Beatty (Dordrecht: Springer), 379–405.

Conflict of Interest Statement: The authors declare that the research was conducted in the absence of any commercial or financial relationships that could be construed as a potential conflict of interest.

Received: 29 June 2013; paper pending published: 17 July 2013; accepted: 02 August 2013; published online: 30 August 2013.

Citation: Zhao N, Lamichhane HP and Hastings G (2013) Comparison of calculated and experimental isotope edited FTIR difference spectra for purple bacterial photosynthetic reaction centers with different quinones incorporated into the Q_A binding site. Front. Plant Sci. ***4****:328. doi: 10.3389/fpls.2013.00328*

This article was submitted to Plant Physiology, a section of the journal Frontiers in Plant Science.

frontiers in
PLANT SCIENCE

ORIGINAL RESEARCH ARTICLE
published: 21 October 2013
doi: 10.3389/fpls.2013.00417

The major thylakoid protein kinases STN7 and STN8 revisited: effects of altered STN8 levels and regulatory specificities of the STN kinases

Tobias Wunder[1], Wenteng Xu[1], Qiuping Liu[1], Gerhard Wanner[2], Dario Leister[1,3]* and Mathias Pribil[1,4]

[1] Plant Molecular Biology (Botany), Department Biology I, Ludwig-Maximilians-Universität München, Planegg-Martinsried, Germany
[2] Ultrastrukturforschung, Department Biology I, Ludwig-Maximilians-Universität München, Planegg-Martinsried, Germany
[3] PhotoLab Trentino - a Joint Initiative of the University of Trento (Centre for Integrative Biology) and the Edmund Mach Foundation (Research and Innovation Centre), San Michele all'Adige (Trento), Italy
[4] Mass Spectrometry Unit, Department Biology I, Ludwig-Maximilians-Universität München, Planegg-Martinsried, Germany

Edited by:
Mohammad M. Najafpour, Institute for Advanced Studies in Basic Sciences, Iran

Reviewed by:
Suleyman I. Allakhverdiev, Russian Academy of Sciences, Russia
Harvey J. M. Hou, Alabama State University, USA

***Correspondence:**
Dario Leister, Plant Molecular Biology (Botany), Department Biology I, Ludwig-Maximilians-Universität München, Großhaderner Str. 2, D-82152 Planegg-Martinsried, Germany
e-mail: leister@lmu.de

Thylakoid phosphorylation is predominantly mediated by the protein kinases STN7 and STN8. While STN7 primarily catalyzes LHCII phosphorylation, which enables LHCII to migrate from photosystem (PS) II to PSI, STN8 mainly phosphorylates PSII core proteins. The reversible phosphorylation of PSII core proteins is thought to regulate the PSII repair cycle and PSII supercomplex stability, and play a role in modulating the folding of thylakoid membranes. Earlier studies clearly demonstrated a considerable substrate overlap between the two STN kinases, raising the possibility of a balanced interdependence between them at either the protein or activity level. Here, we show that such an interdependence of the STN kinases on protein level does not seem to exist as neither knock-out nor overexpression of STN7 or STN8 affects accumulation of the other. STN7 and STN8 are both shown to be integral thylakoid proteins that form part of molecular supercomplexes, but exhibit different spatial distributions and are subject to different modes of regulation. Evidence is presented for the existence of a second redox-sensitive motif in STN7, which seems to be targeted by thioredoxin *f*. Effects of altered STN8 levels on PSII core phosphorylation, supercomplex formation, photosynthetic performance and thylakoid ultrastructure were analyzed in *Arabidopsis thaliana* using STN8-overexpressing plants (oe*STN8*). In general, oe*STN8* plants were less sensitive to intense light and exhibited changes in thylakoid ultrastructure, with grana stacks containing more layers and reduced amounts of PSII supercomplexes. Hence, we conclude that STN8 acts in an amount-dependent manner similar to what was shown for STN7 in previous studies. However, the modes of regulation of the STN kinases appear to differ significantly.

Keywords: chloroplast, protein phosphorylation, PSII supercomplexes, redox, STN kinases, thylakoid ultrastructure

INTRODUCTION

In *Arabidopsis thaliana*, the thylakoid kinase STN8 is predominantly responsible for the quantitative phosphorylation of PSII core proteins (CP43, D1, D2, and PsbH), particularly under high light conditions (Bonardi et al., 2005; Vainonen et al., 2005; Tikkanen et al., 2010). However, inactivation of STN8 alone does not completely abolish PSII core protein phosphorylation: D1 and D2 phosphorylation falls to about 50–60 and 35% of the wild-type level respectively (Vainonen et al., 2005). Only the knock-out of both STN8 and the LHCII kinase STN7 leads to quantitative loss of thylakoid phosphorylation, as monitored by immunodetection (Bonardi et al., 2005; Tikkanen et al., 2008). However, based on MS analyses, Fristedt et al. (2009) were still able to detect residual light-independent D2 phosphorylation in *stn7 stn8* double mutants, corresponding to less than 10% of the wild-type level. These results reveal a degree of overlap in substrate specificity between STN7 and STN8, although their main targets differ, and suggest that they might act in parallel rather than in series (Bonardi et al., 2005). By combining affinity chromatography with mass spectrometry, Reiland et al. (2011) have identified additional substrates of STN8, including the PGR5-like protein 1A (PGRL1A), which is essential for antimycin A (AA)-sensitive cyclic electron flow (CEF) around photosystem I (DalCorso et al., 2008). The differential phosphorylation of PGRL1A in *stn8-1* mutant plants is thought to permit more rapid switching between CEF and linear electron flow (LEF) during dark-light transitions (Reiland et al., 2011). Nevertheless, the function of reversible PSII core phosphorylation, the quantitatively major task of STN8, remains ambiguous.

Initially, the phosphorylated version of photo-damaged D1 was shown to be resistant to proteolysis (Koivuniemi et al., 1995), with the respective PSII complexes being able to move laterally from grana to stroma lamellae for subsequent dephosphorylation, degradation and replacement of damaged D1 (Rintamäki

et al., 1996). The emerging model suggested that the intensity of PSII core protein phosphorylation was correlated with the increase in damage to PSII reaction centers (D1) as light intensity rises, which would be compatible with an involvement of STN8 in D1 turnover during photoinhibition (Baena-Gonzalez et al., 1999). Making use of the STN kinase mutant collection in *A. thaliana*, a later study performed by Bonardi et al. (2005) indicated that STN8-mediated phosphorylation of D1 *per se* is not essential for D1 turnover and PSII repair, challenging the concept that phosphorylation plays a major role in the degradation of D1. Further investigations again provided evidence that lack of STN8 is associated with greater susceptibility to photoinhibition (Nath et al., 2007) and revealed that D1 degradation is delayed in *stn8* and *stn7 stn8* mutants exposed to less intense high-light conditions (Tikkanen et al., 2008). Tikkanen et al. (2008) attribute this difference between WT and the *stn8* and *stn7 stn8* mutants to disturbances in the disassembly of PSII supercomplexes, leading to less efficient exchange of damaged D1 between grana and stroma lamellae due to changes in its migration behavior. More recent studies by Fristedt et al. (2009) confirmed the observed delay in D1 degradation in *stn8* and *stn7 stn8* plants and proposed that the observed increase in the diameter and density of stacked thylakoid membranes (grana) in these lines reduces lateral diffusion of proteins, including photo-damaged D1 and the bulky FtsH complex. The latter is responsible for D1 degradation (Nixon et al., 2005; Adam et al., 2006) and was reported to be spatially separated from PSII in STN8-deficient mutants due to its relocation from the dense grana to the stroma lamellae and grana margins (Fristedt et al., 2009). Therefore, phosphorylation of PSII core proteins is currently assumed to modulate the macroscopic rearrangement of the thylakoid membrane network, as well as the formation of PSII supercomplexes, and to affect lateral movement of proteins within the membrane, thus exerting its effects on D1 turnover indirectly.

In the present study, the effect of increased PSII core phosphorylation in a line overexpressing STN8 (oe*STN8*) was analyzed with respect to its impact on PSII supercomplex formation and modulation of thylakoid membrane structure. Furthermore, we analyzed the topology and localization of the STN kinases and show that neither knock-out nor overexpression of STN7 or STN8 affects the accumulation of the other. Finally, we show that STN8 protein levels in wild-type plants do not depend on ambient light conditions, and present evidence for a direct interaction of STN7 with thioredoxins, which is independent of its N-terminal cysteine motif.

MATERIALS AND METHODS

PLANT MATERIAL

The *Arabidopsis thaliana* L. (*A. thaliana*) ecotype Columbia-0, used in this study as wild type (WT), was obtained from NASC (Nottingham Arabidopsis Stock Center; accession number N1092). Previously described mutant lines employed in this study were *stn7-1, stn8-1, stn7 stn8* (Bonardi et al., 2005), oe*STN7*, $STN7_{C\longrightarrow S:65+70}$ (Wunder et al., 2013), *hcf136* (Meurer et al., 1998), *psad1-1 psad2-1* (Ihnatowicz et al., 2004), *atpd-1,* and *petc-1* (Maiwald et al., 2003).

GENERATION OF STN8 OVEREXPRESSOR LINES (OESTN8)

To generate oe*STN8* lines, the full-length CDS of *STN8* was cloned into the plant vector pLeela, which is a derivative of pJawohl3-RNAi (GenBank Accession No. AF404854) containing a GATEWAY cassette introduced into the HpaI site, using the primers Stn8_attB1_ACC_f (GGGGACAAGTT TGTACAAAAAAGCAGGCTCTACCATGGCCTCTCTTCTCTC TC) and Stn8_attB2_Stop_r (GGGGACCACTTTGTACAA GAAAGCTGGGTTTCACTTGCTGAAACTGAGCTT). The *STN8*-pLeela construct containing a double Cauliflower Mosaic Virus (CMV) 35S promoter was introduced into the *stn8-1* mutant background via the floral-dip method (Clough and Bent, 1998). Plants were selected based on their BASTA resistance, segregation analysis was performed, and independent lines carrying a single T-DNA insertion locus were identified. Lines overexpressing the STN8 kinase (oe*STN8*) were identified by Western blot analysis employing an STN8-specific antibody.

GROWTH CONDITIONS AND LIGHT TREATMENTS

If not stated otherwise, plants to be analyzed were grown for 6 weeks under controlled conditions in a growth chamber on an 8 h/16 h day/night regime providing 100 µmol photons $m^{-2}s^{-1}$ during the light phase (standard lighting conditions). For experiments with the mutants *hcf136*, *petc-1, psad1-1 psad2-1,* and *atpd-1*, plants were grown on 1× MS medium including vitamins (Duchefa®) at 50 µmol photons $m^{-2}s^{-1}$. To study the effects of altered light conditions, plants were adapted to different light conditions specified as follows: 18h dark adaptation (D), adaptation to low light at 60–80 µmol photons $m^{-2}s^{-1}$ (LL) or high light at 800–1,200 µmol photons $m^{-2}s^{-1}$ (HL). The light source used for HL conditions was an Osram Powerstar HQIBT-D/400W lamp. Far-red light (FR) was emitted by LEDs at a wavelength of 740 nm and an intensity of 3.0 µmol photons $m^{-2}s^{-1}$. Adaptation to PSI and PSII light was performed essentially as described previously (Wagner et al., 2008). Briefly, 3-week-old plants were transferred from a climate chamber to either PSI- or PSII-specific light conditions. PSI light (15 µmol $m^{-2}s^{-1}$) was generated by clamping a medium red foil (Lee Filters, 027 Medium Red, transmittance 50% at 650 nm) over red fluorescent lamps (39 W) from Osram. PSII light (15 µmol $m^{-2}s^{-1}$) was generated by wrapping an orange foil (Lee Filters, 405 Orange, transmittance 50% at 560 nm) over white fluorescent lamps of the same type.

ISOLATION OF TOTAL PROTEINS

Total protein extracts were prepared from 6-week-old leaves according to Haldrup et al. (1999). About 0.1 g of leaf material was homogenized in 200 µl solubilization buffer (100 mM Tris pH 8.0, 50 mM EDTA pH 8.0, 0.25 M NaCl, 1 mM DTT, 0.7% SDS) and heated to 65°C for 10 min. Samples were centrifuged for 10 min at 10,000 *g* to remove insoluble debris and the protein concentration in the supernatant was determined with the amido black assay described by Schaffner and Weissmann (1973). The ubiquitously expressed actin protein was used as a loading control.

ISOLATION OF THYLAKOID MEMBRANES

Thylakoids were isolated by a modified procedure based on Bassi et al. (1995). Briefly, leaf material from *A. thaliana* plants was homogenized in ice-cold isolation buffer (0.4 M sorbitol, 0.1 M Tricine-KOH pH 7.8, 0.5% milk powder, 20 mM NaF), filtered through two layers of Miracloth (Calbiochem) and centrifuged at 1,500 *g* for 10 min at 4°C. The membrane pellet was resuspended in ice-cold resuspension buffer (20 mM HEPES-KOH pH 7.5, 10 mM EDTA, 20 mM NaF) followed by a centrifugation step at 10,000 *g* for 10 min at 4°C after 10 min of incubation on ice. Thylakoids were resuspended in TMK buffer (10 mM Tris-HCl pH 6.8, 10 mM $MgCl_2$, 20 mM KCl, 20 mM NaF). The chlorophyll concentration was determined in aqueous 80% acetone according to Porra (2002).

IMMUNOBLOT ANALYSIS

If not stated otherwise, antibodies raised against specific epitopes of STN7 and STN8 were used for Western blot analysis in this study. The peptides CKKVKVGVRGAEEFG of STN8 and LQELREKEPRKKANAQ, located at the C-terminus of STN7, served as immunogens (BioGenes GmbH, Berlin, Germany). Immunoblot analyses with these antibodies, as well as phosphothreonine-specific antibodies (Cell Signaling Technology, Inc., Boston, USA) and polyclonal antibodies raised against actin (Dianova, Germany), RbcL, PsaC, PsaB, PsbO, PsaE, AtpB, Lhcb2, Lhca3 (all Agrisera, Sweden), were performed as previously described (Ihnatowicz et al., 2008).

PAGE ANALYSES

For Blue-native polyacrylamide gel electrophoresis (BN-PAGE), samples of freshly isolated thylakoids corresponding to 50 μg Chl were resuspended in solubilization buffer (750 mM ε-aminocaproic acid, 50 mM Bis-Tris pH 7.0, 5 mM EDTA pH 7.0, 50 mM NaCl) and solubilized for 60 min with 1.5% (w/v) digitonin or for 10 min with n-dodecyl-β-D-maltoside (β-DM) (Sigma) on ice (Pribil et al., 2010). Soluble was then separated from insoluble material by centrifugation (13,100 *g*, 4°C) for either 70 min (digitonin) or 10 min (β-DM). After supplementing with 5% Coomassie brilliant blue G-250 in 750 mM ε-aminocaproic acid, the solubilized material was fractionated by non-denaturing BN-PAGE (4–12% PA) at 4°C as outlined in Heinemeyer et al. (2004). For the second dimension separation, a single lane of the BN gel was incubated in 2× Laemmli buffer with 100 mM DTT for 30 min, then placed on top of a SDS gel and subjected to electrophoresis (two-dimensional (2D) BN/SDS-PAGE) (Schottkowski et al., 2009a,b). Standard 12% SDS-PAGE was performed according to Laemmli (1970) unless indicated otherwise. For non-reducing SDS-PAGE, reducing agents (like DTT) were omitted from the loading dye and samples were not boiled if not otherwise stated.

THYLAKOID FRACTIONATION AFTER STATE 1 AND 2 ADAPTATION

Plants were acclimated to either state 1 or state 2 light and thylakoid fractionation was performed as previously described (Shapiguzov et al., 2010). Briefly, isolated thylakoids at a concentration of 0.6 mg of chlorophyll/mL were solubilized with 1% digitonin for 5 min, followed by stepwise centrifugation of supernatants. Pellets collected after centrifugation at 10,000 *g*, 40,000 *g* and 150,000 *g* represent enriched grana, grana margins and stroma lamellae fractions, respectively. The samples were analyzed by SDS-PAGE and Western blotting.

SUCROSE-GRADIENT FRACTIONATION OF THYLAKOID PROTEIN COMPLEXES

To prepare sucrose gradients, 11-mL aliquots of 0.4 M sucrose, 20 mM Tricine-NaOH (pH 7.5), 0.06% β-DM were subjected to three successive freeze-thaw (4°C) cycles. The gradient was underlaid with a cushion of 1 mL of 60% (w/v) sucrose. Thylakoids, prepared from plants that had been exposed to low light were washed twice with 5 mM EDTA (pH 7.8) and diluted to a final chlorophyll concentration of 2 mg/mL. Solubilization with β-DM at a final concentration of 1% was performed on ice for 10 min and followed by centrifugation (16,000 *g*, 5 min, 4°C). The supernatant was loaded on sucrose gradients and centrifuged at 132,000 *g* for 21 h at 4°C in a swing-out rotor (Beckman SW 40). Gradients were divided into 16 fractions, which were electrophoresed on a 15% SDS-PA gel and analyzed on a Western blot.

CHLOROPLAST ISOLATION AND FRACTIONATION INTO STROMA AND THYLAKOIDS

Chloroplasts were isolated from *A. thaliana* leaves as described (Aronsson and Jarvis, 2002). To obtain thylakoid and stroma fractions, chloroplasts were ruptured by adding 10 volumes of lysis buffer (20 mM HEPES-KOH pH 7.5, 10 mM EDTA) and incubating on ice for 30 min. The supernatant and pellet collected after a 30-min centifugation at 42,000 *g* and 4°C were used as stroma and thylakoid fractions, respectively.

SALT WASHES OF THYLAKOID MEMBRANES

Salt washes of thylakoid membranes were basically performed according to Karnauchov et al. (1997). Freshly isolated thylakoids (chlorophyll concentration 0.5 mg/mL) were incubated for 30 min on ice in HS buffer (0.1 M sucrose, 10 mM HEPES-NaOH pH 8.0) or HS buffer containing 2 mM NaCl, 2 M NaBr, 2 M NaSCN, 0.1 M Na_2CO_3 or 0.1 M NaOH, respectively. After addition of two volumes of HS buffer, the samples were centrifuged at 13,100 *g* for 15 min at 4°C. Proteins in the pellet fraction were subsequently solubilized directly in Laemmli buffer, whereas the supernatant was first precipitated in 80% acetone.

CHLOROPHYLL FLUORESCENCE MEASUREMENTS DURING LIGHT INDUCTION AND PSII INACTIVATION INDUCED BY HIGH LIGHT

Steady-state photosynthetic parameters were measured under actinic red light of increasing light intensity (22, 37, 53, 95, 216, 513, 825, 1,287, and 1,952 μmol photons $m^{-2}s^{-1}$), using the Dual-PAM 100 system (Heinz Walz GmbH, Effeltrich, Germany) in the Dual PAM mode, according to the manufacturer's instructions and with standard settings. Plants were dark-adapted for 10 min prior to measurements and allowed to adapt for 5 min to each new light level. Five plants of each genotype were analyzed for each measurement using always the sixth

true leaf of the respective plant. Photoinhibition of photosystem II (PSII) was induced over a period of 10 h with aid of the Imaging PAM System (Walz) by exposing leaves to blue light alternating every 2 min between HL (1,250 μmol photons $m^{-2}s^{-1}$) and LL (10 μmol photons $m^{-2}s^{-1}$). Maximum PSII quantum yield [Fv/Fm = (Fm − Fo)/Fm] was determined every 60 min after the LL phase and an additional 5-min dark adaptation.

REDOX TITRATION OF STN7 IN THYLAKOID MEMBRANES

Thylakoid proteins were isolated and equilibrated on ice for 3 h with various redox buffers (100 mM MOPS pH 7.0, 330 mM sorbitol) containing DTTred and DTTox in various molar ratios. Reactions were solubilized with 2% SDS and subsequently separated by non-reducing 15% SDS-PAGE. After transfer of proteins to PVDF membrane, reduced and oxidized forms of STN7 were detected by immunoblot analysis.

THIOREDOXIN (TRX) AFFINITY PURIFICATION

Affinity purification was basically performed as described by Motohashi et al. (2001). His-tagged recΔTRX-f (-m) was expressed in *E. coli* and purified by Ni-NTA resin according to the Qiagen protocol for native protein purification (Expressionist, Qiagen), without eluting resin-bound proteins. An aliquot of isolated thylakoid membranes (=1 mg Chl) was solubilized with 1.5% digitonin in 50 mM Tris-HCl pH 8.0 for 60 min. After centrifugation at 16,100 *g* for 70 min, the supernatant was incubated with the TRX-coupled resin (∼5 mg TRX/mL) for 60 min at RT. The column was washed three times with washing buffer (50 mM Tris-HCl pH 8.0, 200 mM NaCl, 0.2% digitonin) and proteins retained by thioredoxin were eluted by adding 10 mM DTT. Samples were analyzed on a Western blot, using STN7-specific antibodies.

MOBILITY SHIFT ASSAY OF TRX

For the TRX mobility shift assay, 10 μg of thylakoids were solubilized with 0.2% deoxycholic acid (DOC) and incubated with 25 μg of recombinant TRX-f (recΔTRX-f) for 30 min in 100 mM MOPS (pH 7.0) and 330 mM sorbitol at RT. Untreated thylakoids (in 0.2% DOC buffer) served as a control. Subsequently, protein mixtures were subjected to non-reducing SDS-PAGE and immunoblotting.

ANALYSIS OF THYLAKOID MEMBRANE ULTRASTRUCTURE BY TRANSMISSION ELECTRON MICROSCOPY (TEM)

Plants were grown for 4 weeks in the climate chamber on a 12 h/12 h day/night regime. 1.5 h after the onset of the light phase the sixth rosette leaf was cut off and fixed for 1 h with 2.5% glutaraldehyde in fixation buffer (75 mM cacodylic acid, 2 mM $MgCl_2$ pH 7.0). The material was washed with buffer, incubated for 2 h with 1% osmium tetroxide in fixation buffer, washed again with fixation buffer and finally with distilled water. Samples were dehydrated by sequential incubation in increasing acetone concentrations, embedded in resin and sectioned with a microtome after complete polymerisation. Micrographs of the sections were taken with an EM-912 electron microscope (Zeiss) equipped with an integrated OMEGA energy filter operated in the zero-loss mode.

RESULTS

STN7 AND STN8 ARE NOT LINKED BY A FEEDBACK LOOP

Previous studies had demonstrated a significant substrate overlap between the kinases STN7 and STN8 (Bonardi et al., 2005). To investigate whether alterations in STN7 levels affect STN8 accumulation and *vice versa*, *A. thaliana* mutant plants either lacking (*stn7-1* and *stn8-1*) or overexpressing (oe*STN7* and oe*STN8*) one of the kinases were analyzed. To this end, STN8 overexpressor lines (oe*STN8*) were generated that express STN8 under the control of the 35S promoter in the *stn8-1* mutant background. This resulted in an increase of 16-fold or more in STN8 protein levels relative to the WT (**Figure 1A**). The analysis of STN7 and STN8 proteins in oe*STN8* plants and the previously described mutant lines *stn7-1*, *stn8-1* and oe*STN7* (Bonardi et al., 2005; Wunder et al., 2013) using epitope-specific STN antibodies (**Figures 1B–D**) revealed no significant alterations in the level of the genetically unperturbed kinase. Thus, fluctuations in the availability of one STN kinase do not lead to compensatory changes in the concentration of the other one.

THE STN KINASES ARE THYLAKOID INTEGRAL MEMBRANE PROTEINS WITH DISTINCT SPATIAL DISTRIBUTIONS THAT FORM PART OF LARGE PROTEIN COMPLEXES

Previous evidence for the localization of the STN8 kinase was based on *in-vitro* import studies with pea chloroplasts (Bonardi et al., 2005). However, localization studies of STN8 with specific antibodies have not been performed. For this purpose, WT *A. thaliana* chloroplasts were fractionated into soluble and membrane components and subjected to immunoblot analysis using antibodies raised against a defined STN8 epitope. STN8 was detected exclusively in the membrane fraction, ruling out the existence of a soluble variant of the protein (**Figure 2A**). The purity of the respective fractions was confirmed by the detection of stroma (RbcL) and thylakoid membrane (Lhcb2) marker proteins. To clarify whether the hydrophobic moieties of the STN kinases truly represent predicted transmembrane domains (TMDs) (Vainonen et al., 2005) or mediate extrinsic attachment to the thylakoid membrane only, WT thylakoids were treated with alkaline buffers or chaotropic agents. Both STN7 and STN8 behaved like the Rieske protein (PetC) (**Figure 2B**), which has been shown to possess a single hydrophobic domain and to associate with the thylakoid membrane predominantly via electrostatic interactions (Karnauchov et al., 1997). Therefore, we conclude that both STN kinases constitute integral membrane proteins as previously suggested (Vainonen et al., 2005; Lemeille et al., 2009).

To monitor possible changes in the sub-thylakoid localization of the STN kinases under either STN7/8-activating or -inhibiting light conditions, thylakoids from WT plants were isolated after exposure to PSI- or PSII-specific light, and fractionated via differential centrifugation after solubilization with 1.5% digitonin. While STN8 was enriched in the grana membranes (10K fraction), STN7 was predominantly located in the stroma lamellae (150K fraction) (**Figure 3A**). The distributions of STN7 and

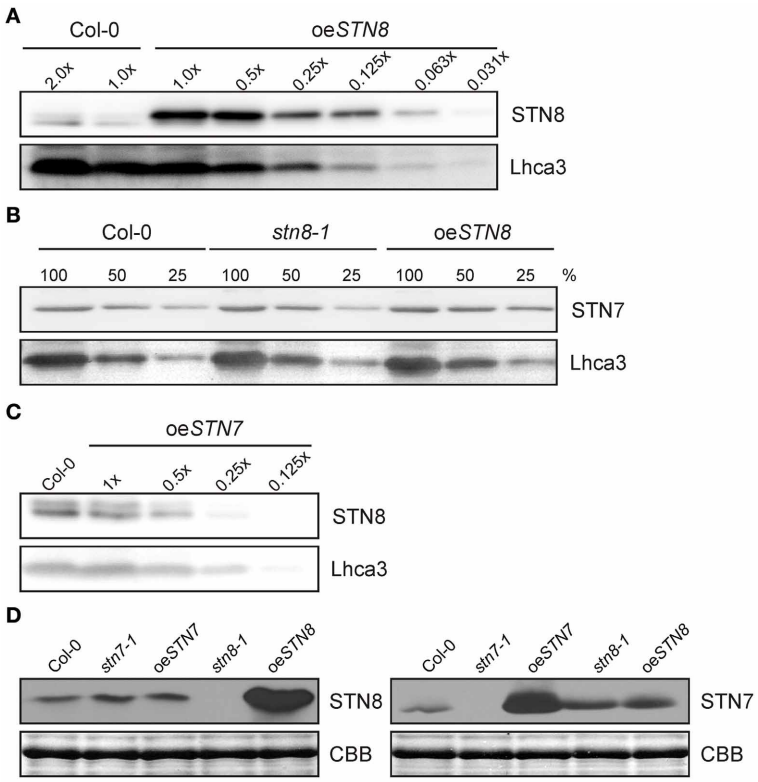

FIGURE 1 | Non-interdependence of STN kinase accumulation. (A) WT (Col-0) thylakoid proteins corresponding to 10 μg (2.0×) and 5 μg (1.0×) of Chl and serial dilutions of oe*STN8* thylakoids were loaded to quantify the levels of STN8 protein in oe*STN8* plants. Proteins were subjected to SDS-PAGE and Western blot analysis using STN8- and Lhca3-specific antibodies. **(B)** STN7 accumulation in thylakoids of WT (Col-0), oe*STN8* and *stn8-1* mutant plants. Thylakoid proteins, corresponding to 8 μg (100%), 4 μg (50%), and 2 μg (25%) of Chl, from each genotype were loaded on a SDS gel and probed using specific antibodies against STN7 and Lhca3 (as loading control). **(C)** Accumulation of STN8 in thylakoids of WT (Col-0) and oe*STN7*. Thylakoids of WT corresponding to 5 μg of Chl and serial dilutions of oe*STN7* thylakoid proteins were separated by SDS-PAGE, and immunoblots were probed with antibodies specific for STN8 and Lhca3 (as loading control). **(D)** Thylakoids of WT (Col-0), *stn8-1*, *stn7-1*, oe*STN8*, and oe*STN7* plants corresponding to 5 μg of Chl were analyzed by Western blotting with antibodies raised against an STN8-specific (left panel) or an STN7-specific (right panel) peptide fragment. Replicate SDS-gels were stained with Coomassie brilliant blue (CBB) and the section with the LHCII signal is shown as loading control.

STN8 between the different membrane fractions were not affected by exposure to PSI- or PSII-favoring light conditions. These data indicate that the major fraction of STN8 resides within the grana stacks close to its assumed primary substrates - the subunits of PSII - irrespective of light conditions. The major proportion of STN7 was localized to the stroma lamellae, with only a minor fraction being found in the grana margins or grana stacks. The distribution of STN7 thus coincides with that of PetC, a subunit of the Cyt b_6f complex known to interact physically with Stt7, the *Chlamydomonas* homolog of STN7 (Lemeille et al., 2009) (**Figure 3A**).

To further refine the localization of the STN kinases within the thylakoid membrane, their association with known thylakoid protein complexes was investigated. To this end, WT thylakoids were solubilized with 1.6% β-DM, separated on BN-PA gels and subsequently resolved via 2D-PAGE. Both STN7- and STN8-specific antibodies gave rise to signals covering the entire molecular weight range, from large supercomplexes down to the free protein fraction (**Figure 3B**), suggesting that they associate at least weakly with some of the major photosynthetic complexes.

Thylakoids were also fractionated by ultracentrifugation on a linear sucrose gradient after β-DM solubilization. Again, STN7 and STN8 were both identified in fractions containing high-molecular-weight (HMW) complexes (Figure S1A). These results agree with previous findings showing that Stt7 associates with a HMW complex (Lemeille et al., 2009), indicating that neither of the STN kinases normally occurs as a monomeric polypeptide, but remains in close association with HMW complexes.

The association of STN8 with HMW complexes was also probed by analyzing different mutant plants devoid of one of the major photosynthetic complexes, following analogous studies previously performed for STN7 (Wunder et al., 2013). Here, absence of PSII (in *hcf136*) also prevented STN8 accumulation, which is in agreement with their co-localization to grana lamellae (Figure S1B). Moreover, a strong decrease in STN8 levels was observed in plants lacking PSI (*psad1-1 psad2-1*), which is probably due to a significant concomitant reduction in PSII amounts rather than to the loss of PSI *per se*. Thus, the presence of PSII, the major constituent of thylakoid protein supercomplexes, seems to be a prerequisite for STN8 accumulation.

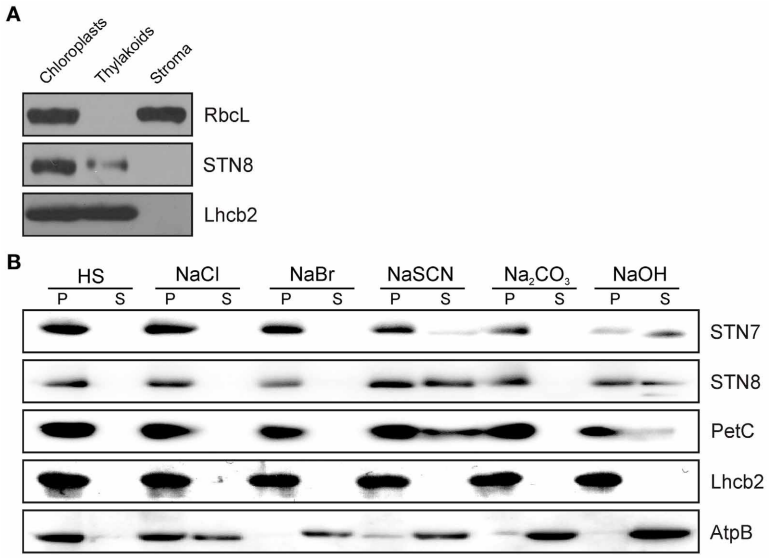

FIGURE 2 | Sub-organellar localization of STN8 and membrane association of the STN kinases. (A) *Arabidopsis* WT chloroplasts were fractionated into soluble and membrane components and subsequently separated by SDS-PAGE. After Western transfer, STN8, RbcL (stroma marker) and Lhcb2 (thylakoid marker) were detected using specific antibodies. **(B)** Extraction of membrane-associated proteins with alkaline buffers or chaotropic salt solutions. Thylakoid membranes from WT plants were resuspended at 0.5 mg chlorophyll/mL in HS buffer containing either 2 M NaCl, 0.1 M NaBr, 2 M NaSCN, 0.1 M Na_2CO_3, 0.1 M NaOH, or no additive. After incubation on ice, samples were fractionated into soluble (S) and membrane-associated proteins (P) and immunolabeled with antibodies specific for STN7, STN8, AtpB (a representative peripheral membrane protein), PetC (a membrane protein with a single hydrophobic domain predominantly anchored by electrostatic interactions), or Lhcb2 (an integral membrane protein with three transmembrane helices).

REDOX SENSITIVITY OF STN7

As recently demonstrated, STN7 activity is redox sensitive, and depends on an N-terminal cysteine motif (Wunder et al., 2013). To analyze possible redox-based effects on the tertiary structure of STN7, thylakoids of WT and $STN7_{C\longrightarrow S:65+70}$ mutant plants devoid of the N-terminal redox-sensitive cysteine motif (Wunder et al., 2013) were incubated in a series of buffers containing reduced and oxidized DTT in different molar ratios, and then subjected to non-reducing SDS-PAGE. Interestingly, both wild-type STN7 and $STN7_{C\longrightarrow S:65+70}$ monomers showed a clear size-shift in response to the redox treatment (**Figure 4A**), suggesting the occurrence of a redox-dependent conformational change in STN7 or the release of a possible redox-sensitive co-factor. This implies that the N-terminal CxxxxC motif is not the only redox-sensitive site in the STN7 protein. Under progressively more reducing conditions the amounts of STN7 detected increased significantly. This may indicate that under oxidizing conditions STN7 associates with various HMW aggregates/complexes, such that less STN7 enters the gel in the absence of reduced DTT. Also the STN7 epitope that is recognized by the peptide-specific antibody might be more accessible under reducing conditions.

STN7 activity, especially its inactivation under HL, is thought to be regulated via stromal thioredoxins such as TRX-f and -m (Rintamäki et al., 2000; Lemeille and Rochaix, 2010). So to search for a direct interaction between STN7 and TRX-f and/ or -m, recombinant TRX-f and TRX-m variants containing a single Cys-to-Ser exchange in their catalytic CGPC motifs (recΔTRXs) were generated. Due to this single cysteine mutation in the conserved TRX motif, stable covalent bonds instead of a transient interaction are formed during the disulfide bridge interchange reaction with the substrate. In this way, potential targets of TRXs are trapped as stable dimeric intermediates. To confirm such covalent binding of STN7 to recΔTRXs, WT thylakoids were solubilized with 1.5% (w/v) digitonin and incubated with either recΔTRX-f or recΔTRX-m immobilized on Ni-NTA resin. After several washing steps proteins interacting with recΔTRX-f and -m were eluted with a DTT-containing buffer, and the presence of STN7 was determined via Western analysis. Although slightly shifted in size, STN7 could indeed be detected in the fraction eluted from the recΔTRX-f resin, whereas no STN7 was detectable in the same fraction from the recΔTRX-m column (**Figure 4B**). In addition, the notion that STN7 can covalently bind to recΔTRX-f was supported by a significant decrease in amounts of STN7 in the flow-through in comparison to the input fraction (**Figure 4B**).

To further assess the possible interaction of STN7 with TRX-f, a TRX mobility-shift assay was performed. To this end, recΔTRX-f was incubated with solubilized thylakoids from WT, *stn7-1* and $STN7_{C\longrightarrow S:65+70}$ plants (**Figure 4C**). Covalent binding of recΔTRX-f to STN7 is expected to reduce the electrophoretic mobility of the STN7 signal due to the increased molecular weight of the resulting complex, but no STN7-TRX-f linkage product was detectable by Western analysis. However, the STN7 monomer disappeared almost completely upon addition of TRX-f (**Figure 4C**), suggesting a direct interaction between the two. Whether TRX-f treatment led to precipitation of STN7 or to formation of cross-linked, HMW aggregates in which

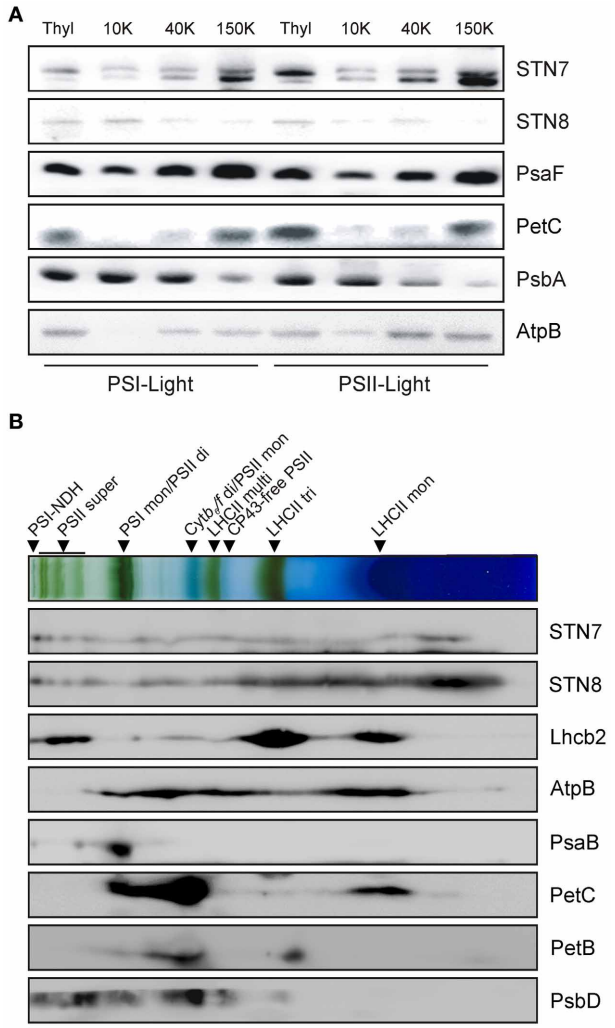

FIGURE 3 | Localization of the STN kinases within the thylakoid membrane. (A) Analysis of STN7 and STN8 localization by thylakoid membrane sub-fractionation. Thylakoids of PSII- or PSI-light adapted WT plants were fractionated into grana lamellae (10 K), grana margins (40 K) and stroma lamellae (150 K) by differential ultracentrifugation after digitonin solubilization. Proteins were separated by SDS-PAGE and analyzed by immunolabeling using antibodies against STN7, STN8, PsaF, PetC, PsbA, and AtpB. **(B)** Analysis of STN7 and STN8 distribution by 2D BN/SDS-PAGE. Thylakoid membranes of WT equivalent to 50 μg of Chl were solubilized with β-DM, subjected to 2D BN/SDS-PAGE and analyzed by Western blotting. STN7, STN8 and various subunits of the major photosynthetic complexes (AtpB, Lhcb2, PsaB, PetC, PetB, and PsbD) were detected with specific antibodies. Protein-Chl complexes are indicated by black arrowheads. The bands detected were identified as specific protein complexes in accordance with previously published profiles (Armbruster et al., 2013): PSI-NDH supercomplex (PSI-NDH), PSII supercomplexes (PSII super), PSI monomers and PSII dimers (PSI mon and PSII di), PSII monomers and dimeric Cyt b_6/f (PSII mon and Cyt b_6/f di), PSII monomers w/o CP43 (CP43-free PSII), multimeric (LHCII multi), trimeric (LHCII tri), and monomeric (LHCII mon) LHCII.

the STN7 epitope is inaccessible to the antibody could not be definitively clarified. Interestingly, the $STN7_{C\longrightarrow S:65+70}$ variant behaved like wild-type STN7 (**Figure 4C**), which supports the inference from the redox titration assay (**Figure 4A**) regarding the existence of a second redox-sensitive site within STN7.

STN8 PROTEIN LEVELS DO NOT RESPOND TO CHANGES IN LIGHT CONDITIONS

STN8 activity was previously shown to be regulated by changes in light quality and quantity (Bonardi et al., 2005; Tikkanen et al., 2010). In particular, FR and HL treatments led to a decrease and increase in PSII core protein phosphorylation respectively (Tikkanen et al., 2008, 2010). To investigate whether these changes are due to alterations in STN8 level or activity, WT plants were exposed for 2 h to LL after 18 h of darkness and subsequently transferred for 4 h to FR or HL (800 μmol photons $m^{-2}s^{-1}$), after which the amounts of STN8 present were determined. In contrast to STN7 (Wunder et al., 2013), STN8 levels did not change markedly upon these light-shift treatments, and showed no significant variations even after exposure to LL for up to 9 h (**Figure 5**). This stable expression profile suggests that STN8 is regulated at the level of specific activity rather than amount.

OVEREXPRESSION OF STN8 INCREASES PSII PROTEIN PHOSPHORYLATION AND DISASSEMBLY OF PSII SUPERCOMPLEXES UNDER HL CONDITIONS

To determine the effects of increased STN8 accumulation on thylakoid protein phosphorylation, WT, *stn8-1*, *stn7 stn8* and oe*STN8* plants were dark-adapted for 18 h, then exposed for 2 h to LL (80 μmol photons $m^{-2}s^{-1}$) followed by either 4 h of HL (1,000 μmol photons $m^{-2}s^{-1}$) or 2 h of FR. The phosphorylation status of isolated thylakoids was then monitored by Western blot using phosphothreonine-specific antibodies (**Figure 6A**). In general, oe*STN8* plants exhibited a significant increase in PSII core protein phosphorylation under all investigated light conditions. While PSII phosphorylation in WT plants decreased in the dark compared to LL conditions, PSII phosphorylation levels in oe*STN8* lines remained high under both conditions. After FR treatment, residual PSII phosphorylation was detectable only in oe*STN8*. The strongest increase in PSII core protein phosphorylation in oe*STN8* relative to WT was observed under HL, which is known to induce STN8 activity (Bonardi et al., 2005). Interestingly, pLHCII levels differed little between oe*STN8* and WT, suggesting that the excess STN8 present in oe*STN8* plants does not significantly affect the phosphorylation status of STN7-specific substrates under the light conditions examined (**Figure 6A**).

Under HL conditions, thylakoid phosphorylation - in particular phosphorylation of the PSII core proteins - has been shown to promote the disassembly of PSII supercomplexes (Tikkanen et al., 2008). To examine effects of increased PSII protein phosphorylation on PSII supercomplexes, BN-PAGE analyses were performed on thylakoids after exposure of oe*STN8* plants to 18 h D and 2 h LL (80 μmol photons $m^{-2}s^{-1}$) or 2 h HL (1,200 μmol photons $m^{-2}s^{-1}$). Solubilization of thylakoid samples from HL-treated plants with 1.5% digitonin prior to BN-PAGE revealed no significant differences between WT and *stn8-1*, while a slight decrease in the amount of PSII supercomplexes was noted in oe*STN8* (**Figure 6B**, left panel). Similar, but more pronounced, effects on PSII supercomplex accumulation were observed when

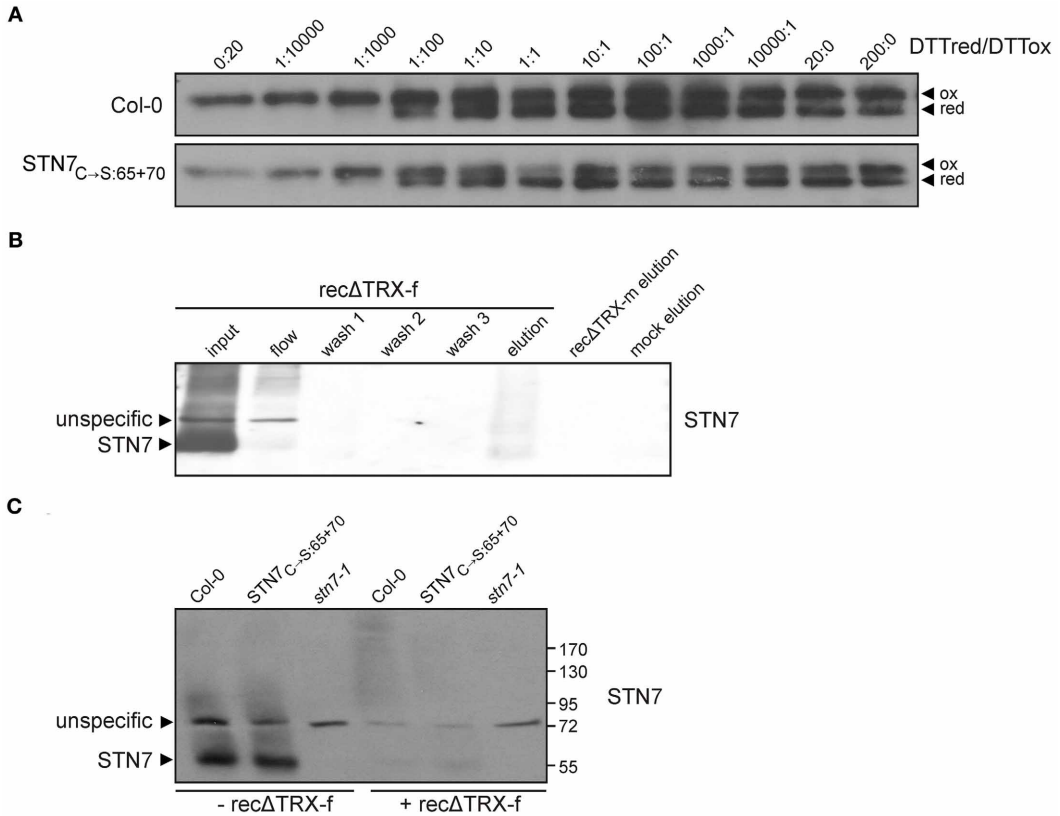

FIGURE 4 | Redox sensitivity of STN7. (A) Redox titration of STN7 variants. Thylakoids of WT (Col-0) and $STN7_{C\longrightarrow S:65+70}$ were equilibrated at various redox potentials using the DTTred/DTTox redox couple. After separation by non-reducing SDS-PAGE, STN7 was detected by immunoblotting. DTTred/DTTox ratios are indicated above each lane. Oxidized (ox) and reduced (red) forms of the STN7 monomer are indicated by black arrowheads. **(B)** STN7—TRX-f interaction assayed by thioredoxin affinity chromatography. His-tagged recombinant thioredoxins f and m, with one cysteine replaced by serine (recΔTRX-f, -m), were bound to Ni-NTA and incubated with thylakoids solubilized with 1.5% digitonin corresponding to 2 mg of Chl. After several washes, the eluates from recΔTRX-f and -m resins were subjected to Western blot analysis using STN7-specific antibodies. Solubilized WT (Col-0) thylakoids (input; corresponding to 10 μg of Chl), the flow through off the recΔTRX-f resin (flow; equivalent to 10 μg Chl), washes 1–3 of the recΔTRX-f resin and the eluate from a similarly treated Ni-NTA resin not coupled to recΔTRX (mock elution) were loaded as controls. **(C)** TRX-f mobility shift assay. Thylakoid membranes (10 μg Chl) from WT (Col-0), $STN7_{C\longrightarrow S:65+70}$ and *stn7-1* mutants were solubilized with 0.2% DOC and incubated with either 25 μg of recΔTRX-f or without additives. Proteins were separated by non-reducing SDS-PAGE and Western analysis was performed using STN7-specific antibodies.

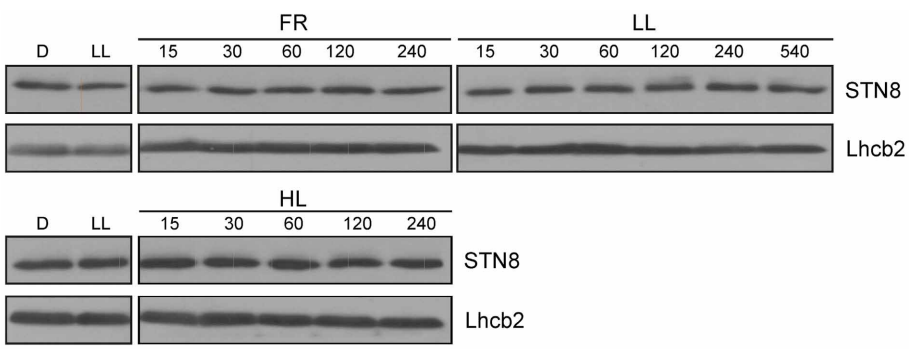

FIGURE 5 | STN8 protein accumulation upon exposure to D, LL, FR, and HL. WT plants were dark-adapted for 18 h, transferred to low light (LL; 80 μmol photons $m^{-2}s^{-1}$) for 2 h and then to FR or HL (HL; 800 μmol photons $m^{-2}s^{-1}$) for an additional 4 h. Leaf material was collected after each treatment and thylakoids were fractionated by SDS-PAGE and analyzed using antibodies specific for STN8 and Lhcb2 (loading control).

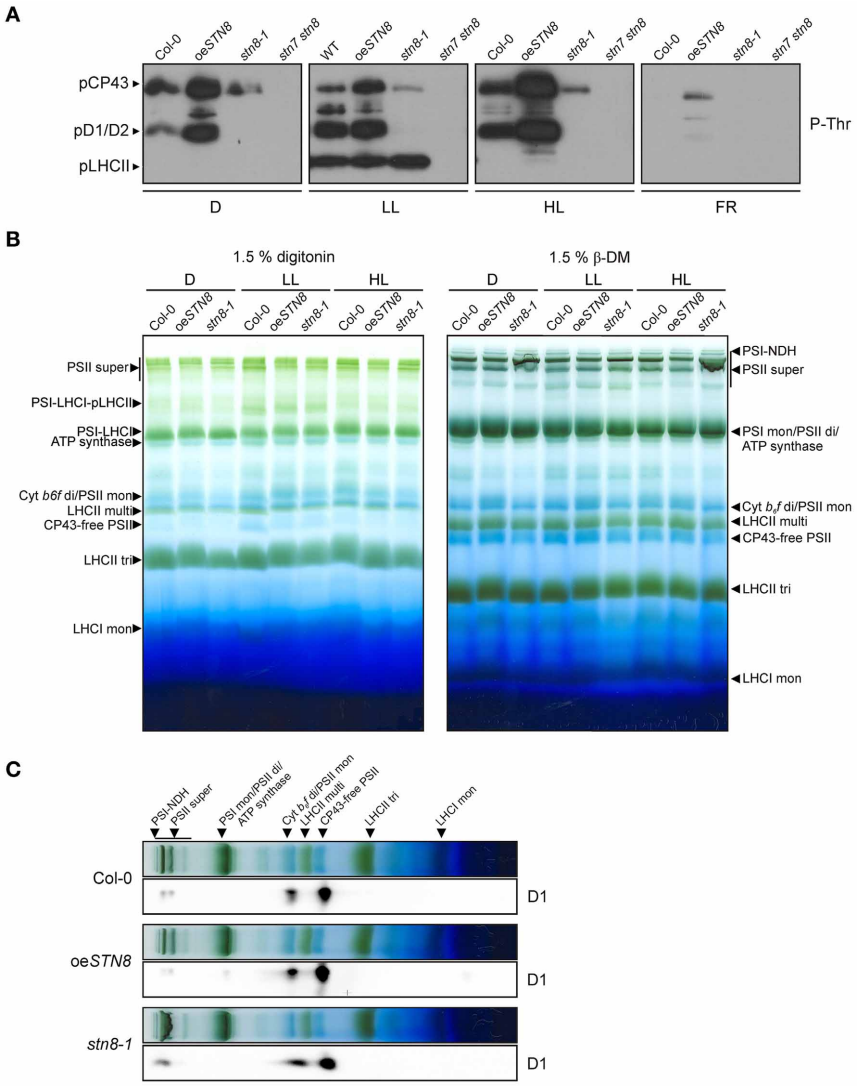

FIGURE 6 | Effects of altered STN8 levels on thylakoid phosphorylation and PSII supercomplex formation. (A) Thylakoid protein phosphorylation in WT (Col-0), oe*STN8, stn8-1*, and *stn7 stn8* plants dark-adapted for 18 h (D), subsequently transferred to LL (80 μmol photons $m^{-2}s^{-1}$) for 2 h and for additional 2 h to FR or 4 h to HL (1,000 μmol photons $m^{-2}s^{-1}$). After these light treatments, isolated thylakoids were analyzed by immunodetected using phosphothreonine (pThr) -specific antibodies (Cell Signaling). The positions of phosphorylated LHCII (pLHCII), CP43 (pCP43) and D1/2 (pD1/2) are indicated by black arrowheads. **(B)** Patterns of protein complexes solubilized from WT (Col-0), oe*STN8* and *stn8-1* thylakoids and separated on BN-PA gels. Thylakoid membranes of WT, oe*STN8* and *stn8-1* plants exposed to either LL (80 μmol photons m^{-2} s^{-1}) or HL (1,200 μmol photons $m^{-2}s^{-1}$) for 2 h, or kept in the dark for 18 h, were solubilized with 1.5% digitonin (left panel) or 1.5% β-DM (right panel) and separated by BN-PAGE. Protein-Chl complexes are indicated by black arrowheads. The bands detected were identified as specific protein complexes in accordance with previously published profiles (Armbruster et al., 2013): PSI-LHCI-pLHCII supercomplex (PSI-LHCI-pLHCII), PSI-LHCI supercomplex (PSI-LHCI), PSI-NDH supercomplex (PSI-NDH), PSII supercomplexes (PSII super), PSI monomers and PSII dimers (PSI mon and PSII di), PSII monomers and dimeric Cyt b_6f (PSII mon and Cyt b_6f di), PSII monomers w/o CP43 (CP43-free PSII), multimeric (LHCII multi), trimeric (LHCII tri) and monomeric (LHCII mon) LHCII. **(C)** BN-PAGE lanes bearing HL-treated samples corresponding to those shown in the right panel of **(B)** were subjected to SDS-PAGE in the second dimension and probed with D1-specific antibodies.

thylakoids were solubilized with 1.5% β-DM. Here, WT plants exposed to HL once again contained more PSII supercomplexes than oe*STN8* and fewer than *stn8-1* (**Figure 6B**, right panel), which is in accordance with earlier reports (Tikkanen et al., 2008).

2D-PAGE analysis was performed on HL-treated samples to assess the distribution of the PSII core proteins between PSII supercomplexes, dimers and monomers. Greater accumulation of D1 in PSII supercomplexes was observed in *stn8-1* compared to WT, whereas the opposite was the case for oe*STN8* (**Figure 6C**). In oe*STN8* a clear shift in the ratio of PSII supercomplexes to PSII dimers and monomers in favor of the latter two was observed in comparison to the situation in WT and the *stn8-1* mutant.

This suggests that disassembly of PSII supercomplexes is indeed enhanced by an increase in PSII core protein phosphorylation, as previously described (Tikkanen et al., 2008).

INCREASED STN8 LEVELS REDUCE SUSCEPTIBILITY TO PSII PHOTOINHIBITION AND LEAD TO A MODERATE RISE IN THE OXIDATION STATE OF THE PQ POOL

In previous studies, a decrease in the turnover of damaged D1 was observed in leaves of *stn7 stn8* and *stn8-1* plants exposed to high light. This was attributed to the lack of PSII core protein phosphorylation, which is a prerequisite for the disassembly of PSII supercomplexes and the migration of damaged PSII complexes from grana to stroma lamellae (Tikkanen et al., 2008; Fristedt et al., 2009). Accordingly, a reduction in PSII phosphorylation is expected to increase sensitivity to photoinhibition during HL treatment, which translates into lower Fv/Fm values relative to WT. To address the question whether increased PSII phosphorylation levels affect susceptibility to photoinhibition, WT, *stn8-1* and oe*STN8* plants were exposed to fluctuating light intensities by switching from LL (10 μmol photons $m^{-2}s^{-1}$) to HL (1,250 μmol photons $m^{-2}s^{-1}$) and back every 3 min. While *stn8-1* and WT plants did not differ significantly in their Fv/Fm values, as previously shown (Bonardi et al., 2005), Fv/Fm values in oe*STN8* plants were slightly higher than in WT (**Figure 7A**). This can be explained if one assumes that light fluctuations enhance the positive effect of elevated STN8 levels at the onset of HL by allowing a more rapid response to sudden light stress. Overall, enhanced disassembly of PSII supercomplexes under HL conditions, as in the case of oe*STN8* (**Figure 6**), seems to have only a moderate effect on PSII repair.

To explore general effects of altered PSII core phosphorylation on photosynthesis, Chl a fluorescence and absorption parameters were recorded for WT, oe*STN8*, *stn8-1* and *stn7 stn8* plants during dark-light transitions (**Figures 7B,C**). When dark-adapted plants were exposed to LL (22 μmol photons $m^{-2}s^{-1}$) for 6 min, no significant differences in the effective quantum yield of PSII (Φ_{II}) were detected between WT and *stn8-1*, while in oe*STN8* plants the Φ_{II} was initially higher and gradually converged to WT levels during the course of the measurement (**Figure 7B**). 1-qL, a measure of the excitation pressure of PSII, was somewhat lower in oe*STN8* compared to WT and *stn8-1*, which suggests a slightly more oxidized PQ pool (**Figure 7C**). As expected, the *stn7 stn8* mutant showed higher 1-qL and lower Φ_{II} values than the WT. Due to the slightly increased resistance of oe*STN8* plants to photoinhibition (**Figure 7A**), a degree of alteration in photosynthetic performance could be expected even under short-term exposure to high light. However, upon stepwise increase in light intensity (in 5-min steps), Φ_{II} and 1-qL measurements revealed no significant differences between oe*STN8* and WT plants (**Figures 7D–F**). Non-photochemical quenching (NPQ) alone showed a slight increase in oe*STN8* under strong light intensities, as in the case of *stn7 stn8* (**Figure 7F**).

To assess the performance of PSI in oe*STN8*, the photochemical quantum yield of PSI (Φ_I) and the quantum yield of non-photochemical energy dissipation in PSI due to donor (Φ_{ND}) or acceptor side limitation (Φ_{NA}) were determined in WT, oe*STN8, stn8-1* and *stn7 stn8* plants by performing a light curve with increasing light intensities (Figure S2). All PSI values determined for all mutant lines, except *stn7 stn8*, lay within the standard deviation of the WT. Only at weaker light intensities up to 216 μmol photons $m^{-2}s^{-1}$ did oe*STN8* show a slight tendency to higher (and *stn8-1* to lower) Φ_I values compared to WT (Figure S2).

INCREASED STN8 ACTIVITY RESULTS IN HIGHER GRANA STACKS

PSII phosphorylation, primarily mediated by STN8, has been proposed to alter the macroscopic folding of the thylakoid membrane (Fristedt et al., 2009). Specifically, a reduction in thylakoid protein phosphorylation, as in *stn8-1*, is associated with an increase in grana diameter (Fristedt et al., 2009). This effect was even more pronounced in the *stn7 stn8* double mutant (Fristedt et al., 2009; Herbstova et al., 2012; Armbruster et al., 2013), which in addition has fewer membrane layers per granum and therefore shows a reduction in grana height (Armbruster et al., 2013). To determine the effects of enhanced STN8-mediated phosphorylation on thylakoid ultrastructure, WT, oe*STN8* and *stn8-1* plants were adapted to LL for 1.5 h after 12 h of darkness, and the chloroplasts in thin sections of leaves were analyzed by transmission electron microscopy (**Figures 8A–C**). While grana stacks of WT exhibited an average ratio of diameter to height of 0.47/0.11 (±0.01/0.01) μm, the corresponding value for *stn8-1* grana was 0.58/0.06 (±0.02/0.00) μm (**Figure 8D**). These observations confirmed the significant tendency toward an increase in grana diameter in *stn8-1* (Fristedt et al., 2009), and the detected decrease in grana height is in good agreement with the measurements by Armbruster et al. (2013), giving a diameter/height ratio for *stn8-1* that lies between those for WT and *stn7 stn8* double mutant plants. oe*STN8* on the other hand showed an average grana diameter/height ratio of 0.54/0.15 (± 0.01/0.01) μm (**Figure 8D**). The moderate but significant increase in grana height compared to WT is in accordance with that seen in other mutant lines (i.e., *tap38*) showing enhanced thylakoid phosphorylation (Armbruster et al., 2013). However, this increase in grana height does not seem to be compensated by a decrease in grana diameter. All differences in grana diameter and height between the lines are significant at p-values of <0.05. Whether the observed changes in thylakoid ultrastructure associated with increased levels of STN8 result from (i) enhanced PSII phosphorylation, (ii) the concomitant alterations in PSII supercomplex composition or (iii) possible changes in the phosphorylation state of the CURT1 proteins, which were recently shown to mediate grana formation by inducing membrane curvature (Armbruster et al., 2013), remains to be elucidated.

DISCUSSION

STN KINASES: SIMILAR BIOCHEMICAL FEATURES BUT NO FUNCTIONAL INTERDEPENDENCE

When STL1, the STN8 homolog in *Chlamydomonas reinhardtii,* was shown to be phosphorylated in an Stt7-dependent manner (Lemeille et al., 2010), the idea was proposed that STN7 and STN8 might also form part of a kinase cascade (Lemeille and Rochaix, 2010). It was later shown that the phosphorylation status of STN7 is not affected in the *stn8-1* mutant, indicating that STN7 is not phosphorylated by STN8 (Reiland et al.,

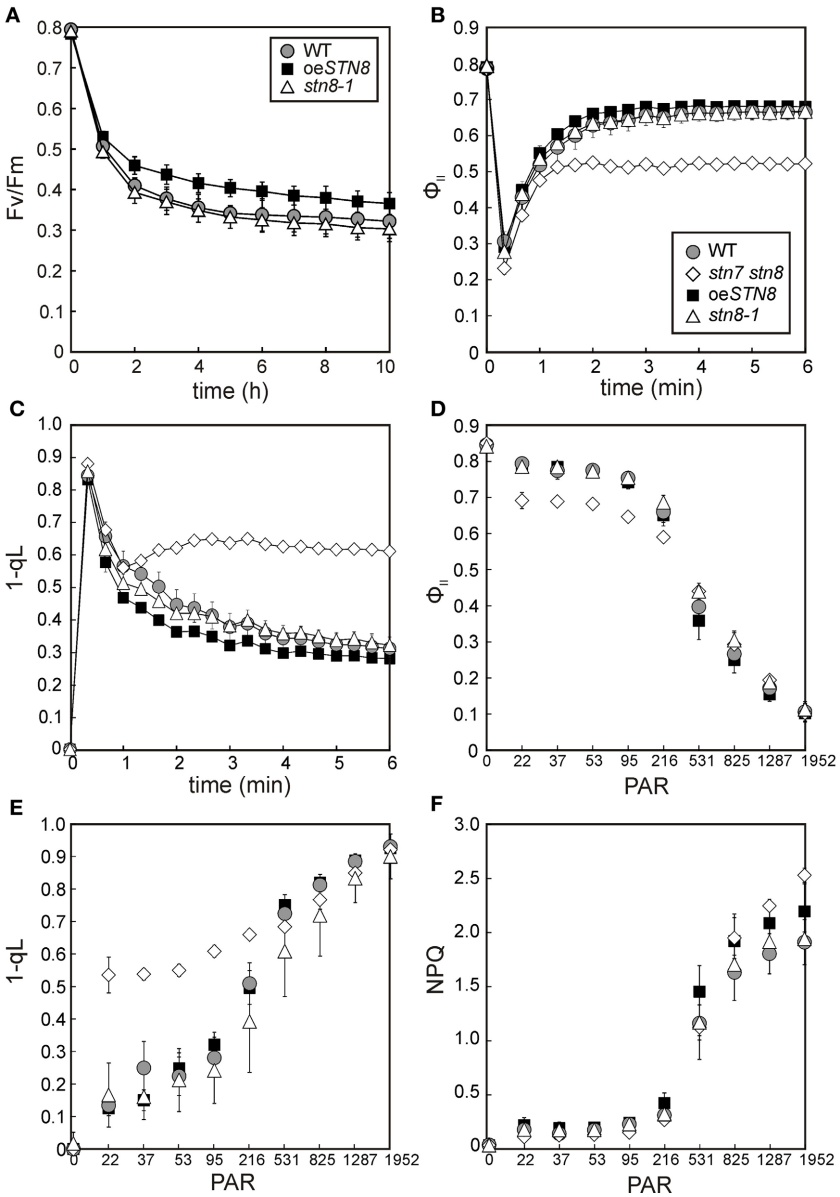

FIGURE 7 | Kinetics of Chl a fluorescence and time-course of PSII photoinhibition in WT, *stn8-1* and oe*STN8* plants. (A) WT, *stn8-1* and oe*STN8* plants were exposed to fluctuating (blue) light intensities for 10 h by switching from HL (1,250 μmol photons m^{-2} s^{-1}) to LL (10 μmol photons $m^{-2}s^{-1}$) and back every 3 min. The maximum quantum yield of PSII (Fv/Fm) was measured every 60 min after the LL phase and additional 5 min dark adaptation. HL exposure and PAM measurements were performed using an Imaging PAM system (Heinz Walz GmbH). **(B,C)** Time-course of the effective quantum yield of PSII (Φ_{II}) **(B)** and excitation pressure of PSII (1-qL) **(C)** of plants pre-incubated for 10 min in the dark and exposed to actinic red light (22 μmol photons $m^{-2}s^{-1}$) for 6 min. **(D–F)** Dependence of Chl a fluorescence on light intensity. The effective quantum yield of PSII (Φ_{II}) **(D)**, the excitation pressure of PSII (1-qL) **(E)** and non-photochemical quenching of chlorophyll fluorescence (NPQ) **(F)** were monitored as red light intensity was increased stepwise at 5-min intervals (22, 37, 53, 95, 216, 513, 825, 1,287, and 1,952 μmol photons $m^{-2}s^{-1}$) after 10 min of dark adaptation. PAR, photosynthetically active radiation (μmol photons $m^{-2}s^{-1}$); circles with gray filling, WT; squares with black filling, oe*STN8*; triangles; *stn8-1*; diamonds, *stn7 stn8*. **(A–F)** Plants were grown under an 8 h/16 h day/night regime at 100 μmol photons $m^{-2}s^{-1}$ prior to measurements. Average values (±SD) of at least five individual plants are shown.

2011). Therefore, it remains unclear whether STN7 and STN8 interact functionally, either directly or indirectly. It is however accepted that there is some substrate overlap between the two (Bonardi et al., 2005; Tikkanen et al., 2008, 2010), and this also applies to the corresponding protein phosphatases, with TAP38/PPH1 potentially targeting STN8 substrates (Vainonen et al., 2008; Pribil et al., 2010) and overexpression of PBCP - the PSII core protein phosphatase - affecting state transitions (Samol et al., 2012). Here, we show that, despite this complex interplay of these two protein kinase/phosphatase couples, knockout or

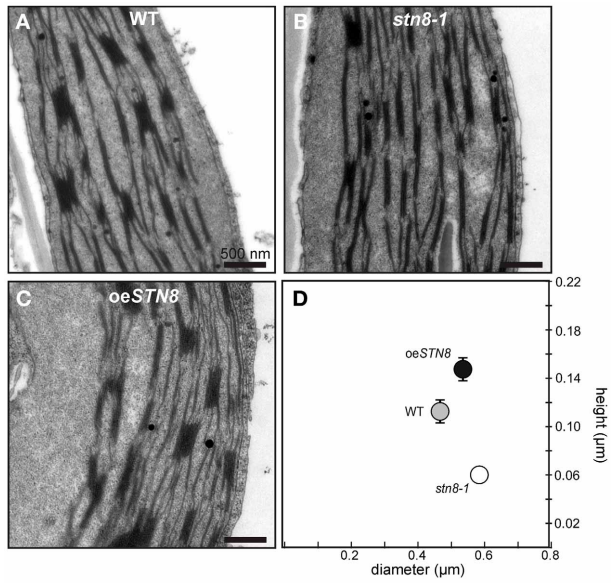

FIGURE 8 | Altered STN8 levels affect thylakoid ultrastructure. (A–C) True leaves of 4-week-old WT (Col-0), *stn8-1* and oe*STN8* plants grown at 100 µmol photons $m^{-2}s^{-1}$ at a 12/12 h night/day cycle were fixed 2 h after the onset of light and analyzed by transmission electron microscopy (TEM). Representative cross-sections of chloroplasts are shown for WT **(A)**, *stn8-1* **(B)** and oe*STN8* **(C)**, respectively. Bars represent 500 nm. **(D)** Scatter plot of the average grana diameter and height values ($n = 30$) in the genotypes shown in **(A–C)**. Bars represent the respective standard errors of the mean (SEM).

overexpression of one STN kinase does not significantly affect the activity or steady-state level of the other (**Figure 1**). Therefore, the overlap in substrate specificity of STN7 and STN8 is not reflected in a reciprocal response to changes in the level of either protein.

While the topology of Stt7 has been clarified experimentally (Lemeille et al., 2009), the assumption that STN8 is a single-pass transmembrane thylakoid protein with its kinase domain facing the stroma has been based solely on sequence predictions and the inference that PSII proteins are phosphorylated exclusively on their stromal moieties (Vainonen et al., 2005). However, the predictions of the putative transmembrane domain (TM) are not clear-cut, with some algorithms for TM prediction (i.e., TMHMM and SOSUI) suggesting that STN8 is a soluble protein. We have now confirmed that STN8 is an intrinsic thylakoid membrane protein, very similar in character to STN7 (**Figure 2**).

Furthermore, this study has also addressed the question whether STN7 and STN8 exist as monomeric enzymes or are associated with HMW complexes, as previously shown for Stt7 under state 1 and state 2 conditions (Lemeille et al., 2009). In 2D BN-/SDS-PAGE analyses we show that both STN kinases were associated with HMW complexes, and their presence in multiple assembly states of high molecular weight was further supported by data from sucrose-density-gradient centrifugations (**Figures 3**, S1). Interestingly, alterations in light quality had no significant effects on the localization of the STN kinases within the thylakoid membrane (**Figure 3A**). Thus, there is now comprehensive evidence that both STN7 and STN8 operate in close association with the major photosynthetic complexes. A lack of STN8 accumulation in plants devoid of PSII complexes (Figure S1) might further reflect the necessity for a close spatial relationship between STN8 and PSII core proteins, its most likely substrates. In line with these findings, STN8 was mainly detected in grana stacks or grana margins, the thylakoid fractions in which PSII accumulates (**Figure 3A**). These observations suggest that phosphorylation of PSII subunits by STN8 occurs directly. However, a kinase cascade residing in close proximity to the PSII complex cannot be ruled out. The latter scenario would explain results obtained by Hou et al. (2003), who showed that washing thylakoids with 2 M NaBr led to loss of the capacity for PSII core protein phosphorylation, whereas we showed here that most of the STN8 protein remained bound to the membrane after similar treatments (**Figure 2B**). Therefore, it is tempting to speculate that, instead of affecting the presence or activity of STN8, washing with NaBr removes downstream components that are part of a putative PSII core phosphorylation cascade.

THE STN KINASES EXHIBIT DISTINCTLY DIFFERENT REGULATORY FEATURES

It is generally accepted that STN7 activity can be inhibited via the stromal ferredoxin-thioredoxin pathway, but the precise site of inactivation remains a matter of speculation. Two main scenarios have been considered: (i) thioredoxins directly target the stroma-exposed cysteines Cys 187 and Cys 191, which reside within the ATP binding pocket (Puthiyaveetil, 2011) and (ii) the redox signal is transferred to the lumen via the putative CcdA/Hcf164 pathway targeting the lumenal cysteines Cys 65 and Cys 70 (Lemeille and Rochaix, 2010). Here, we have presented experimental evidence for a direct physical interaction between STN7 and recombinant thioredoxin-f (recΔTRX-f), which is not affected by replacement of the luminal STN7 cysteines Cys 65 and Cys 70 (**Figures 4B,C**). This observation supports the idea that STN7 is targeted by thioredoxins at its stromal CxxxC motif, which presumably interferes with the binding of ATP to the ATP binding pocket, especially under HL conditions, and thereby leads to the inactivation of STN7. The lack of this stromal cysteine motif in Stt7 and the fact that no thioredoxin-dependent inhibition of Stt7 has been found in *C. reinhardtii* (Puthiyaveetil, 2011) both argue in favor of this scenario. Further evidence for disulfide bridge formation in STN7, involving cysteines other than the known N-terminally located ones, was provided by redox titration experiments, which showed that STN7 reduction results in a shift in its migration behavior even in the absence of the N-terminal cysteine motif (**Figure 4A**). This suggests the presence of a second redox-sensitive motif besides the confirmed N-terminally located one, which could be regulated by thioredoxins. The observation that the electrophoretic mobility of STN7 is increased under reducing conditions is rather unusual for the opening of a disulfide bridge and might therefore be attributable to the release of an as yet unknown STN7-bound cofactor.

At least one of two conserved cysteine motifs, both of which are absent in STN8, is thought to be involved in thioredoxin-mediated down-regulation of Stt7/STN7 activity and protein levels under HL conditions (Rintamäki et al., 2000; Lemeille et al., 2009; Puthiyaveetil, 2011; Wunder et al., 2013). Thus, in contrast to STN7, STN8 activity is retained or even increased under these lighting conditions (Bonardi et al., 2005; Tikkanen et al., 2008).

As STN8 has none of the cysteine motifs that are commonly subject to redox-dependent regulation (Depège et al., 2003), it seemed possible that STN8 activity might be controlled on the level of protein amounts. However, in contrast to STN7, levels of the STN8 protein remained surprisingly stable both under activity-promoting and inactivating light conditions (**Figure 5**), suggesting that an activity-modulating mechanism must act on STN8. As such, reversible phosphorylation of STN8 could represent an essential mode of regulation. The phosphorylation of STL1, the STN8 homolog in *C. reinhardtii*, in a Stt7-dependent manner (Lemeille et al., 2010) argues in favor of this scenario.

PHYSIOLOGICAL EFFECTS OF VARYING STN8 PROTEIN LEVELS

Elevated STN8 levels resulted in an overall increase in CP43, D1 and D2 phosphorylation under all light conditions tested (**Figure 6A**). Only FR conditions, which cause a strong oxidation of the PQ pool, led to a substantial decrease in PSII phosphorylation even in the presence of increased amounts of STN8, supporting the notion that redox-responsive mechanisms act (presumably indirectly; see above) on STN8 activity. This PSI light-dependent dephosphorylation of PSII core proteins was proposed to be relevant for the formation of PSII supercomplexes, the photosynthetically most efficient conformation of PSII (Tikkanen et al., 2008; Tikkanen and Aro, 2012). In contrast, under HL conditions, LHCII is preferentially released from the photosystems to participate in heat dissipation (Allakhverdiev and Murata, 2004; Murata et al., 2007; Allakhverdiev et al., 2008) and amounts of PSII supercomplexes are decreased due to increased PSII protein phosphorylation (Tikkanen et al., 2008, 2010). While studies on the role of PSII core phosphorylation in D1 turnover based on the protein kinase mutants *stn8* and *stn7 stn8* have led to somewhat contradictory results (Bonardi et al., 2005; Tikkanen et al., 2008; Fristedt et al., 2009), more recently the consensus has emerged that PSII phosphorylation exerts a rather indirect influence on PSII turnover via the modulation of thylakoid ultrastructure and PSII complex formation and migration (Grouneva et al., 2013). Here we show that the increased PSII core phosphorylation in oe*STN8* plants (**Figure 6A**) indeed leads to a slight reduction in photoinhibition after long-term exposure to fluctuating HL (**Figure 7A**). The underlying increase in D1 turnover efficiency can be ascribed to mechanisms that involve (i) PSII supercomplex disassembly and/or (ii) the modulation of thylakoid membrane stacking.

(i) While Tikkanen et al. (2008) interpreted the observed delay in D1 degradation in the *stn8-1* mutants under HL as a consequence of slower disassembly of PSII supercomplexes, no such changes in the ratio of PSII supercomplexes to PSII monomers could be detected by Fristedt et al. (2009) after 3 h of HL treatment. Interestingly, the direct comparison of PSII supercomplex formation in WT, oe*STN8* and *stn8-1* of this study revealed an obvious discrepancy between the respective genotypes under D and LL, and even more so under HL conditions (**Figures 6B,C**). While the disassembly of PSII supercomplexes was slightly promoted in oe*STN8*, PSII supercomplexes clearly accumulated in *stn8-1*, suggesting clear effects of altered STN8 levels. However, these observations do not fully explain the altered resistance to photoinhibition seen for oe*STN8* but not for *stn8-1* (**Figure 7A**), as both genotypes exhibit aberrant PSII supercomplex formation compared to WT.

(ii) The slightly higher resistance of oe*STN8* to photoinhibition could also be due to an increase in charge-dependent repulsion of the thylakoid membranes, which is reported to cause looser grana stacking and therefore allows faster lateral movement of proteins (Fristedt et al., 2009). In fact, compared to WT, slight changes in macroscopic thylakoid membrane folding could be observed in oe*STN8* under low light intensities (**Figure 8**), where differences in PSII phosphorylation between oe*STN8* and WT are only marginal (**Figure 6A**). Surprisingly, both height and diameter of the grana stacks seemed to be slightly increased in oe*STN8* (**Figure 8**), which argues against facilitated movement of membrane proteins between grana and stroma thylakoids, at least from the perspective of the grana diameter (Fristedt et al., 2009). The idea that the association of HL-induced PSII phosphorylation with altered grana stacking is purely coincidental, and that other HL-induced, STN8-independent processes are actually responsible for the modulation of grana stacking can probably be ruled out also, as oe*STN8* shows somewhat increased grana stacking already under LL (**Figure 8**). This provides evidence that thylakoid protein phosphorylation mediated by STN8 is indeed responsible for the observed changes in thylakoid remodeling. Nevertheless, it remains unclear whether STN8-dependent changes in grana formation actually result from alterations in PSII core protein phosphorylation or possible changes in the phosphorylation state of the CURT1 proteins, which were shown to mediate grana formation by inducing membrane curvature (Armbruster et al., 2013), or other so far unknown thylakoid components. In this respect, whether the differences in PSII supercomplex composition are the cause or the consequence of the altered macroscopic thylakoid membrane folding remains to be elucidated. In conclusion, it can be stated that the aberrant phosphorylation of PSII core proteins in oe*STN8* and *stn8-1* plants has only a minor impact on photosynthetic performance (**Figures 7**, S2).

AUTHOR CONTRIBUTIONS

Research was designed by Tobias Wunder, Mathias Pribil and Dario Leister. Research was performed by Tobias Wunder, Wenteng Xu, Qiuping Liu, Gerhard Wanner, and Mathias Pribil. The manuscript was prepared by Mathias Pribil, Tobias Wunder, and Dario Leister. The whole study was supervised by Dario Leister.

ACKNOWLEDGMENTS

We thank the Deutsche Forschungsgemeinschaft (grant LE1265/21-1) for support and Paul Hardy for critical reading

of the manuscript. Further we thank Prof. Dr. Roberto Barbato (Alessandria, Italy) and Dr. Paolo Pesaresi (Milan, Italy) for providing antibodies against mature STN7 and STN8 and Dr. Alexander Hertle for providing recombinant TRX-f and -m.

SUPPLEMENTARY MATERIAL

The Supplementary Material for this article can be found online at: http://www.frontiersin.org/journal/10.3389/fpls.2013.00417/abstract

REFERENCES

Adam, Z., Rudella, A., and Van Wijk, K. J. (2006). Recent advances in the study of Clp, FtsH and other proteases located in chloroplasts. *Curr. Opin. Plant Biol.* 9, 234–240. doi: 10.1016/j.pbi.2006.03.010

Allakhverdiev, S. I., and Murata, N. (2004). Environmental stress inhibits the synthesis *de novo* of proteins involved in the photodamage-repair cycle of Photosystem II in Synechocystis sp. PCC 6803. *Biochim. Biophys. Acta* 1657, 23–32. doi: 10.1016/j.bbabio.2004.03.003

Allakhverdiev, S. I., Kreslavski, V. D., Klimov, V. V., Los, D. A., Carpentier, R., and Mohanty, P. (2008). Heat stress: an overview of molecular responses in photosynthesis. *Photosynth. Res.* 98, 541–550. doi: 10.1007/s11120-008-9331-0

Armbruster, U., Labs, M., Pribil, M., Viola, S., Xu, W., Scharfenberg, M., et al. (2013). Arabidopsis CURVATURE THYLAKOID1 Proteins modify thylakoid architecture by inducing membrane curvature. *Plant Cell* 25, 2661–2678. doi: 10.1105/tpc.113.113118

Aronsson, H., and Jarvis, P. (2002). A simple method for isolating import-competent Arabidopsis chloroplasts. *FEBS Lett.* 529, 215–220. doi: 10.1016/S0014-5793(02)03342-2

Baena-Gonzalez, E., Barbato, R., and Aro, E. M. (1999). Role of phosphorylation in the repair cycle and oligomeric structure of photosystem II. *Planta* 208, 196–204. doi: 10.1007/s004250050550

Bassi, R., Marquardt, J., and Lavergne, J. (1995). Biochemical and functional properties of photosystem II in agranal membranes from maize mesophyll and bundle sheath chloroplasts. *Eur. J. Biochem.* 233, 709–719. doi: 10.1111/j.1432-1033.1995.709_3.x

Bonardi, V., Pesaresi, P., Becker, T., Schleiff, E., Wagner, R., Pfannschmidt, T., et al. (2005). Photosystem II core phosphorylation and photosynthetic acclimation require two different protein kinases. *Nature* 437, 1179–1182. doi: 10.1038/nature04016

Clough, S. J., and Bent, A. F. (1998). Floral dip: a simplified method for Agrobacterium-mediated transformation of *Arabidopsis thaliana*. *Plant J.* 16, 735–743. doi: 10.1046/j.1365-313x.1998.00343.x

DalCorso, G., Pesaresi, P., Masiero, S., Aseeva, E., Schünemann, D., Finazzi, G., et al. (2008). A complex containing PGRL1 and PGR5 is involved in the switch between linear and cyclic electron flow in Arabidopsis. *Cell* 132, 273–285. doi: 10.1016/j.cell.2007.12.028

Depège, N., Bellafiore, S., and Rochaix, J. D. (2003). Role of chloroplast protein kinase Stt7 in LHCII phosphorylation and state transition in Chlamydomonas. *Science* 299, 1572–1575. doi: 10.1126/science.1081397

Fristedt, R., Willig, A., Granath, P., Crevecoeur, M., Rochaix, J. D., and Vener, A. V. (2009). Phosphorylation of photosystem II controls functional macroscopic folding of photosynthetic membranes in Arabidopsis. *Plant Cell* 21, 3950–3964. doi: 10.1105/tpc.109.069435

Grouneva, I., Gollan, P. J., Kangasjärvi, S., Suorsa, M., Tikkanen, M., and Aro, E. M. (2013). Phylogenetic viewpoints on regulation of light harvesting and electron transport in eukaryotic photosynthetic organisms. *Planta* 237, 399–412. doi: 10.1007/s00425-012-1744-5

Haldrup, A., Naver, H., and Scheller, H. V. (1999). The interaction between plastocyanin and photosystem I is inefficient in transgenic Arabidopsis plants lacking the PSI-N subunit of photosystem I. *Plant J.* 17, 689–698. doi: 10.1046/j.1365-313X.1999.00419.x

Heinemeyer, J., Eubel, H., Wehmhöner, D., Jänsch, L., and Braun, H. P. (2004). Proteomic approach to characterize the supramolecular organization of photosystems in higher plants. *Phytochemistry* 65, 1683–1692. doi: 10.1016/j.phytochem.2004.04.022

Herbstova, M., Tietz, S., Kinzel, C., Turkina, M. V., and Kirchhoff, H. (2012). Architectural switch in plant photosynthetic membranes induced by light stress. *Proc. Natl. Acad. Sci. U.S.A.* 109, 20130–20135. doi: 10.1073/pnas.1214265109

Hou, C. X., Rintamäki, E., and Aro, E. M. (2003). Ascorbate-mediated LHCII protein phosphorylation–LHCII kinase regulation in light and in darkness. *Biochemistry* 42, 5828–5836. doi: 10.1021/bi0343119

Ihnatowicz, A., Pesaresi, P., Lohrig, K., Wolters, D., Müller, B., and Leister, D. (2008). Impaired photosystem I oxidation induces STN7-dependent phosphorylation of the light-harvesting complex I protein Lhca4 in *Arabidopsis thaliana*. *Planta* 227, 717–722. doi: 10.1007/s00425-007-0650-8

Ihnatowicz, A., Pesaresi, P., Varotto, C., Richly, E., Schneider, A., Jahns, P., et al. (2004). Mutants for photosystem I subunit D of *Arabidopsis thaliana*: effects on photosynthesis, photosystem I stability and expression of nuclear genes for chloroplast functions. *Plant J.* 37, 839–852. doi: 10.1111/j.1365-313X.2004.02011.x

Karnauchov, I., Herrmann, R. G., and Klösgen, R. B. (1997). Transmembrane topology of the Rieske Fe/S protein of the cytochrome b6/f complex from spinach chloroplasts. *FEBS Lett.* 408, 206–210. doi: 10.1016/S0014-5793(97)00427-4

Koivuniemi, A., Aro, E. M., and Andersson, B. (1995). Degradation of the D1- and D2-proteins of photosystem II in higher plants is regulated by reversible phosphorylation. *Biochemistry* 34, 16022–16029. doi: 10.1021/bi00049a016

Laemmli, U. K. (1970). Cleavage of structural proteins during the assembly of the head of bacteriophage T4. *Nature* 227, 680–685. doi: 10.1038/227680a0

Lemeille, S., and Rochaix, J. D. (2010). State transitions at the crossroad of thylakoid signalling pathways. *Photosynth. Res.* 106, 33–46. doi: 10.1007/s11120-010-9538-8

Lemeille, S., Turkina, M. V., Vener, A. V., and Rochaix, J. D. (2010). Stt7-dependent phosphorylation during state transitions in the green alga *Chlamydomonas reinhardtii*. *Mol. Cell Proteomics* 9, 1281–1295. doi: 10.1074/mcp.M000020-MCP201

Lemeille, S., Willig, A., Depège-Fargeix, N., Delessert, C., Bassi, R., and Rochaix, J. D. (2009). Analysis of the chloroplast protein kinase Stt7 during state transitions. *PLoS Biol.* 7:e45. doi: 10.1371/journal.pbio.1000045

Maiwald, D., Dietzmann, A., Jahns, P., Pesaresi, P., Joliot, P., Joliot, A., et al. (2003). Knock-out of the genes coding for the Rieske protein and the ATP-synthase delta-subunit of *Arabidopsis*. effects on photosynthesis, thylakoid protein composition, and nuclear chloroplast gene expression. *Plant Physiol.* 133, 191–202. doi: 10.1104/pp.103.024190

Meurer, J., Plücken, H., Kowallik, K. V., and Westhoff, P. (1998). A nuclear-encoded protein of prokaryotic origin is essential for the stability of photosystem II in *Arabidopsis thaliana*. *EMBO J.* 17, 5286–5297. doi: 10.1093/emboj/17.18.5286

Motohashi, K., Kondoh, A., Stumpp, M. T., and Hisabori, T. (2001). Comprehensive survey of proteins targeted by chloroplast thioredoxin. *Proc. Natl. Acad. Sci. U.S.A.* 98, 11224–11229. doi: 10.1073/pnas.191282098

Murata, N., Takahashi, S., Nishiyama, Y., and Allakhverdiev, S. I. (2007). Photoinhibition of photosystem II under environmental stress. *Biochim. Biophys. Acta* 1767, 414–421. doi: 10.1016/j.bbabio.2006.11.019

Nath, K., Mishra, S., Zulfugarov, I., Raffi, S., An, G., and Lee, C. H. (2007). Characterization of a T-DNA inserted STN8 kinase mutant of *Ozyra sativa* L. *Photosynth. Res.* 91, 289.

Nixon, P. J., Barker, M., Boehm, M., De Vries, R., and Komenda, J. (2005). FtsH-mediated repair of the photosystem II complex in response to light stress. *J. Exp. Bot.* 56, 357–363. doi: 10.1093/jxb/eri021

Porra, R. J. (2002). The chequered history of the development and use of simultaneous equations for the accurate determination of chlorophylls a and b. *Photosynth. Res.* 73, 149–156. doi: 10.1023/A:1020470224740

Pribil, M., Pesaresi, P., Hertle, A., Barbato, R., and Leister, D. (2010). Role of plastid protein phosphatase TAP38 in LHCII dephosphorylation and thylakoid electron flow. *PLoS Biol.* 8:e1000288. doi: 10.1371/journal.pbio.1000288

Puthiyaveetil, S. (2011). A mechanism for regulation of chloroplast LHC II kinase by plastoquinol and thioredoxin. *FEBS Lett.* 585, 1717–1721. doi: 10.1016/j.febslet.2011.04.076

Reiland, S., Finazzi, G., Endler, A., Willig, A., Baerenfaller, K., Grossmann, J., et al. (2011). Comparative phosphoproteome profiling reveals a function of the STN8 kinase in fine-tuning of cyclic electron flow (CEF). *Proc. Natl. Acad. Sci. U.S.A.* 108, 12955–12960. doi: 10.1073/pnas.1104734108

Rintamäki, E., Kettunen, R., and Aro, E. M. (1996). Differential D1 dephosphorylation in functional and photodamaged photosystem II centers. Dephosphorylation is a prerequisite for degradation of damaged D1. *J. Biol. Chem.* 271, 14870–14875. doi: 10.1074/jbc.271.25.14870

Rintamäki, E., Martinsuo, P., Pursiheimo, S., and Aro, E. M. (2000). Cooperative regulation of light-harvesting complex II phosphorylation via the plastoquinol and ferredoxin-thioredoxin system in chloroplasts. *Proc. Natl. Acad. Sci. U.S.A.* 97, 11644–11649. doi: 10.1073/pnas.180054297

Samol, I., Shapiguzov, A., Ingelsson, B., Fucile, G., Crevecoeur, M., Vener, A. V., et al. (2012). Identification of a photosystem II phosphatase involved in light acclimation in *Arabidopsis*. *Plant Cell* 24, 2596–2609. doi: 10.1105/tpc.112.095703

Schaffner, W., and Weissmann, C. (1973). A rapid, sensitive, and specific method for the determination of protein in dilute solution. *Anal. Biochem.* 56, 502–514. doi: 10.1016/0003-2697(73)90217-0

Schottkowski, M., Gkalympoudis, S., Tzekova, N., Stelljes, C., Schünemann, D., Ankele, E., et al. (2009a). Interaction of the periplasmic PratA factor and the PsbA (D1) protein during biogenesis of photosystem II in *Synechocystis sp*. PCC 6803. *J. Biol. Chem.* 284, 1813–1819. doi: 10.1074/jbc.M806116200

Schottkowski, M., Ratke, J., Oster, U., Nowaczyk, M., and Nickelsen, J. (2009b). Pitt, a novel tetratricopeptide repeat protein involved in light-dependent chlorophyll biosynthesis and thylakoid membrane biogenesis in *Synechocystis sp*. PCC 6803. *Mol. Plant* 2, 1289–1297. doi: 10.1093/mp/ssp075

Shapiguzov, A., Ingelsson, B., Samol, I., Andres, C., Kessler, F., Rochaix, J. D., et al. (2010). The PPH1 phosphatase is specifically involved in LHCII dephosphorylation and state transitions in *Arabidopsis*. *Proc. Natl. Acad. Sci. U.S.A.* 107, 4782–4787. doi: 10.1073/pnas.0913810107

Tikkanen, M., and Aro, E. M. (2012). Thylakoid protein phosphorylation in dynamic regulation of photosystem II in higher plants. *Biochim. Biophys. Acta* 1817, 232–238. doi: 10.1016/j.bbabio.2011.05.005

Tikkanen, M., Grieco, M., Kangasjärvi, S., and Aro, E. M. (2010). Thylakoid protein phosphorylation in higher plant chloroplasts optimizes electron transfer under fluctuating light. *Plant Physiol.* 152, 723–735. doi: 10.1104/pp.109.150250

Tikkanen, M., Nurmi, M., Kangasjärvi, S., and Aro, E. M. (2008). Core protein phosphorylation facilitates the repair of photodamaged photosystem II at high light. *Biochim. Biophys. Acta* 1777, 1432–1437. doi: 10.1016/j.bbabio.2008.08.004

Vainonen, J. P., Hansson, M., and Vener, A. V. (2005). STN8 protein kinase in *Arabidopsis thaliana* is specific in phosphorylation of photosystem II core proteins. *J. Biol. Chem.* 280, 33679–33686. doi: 10.1074/jbc.M505729200

Vainonen, J. P., Sakuragi, Y., Stael, S., Tikkanen, M., Allahverdiyeva, Y., Paakkarinen, V., et al. (2008). Light regulation of CaS, a novel phosphoprotein in the thylakoid membrane of *Arabidopsis thaliana*. *FEBS J.* 275, 1767–1777. doi: 10.1111/j.1742-4658.2008.06335.x

Wagner, R., Dietzel, L., Bräutigam, K., Fischer, W., and Pfannschmidt, T. (2008). The long-term response to fluctuating light quality is an important and distinct light acclimation mechanism that supports survival of *Arabidopsis thaliana* under low light conditions. *Planta* 228, 573–587. doi: 10.1007/s00425-008-0760-y

Wunder, T., Liu, Q., Aseeva, E., Bonardi, V., Leister, D., and Pribil, M. (2013). Control of STN7 transcript abundance and transient STN7 dimerisation are involved in the regulation of STN7 activity. *Planta* 237, 541–558. doi: 10.1007/s00425-012-1775-y

Conflict of Interest Statement: The authors declare that the research was conducted in the absence of any commercial or financial relationships that could be construed as a potential conflict of interest.

Received: 16 August 2013; accepted: 01 October 2013; published online: 21 October 2013.

*Citation: Wunder T, Xu W, Liu Q, Wanner G, Leister D and Pribil M (2013) The major thylakoid protein kinases STN7 and STN8 revisited: effects of altered STN8 levels and regulatory specificities of the STN kinases. Front. Plant Sci. **4**:417. doi: 10.3389/fpls.2013.00417*

This article was submitted to Plant Physiology, a section of the journal Frontiers in Plant Science.

frontiers in
PLANT SCIENCE

ORIGINAL RESEARCH ARTICLE
published: 12 September 2013
doi: 10.3389/fpls.2013.00334

Photosynthetic acclimation responses of maize seedlings grown under artificial laboratory light gradients mimicking natural canopy conditions

Matthias Hirth†, Lars Dietzel†, Sebastian Steiner†, Robert Ludwig†, Hannah Weidenbach, Jeannette Pfalz and Thomas Pfannschmidt*†

Institut für Allgemeine Botanik und Pflanzenphysiologie, Lehrstuhl für Pflanzenphysiologie, Friedrich-Schiller-Universität Jena, Jena, Germany

Edited by:
Mohammad Mahdi Najafpour, Institute for Advanced Studies in Basic Sciences, Iran

Reviewed by:
Suleyman I. Allakhverdiev, Russian Academy of Sciences, Russia
Helmut Kirchhoff, Washington State University, USA

****Correspondence:***
Thomas Pfannschmidt, Laboratoire de Physiologie Cellulaire & Végétale, Univ. Grenoble Alpes, 17 rue des Martyrs, F-38054 Grenoble, France
e-mail: Thomas.Pfannschmidt@ujf-grenoble.fr

†Present address:
Matthias Hirth, Institut für Allgemeine Botanik und Pflanzenphysiologie, Professur für Molekulare Botanik, Friedrich-Schiller-Universität Jena, Dornburger Straße 159, Jena 07743, Germany;
Lars Dietzel, Institut für Molekulare Biowissenschaften, Pflanzliche Zellphysiologie, Biozentrum Goethe-Universität Frankfurt, Max-von-Laue-Straße 9, Frankfurt am Main 60438, Germany;
Sebastian Steiner, Klein Wanzlebener Saatzucht Saat AG, Grimsehlstraße 31, Einbeck 37574, Germany;
Robert Ludwig, Institut für Diagnostische und Interventionelle Radiologie I – AG Experimentelle Radiologie, Universitätsklinikum Jena – Friedrich-Schiller Universität Jena, Erlanger Allee 101, Jena 07747, Germany;
Thomas Pfannschmidt, Laboratoire de Physiologie Cellulaire & Végétale, Univ. Grenoble Alpes, 17 rue des Martyrs, Grenoble F-38054, France

In this study we assessed the ability of the C4 plant maize to perform long-term photosynthetic acclimation in an artificial light quality system previously used for analyzing short-term and long-term acclimation responses (LTR) in C3 plants. We aimed to test if this light system could be used as a tool for analyzing redox-regulated acclimation processes in maize seedlings. Photosynthetic parameters obtained from maize samples harvested in the field were used as control. The results indicated that field grown maize performed a pronounced LTR with significant differences between the top and the bottom levels of the plant stand corresponding to the strong light gradients occurring in it. We compared these data to results obtained from maize seedlings grown under artificial light sources preferentially exciting either photosystem II or photosystem I. In C3 plants, this light system induces redox signals within the photosynthetic electron transport chain which trigger state transitions and differential phosphorylation of LHCII (light harvesting complexes of photosystem II). The LTR to these redox signals induces changes in the accumulation of plastid *psaA* transcripts, in chlorophyll (Chl) fluorescence values F_s/F_m, in Chl *a/b* ratios and in transient starch accumulation in C3 plants. Maize seedlings grown in this light system exhibited a pronounced ability to perform both short-term and long-term acclimation at the level of *psaA* transcripts, Chl fluorescence values F_s/F_m and Chl a/b ratios. Interestingly, maize seedlings did not exhibit redox-controlled variations of starch accumulation probably because of its specific differences in energy metabolism. In summary, the artificial laboratory light system was found to be well-suited to mimic field light conditions and provides a physiological tool for studying the molecular regulation of the LTR of maize in more detail.

Keywords: photosynthesis, redox regulation, light quality, light acclimation, maize fields

INTRODUCTION

Plants need to cope with natural variations in illumination and temperature during their vegetation period. The major process affected by both parameters is photosynthesis, which is both light- and temperature-sensitive due to the tight coupling between light and dark reaction (Hüner et al., 1998; Blankenship, 2002). Photosynthesis, therefore, represents an attractive target for biotechnological improvements in order to promote growth and yield of crop plants (Long et al., 2006; Zhu et al., 2010).

Natural illumination of plants is highly fluctuating in intensity and quality mainly because of seasonal and daily periodicity and of short-term disturbances caused from, e.g., clouding or leaf movement. Beside these abiotic influences plants themselves create strong light gradients especially within dense plant populations where leaves of neighboring plants shade each other and

compete for light. This competition for light results in strong decreases in light intensity and a relative enrichment in far-red wavelengths within the canopy (Terashima et al., 2005). The latter effect is sensed by photoreceptors which control photomorphogenesis or shade avoidance responses (Ballare, 1999; Smith, 2000). The enrichment in far-red light wavelengths has an additional strong impact on photosynthesis since it can be partly used by photosystem I (PSI) but not or less effectively by photosystem II (PSII) causing imbalanced distribution of excitation energy between the photosystems. During evolution plants developed a number of responses which optimize light utilization under these variable conditions (Aro and Andersson, 2001; Blankenship, 2002). Developmental responses at the whole-plant or leaf level include variation of photosynthetic capacity by modification of leaf thickness (e.g., sun and shade leaves) which take place within weeks and months. They act in concert with more dynamic molecular acclimation mechanisms at the chloroplast level which work within the range of minutes to several hours. These physiological responses are fully reversible. In the short-term functionality of the photosystem antennae is adjusted by important regulatory processes such as non-photochemical quenching for pH dependent dissipation of excess excitation energy under high light as well as state transitions – a posttranslational modification, which counteracts imbalanced excitation of the photosystems under low light. In the long-term, changes in gene expression control an adjustment of photosystem stoichiometry which work in the same functional direction as state transitions, but create a longer lasting effect (Melis, 1991; Anderson et al., 1995; Allen and Pfannschmidt, 2000; Haldrup et al., 2001; Allen, 2003; Holt et al., 2004; Pons and de Jong-Van Berkel, 2004; Kanervo et al., 2005; Walters, 2005; Eberhard et al., 2008; Horton et al., 2008; Kargul and Barber, 2008). These different responses generate a hierarchical framework which countervails the high variability in illumination and optimize photosynthetic electron transport (Frenkel et al., 2007; Dietzel et al., 2008). Therefore, it was proposed that manipulation of photosynthetic acclimation might help to improve photosynthesis (Horton et al., 2001; Murchie et al., 2009). In general, photosynthetic acclimation appears to be a chloroplast-autonomous regulation being independent of photoreceptors (Walters et al., 1999; Fey et al., 2005a); however, because of the numerous interactions in the plant cellular signaling network indirect photoreceptor and hormone influences must be also taken into account (Boonman et al., 2007, 2009).

Photosystem stoichiometry adjustment could be found in shade- and sun- as well as in mono- and dicot plants (Chow et al., 1988, 1990a; Pfannschmidt et al., 1999a; Fan et al., 2007) and appears to be an ubiquitous acclimation response in photosynthetic organisms (Melis, 1991; Allen and Pfannschmidt, 2000). Recent studies with the model organism *Arabidopsis thaliana* have revealed that the thylakoid-associated kinase STN7 is a key regulator of this long-term response (LTR; Bonardi et al., 2005; Pesaresi et al., 2009). Using knock out mutants as negative control it could be demonstrated that state transitions and LTR provide a physiological advantage under permanently changing conditions resulting in enhanced growth and seed production (Bellafiore et al., 2005; Frenkel et al., 2007; Wagner et al., 2008). Furthermore, systems biology approaches revealed that photosynthetic acclimation responses not only reconfigure the photosynthetic apparatus to the instantaneous light environment but also trigger a metabolic reprogramming which coordinates the energetic demands with the light harvesting efficiencies of the plant (Bräutigam et al., 2009; Frenkel et al., 2009). The studies demonstrated that starch accumulation in *Arabidopsis* significantly differs between different light quality acclimation states and, thus, represents a well-suited reporter for the metabolic reprogramming that finally controls plant growth efficiency (Bräutigam et al., 2009).

Maize is one of the world's most important field crops and improvement of its photosynthetic yield would be of great interest (Zhu et al., 2010). Maize fields generate tall and dense plant stands during its vegetation period, which contains strong light gradients and, hence, a high degree of photosynthetic acclimation should be expected. Recent observations demonstrated that maize exhibit a high ability for photosynthetic acclimation when grown under different white light (WL) intensities in growth chambers. Variations in antenna structures and LHC protein accumulation were found both in mesophyll and bundle sheath chloroplasts (Drozak and Romanowska, 2006).

Here, we analyzed the degree of photosynthetic acclimation in maize grown under low-intensity artificial light qualities, which preferentially excite either PSI or PSII. This test system was successfully used previously for understanding redox-controlled photosynthetic acclimation in C3 plants like mustard, tobacco and *Arabidopsis* (Pfannschmidt et al., 1999a,b, 2001; Fey et al., 2005b; Wagner et al., 2008). Light quality acclimation to artificial light quality gradients could be demonstrated to be efficient and beneficial in various C3 species (Chow et al., 1990b; Hogewoning et al., 2012). In order to test the corresponding response of the C4 plant we determined chlorophyll (Chl) a fluorescence, Chl a/b ratios, transcript accumulation of plastid gene *psaA* (encoding the core protein of PSI), phosphorylation state of light harvesting complexes of PSII (LHCII) and the ability to perform state transitions. The detected acclimation ability was compared to that of samples harvested from maize plants grown under natural conditions. Our study indicates a high ability of maize to acclimate to light quality gradients in low-intensity light conditions in a lab based system providing a tool for analyzing the potential of the maize LTR for biotechnology applications.

RESULTS

LIGHT GRADIENTS AND PHOTOSYNTHETIC ACCLIMATION OF MAIZE UNDER FIELD CONDITIONS

Light intensity within plant populations decreases as a function of the leaf area index (LAI) while at the same time an enrichment of far-red wavelengths occurs (Smith, 2000; Hirose, 2005). We wanted to test if we could use a laboratory light set-up to study acclimation responses of maize seedlings to natural light gradients. In order to have a reference we analyzed the course of light gradients in a maize field trail by determination of light intensity and spectrum at different heights (**Figure 1**) of full-grown maize plants. 80% of the light was absorbed within the top 10–20% of the field, all lower parts obtained low light intensities with a strong enrichment in the far-red range (**Table 1**).

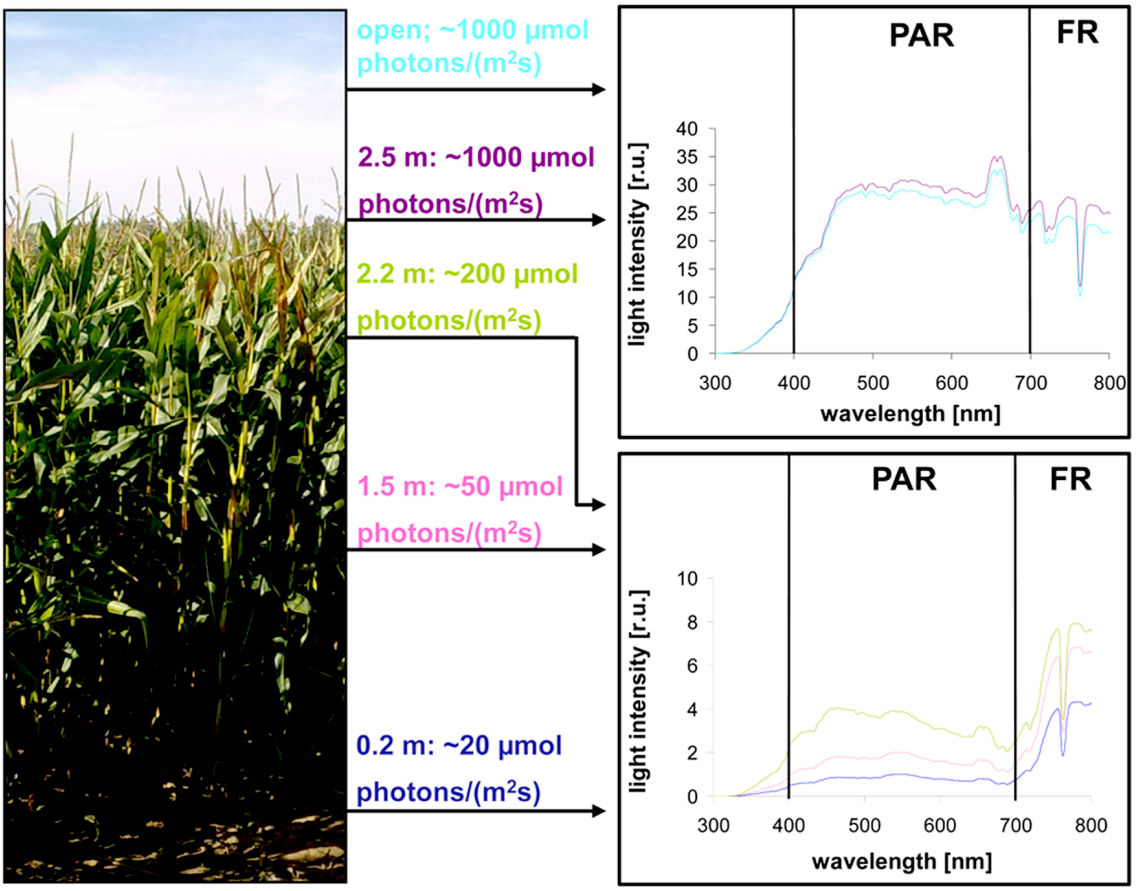

FIGURE 1 | Natural illumination conditions within the maize field used for sampling. Left picture displays the plant stand used for measurements. Light intensities determined at indicated heights within the stand are given in the middle panel. Corresponding light spectra (indicated by the same color) at the respective position are shown on the right. Open: intensity and spectrum of full sunlight outside the field. PAR: photosynthetic active radiation. FR: far-red region.

Thus, even under sunny conditions the majority of the leaves in the field perceived only a sub-saturating photosynthetic active radiation (PAR) with a three- to four-times higher proportion of far-red light. To analyze effects on the photosynthetic performance of the plants we harvested plant leaf samples from the top, the middle and the bottom region of the stand. To include possible effects of the leaf blade position and the developmental gradient in chloroplast biogenesis we studied three segments of the leaves (basal, middle, and top segment; **Figure 2A**). In order to study the potential light acclimation we probed the Chl *a/b* ratio as indicator for changes in the amount of LHCII and the Chl fluorescence value F_s/F_m as physiological marker for the LTR, This value represents the fraction of light which is absorbed by the PSII antenna and subsequently lost by constitutive dissipation *via* fluorescence and heat emission in the steady state. Photosystem stoichiometry adjustment creates significant changes in this parameter (Pfannschmidt et al., 2001). The Chl *a/b* ratio was found to be significantly higher in level 1 than in level 2 and 3 (**Figure 2B**) while the measured F_s/F_m values were lower in level 1 and increased step-wise toward level 2 and 3 (**Figure 2C**) with a significant difference in section 2 of level 1 and 3. Effects of the leaf gradient were hardly detectable with the exception of segment 1 in level 2 which displayed a slightly more pronounced increase in the F_s/F_m values than segments 2 and 3. The starch content was found to be relatively stable at the different levels of sampling (**Figure 2D**) with a weak tendency to increase toward the bottom level which, however, was only significant in segment 2 of level 3. In summary, the measured parameters F_s/F_m and Chl *a/b* demonstrated typical changes between top and bottom level being indicative for a functional LTR in maize under field conditions.

PHOTOSYNTHETIC ACCLIMATION OF MAIZE SEEDLINGS TO LIGHT QUALITY GRADIENTS

Recently, we described the physiological and molecular acclimation of the dicotyledonous C3 plants *A. thaliana, Nicotiana tabacum*, and *Sinapis alba* grown in a light system which preferentially excites either PSI or PSII (Pfannschmidt et al., 2001; Fey et al., 2005b; Wagner et al., 2008; Steiner et al., 2009). Here, we used the same set-up to analyze photosynthetic acclimation in the monocotyledonous C4 plant *Zea mays*. Seedlings were grown under WL as control and under PSI- or PSII-light (PSI, PSII) in

Table 1 | Ratio of short and long wavelengths in the different field stories.

Position in field	R/FR
Outside	1.413 ± 0.002
2.5 m	1.351 ± 0.012
2.2 m	0.483 ± 0.068
1.5 m	0.561 ± 0.147
0.2 m	0.400 ± 0.070

The ratio has been calculated from integration of the values measured in the wavelength ranges 655–665 (R: red) and 725–735 (FR: far-red) nm. Results represent means of three measurements, standard deviation is given.

order to test their ability to perform a LTR. Additional controls were shifted between the PSI- and PSII-lights (PSI-II; PSII-I) to test the reversibility of the response, an important criterion to distinguish between acclimation and development. The general appearance of the plants grown under the different light regimes did not reveal major morphological differences which is consistent with earlier observations in C3 plants (**Figure 3A**). For detection of a LTR the second true leaves of 10-day-old plants were used for measuring the F_s/F_m parameter by video imaging (**Figure 3A**). In this experimental set-up PSI-light acclimated plants absorb more light than they can use and dissipate the excess as fluorescence which usually is significantly higher in the steady-state than that from PSII-light acclimated plants. A deficiency in performing a LTR, however, is indicated by a loss of significant changes in F_s/F_m as observed in the *stn7* mutant of *Arabidopsis* (Bonardi et al., 2005). WL plants exhibited a low F_s/F_m value while PSI plants displayed a high one. After a shift from PSI-light to PSII-light the F_s/F_m value in the seedlings declined. In PSII-plants it was low and increased after a shift of the plants to PSI-light. This result is consistent with earlier measurements of F_s/F_m values in C3 plants indicating that maize seedlings are able to perform a LTR in the same manner.

2D images of the Chl fluorescence revealed some variations in the fluorescence values between different areas of the leaf blade (**Figure 3A**) which could be caused by the characteristic developmental gradient of the plastids in young monocotyledonous leaves which is more pronounced than in fully developed leaves as investigated in **Figure 2**. To examine this in more detail leaf blades were dissected into three segments containing young plastid from the leaf base (segment 3), middle aged plastids (segment 2), and mature plastids from the leaf tip (segment 1; **Figure 3B**). The F_s/F_m values were determined 6 h and 4 days after either a PSI-II or a PSII-I light shift (**Figure 4A**) in comparison to the respective controls. 6 h after a light shift only segment 1 revealed significant changes in F_s/F_m values. Segment 2 and 3 exhibited very weak Chl fluorescence without any recognizable differences between the growth light regimes. Four days after the light shift the Chl fluorescence in general was increased indicating the progress in the build-up of the photosynthetic machinery during the time range of observation. However, again segment 1 was the only segment displaying significant F_s/F_m fluorescence changes characteristically for a LTR.

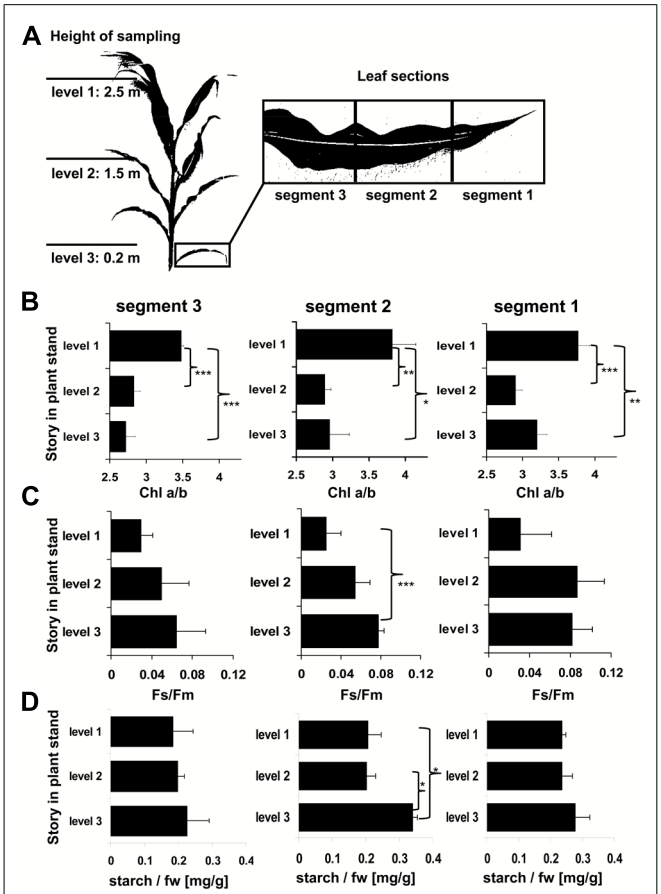

FIGURE 2 | Analysis of field grown maize. (A) Left panel displays height of leaf harvesting. Magnification on right defines the analyzed sections of the respective leaves. Three to five leaves of each level were harvested from different individuals distributed randomly over the field. **(B)** Chl *a/b* ratio, **(C)** Chl fluorescence, and **(D)** starch contents in field grown maize. Story of harvest is given on the left, respective leaf segment analyzed on top. Acclimation parameters Chl *a/b* and F_s/F_m were determined as described in Section "Materials and Methods." Starch content is given relative to the fresh weight (fw). Data represent means from at least three independent biological replicates, standard deviation is given. A Student's *t*-test was performed to test significance of differences (*$P < 0.05$, **$P < 0.01$, ***$P < 0.005$).

In the same experiments we analyzed the Chl *a/b* ratios of the respective samples (**Figure 4B**) which represents a second reporter for the LTR. After 6 h of acclimation it was found to be stable and comparable to the controls. After 4 days, however, the Chl *a/b* ratio of the PSI-II plants was significantly higher than that of PSI plants resembling that of PSII and WL plants. In contrast, PSII-I plants exhibited the opposite behavior with a lower Chl *a/b* ratio as in PSI plants. This pattern was found in all three segments analyzed indicating that even the younger leaf segments had begun to acclimate to the light condition although the Chl fluorescence measurements yet did not indicate this. A more detailed time course experiment indicated that the changes in Chl *a/b* ratios were largely finished after 2 days of acclimation (**Figure A1** in Appendix) which is similar to the dynamics observed earlier in *Arabidopsis* (Wagner et al., 2008).

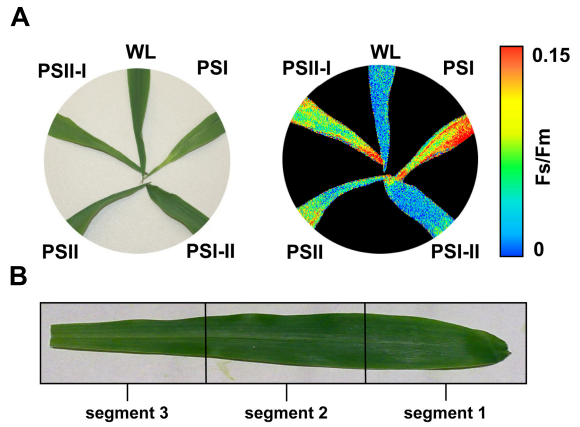

FIGURE 3 | Chl fluorescence of maize seedlings acclimated in long-term to different artificial light regimes affecting the redox state of photosynthetic electron transport. The growth light regime is indicated next to each leaf. **(A)** Left: appearance of leaves of differently acclimated plants under white light. Right: F_s/F_m values of the same leaves as detected by a CCD camera for Chl fluorescence detection given in false colors. Color bar on the right indicates the measured values. First and second true leaves were used for all analyses, the figures display representative samples. **(B)** Leaf sections used for more detailed analyses (compare **Figures 4** and **5**) were selected according to the field sampling.

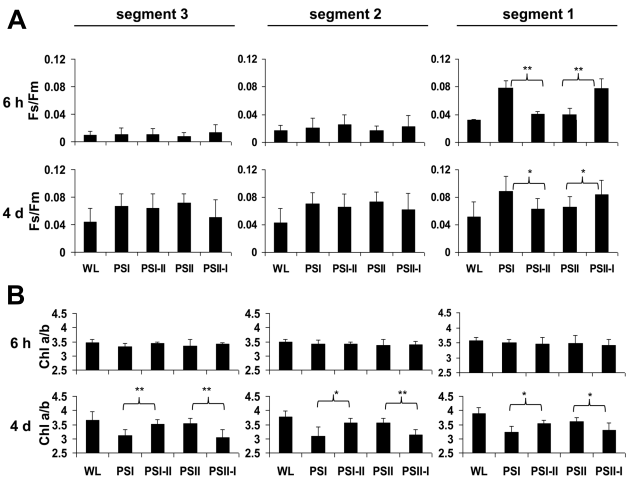

FIGURE 4 | Chl fluorescence and Chl *a/b* ratios in defined segments of maize seedlings acclimated in long-term to different artificial light qualities. Growth light conditions are given below the charts. Plants under PSI-light were shifted to PSII-light and *vice versa* and harvested 6 h of 4 days after the shift (indicated in the left margin) and compared to non-shifted controls. **(A)** F_s/F_m and **(B)** Chl *a/b* were determined from the same segments (indicated on top, compare **Figure 3**). Data represent at least three independent biological replicates, standard deviation is given. A Student's *t*-test was performed to test significance of differences ($*P < 0.05$, $**P < 0.01$).

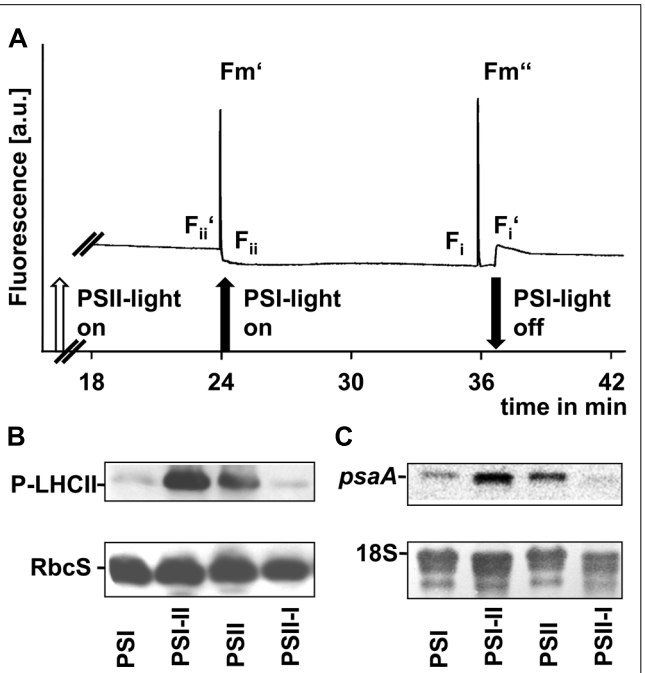

FIGURE 5 | Redox-controlled processes in photosynthetic acclimation of maize seedlings. (A) Artificial growth lights were used as actinic light sources in state transition experiments to indicate the short-term redox effects on linear electron transport. Chl fluorescence given in arbitrary units was recorded using a PAM fluorometer. Measurements were done three times with leaves from three different biological samples. A typical trace is shown. On–off switches of the lights are given below the trace. Nomenclature of fluorescence parameters follows established conventions (see Materials and Methods). **(B)** Plastid protein extracts of maize seedlings grown under the different long-term light quality regimes as indicated in Section "Material and Methods" (indicated on bottom, compare **Figures 3** and **4**) were used to analyze the phosphorylation state of LHCII using a anti-phosphothreonine antibody. As loading control a corresponding experiment with the same membrane targeted to the small subunit of RubisCO (RbcS) is shown. **(C)** RNA isolates from the same samples isolated in parallel were used to determine the accumulation of *psaA* transcripts by northern analysis. As loading control a hybridization of the same membrane with a probe directed against the 18S rRNA is shown.

REDOX-CONTROLLED MOLECULAR PROCESSES IN PHOTOSYNTHETIC ACCLIMATION

Shifts between the PSI- and PSII-lights (and *vice versa*) induce reduction or oxidation of the plastoquinone pool (Wagner et al., 2008), respectively, which serves as a sensor for the balanced action of the two photosystems. In C3 plants, it controls the transcriptional regulation of the plastid gene *psaA*, targets the phosphorylation of the LHCII and the performance of state transitions. We tested all three processes in segment 1 of the leaf blades (**Figure 5**).

To demonstrate the effect of light sources on the redox state of the electron transport chain we used actinic lights in standard state transitions measurements (Haldrup et al., 2001). Chl fluorescence was detected using a pulse amplitude modulation (PAM) fluorometer (**Figure 5A**). The Chl fluorescence traces displayed changes characteristic for state transitions as observed earlier in C3 plants, i.e., a slow transient rise after a sudden drop when the far-red light was switched on and a more rapid transient decrease after a sharp rise when it was switched off again. These fluorescence transients are caused by the lateral migration of the LHCII between PSII and PSI and indicate that the time range necessary for state transitions in maize corresponded to that observed in *Arabidopsis* (Wagner et al., 2008).

Western analyses of thylakoid membrane phosphorylation state using an anti-phosphothreonine antibody (**Figure 5B**) indicated a strong phosphorylation of the LHCII proteins under PSII- and PSI-II light conditions while only weak phosphorylation signals could be detected in samples obtained from PSI- and PSII-I plants. This observation is consistent with the Chl fluorescence measurements and indicates the activity of a redox-sensitive kinase catalyzing state transitions *via* LHCII phosphorylation.

Northern analyses of total RNA preparations indicated a *psaA* transcript pool in PSI-light adapted plants which increased after a shift into PSII-light (**Figure 5C**). A similar transcript accumulation was observable in PSII-light grown plants and a down-regulation of *psaA* transcript amounts became apparent after a shift to PSI-light (**Figure 5C**).

In total all three parameters clearly demonstrated that redox-controlled acclimation responses occur in maize and that the seedlings perform a proper LTR at least in segment 1 under the artificial light quality regimes.

Recently, it could be demonstrated that the LTR includes targeted changes in the metabolic state of *Arabidopsis* and that this is reflected by a characteristic increase in the starch content of the leaves under PSII and PSI-II lights when compared to PSI and PSII-I conditions. The *stn7* mutant was unable to perform this increase indicating that it is an redox-controlled process (Bräutigam et al., 2009). To test whether this regulation is also present in maize, seedlings were grown under the four light regimes and starch accumulation was determined in each segment (**Figure 6**). In contrast to *Arabidopsis* we could not observe any distinct pattern of starch accumulation in response to the light quality indicating that this regulation does not work in maize although the photosynthetic acclimation processes appeared to be fully functional. This result is consistent with the findings in plants collected from the field.

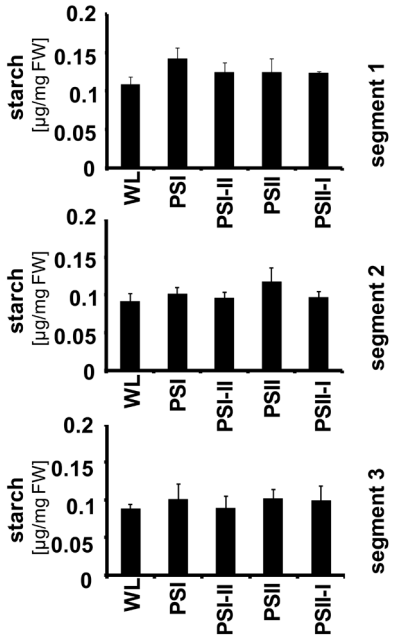

FIGURE 6 | Starch accumulation in segments of maize seedlings grown in long-term under the different light quality regimes. Starch per fresh weight (FW) was determined from the three leaf segments (indicated on the right) as described before. Growth light regimes of the respective plant samples are indicated at the bottom of each panel. All determinations were done in triplicate, standard deviations are given.

REDOX-DEPENDENT PHOSPHORYLATION OF LHCII IN MAIZE GROWN IN THE FIELD OR UNDER VARIOUS LABORATORY CONDITIONS

In order to obtain a direct comparison of acclimation abilities of maize under field and laboratory conditions we determined the phosphorylation state of the LHCII using immunoblotting analyses with antibodies directed against phosphothreonine. We harvested leaf material in the field corresponding to the levels 1–3 (compare **Figure 2**) and isolated total leaf protein extracts. 20 µg protein were separated by SDS gel electrophoresis and subjected to immunoblot analysis (**Figure 7**). In parallel, we separated the same amounts of protein extracts isolated from 2 months old maize plants grown in growth chambers where they experienced mainly a light intensity gradient due to vertical growth without neighboring plants. In addition, we grew maize seedlings for 10 days directly under two different WL intensities (170 and 35 µE) as well as in our light quality regime. For the latter *Arabidopsis* plants grown in parallel were used as control. Redox-mediated LHCII phosphorylation induced by growth under PSII- and PSI-lights appeared to be comparable for *Arabidopsis* and maize seedlings (**Figure 7**, lanes 1, 2 and 12, 13) and resulted in a strong phosphorylation of LHCII under PSII-light and a weak phosphorylation under PSI-light, respectively. This result is in accordance with our earlier observations (Wagner et al., 2008, **Figure 5**). Field grown maize exhibited a phosphorylation state of LHCII at levels 2 and 3 (lanes 5, 6) being comparable to that of the PSI-light control (lane 13) while that of level 1 (lane 4) was clearly reduced. The latter observation corresponds to reports demonstrating that the LHCII kinase is inhibited at high light intensities by a thiol-dependent repression mechanism (Rintamaki et al., 2000). Interestingly, the phosphorylation signal occurring above the LHCII remained stable under all conditions. Because of size and regulation behavior of this band under lab conditions it is likely the D1 protein which requires experimental proof in the future. If this assumption is correct then the stable phosphorylation contrasts results from laboratory experiments with *Arabidopsis* which suggest that D1 phosphorylation is affected by light intensity (Tikkanen et al., 2008; compare also lanes 7–9) pointing to potential additional control mechanisms in field grown maize besides light-dependent redox control. Maize from growth chambers not subjected to dense planting displayed a regular increase in LHCII phosphorylation from the top level to the bottom (lanes 7–9) which can be easily explained by the light-intensity dependent repression of the kinases. The additional experiment with the 10-day-old maize seedlings grown under 170 and 35 µE WL (lanes 10 and 11) displaying high phosphorylation states under both conditions indicates that a significant high light repression of LHCII phosphorylation in maize likely starts beyond the 330 µE light intensity point (Lane 8). This is much higher as the corresponding point in *Arabidopsis* (about 150 µE, compare Bonardi et al., 2005), probably since maize is genotypically adapted to much higher light intensities for growth than *Arabidopsis*. In

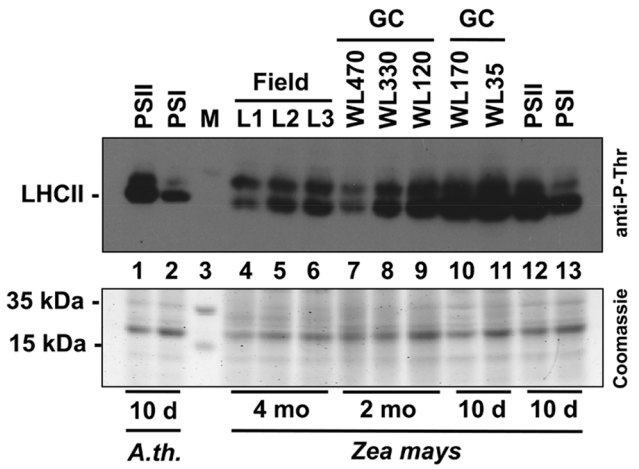

FIGURE 7 | Redox-dependent phosphorylation of LHCII in maize grown under field conditions or various laboratory conditions. Protein extracts of differentially grown plants were separated on a denaturing 10% SDS-PAGE, blotted to a PVDF membrane and subjected to an immunoblot analysis using an anti-phosphothreonine antibody (top panel). Signals were visualized by enhanced chemiluminescence. 20 μg total protein were loaded per lane. A parallel control gel was loaded with the same protein amounts from the same samples and subjected to Coomassie staining as loading control (bottom panel). Lanes 1 and 2: extracts of 10-day-old *Arabidopsis* seedlings grown under artificial PSII- and PSI-light serving as control. Lane 3: size marker. Lanes 4–6: Leaf protein extracts of 4 months old field grown maize (L1–L3 correspond to the respective height levels given in **Figures 1** and **2**). Lanes 7–9: leaf protein extracts of 2 months old maize plants grown in a growth chamber (GC) equipped with mercury vapor white light sources. Light intensity at the height of leaf harvest is given in μmol photons per m^2 and s. Lanes 10 and 11: leaf protein extracts from 10-day-old maize plants grown in growth cabinets equipped with cool white light fluorescent stripe lamps (light intensity is given in μmol photons per m^2 and s). Lanes 12 and 13: leaf protein extracts of 10-day-old maize plants grown under the same PSII- and PSI-light conditions as given for extracts from *Arabidopsis* seedlings presented in lanes 1 and 2. All plants used for experiments given in lanes 7–13 were grown in the same growth chamber being subjected to 60% relative humidity and 18–21°C.

summary, we conclude that the principal LHCII phosphorylation events occurring in the field can be mimicked by our artificial light quality system. Phosphorylation of the putative D1 protein, however, appears to be potentially under a more complex control including additional influences besides the light environment and requires more complex physiological set-ups in order to study it.

DISCUSSION

Maize is one of the major crops in worldwide agriculture and, therefore, its ability to respond and acclimate to changing environmental conditions is of great interest, especially with regard to rising CO_2 concentrations in the atmosphere (Prins et al., 2007). Recent analyses have demonstrated that the acclimation to CO_2 is closely related to the water status and the developmental stage of the leaf investigated reflecting the multiple effects on photosynthesis (Prins et al., 2011). The efficiency of CO_2 fixation, however, also largely depends on the energy provided by the light reaction which might create a limiting factor since it is well-known that maize fields possess a very high LAI. Our measurements of the light gradients within such a field confirm this and demonstrate that in a fully grown maize field approximately 70–80% of the biomass can perform photosynthesis only in a very sub-optimal way since the useful light wavelengths as driving force for the light reaction are very limited. This occurs even under optimal sun light conditions suggesting that there is a high potential for improvement of light usage efficiency in the same way as discussed for rice (Horton et al., 2001).

Recently, molecular studies investigated the molecular changes of the photosynthetic apparatus in maize in response to WL intensity gradients (Romanowska and Drozak, 2006; Romanowska et al., 2008). In the present study we focused on potential changes in photosynthetic functions in maize caused by long-term variations of incident light quality using artificial light sources exciting preferentially PSI or PSII. A similar approach has been performed earlier, however, with the main focus on the effectiveness of the phytochrome system (Eskins et al., 1986). A recent study explains photosynthetic acclimation to canopy density of tobacco and *Arabidopsis* as an interplay of photoreceptors and cytokinins, but the results also suggest a possible existence of alternative signaling pathways (Boonman et al., 2009). Our physiological set-up was originally established to analyze processes controlled by redox signals from photosynthetic electron transport in C3 plants. Our experiments presented here demonstrate that the system is able to induce a prominent short-term response also in the maize seedlings. Redox-controlled state transitions as measured by Chl fluorescence and corresponding changes in LHCII phosphorylation (**Figure 5**) were observable in a comparable way as reported earlier (Andrews et al., 1993). In addition, we could detect a pronounced LTR with corresponding changes in *psaA* transcript accumulation (**Figure 5C**) and characteristic changes in F_s/F_m and Chl *a/b* values (**Figure 4**). The LTR, however, was fully observable only in the top leaf segment of the maize seedlings indicating a developmental dependency of the LTR on the gradient of chloroplast biogenesis at least under the conditions of the present study (**Figure 4**). In contrast, in mature leaves of field grown plants the LTR as reported by respective changes of F_s/F_m and Chl *a/b* was readily detectable in all segments (**Figure 2**) supporting this conclusion. Our light measurements in the field confirm earlier results demonstrating that in dense plant population strong light quality gradients exist which are present even under sunny conditions (**Figure 1**). It can be concluded that fluctuations of illumination from outside are dampened in their absolute values by the top layers of the field and that within the field canopy the light environment is a rather stable low-intensity, far-red enriched light condition. Thus, leaves in the top level mainly require to perform high light acclimation using mechanisms such as non-photochemical quenching (NPQ). In contrast, for the largest portion of the biomass in the field a long-term acclimation to the non-saturating low light conditions appears to be more desirable. We could observe a distinct difference between the F_s/F_m and Chl *a/b* values for the top storey of the field when compared to middle or bottom storey indicating an adjustment of the photosynthetic apparatus to the respective illumination conditions (**Figure 2**). Leaf autonomous regulation of photosynthetic acclimation *via* redox signals from photosynthesis would provide

an efficient and simple regulation principle allowing the individual plants to adapt to the strong gradient in light intensity on one hand and the parallel light quality gradient on the other. Thus, our physiological light system and the reporter for the LTR provide a useful test system not only for redox-controlled processes, but also for mimicking field conditions in dense canopies.

In *Arabidopsis* we observed a concomitant variation of the starch amount during the LTR which was reported to be a reporter for the metabolic changes occurring in the background of the light acclimation response (Bräutigam et al., 2009). Interestingly, this was not observable in maize, neither in the seedlings nor in the mature plants. In *Arabidopsis,* it was shown that starch synthesis is dependent on redox regulation of the entry enzyme ADP-glucose-pyrophosphorylase (AGPase) *via* the thioredoxin-like NtrC (Michalska et al., 2009). It is not clear yet whether the changes in starch accumulation during the LTR are also mediated by NtrC, however, it is a likely candidate. In maize obviously the regulatory link between LTR and starch accumulation has been uncoupled. A possible explanation would be the C4 syndrome of maize, since in C4 metabolism starch is mainly produced in the bundle sheath cells which do not contribute significantly to overall linear electron transport, thus lacking the basic requirement for photosynthetic redox signaling. However, it could be shown that even the agranal chloroplasts of the bundle sheath cells of maize contain a certain amount of PSII providing at least a limited capacity for redox signaling (Romanowska et al., 2008). BLAST searches done with the NtrC protein sequence of *Arabidopsis* identify an ortholog in maize with 92% positive amino acids strongly suggesting the existence of this key redox regulator in maize. Interestingly, starch accumulation in bottom leaves of the field grown plants is comparable or even slightly higher than in the top level leaves. Thus, starch accumulation appears to be uncoupled from the major site of primary photosynthesis implying a number of questions concerning the source–sink relationships in this plant which are an interesting topic for future work.

Regarding the high proportion of the field biomass performing a LTR the question arises for the beneficial effects of this acclimation response. In *Arabidopsis,* a clear negative impact on rosette growth and seed production could be demonstrated when the LTR is lacking (Wagner et al., 2008; Bräutigam et al., 2009). A recent study analyzed in detail the wavelengths dependency of photosynthetic quantum yield indicating significant positive effects for plants when performing a corresponding acclimation response (Hogewoning et al., 2012). Comparable experiments in maize require the isolation of corresponding LTR mutants which are currently under way. In addition, further field experiments are required to understand temporal and spatial occurrence of the LTR during the development of the plant stand. Young and small maize seedlings in the field perceive much more high light per total leaf area than the older plants which need to compete for light. Thus, the requirement for a LTR in the lower parts of the plants increases with the development of the plant stand. Understanding the molecular regulation of these processes will help to assess the potential of yield improvement in crop field *via* engineering of photosynthetic acclimation responses.

MATERIALS AND METHODS

FIELD GROWN PLANT MATERIAL

For field analyses we characterized a plot in the middle of a fully grown maize field near Jena on the 9th of September 2009 at a time point when development of the corncobs has not yet started. The density of plants within the field was between 16 and 20 plants/m^2. Light conditions in the maize field were measured at different indicated heights at noon under sunny and dry conditions and 22°C air temperature. Light intensity of PAR was determined with a Licor LI-250 (Heinz Walz GmbH, Effeltrich, Germany). Light spectra were determined with a spectroradiometer GER 1.500 (Geophysical and Environmental Research Corp., Millbrook, NY, USA). Reference data were obtained outside the field in a plant free area nearby which was also free of reflecting light from the fields around. Based on these measurements leaves were harvested at three different heights with characteristic light conditions. Only healthy, green leaves without any sign of beginning senescence or pathogen attack were chosen. Leaves were put in a light-proof box on ice and transported immediately to the lab. Chl fluorescence measurements were started within 30 min after harvest and after acclimation to room temperature. Material for Chl and starch determination was frozen in liquid nitrogen and kept at −80°C until further use.

PLANT MATERIAL GROWN IN CLIMATE CHAMBERS

For analysis of young maize seedlings *Z. mays* (L.) var seeds were sown in pots on soil/vermiculite (4:1) and grown in growth chambers at 25°C, 80% humidity and a 16 h light/8 h dark cycle. Illumination was ∼30 μmol photons/m^2s provided by cool white fluorescence lamps. Seedlings were grown for 3–4 days until the first leaf had developed. Then pots were shifted for further 3 days to light cabinets equipped with light sources preferentially exciting PSI or PSII (PSI- or PSII-light, respectively). The spectral composition of the light sources have been described in detail earlier (Wagner et al., 2008). Both light sources (PSI- and PSII-light) had an comparable PAR of 20–30 μmol photons/m^2s which was found to be sufficient to sustain photoautotrophic growth. After this pre-acclimation one half of the plants were shifted from PSII- to PSI-light (PSII-I plants) and from PSI- to PSII-light (PSI-II plants) while the other half remained in the light cabinets (PSI and PSII plants). Plants were then re-acclimated for further 4 days before they were harvested for analyses. In time course experiments samples were taken 6, 24, 48, and 96 h after the light shift. Maize plants grown under high WL conditions or for prolonged growth under WL were subjected to illumination from mercury vapor WL sources in the same growth chambers as the PSI- and PSII-light sources. Light intensities as indicated in the figures were obtained by adjusting the distance of the plants to the light sources placed on top of them. The respective PAR intensity was detected using the Licor LI-250 (see above).

CHLOROPHYLL FLUORESCENCE MEASUREMENTS

In vivo Chl *a* fluorescence parameters were determined by video imaging under room temperature using a pulse amplitude-modulated FluorCam 700 MF device (Photon Systems Instruments, Brno, Czech Republic). F_s/F_m and F_v/F_m of plants

acclimated to different light qualities were determined as described earlier (Wagner et al., 2008). We also compared basic photosynthetic parameters such as F_v/F_m detected by the Fluorcam with that of a PAM2000 (Heinz Walz GmbH, Effeltrich, Germany) and found the saturation flash of approximately 2000 μE sufficient to close all PSII centers for determination of F_m. State transitions were determined as described earlier (Lunde et al., 2000; Damkjaer et al., 2009) with intact single plant leaves using a PAM-101 fluorometer equipped with a PDA100 for digital data recording (WALZ, Effeltrich, Germany). PSII- and PSI-favoring light was provided by the growth light sources as described (Wagner et al., 2008). Saturation pulses were given for 800 ms by a Schott KL-1500 lamp at 5000 μmol photons/m^2s. One representative of three replicates is shown.

CHLOROPHYLL AND STARCH DETERMINATION

Plant material was ground in liquid nitrogen in a mortar. For determination of Chl concentration the pigments were extracted with 80% buffered acetone. Chl *a* and *b* concentrations were then spectroscopically determined according to Porra et al. (1989). Starch was determined using a standard colorimetric method (Magel, 1991) and the absorption coefficients described by Appenroth et al. (2010).

NORTHERN ANALYSIS

Preparation of total RNA from the top section of 10-day-old maize seedlings grown in the light quality system as described above was performed as established earlier (Fey et al., 2005b). 10 μg of total RNA were separated on a 1% denaturing agarose gel containing 7% formaldehyde, transferred to a nylon membrane and hybridized to a probe directed against a highly conserved sequence in the *psaA* gene (encoding the apoprotein of PSI) of *Arabidopsis* following established standard protocols (Sambrook et al., 1989).

PHOSPHORYLATION STATE OF LHCII

Fresh leaf tissue of differentially grown plants was homogenized using a Waring® blender in ice cold homogenization buffer (HB; 50 mM HEPES-KOH, 0.33 M sorbitol, 10 mM KCl, 5 mM $MgCl_2$, 10 mM NaF) at 4°C. Chloroplasts were recovered by centrifugation for 2 min at 2000 × *g*. Total chloroplast protein extracts containing 20 μg Chl were solubilized for 10 min in 40 μl buffer containing β-dodecyl-maltoside (BDM) at a final concentration of 1%. Proteins were denatured with 40 mM DTT, 2% SDS, 4% glycerol, and 150 mM Tris–HCL *pH* 6.8 for 10 min and subjected to SDS-PAGE using a 12% gel. The gel was either stained with colloidal Coomassie following manufacturer's recommendations (Roth, Karlsruhe, Germany) or used for western analysis. The stained gel was scanned with a LI-COR Odyssey infrared laser scanner at 700 nm to detect the dye fluorescence and protein loading was determined by quantification of fluorescence signals. Calculations of relative protein amounts were done with LI-COR Odyssey2.1 software (median background correction). For immunoblot analysis gels were electro-transferred to a polyvinylidene difluoride (PVDF) membrane (Roti-PVDF, Roth, Karlsruhe, Germany) and de-stained according to current protocols (Wittig et al., 2006). Phosphorylated proteins were detected with a polyclonal primary anti-phosphothreonine antibody (Cell Signaling Technology Inc., Danvers, MA, USA) and a fluorophore-coupled secondary antibody IRD800-anti-rabbit (Rockland Immunochemicals Inc., Gilbertsville, PA, USA). For testing phosphorylation state of field material the harvested leaves were frozen on dry ice directly at the site of harvest to avoid any change in phosphorylation during transportation. Total leaf protein extracts were isolated according to Pfalz et al. (2009) and used for immune-western analysis with anti-phosphothreonine antibodies as described above with the exception that the detection was performed with enhanced chemiluminescence (ECL). Samples collected from lab growth chamber-grown plants were treated in an identical manner to allow direct comparison.

ACKNOWLEDGMENTS

We thank N. L. Chrestensen Erfurter Samen- und Pflanzenzucht GmbH for providing seed material. This work was supported by the Deutsche Forschungsgemeinschaft.

REFERENCES

Allen, J. F. (2003). State transitions – a question of balance. *Science* 299, 1530–1532. doi: 10.1126/science.1082833

Allen, J. F., and Pfannschmidt, T. (2000). Balancing the two photosystems: photosynthetic electron transfer governs transcription of reaction centre genes in chloroplasts. *Philos. Trans. R. Soc. Lond. B Biol. Sci.* 355, 1351–1357. doi: 10.1098/rstb.2000.0697

Anderson, J. M., Chow, W. S., and Park, Y.-I. (1995). The grand design of photosynthesis: acclimation of the photosynthetic apparatus to environmental cues. *Photosyn. Res.* 46, 129–139. doi: 10.1007/BF00020423

Andrews, J. R., Bredenkamp, G. J., and Baker, N. R. (1993). Evaluation of the role of state transitions in determining the efficiency of light utilisation for CO2 assimilation in leaves. *Photosyn. Res.* 38, 15–26. doi: 10.1007/BF00015057

Appenroth, K. J., Krech, K., Keresztes, A., Fischer, W., and Koloczek, H. (2010). Effects of nickel on the chloroplasts of the duckweeds *Spirodela polyrhiza* and *Lemna minor* and their possible use in biomonitoring and phytoremediation. *Chemosphere* 78, 216–223. doi: 10.1016/j.chemosphere.2009.11.007

Aro, E.-M., and Andersson, B. (2001). *Regulation of Photosynthesis*, Vol. 11. Dordrecht: Kluwer Academic Publishers.

Ballare, C. L. (1999). Keeping up with the neighbours: phytochrome sensing and other signaling mechanisms. *Trends Plant Sci.* 4, 97–102. doi: 10.1016/S1360-1385(99)01383-7

Bellafiore, S., Barneche, F., Peltier, G., and Rochaix, J. D. (2005). State transitions and light adaptation require chloroplast thylakoid protein kinase STN7. *Nature* 433, 892–895. doi: 10.1038/nature03286

Blankenship, R. E. (2002). *Molecular Regulation of Photosynthesis*. Oxford: Blackwell Science Ltd. doi: 10.1002/9780470758472

Bonardi, V., Pesaresi, P., Becker, T., Schleiff, E., Wagner, R., Pfannschmidt, T., et al. (2005). Photosystem II core phosphorylation and photosynthetic acclimation require two different protein kinases. *Nature* 437, 1179–1182. doi: 10.1038/nature04016

Boonman, A., Prinsen, E., Gilmer, F., Schurr, U., Peeters, A. J. M., Voesenek, L. A. C. J., et al. (2007). Cytokinin import rate as a signal for photosynthetic acclimation to canopy light gradients. *Plant Physiol.* 143, 1841–1852. doi: 10.1104/pp.106.094631

Boonman, A., Prinsen, E., Voesenek, L. A. C. J., and Pons, T. L. (2009). Redundant roles of photoreceptors and cytokinins in regulating photosynthetic acclimation to canopy density. *J. Exp. Bot.* 60, 1179–1190. doi: 10.1093/jxb/ern364

Bräutigam, K., Dietzel, L., Kleine, T., Ströher, E., Wormuth, D., Dietz, K. J., et al. (2009). Dynamic plastid redox signals integrate gene expression and metabolism to induce distinct metabolic states in photosynthetic acclimation in *Arabidopsis*. *Plant Cell* 21, 2715–2732. doi: 10.1105/tpc.108.062018

Chow, W. S., Anderson, J. M., and Hope, A. B. (1988). Variable stoichiometries of photosystem II to photosystem I reaction centres. *Photosyn. Res.* 17, 277–281. doi: 10.1007/BF00035454

Chow, W. S., Anderson, J. M., and Melis, A. (1990a). The photosystem stoichiometry in thylakoids of some Australian shade-adapted plant-species. *Aust. J. Plant Physiol.* 17, 665–674. doi: 10.1071/PP9900665

Chow, W. S., Melis, A., and Anderson, J. M. (1990b). Adjustments of photosystem stoichiometry in chloroplasts improve the quantum efficiency of photosynthesis. *Proc. Natl. Acad. Sci. U.S.A.* 87, 7502–7506. doi: 10.1073/pnas.87.19.7502

Damkjaer, J. T., Kereiche, S., Johnson, M. P., Kovacs, L., Kiss, A. Z., Boekema, E. J., et al. (2009). The photosystem II light-harvesting protein Lhcb3 affects the macrostructure of photosystem II and the rate of state transitions in *Arabidopsis*. *Plant Cell* 21, 3245–3256. doi: 10.1105/tpc.108.064006

Dietzel, L., Bräutigam, K., and Pfannschmidt, T. (2008). Photosynthetic acclimation: state transitions and adjustment of photosystem stoichiometry – functional relationships between short-term and long-term light quality acclimation in plants. *FEBS J.* 275, 1080–1088. doi: 10.1111/j.1742-4658.2008.06264.x

Drozak, A., and Romanowska, E. (2006). Acclimation of mesophyll and bundle sheath chloroplasts of maize to different irradiances during growth. *Biochim. Biophys. Acta* 1757, 1539–1546. doi: 10.1016/j.bbabio.2006.09.001

Eberhard, S., Finazzi, G., and Wollman, F. A. (2008). The dynamics of photosynthesis. *Annu. Rev. Genet.* 42, 463–515. doi: 10.1146/annurev.genet.42.110807.091452

Eskins, K., Mccarthy, S. A., Dybas, L., and Duysen, M. (1986). corn chloroplast development in weak fluence rate red-light and in weak fluence rate red plus far-red light. *Physiol. Plant.* 67, 242–246. doi: 10.1111/j.1399-3054.1986.tb02450.x

Fan, D. Y., Hope, A. B., Smith, P. J., Jia, H., Pace, R. J., Anderson, J. M., et al. (2007). The stoichiometry of the two photosystems in higher plants revisited. *Biochim. Biophys. Acta* 1767, 1064–1072. doi: 10.1016/j.bbabio.2007.06.001

Fey, V., Wagner, R., Brautigam, K., and Pfannschmidt, T. (2005a). Photosynthetic redox control of nuclear gene expression. *J. Exp. Bot.* 56, 1491–1498. doi: 10.1093/jxb/eri180

Fey, V., Wagner, R., Brautigam, K., Wirtz, M., Hell, R., Dietzmann, A., et al. (2005b). Retrograde plastid redox signals in the expression of nuclear genes for chloroplast proteins of *Arabidopsis thaliana*. *J. Biol. Chem.* 280, 5318–5328. doi: 10.1074/jbc.M406358200

Frenkel, M., Bellafiore, S., Rochaix, J. D., and Jansson, S. (2007). Hierarchy amongst photosynthetic acclimation responses for plant fitness. *Physiol. Plant.* 129, 455–459. doi: 10.1111/j.1399-3054.2006.00831.x

Frenkel, M., Kulheim, C., Johansson Jankanpaa, H., Skogstrom, O., Dall'Osto, L., Agren, J., et al. (2009). Improper excess light dissipation in *Arabidopsis* results in a metabolic reprogramming. *BMC Plant Biol.* 9:12. doi: 10.1186/1471-2229-9-12

Haldrup, A., Jensen, P. E., Lunde, C., and Scheller, H. V. (2001). Balance of power: a view of the mechanism of photosynthetic state transitions. *Trends Plant Sci.* 6, 301–305. doi: 10.1016/S1360-1385(01)01953-7

Hirose, T. (2005). Development of the Monsi–Saeki theory on canopy structure and function. *Ann. Bot.* 95, 483–494. doi: 10.1093/aob/mci047

Hogewoning, S. W., Wientjes, E., Douwstra, P., Trouwborst, G., van Ieperen, W., Croce, R., et al. (2012). Photosynthetic quantum yield dynamics: from photosystems to leaves. *Plant Cell* 24, 1921–1935. doi: 10.1105/tpc.112.097972

Holt, N. E., Fleming, G. R., and Niyogi, K. K. (2004). Toward an understanding of the mechanism of nonphotochemical quenching in green plants. *Biochemistry* 43, 8281–8289. doi: 10.1021/bi0494020

Horton, P., Johnson, M. P., Perez-Bueno, M. L., Kiss, A. Z., and Ruban, A. V. (2008). Photosynthetic acclimation: does the dynamic structure and macro-organisation of photosystem II in higher plant grana membranes regulate light harvesting states? *FEBS J.* 275, 1069–1079. doi: 10.1111/j.1742-4658.2008.06263.x

Horton, P., Murchie, E. H., Ruban, A. V., and Walters, R. G. (2001). "Increasing rice photosynthesis by manipulation of the acclimation and adaptation to light," in *Rice Biotechnology: Improving Yield, Stress Tolerance and Grain Quality*, Vol. 236, ed. Novartis Foundation (Hoboken John Wiley & Sons) 117–134.

Hüner, N. P. A., Oquist, G., and Sarhan, F. (1998). Energy balance and acclimation to light and cold. *Trends Plant Sci.* 3, 224–230. doi: 10.1016/S1360-1385(98)01248-5

Kanervo, E., Suorsa, M., and Aro, E. M. (2005). Functional flexibility and acclimation of the thylakoid membrane. *Photochem. Photobiol. Sci.* 4, 1072–1080. doi: 10.1039/b507866k

Kargul, J., and Barber, J. (2008). Photosynthetic acclimation: structural reorganisation of light harvesting antenna – role of redox-dependent phosphorylation of major and minor chlorophyll a/b binding proteins. *FEBS J.* 275, 1056–1068. doi: 10.1111/j.1742-4658.2008.06262.x

Long, S. P., Zhu, X.-G., Naidu, S. L., and Ort, D. R. (2006). Can improvement in photosynthesis increase crop yields? *Plant Cell Environ.* 29, 315–330. doi: 10.1111/j.1365-3040.2005.01493.x

Lunde, C., Jensen, P. E., Haldrup, A., Knoetzel, J., and Scheller, H. V. (2000). The PSI-H subunit of photosystem I is essential for state transitions in plant photosynthesis. *Nature* 408, 613–615. doi: 10.1038/35046121

Magel, E. (1991). Qualitative and quantitative determination of starch by a colorimetric method. *Starch* 43, 384–387. doi: 10.1002/star.19910431003

Melis, A. (1991). Dynamics of photosynthetic membrane composition and function. *Biochim. Biophys. Acta* 1058, 87–106. doi: 10.1016/S0005-2728(05)80225-7

Michalska, J., Zauber, H., Buchanan, B. B., Cejudo, F. J., and Geigenberger, P. (2009). NTRC links built-in thioredoxin to light and sucrose in regulating starch synthesis in chloroplasts and amyloplasts. *Proc. Natl. Acad. Sci. U.S.A.* 106, 9908–9913. doi: 10.1073/pnas.0903559106

Murchie, E. H., Pinto, M., and Horton, P. (2009). Agriculture and the new challenges for photosynthesis research. *New Phytol.* 181, 532–552. doi: 10.1111/j.1469-8137.2008.02705.x

Pesaresi, P., Hertle, A., Pribil, M., Kleine, T., Wagner, R., Strissel, H., et al. (2009). *Arabidopsis* STN7 kinase provides a link between short- and long-term photosynthetic acclimation. *Plant Cell* 21, 2402–2423. doi: 10.1105/tpc.108.064964

Pfalz, J., Bayraktar, O. A., Prikryl, J., and Barkan, A. (2009). Site-specific binding of a PPR protein defines and stabilizes 5′ and 3′ mRNA termini in chloroplasts. *EMBO J.* 28, 2042–2052. doi: 10.1038/emboj.2009.121

Pfannschmidt, T., Nilsson, A., and Allen, J. F. (1999a). Photosynthetic control of chloroplast gene expression. *Nature* 397, 625–628. doi: 10.1038/17624

Pfannschmidt, T., Nilsson, A., Tullberg, A., Link, G., and Allen, J. F. (1999b). Direct transcriptional control of the chloroplast genes psbA and psaAB adjusts photosynthesis to light energy distribution in plants. *IUBMB Life* 48, 271–276.

Pfannschmidt, T., Schutze, K., Brost, M., and Oelmuller, R. (2001). A novel mechanism of nuclear photosynthesis gene regulation by redox signals from the chloroplast during photosystem stoichiometry adjustment. *J. Biol. Chem.* 276, 36125–36130. doi: 10.1074/jbc.M105701200

Pons, T., and de Jong-Van Berkel, Y. (2004). Species-specific variation in the importance of the spectral quality gradient in canopies as a signal for photosynthetic resource partitioning. *Ann. Bot.* 94, 725–732. doi: 10.1093/aob/mch197

Porra, R. J., Thompson, W. A., and Kriedemann, P. E. (1989). Determination of accurate extinction coefficients and simultaneous-equations for assaying chlorophyll-a and chlorophyll-B extracted with 4 different solvents – verification of the concentration of chlorophyll standards by atomic-absorption spectroscopy. *Biochim. Biophys. Acta* 975, 384–394. doi: 10.1016/S0005-2728(89)80347-0

Prins, A., Muchwezi, J., Verrier, P., and Foyer, C. (2007). Acclimation of photosynthesis in maize plants to high CO2. *Photosyn. Res.* 91, 294–295.

Prins, A., Mukubi, J. M., Pellny, T. K., Verrier, P. J., Beyene, G., et al. (2011). Acclimation to high CO2 in maize is related to water status and dependent on leaf rank. *Plant Cell Environ.* 34, 314–331. doi: 10.1111/j.1365-3040.2010.02245.x

Rintamaki, E., Martinsuo, P., Pursiheimo, S., and Aro, E. M. (2000). Cooperative regulation of light-harvesting complex II phosphorylation via the plastoquinol and ferredoxin-thioredoxin system in chloroplasts. *Proc. Natl. Acad. Sci. U.S.A.* 97, 11644–11649. doi: 10.1073/pnas.180054297

Romanowska, E., and Drozak, A. (2006). Comparative analysis of biochemical properties of mesophyll and bundle sheath chloroplasts from various subtypes of C-4 plants grown at moderate irradiance. *Acta Biochim. Pol.* 53, 709–719.

Romanowska, E., Kargul, J., Powikrowska, M., Finazzi, G., Nield, J., Drozak, A., et al. (2008). Structural organization of photosynthetic apparatus in agranal chloroplasts of Maize. *J. Biol. Chem.* 283, 26037–26046. doi: 10.1074/jbc.M803711200

Sambrook, J., Fritsch, E. F., and Maniatis, T. (1989). *Molecular Cloning: A Laboratory Manual.* Cold Spring Harbor: Cold Spring Harbor Laboratory Press.

Smith, H. (2000). Phytochromes and light signal perception by plants-an emerging synthesis. *Nature* 407, 585–591. doi: 10.1038/35036500

Steiner, S., Dietzel, L., Schröter, Y., Fey, V., Wagner, R., and Pfannschmidt, T. (2009). The role of phosphorylation in redox regulation of photosynthesis genes psaA and psbA during photosynthetic acclimation of mustard. *Mol. Plant* 2, 416–429. doi: 10.1093/mp/ssp007

Terashima, I., Araya, T., Miyazawa, S., Sone, K., and Yano, S. (2005). Construction and maintenance of the optimal photosynthetic systems of the leaf, herbaceous plant and tree: an eco-developmental treatise. *Ann. Bot.* 95, 507–519. doi: 10.1093/aob/mci049

Tikkanen, M., Nurmi, M., Kangasjarvi, S., and Aro, E. M. (2008). Core protein phosphorylation facilitates the repair of photodamaged photosystem II at high light. *Biochim. Biophys. Acta* 1777, 1432–1437. doi: 10.1016/j.bbabio.2008.08.004

Wagner, R., Dietzel, L., Bräutigam, K., Fischer, W., and Pfannschmidt, T. (2008). The long-term response to fluctuating light quality is an important and distinct light acclimation mechanism that supports survival of *Arabidopsis thaliana* under low light conditions. *Planta* 228, 573–587. doi: 10.1007/s00425-008-0760-y

Walters, R. G. (2005). Towards an understanding of photosynthetic acclimation. *J. Exp. Bot.* 56, 435–447. doi: 10.1093/jxb/eri060

Walters, R. G., Rogers, J. J. M., Shephard, F., and Horton, P. (1999). Acclimation of *Arabidopsis thaliana* to the light environment: the role of photoreceptors. *Planta* 209, 517–527. doi: 10.1007/s004250050756

Wittig, I., Braun, H. P., and Schagger, H. (2006). Blue native PAGE. *Nat. Protoc.* 1, 418–428. doi: 10.1038/nprot.2006.62

Zhu, X.-G., Long, S. P., and Ort, D. R. (2010). Improving photosynthetic efficiency for greater yield. *Annu. Rev. Plant Biol.* 61, 235–261. doi: 10.1146/annurev-arplant-042809-112206

Conflict of Interest Statement: The authors declare that the research was conducted in the absence of any commercial or financial relationships that could be construed as a potential conflict of interest.

Received: 27 June 2013; paper pending published: 29 July 2013; accepted: 08 August 2013; published online: 12 September 2013.

Citation: Hirth M, Dietzel L, Steiner S, Ludwig R, Weidenbach H, Pfalz J and Pfannschmidt T (2013) Photosynthetic acclimation responses of maize seedlings grown under artificial laboratory light gradients mimicking natural canopy conditions. Front. Plant Sci. ***4****:334. doi: 10.3389/fpls.2013.00334*

This article was submitted to Plant Physiology, a section of the journal Frontiers in Plant Science.

APPENDIX

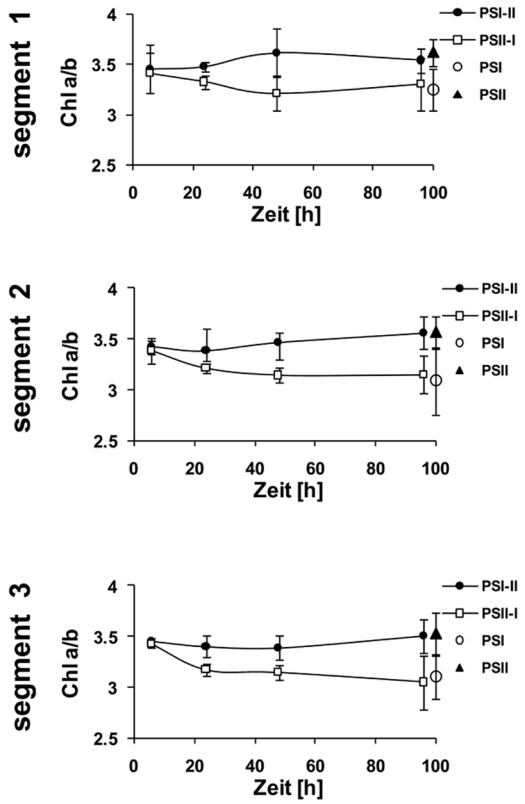

FIGURE A1 | Kinetic changes of Chi a/b ratio in defined segments of maize seedlings acclimated to different light qualities. Growth light conditions are given in the right margins. Plants under PSI-light were shifted to PSII-light and *vice versa* and harvested at indicated time points after the shift and compared to non-shifted controls. Data represent at least three independent biological replicates, standard deviation is given.

frontiers in
PLANT SCIENCE

ORIGINAL RESEARCH ARTICLE
published: 25 February 2014
doi: 10.3389/fpls.2014.00067

Optimization and effects of different culture conditions on growth of *Halomicronema hongdechloris* – a filamentous cyanobacterium containing chlorophyll *f*

Yaqiong Li, Yuankui Lin, Patrick C. Loughlin and Min Chen*

School of Biological Sciences, University of Sydney, Sydney, NSW, Australia

Edited by:
Suleyman I. Allakhverdiev, Russian Academy of Sciences, Russia

Reviewed by:
Suleyman I. Allakhverdiev, Russian Academy of Sciences, Russia
Nabil I. Elsheery, Tanta University, Egypt

***Correspondence:**
Min Chen, School of Biological Sciences (A08), University of Sydney, Sydney, NSW 2006, Australia
e-mail: min.chen@sydney.edu.au

A chlorophyll *f* containing cyanobacterium, *Halomicronema hongdechloris* (*H. hongdechloris*) was isolated from a stromatolite cyanobacterial community. The extremely slow growth rate of *H. hongdechloris* has hindered research on this newly isolated cyanobacterium and the investigation of chlorophyll *f*-photosynthesis. Therefore, optimizing *H. hongdechloris* culture conditions has become an essential requirement for future research. This work investigated the effects of various culture conditions, essential nutrients and light environments to determine the optimal growth conditions for *H. hongdechloris* and the biosynthetic rate of chlorophyll *f*. Based on the total chlorophyll concentration, an optimal growth rate of 0.22 ± 0.02 day^{-1} (doubling time: 3.1 ± 0.3 days) was observed when cells were grown under continuous illumination with far-red light with an intensity of 20 μE at 32°C in modified K + ES seawater (pH 8.0) with additional nitrogen and phosphor supplements. High performance liquid chromatography on *H. hongdechloris* pigments confirmed that chlorophyll *a* is the major chlorophyll and chlorophyll *f* constitutes ~10% of the total chlorophyll from cells grown under far-red light. Fluorescence confocal image analysis demonstrated changes of photosynthetic membranes and the distribution of photopigments in response to different light conditions. The total photosynthetic oxygen evolution yield per cell showed no changes under different light conditions, which confirms the involvement of chlorophyll *f* in oxygenic photosynthesis. The implications of the presence of chlorophyll *f* in *H. hongdechloris* and its relationship with the ambient light environment are discussed.

Keywords: cyanobacteria, chlorophyll *a*, chlorophyll *f*, *Halomicronema hongdechloris* (*H. hongdechloris*), light, photopigments

INTRODUCTION

Cyanobacteria are oxygenic photosynthetic prokaryotes that convert CO_2 into organic biomass by means of photosynthesis. Their metabolic flexibility to adapt and to thrive in various ecological niches is remarkable, and the optimal culture conditions of cyanobacteria are diverse among genera, species and strains (Pikuta et al., 2007; Singh, 2009). As with other bacteria, cyanobacteria have four different phases of growth: lag phase, exponential (or log) phase, stationary phase and the death phase (Fogg and Thake, 1987; Wood et al., 2005). The growth rate can be represented as the doubling time (the period of time required for the cell number or biomass to double). In addition to the direct measure of the growth rate of an organism by cell counting and/or the changes of total biomass (dry or wet weight), the growth rate of cyanobacteria can be measured indirectly using the changes of cellular components such as total organic carbon, lipids, protein, or chlorophyll (Hansmann, 1973; Moheimani et al., 2013). The total chlorophyll concentration has been widely used for the measurement of growth, particularly in the case of filamentous cyanobacteria, where the number of cells cannot be counted directly.

In order to maintain a culture successfully and to optimize the culture growth conditions, various environmental and nutritional parameters need to be taken into account. The most commonly studied parameters are light quality and quantity, pH, salinity, temperature, and macronutrients, mainly nitrogen (N) and phosphorus (P). Light is the major energy source for cyanobacteria and light quality and quantity strongly affect the light-harvesting systems and photosynthetic efficiency (Smith, 1986; Bibby et al., 2009; Chen and Scheer, 2013). *Synechocystis* sp. PCC6803 can be cultured easily under the laboratory conditions and is used as a model cyanobacterium for understanding the mechanism of photosynthesis. Recently, additional chlorophylls have been found in some cyanobacteria and the function of these novel chlorophylls in photosynthesis challenges the traditional belief of oxygenic photosynthesis: Chl *a* is the only chlorophyll that can involve the charge separation in the photosynthetic reaction centers (Miyashita et al.,

Abbreviation: Car, carotenoid; Chl, chlorophyll; Cm, cytoplasmic membrane; FR, far-red light; fs, fibril sheath; *H. hongdechloris*, *Halomicronema hongdechloris*; HPLC, high performance liquid chromatography; *k*, growth rate; LEDs, light emitting diodes; N, nitrogen; OR, orange-red light; P, phosphorus; PC index, the relative amount of phycobiliprotein to Chl *a* ratio; Pg, peptidoglycan layer; PS, photosystem; R^2, the coefficient of determination; RL, red light; *t*, doubling time; Th, thylakoid membranes; WL, cool white fluorescent light or white light.

1996; Chen et al., 2010). Cyanobacteria take advantage of having different compositions of photopigments to capture the available sunlight present in a particular ecological niche (Chen and Scheer, 2013; Hou et al., 2013). For example, *Acaryochloris marina* synthesizes chlorophyll *d* (Chl *d*) to capture far-red light that is the leftover light from phototrophs using Chl *a* existing in the upper stacked biolayers (Kühl et al., 2005; Loughlin et al., 2013). Chlorophyll *f* (Chl *f*) is the most recently identified chlorophyll, having the most red-shifted absorption peak of 707 nm found in oxygenic photosynthetic organisms to date (Chen et al., 2010). The presence of the red-shifted chlorophylls (Chl *d* and Chl *f*) enables oxygenic photosynthetic organisms to expand their absorbance spectral region beyond visible light region and to enhance their photosynthesis efficiency (Chen and Blankenship, 2011).

Halomicronema hongdechloris (*H. hongdechloris*) is the first reported filamentous cyanobacterium containing Chl *f* together with Chl *a* (Chen et al., 2012). A previous study suggested that phycobiliproteins are the main antenna system utilized by *H. hongdechloris* under white light conditions. However, Chl *f* is reported to be a "red-light-induced" chlorophyll with increased amount when *H. hongdechloris* is cultured under far-red light (Chen et al., 2012). *H. hongdechloris* offers an opportunity for exploring the function of Chl *f* in oxygenic photosynthesis. At the time when *H. hongdechloris* was isolated and purified, its doubling time was approximately 1 week (more than 150 h). Compared with the doubling time <20 h for *Synechocystis* sp. PCC 6803 (Saha et al., 2012), and ∼33 h for *A. marina* (Miyashita et al., 2003) the growth rate of *H. hongdechloris* was extremely slow and became a hindrance to research on this newly isolated cyanobacterium and the investigation of Chl *f*-photosynthesis. With such slow growth, obtaining enough biomass of cells and Chl *f* is a major challenge for molecular, biochemical and biophysical studies. Therefore, optimizing *H. hongdechloris* culture conditions has become an essential requirement for future research.

Here we characterize *H. hongdechloris* growth kinetics and describe its light, pH, salinity, temperature and nitrogen/phosphorus requirements for the first time. The significantly improved growth rate of 0.22 ± 0.02 day^{-1} is achieved under enriched nitrogen and phosphorus nutrient conditions and continuous illumination of 730 nm monochromatic light with an intensity of 20 μE at 32°C. The influence of various light conditions and nutrient combinations on *H. hongdechloris* morphology and physiological features is observed using confocal fluorescence microscopy and transmission electron microscopy.

MATERIALS AND METHODS

CULTURE CONDITIONS

Halomicronema hongdechloris was isolated from stromatolites, Shark Bay, Western Australia (Chen et al., 2012). This strain was initially grown in modified K + ES seawater medium (**Table 1A**) with 100 rpm shaking under the control condition given in **Table 1B**. Seven days after inoculation, cells were homogenized using a glass homogenizer with K + ES seawater medium at a ratio of 1:10 (v/v) and used to inoculate 24 well plates (maximum capacity of 3.6 ml/well) with a final volume of 2 ml of cell culture per well. All cultures were inoculated with an equal cell amount containing a total chlorophyll concentration of 3.4 ± 0.4 μg/ml ($n = 100$).

GROWTH RATE, PIGMENT COMPOSITION AND STATISTICAL ANALYSIS

The growth rate of *H. hongdechloris* cultures was monitored using total chlorophyll concentration by sampling every 2–3 days over a period of 30 days. Cells from each well were sampled by centrifugation, and the methanolic total pigment extractions were directly used for spectral and high performance liquid chromatography (HPLC) analysis (Willows et al., 2013). All experiments were carried out on ice under dim green light to prevent photodamage of the pigment. Each experiment was repeated once in new culture plates and each sampling point had four technical replicates. Therefore, each point in the growth curve represents the mean of eight replicates.

Cell concentration was determined using total chlorophyll concentration as a proxy measure. The amount of total chlorophyll (Chl *a* and Chl *f*) was calculated according to the following equations based on the extinction coefficient published in Li et al. (2012).

$$\text{Chl } a\ (\mu\text{g/ml}) = 12.52A_{665-750\text{nm}} - 2.28A_{707-750\text{nm}} \quad (1)$$

Table 1 | Control culture condition.

A. Modified K + ES seawater medium

Major nutrient (mM)	$NaNO_3$	2.35
	K_2HPO_4	0.03
Iron (μM)	Fe-Mn-EDTA	7.2
	Thiamine HCl	200
Vitamin (μg/L)	Biotin	1.5
	B12	1.5
Trace minerals (μg/L)	$MnCl_2{\cdot}4H_2O$	178
	$ZnSO_4{\cdot}\ 7H_2O$	2.3
	$CoSO_4{\cdot}\ 7H_2O$	1.2
	$Na_2MO_4{\cdot}H_2O$	7.2
	$CuSO_4{\cdot}5H_2O$	2.5
pH	TES[a] (pH = 8.0)	25 mM

B. Culture condition

Light quality	Far-red light[b]
Illumination time (h)	Continuous (24 h)
Light intensity (μE)	20
Temperature (°C)	32
Salinity (‰)	33[c]

[a] *TES is 2-[[1,3-dihydroxy-2-(hydroxymethyl)propan-2-yl]amino]ethanesulfonic acid.*
[b] *Single wavelength light emitting diodes (LEDs) 730 nm with 20 nm half width and viewing angle 30° (Nanning Lvxing Light Electronics Co., Ltd., China).*
[c] *The sea salt concentration of 33.3 g in 1 L water is equivalent to 1 × natural seawater.*

$$\text{Chl } f(\mu\text{g/ml}) = 12.78A_{707-750\text{nm}} - 0.07A_{665-750\text{nm}} \quad (2)$$

The in vivo spectra of cells grown under different conditions were recorded using Shimadzu UV–Vis spectrophotometer (UV-2550) with a Taylor-sphere attachment (ISR-240A, Shimadzu, Japan). The cells were homogenized prior to measurement. The recorded spectra were smoothed using the Savitzky-Golay method with a window of <15 points (Origin version 8.0). Spectra were then re-plotted in Microsoft Office Excel 2007.

In this study, the growth rates (k) were the slope estimated based on the linear regression equation of the logarithm of total chlorophyll concentration in logarithmic growth phase in all conditions. The coefficient of determination, R^2, determined using Microsoft Office Excel 2007 based on the linear regression equation. Cells grown under control culture conditions (**Table 1**) were used as the experimental reference for all factors tested in this study. When the relative growth rate is constant, the cell culture has a constant doubling time which can be calculated based on:

$$\text{Doubling time (t)} = \ln 2/\text{k} \quad (3)$$

where k (day^{-1}) is the growth rate.

STATISTICAL ANALYSES

The mean values, confidence intervals and SD values of the replicates for each treatment were calculated by Microsoft Office Excel 2007. The SE of growth rate generated by linear regression were calculated as described in Kenney and Keeping (1962). The effects on growth characters as growth rate and cell sizes caused by different growth conditions were analyzed by ANOVA using R (version 3.0.0). The post hoc multiple comparisons were made by a F-test if a significant difference was detected. The level of significance was set at 0.05 for all testing conditions. All errors quoted in this study are ±95% confidence intervals with the numbers of replicate presented in brackets (n).

VARIATIONS OF LIGHT CONDITIONS

The effects of light qualities and quantities for H. hongdechloris were examined by setting seven different light conditions at various intensities: far-red light (FR, 730 nm LEDs with 20 nm half width and 30° viewing angle) with intensities ranging from 10 to 60 μE; red (RL, 650 nm LEDs with 20 nm half width at a 15° viewing angle), orange-red (OR, 625 nm LEDs with 20 nm half width at a 15° viewing angle), green (520 nm) LEDs with 20 nm half width at a 30° viewing angle), or blue (470 nm) LEDs with 20 nm half width at a 30° viewing angle) light with intensities of 10 and 20 μE; white light (cool white fluorescent light, WL) with intensities of 10–100 μE. LEDs lights utilized in this study are all mono-wavelength LED clusters (Nanning Lvxing Light Electronics Co., Ltd., China). The radiation spectra of various light conditions were monitored using an USB2000+ Miniature Fiber Optic Spectrometer (Ocean Optics, Inc., Australia). Different light intensities were obtained by adjusting the distance between sample and light source, and monitored using a SKP200 light meter (Skye Instruments Ltd., UK) for the OR, RL and FR lights or a Quantum LI-light meter (LI-COR, Inc., USA) for the other light sources. All illumination was continuous. Except for differences in light conditions, cells were all incubated in the same conditions as the control (**Table 1**).

RELATIONSHIP BETWEEN TOTAL CHLOROPHYLL AND WET WEIGHT OF CELLS

The wet weight of cells grown under FR light/10–20 μE or WL light/40–60 μE at the period of exponential phase was obtained by rinsing the cells using milliQ water and removing any remaining surface water by vacuum filtration before weighing. Subsequently, total chlorophyll was extracted from the same samples using 100% methanol (HPLC grade) and the total chlorophyll concentration was determined as described above (Eqs 1 and 2). The rinsed cells were extracted by 100% methanol several times until no detectable pigment was observed in the absorption spectrum (absorbance reading at 665 nm < 0.05). This process was repeated ($n = 10$) for each culture treatment using different amount of cells ranging from 0.25 to 1.50 g. The relationship between total chlorophyll and wet weight were re-plotted in Microsoft Office Excel 2007.

VARIATIONS OF SELECTED ENVIRONMENTAL AND NUTRITIONAL FACTORS

The environmental factors tested in this study were: pH, temperature and salinity. The pH of the medium was maintained using Good's buffers (Good et al., 1966) at a concentration of 25 mM: 2-(N-morpholino)ethanesulfonic acid (MES; pH 6.0), TES (pH 7.0 and 8.0), and N-Cyclohexyl-2-aminoethanesulfonic acid (CHES; pH 9.0 and 10.0). To determine the best culture temperature, cells were cultivated under four selected temperatures (20°C, 27°C, 32°C, and 39°C). The effects of salinity on the growth of the cells were characterized by monitoring the growth rates in modified K + ES medium with different concentrations of commercial premium Sea Salt (AQUASONIC, Australia) from 0.0 g (fresh water) to 3.3 g per 100 ml medium (1 × salinity of nature seawater = 33‰). When the salt concentration of the medium exceeded 1 × seawater, additional NaCl was used to reach the required level of salinity. In all cases, apart from the parameter being tested, conditions were the same as the control condition (**Table 1**).

The effect of different inorganic nitrogen sources ($(NH_4)_2SO_4$, NH_4Cl, $NaNO_3$, $NaNO_2$) and ratio of N:P (mM:mM) on the growth of *H. hongdechloris* were also examined. The ratio of N:P was varied from 7.8 to 780 (with control conditions from **Table 1** being 78) by maintaining the control nitrogen concentration and increasing the phosphorus concentration by 5- or 10-fold or maintaining the control phosphorus concentration and increasing the nitrogen.

PHOTOSYNTHETIC OXYGEN EVOLUTION RATE

The oxygen evolution rates of *H. hongdechloris* cultures were measured using a Hanstech DW2/2 Liquid-Phase Oxygen Electrode Chamber with a circulating thermostat-regulated water bath. All oxygen evolution rate experiments were done at 25°C, except the high temperature measurement (32°C). To avoid large filamentous cell aggregation, the cell culture was homogenized and re-cultured under the same conditions for approximately a week until their biological activity recovered and cell growth was in the exponential phase. One ml of pre-homogenized cell culture with

a total chlorophyll content of 4–8 μg was added to the chamber for oxygen evolution rate measurement. The light source was provided by either a Leica Pradovit color 250 (Autofocus) projector with different transmission filters or a FR light (730 nm with 20 nm half width and 30° viewing angle, Nanning Lvxing Light Electronics Co., Ltd., China).

CONFOCAL MICROSCOPY

The cell morphology of exponential phase *H. hongdechloris* cells grown under different light regimes was examined on a Zeiss LSM Pascal 410 confocal microscope (Oberkochen, Germany) using an Achroplan 63 × water immersion objective or Plan-Neofluar 100 × oil immersion object. Cells were excited using a 458 nm argon laser and autofluorescence was collected using either a 600–680 nm band-pass filter or a 692 nm long-pass filter.

TRANSMISSION ELECTRON MICROSCOPY

Exponential phase cells grown under FR and WL conditions were fixed in 2.5% (v/v) glutaraldehyde with 6% (w/v) sucrose in 0.1 M phosphate buffer pH 7.5 overnight at 4°C. Cells were rinsed 3 × 10 min in the same buffer, and then embedded in 1% (w/v) low melting agarose and further fixed in 1% (w/v) osmium tetroxide with 6% (w/v) sucrose in 0.1 M phosphate buffer pH 7.5 overnight at room temperature. Cells were rinsed 3 × 10 min with milliQ water, and then dehydrated in a series of ethanol concentrations from 50 to 100% for 10 min each. The dehydrated cells were infiltrated with Spurr's resin (Proscitech, Australia) and embedded in gelatin capsules. The samples were polymerized at 65°C for 24 h. Semi-thin sections (1 μm) were cut using a glass knife on an ultramicrotome (Ultracut T, Leica, Austria), mounted and dried on glass slides and stained with 0.5% (w/v) Toluidine blue. Ultrathin sections (70 nm) were cut on the ultramictrotome, placed on 200 mesh thin bar copper grids (Proscitech, Australia) and stained with 2% uranyl acetate for 10 min and lead citrate (Reynold's) for 10 min. All sections were visualized using a transmission electron microscope (JEOL 1400, JEOL Ltd.) at 120 kV. Images were captured using a Gatan Erlangshen ES500W camera and processed using Gatan DigitalMicrograph^{TM} software (Gatan, USA).

RESULTS

To determine the optimal culture conditions, more than 20 different light conditions, covering four different light sources with a series light intensities were tested initially to investigate the best light condition for growing *H. hongdechloris* under laboratory conditions (**Figure 1**). The optimized light conditions were applied in the subsequent studies on optimizing the growth factors. Optimization of environmental and nutritional conditions was performed in a step-wise fashion as follows: optimal culture salinity was determined following by pH, then temperature and finally nitrogen and phosphorus requirements were examined under these optimized conditions (**Figure 1**).

THE LINEAR RELATIONSHIP BETWEEN TOTAL CHLOROPHYLL AND BIOMASS

A linear relationship between the total chlorophyll and cell wet weight for *H. hongdechloris* cells grown was observed under both

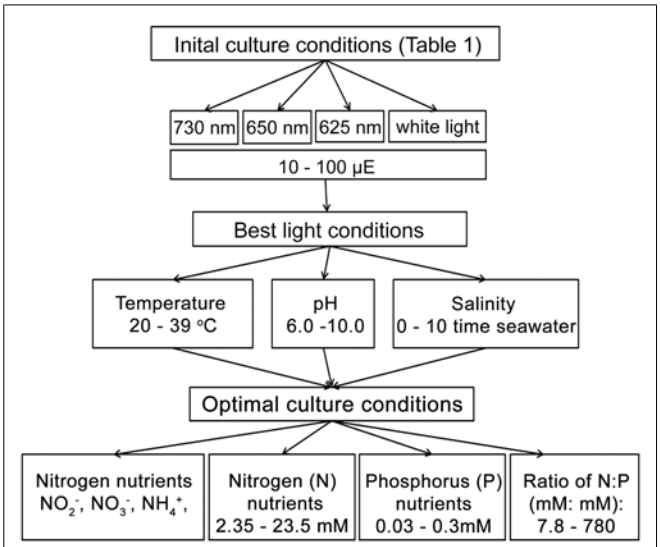

FIGURE 1 | Experimental scheme.

FR light/10–20 μE and WL/40–60 μE conditions (**Figure 2A**). The significant linear relationship indicates that the content of total chlorophyll is relatively constant per cell under the same light conditions. It is of interest to note that the chlorophyll content per cell was ∼1.54 (mg chlorophyll) g^{-1} cell wet weight for the cells grown under FR light, which is about 50% more chlorophyll content compared to the cells grown under WL light. The cells grown under WL light have about 1.0 mg chlorophyll/g cell wet weight (**Figure 2A**). Both Chl *a* and Chl *f* showed a linear relationship with the cell wet weight, 1.39 (mg Chl *a*) g^{-1} and 0.15 (mg Chl *f*) g^{-1} cell wet weight in FR light-grown cells (**Figure 2B**). Cell size did not vary under the different light qualities according to the microscopic observation based on the average measurement of >100 cells per treatment (**Table 2**). There are no significant differences observed in both cell length ($F(3,346) = 2.17$, $p = 0.091 > 0.05$) and width ($F(3,346) = 0.93$, $p = 0.428 > 0.05$) according to a one-way ANOVA analysis (**Table 2**). Hence, the total chlorophyll content is used as a measure of growth throughout this report.

THE INFLUENCE OF VARIOUS LIGHT CONDITIONS ON CELL GROWTH

H. hongdechloris pigment composition has previously been reported to change in response to two light conditions: WL light/20 μE and 720 nm LED light/10–15 μE (Chen et al., 2012). *H. hongdechloris* cells grow under the all tested orange to red LED lights and also WL light (**Figure 3A**). However, no growth was observed when cells were grown under green or blue light at intensities of either 10 or 20 μE (data not shown). The growth rates under the white and red light conditions examined vary considerably with an increased growth rate observed in the following order: FR/20 μE ≥ WL/40 μE > OR/20 μE > RL/20 μE based on total chlorophyll content.

The highest growth rate (k) of ∼0.17 ± 0.01 day^{-1} was obtained under either FR/20 μE or WL/40 μE (**Figures 3B,C**). However, the shape of growth curve and the maximum chlorophyll content at stationary phase are different under the two

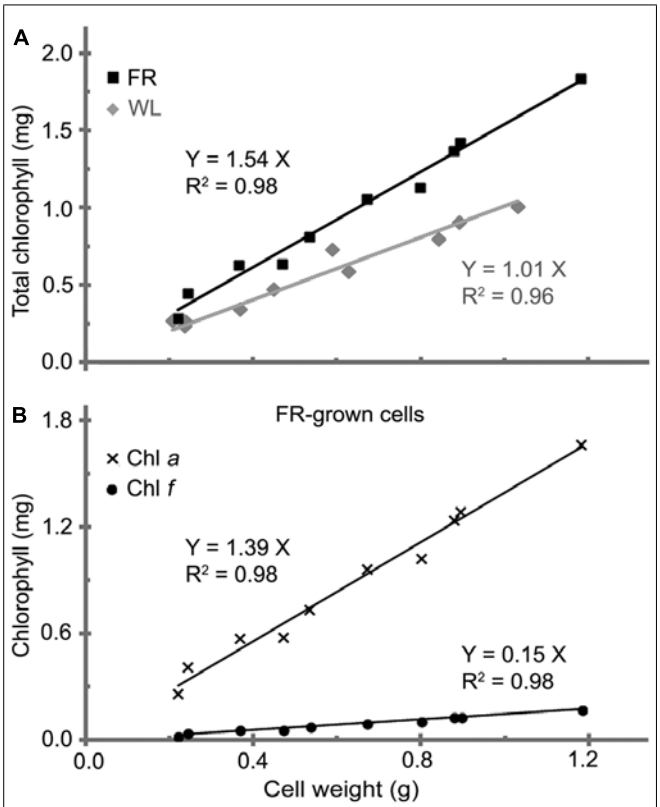

FIGURE 2 | The relationship between cell weight and chlorophyll contents in *H. hongdechloris*. (A) Comparison of total chlorophyll per cell weight (mg/g) for white light-grown (WL, gray line) and far-red light-grown (FR, black line) cells. **(B)** Comparison of Chl *a* (line with crosses) and Chl *f* (line with dots) per cell wet weight (mg/g) for FR-grown cells.

light conditions. Under WL/40 μE, the *H. hongdechloris* culture reaches stationary phase at ∼11 days after a relatively short exponential phase of ∼7 days, resulting in a significantly lower biomass (based on total chlorophyll content) compared with cultures grown under red light conditions. Under FR/20 μE and other red light conditions, the exponential growth phase was extended to >15 days and the maximum chlorophyll content of ∼26 mg $ml^{-1}$was achieved (**Figure 3A**). Surprisingly, the growth rate decreased sharply when the light intensity was increased above 30 μE for FR light and 50 μE for WL light (**Figures 3B,C**). The lowest growth rate of ∼0.08 ± 0.01 day^{-1} was observed when the FR light intensity was increased to 60 μE, the highest light intensity using the available LED light source in the laboratory. No cell growth was detected when WL light intensity was increased to 80 μE or greater (**Figures 3B,C**). These data suggest *H. hongdechloris* prefers a low light intensity and to use FR light for growth.

THE INFLUENCE OF VARIOUS CULTURE CONDITIONS ON CELL GROWTH

Understanding the impacts of environmental as well as other physico-chemical parameters are important for a newly purified cyanobacterial culture. Effects of pH, temperature, and salinity on the cell growth are shown in **Figure 4**. The cells grew at temperature ranges from 20 to 39°C with a best *k* of 0.17 ± 0.02 $day^{-1}$and *t* of 4.2 ± 0.4 days were obtained at 32°C, which was assigned as the optimal temperature (**Figure 4A**). No significant reductions were observed when the temperature was reduced to 27°C or increased to 39°C ($F(2,21) = 1.07$, $p = 0.3617$).

The optimal pH for *H. hongdechloris* culture was determined to be pH 8 ($k = 0.16 \pm 0.02$ day^{-1}, $t = 4.4 \pm 0.4$ days; **Figure 4B**). Cells died in acidic (pH ≤ 6.0) media conditions (**Figure 4B**); however, they were tolerant of alkaline media conditions up to pH 10, the highest pH tested in this study, although the growth rate is much lower than the cells under optimal pH conditions (**Figure 4B**). These data highlight the relative acid sensitivity of *H. hongdechloris*.

Variations in salinity impact a cell's ability to absorb water and nutrients from the medium (Moisander et al., 2002). Culturing of *H. hongdechloris* in different salinities revealed the best *k* of 0.17 ± 0.02 day^{-1} ($t = 4.2 \pm 0.4$ day) is obtained in 1× salinity of natural seawater (33‰(w/v) artificial sea salt); however, similar growth rate was observed in seawater salt concentration between 25‰(w/v) and 67‰(w/v); (**Figure 4C**). *H. hongdechloris* exhibited resistance to the changes in salinity ranging from 8 to 133‰(w/v); however, it cannot survive in the K + ES fresh water medium or salinity higher than 167‰(5 × the salinity of natural seawater; **Figure 4C**).

THE INFLUENCE OF VARIOUS NUTRIENT CONDITIONS ON CELL GROWTH

All nitrogen sources studied were initially provided to *H. hongdechloris* at 2.35 mM nitrogen content (**Table 1**). The best growth rate of 0.17 ± 0.01 day^{-1}($t = 4.1 \pm 0.4$ day) was observed using nitrate ($NaNO_3$) as a nitrogen source, although there were no significant difference among the nitrogen nutrient forms, NH_4^+, NO_2, and NO_3 (**Figure 5A**). $NaNO_3$was used as the best nitrogen nutrient source for *H. hongdechloris* culture.

The amounts and ratio of nitrogen and phosphorus are an important correlated requirement for algal culture (Smith, 1983; Stockner and Shortreed, 1988; Dolman et al., 2012). **Figure 5B** illustrates that growth rates were affected by changing the ratios of

Table 2 | Cell sizes of *H. hongdechloris* cells grown under different light conditions.

		Light conditions			
		White (WL)	**Far red (FR)**	**Orange red (OR)**	**Red light (RL)**
Cells Size	Length	1.81 ± 0.20 ($n = 100$)	1.86 ± 0.23 ($n = 100$)	1.80 ± 0.13 ($n = 100$)	1.79 ± 0.25 ($n = 50$)
	Width	0.86 ± 0.12 ($n = 100$)	0.88 ± 0.06 ($n = 100$)	0.88 ± 0.07 ($n = 100$)	0.87 ± 0.08 ($n = 50$)

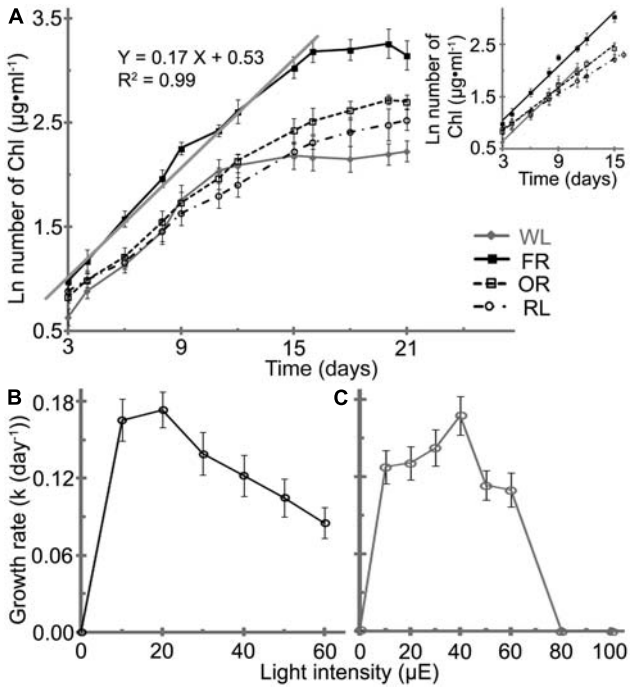

FIGURE 3 | Effects of light conditions on the growth profile of *H. hongdechloris*. **(A)** Growth profile of *H. hongdechloris* under different light conditions. Optimal intensities for all red/orange LED lights were 20 μE, but 40 μE for white light. The solid gray line and equation denotes the trend line of linear regressions of the logarithm of total chlorophyll concentration in the exponential phase under the FR/20 μE condition. **A** insert: Comparison of the trend lines of linear regressions of the logarithm of total chlorophyll concentration in the exponential phase for cells grown under different light conditions. FR, far-red; OR, orange-red; RL, red light and WL, white light. Error bars represent SDs ($n = 8$). Effects of **(B)** FR and **(C)** WL light intensities on the growth rate of *H. hongdechloris*. Error bars represent SE ($n = 8$).

N:P (mM:mM)) and the total concentration of nitrogen and phosphorus nutrients. The highest growth rate of 0.22 ± 0.02 day^{-1} and a doubling time of 3.1 ± 0.2 days were observed when both total nitrogen and phosphorus nutrient concentration were increased fivefold compared with the standard amount in K + ES but the ratio of N:P remained the same, i.e., the best nutrient condition is: 11.75 mM nitrogen in the form of $NaNO_3$, 0.15 mM phosphorus in the form of PO_4^{3-} and the ratio of N:P is 78 (**Figure 5B**). Under these conditions, the maximum biomass, calculated based on the rate of total chlorophyll to cell wet weight shown in **Figure 2**, was >35.7 mg ml^{-1} (data not shown), which is almost double the biomass observed in cells grown under normal N:P concentrations (**Table 1**). The imbalance of the ratio of N:P, either <7.8 or >780 inhibited the growth of *H. hongdechloris* (**Figure 5B**).

CHARACTERIZED PHYSIOLOGICAL PROPERTIES

Photopigment composition

In vivo absorption spectra of *H. hongdechloris* cells indicated that Chl *a* (678 nm peak) and phycobiliprotein (625 nm peak) are the main photopigments in cultures grown under WL, OR or RL conditions (**Figure 6**). The absorption spectral profiles are similar to most other typical cyanobacteria using Chl *a* and phycobiliproteins. Further HPLC analysis confirmed that no detectable Chl *f* existed in cultures grown under WL, OR or RL conditions (data not shown). However, the pigment composition of *H. hongdechloris* under FR light is unique, having an absorption spectrum indicative of the presence of Chl *a* (678 nm) and Chl *f* (730 nm), with a limited amount of phycobiliproteins (**Figure 6A**), which is consistent with the previous report (Chen et al., 2012). Despite the presence of Chl *f* in FR light-grown cells, Chl *a* still remains the main chlorophyll of *H. hongdechloris* under all light conditions tested (**Figure 6A**).

To enhance the content of Chl *f* and the total biomass, different light intensities of FR light were tested and compared with the equivalent intensities of white light. The highest Chl *f*/Chl *a* index ($A_{730-780\ nm}/A_{678-780\ nm}$) of 0.29 is observed under the FR light intensities of 10–20 μE (**Figure 6B**). Increased FR light intensities resulted in a decreased Chl *f*/Chl *a* index of 0.13 and the increased carotenoids to Chl *a* index (Car/Chl *a*, $A_{495-780\ nm}/A_{678-780\ nm}$), which may indicate the culture was under high-light stress. Interestingly, the cells grown under WL light showed a more stable pigment content beside the increased Car/Chl *a* index under increased light intensities. The highest Car/Chl *a* index of ∼1.9 was observed in the cells grown under FR light/60 μE light, suggesting the high-light stressed situation for *H. hongdechloris* cells (**Figure 7B** insert). The relatively stable amount of phycobiliprotein and the dramatic changes in Chl *f* concentration (**Figure 6B** insert) observed in cells grown under different intensities of FR light suggest that Chl *f* plays an important role in the capture and use of FR light for driving photosynthetic reactions. Increases in the Car/Chl *a* index observed in the cells under possible high-light stress agree well with the decreased growth rate for the cells grown under these higher intensities of either FR or WL light (**Figures 3B,C**). The optimized light condition for *H. hongdechloris* culture is FR light with lower light intensity of 10–20 μE.

Photosynthetic activities (photosynthetic oxygen evolution rate)

H. hongdechloris cells grown under FR light and WL light conditions were subjected to oxygen evolution measurements. When WL was used as the incident light source, the FR light-grown cells had a maximum oxygen evolution rate of 23 μmol O_2 (mg Chl)$^{-1}$ h^{-1} and reached its light saturation point at ∼50 μE at 25°C (**Figure 7A**). However, under the same conditions the WL light-grown cells had a higher maximum oxygen evolution rate of 39 μmol O_2 (mg Chl)$^{-1}$ h^{-1} and reached its light saturation point at about 90 μE at 25°C (**Figure 7B**). *H. hongdechloris* cells cultured in both conditions show lower oxygen evolution rates than typical cyanobacteria (Lee et al., 1998; Gloag et al., 2007; Milligan et al., 2007). Given the slower growth rate of *H. hongdechloris*, this lower oxygen evolution rate is unsurprising.

When a FR light was used as the incident light source for detecting oxygen evolution, the maximum evolution rate for FR light grown cells is only about 12 μmol O_2 (mg Chl)$^{-1}$ h^{-1}, ∼50% oxygen evolution rate using WL as incident light at the equivalent intensity (**Figure 7A**). White light grown cells did not show any detectable oxygen production under illumination of FR light

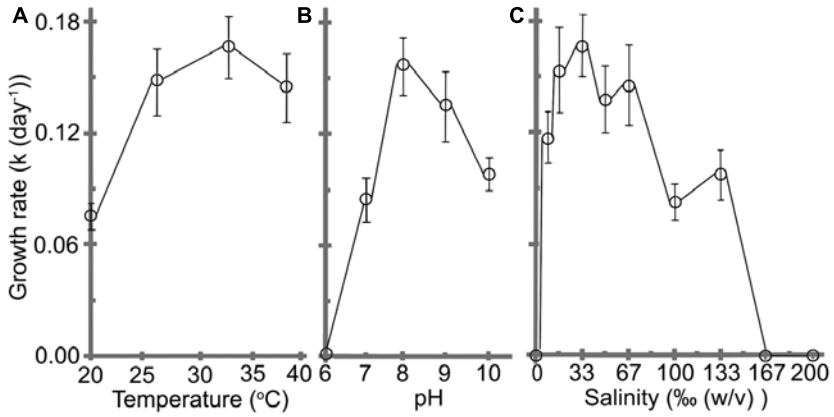

FIGURE 4 | Effects of (A) temperature, (B) pH, and (C) salinity on the growth rate of *H. hongdechloris*. Error bars represent SE ($n = 8$).

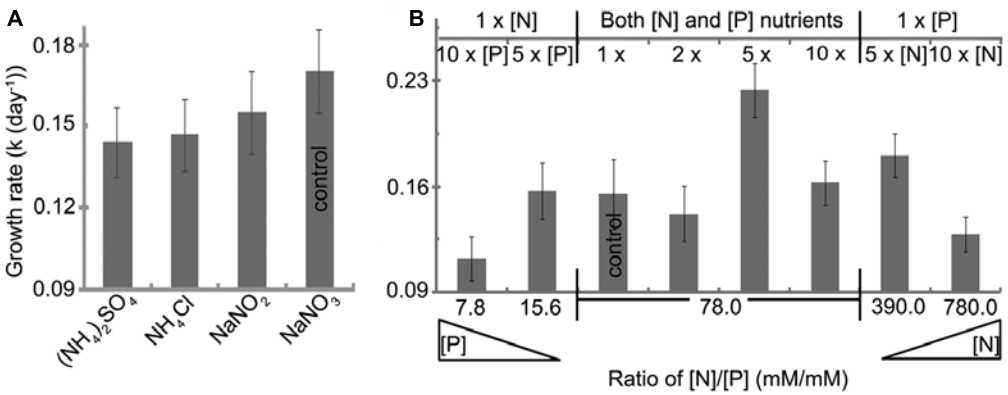

FIGURE 5 | Effect of (A) nitrogen source and (B) nitrogen and phosphorus concentration on the growth rate of *H. hongdechloris*. All concentrations are relative to the concentrations outlined in **Table 1**. Error bars represent SE ($n = 8$).

when the light intensity was <60 μE (**Figure 7B**). This result suggests that Chl *f* in *H. hongdechloris* plays an important role in capturing FR light and transferring the energy to the reaction center for photosynthetic activity. As reported in **Figure 2**, the chlorophyll content in WL light-grown cells is lower than that in FR light grown cells (**Figure 2A**). Taking this parameter into account, a similar maximum oxygen evolution rate of about 35–40 μmol O_2 (cell weight g)$^{-1}$ h^{-1} is observed for cells grown under both light conditions (**Figure 7C**) when using WL as the incident light. The oxygen evolution rate is almost doubled when the measurement temperature is increased from a standard 25 to 32°C (**Figure 7A** insert), which is in agreement with the optimized *H. hongdechloris* culture temperature (**Figure 7A**).

The morphology of H. hongdechloris grown under various light conditions

Different wavelength pass filters were applied for detecting the fluorescence generated from different photopigments using confocal fluorescence microscope. The fluorescence detected by an emission band pass filter of 600–680 nm is mainly generated from phycobiliproteins (Blankenship, 2002; Collins et al., 2012), and the fluorescence detected using a 692 nm long pass filter is largely due to the presence of Chl *f*. Strong >692 nm fluorescence was only observed in *H. hongdechloris* cells grown under FR light, and not in the cells grown under WL, OR or RL light (**Figure 8A**). This >692 nm fluorescence observed from FR light-grown cells was distributed evenly around the peripheral thylakoid membranes (Th) of the cells, suggesting that Chl *f*-binding protein complexes are also distributed through these membranes (**Figure 8B**). Using the emission band pass filter (600–680 nm), strong and uniform fluorescence was observed in cells grown under white, orange-red or red light. However, the fluorescence recorded using this filter was much weaker for the cells grown under FR light; and strikingly, the strongest fluorescence was localized at the septa region. This phenomenon was also observed in our previous report (Chen et al., 2012). Both 600–680 nm and >692 nm fluorescence patterns for white and OR light grown cells overlayed well with one another; however, for FR light grown cells, a clear inverse pattern of fluorescence was observed (**Figure 8B**).

Comparison of the ultrastructure of *H. hongdechloris* grown under either WL or FR light demonstrated no obvious difference in

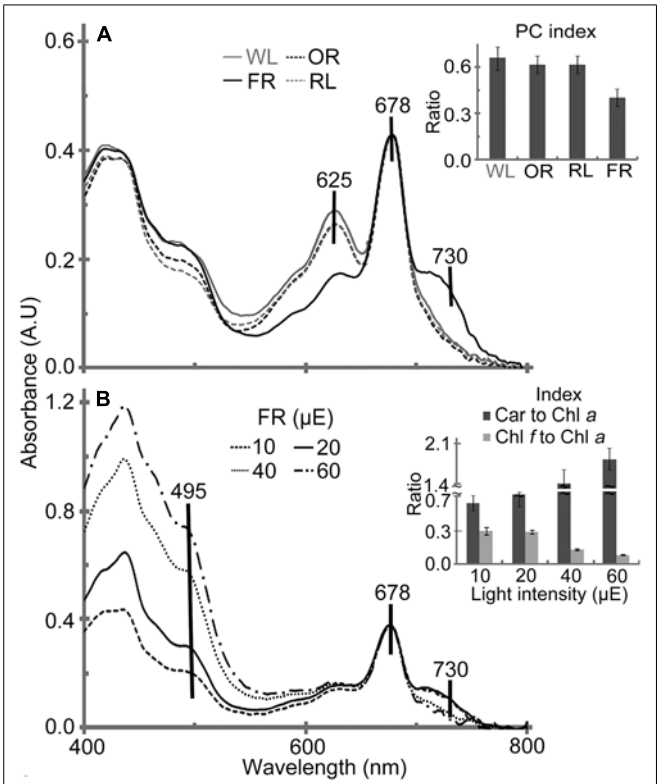

FIGURE 6 | *In vivo* absorption spectra of *H. hongdechloris* grown under different light qualities (A) and different intensities of FR light (B). Absorption peaks corresponding to carotenoid (495 nm), phycobiliprotein (625 nm), Chl *a* (678 nm) and Chl *f* (730 nm) are indicated. **A** insert: PC index [phycobiliprotein to Chl *a* ratio ($A_{625-780\ nm}/A_{678-780\ nm}$)] of *H. hongdechloris* grown under different light qualities; FR, far-red; OR, orange-red; RL, red light and WL, white light. **B** insert: Car to Chl *a* (carotenoid to Chl *a*, $A_{495-780\ nm}/A_{678-780\ nm}$) and Chl *f* to Chl *a* index ($A_{730-780\ nm}/A_{678-780\ nm}$) index of *H. hongdechloris* under different intensities of 730 nm light. All data represent the means of five replicates ($n = 5$).

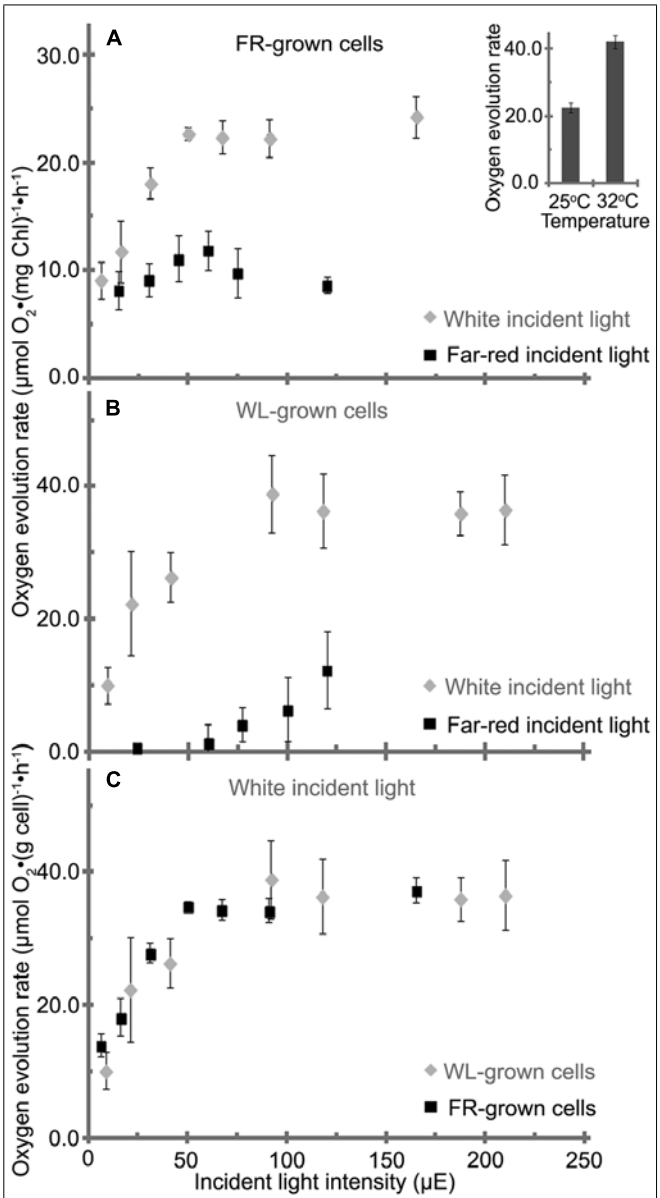

FIGURE 7 | Oxygen evolution rate of *H. hongdechloris* grown under (A) far-red light (FR) or (B) white light (WL), with either FR or WL light as the incident light source as indicated. Data are based on total chlorophyll content. **A** insert: oxygen evolution rate of *H. hongdechloris* cells at 25°C or 32°C with 67 μE white light illumination. **(C)** The oxygen evolution rate of *H. hongdechloris* cells grown under either FR or WL conditions based on biomass, using white light as the incident light source. Error bars represent SDs ($n = 9$).

cell morphology, apart from a slight difference in the thicknesses of appressed Th (**Figure 9**). The cells grown under WL demonstrate that phycobilisome-like structures are uniformly distributed along the Th (white arrows in **Figures 9B,C**). The Th in the FR light grown cells were more appressed, which seems likely consistent with the reduction in the amount of phycobilisomes between the Th (**Figure 9A**). Conversely, the phycobilosome-like structures can be only observed between the plasma membrane and Th in the cells grown under FR light (**Figure 9A**). Under both FR and WL light conditions, cells have a filamentous structure surrounded by a fibrous sheath (fs)-like layer with a thickness of 0.08–0.15 μm ($n = 200$) and a peptidoglycan layer (Pg) shared between the cells. No branching was observed (**Figure 9**).

DISCUSSION

In liquid culture, *H. hongdechloris* has a propensity to attach to surfaces and to aggregate. This strong adhesion creates difficulties for cell counting and other measurements. Cells used in this study were homogenized before inoculation in order to obtain an equal number of cells at the start of each experiment (total chlorophyll concentration of 3.4 ± 0.4 μg/ml). A consequence of this homogenization process is some apparent damage to the cells that contributes to the lag phase after inoculation (**Figure 3A**). To avoid the effects of this reduction, growth rate was only calculated using the data collected from exponential phase, where more than six measuring points are recorded. All growth curves presented in this study start from day three after lag phase. The coefficient of determination, R^2, was over 0.95 in most of the conditions, which

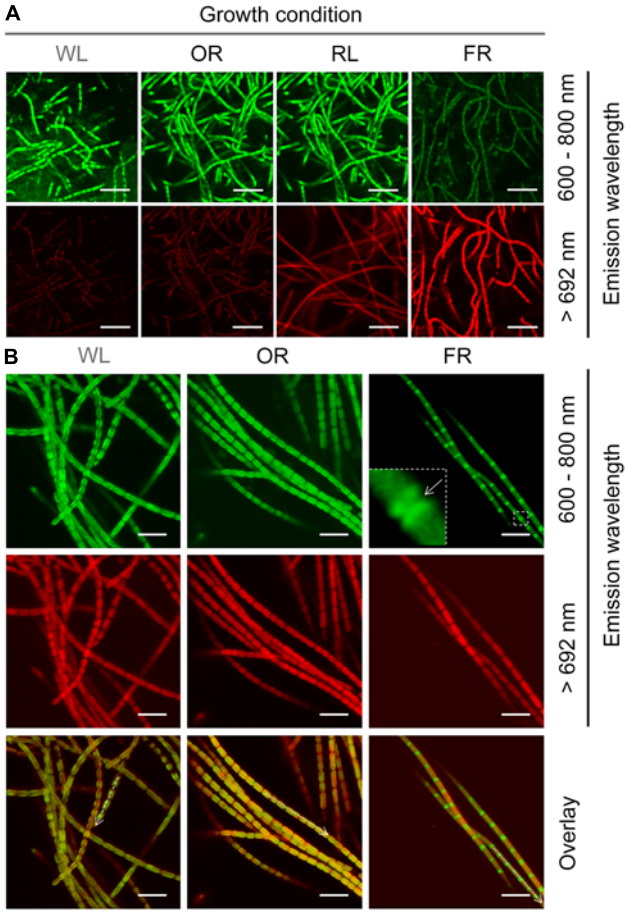

FIGURE 8 | Confocal fluorescence images of *H. hongdechloris* cells grown under different light conditions. Autoflourescence of cells excited with 458 nm light were collected using either a 600–680 nm band-pass filter or a 692 nm long-pass filter (>692 nm). **(A)** Confocal fluorescence images of cells grown under WL, FR, OR, or RL light. All data were collected using identical laser intensity and gain settings. Bar = 10 μm. **(B)** Confocal fluorescence images of cells grown in WL, OR, or FR light conditions. Fluorescence emission at 600–680 nm was detected uniformly around the periphery of cells grown in other selected lights whereas in FR light grown cells this fluorescence was concentrated in the septa. Intensities of the different fluorescence wavelengths along the axis of the dotted arrows in the overlay are plotted in the lower panel. Different laser intensities and gain settings were used in order to collect normalized fluorescence intensities. Bar = 5 μm.

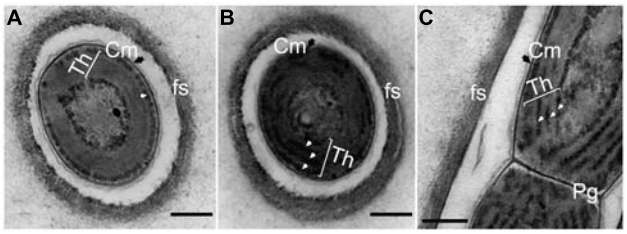

FIGURE 9 | Transmission electron micrograph of ultrathin section of *H. hongdechloris* cells grown under white and far-red light conditions. **(A)** Cross section of a cell grown under FR light; **(B)** Cross section of a cell grown under white light; **(C)** Longitudinal section of the intersection (septum region) between filamentous cells grown under white light. White arrows indicate phycobilisome-like structures filling the stromal side of the thylakoid membranes (Th). Pg, peptidoglycan layer; fs, fibrils sheath and Cm (black arrows), cytoplasmic membrane. Bar = 0.2 m.

represents over 95% of data that is closest to the line of best fit. The statistical analysis indicates that the calculation of growth rate is reliable. Furthermore, the reproducibility of the results is confirmed by the consistent doubling time of the control treatment, which was always in the range of 4.1–4.4 days ($n = 10$) throughout the whole study.

All growth curves are generated from at least two biological repeats and four technical repeats, and each set of measurement requires minimum five weeks for completion. Such time-consuming experiments forced us to design one-way optimizing strategy, that is, we tested one environmental element at once and used the optimized condition for the next test (**Figure 1**).

Comparison of the maximum biomass based on the total chlorophyll under a particular test condition may not be an appropriate method since we observed a difference in the total chlorophyll present in cells grown under FR light compared to WL light (**Figure 2**). However, the measured growth rate should be reliable as there is a linear relationship observed between total chlorophyll content and biomass under the same light conditions, and therefore chlorophyll content can be used as a proxy measure for biomass for each light condition. Additionally, there were no observable differences in the cell size or filamentous features from the cells cultured under different light conditions (**Table 2** and **Figure 8**).

The decreased amount of total chlorophyll per gram cells under WL light conditions (**Figure 2**) is likely complemented by the dramatically increased amount of phycobiliprotein, compared with the higher chlorophyll content in the FR light grown cells. With the aid of phycobiliprotein to capture light under WL, OR or RL conditions, cells are unlikely to require as much chlorophyll as that which is needed under the FR light environment, beyond the phycobiliprotein absorption region. The mechanism of this pigment adaptation process remains undefined.

Pigment analysis of cell cultures grown under different light qualities demonstrate the increase in the PC index [phycobiliprotein to Chl *a* ratio ($A_{625-780\ \mathrm{nm}}/A_{678-780\ \mathrm{nm}}$)] for the cells grown under OR, RL or WL light, and the decrease of Chl *f* composition in total chlorophyll relative to FR light grown cells (**Figure 6A** insert). These results strongly suggest that *H. hongdechloris* acclimates to the shifted accessible light environment by varying the pigment composition. The experiments using a mixture of OR light/10 μE and FR light/10 μE light were also performed in order to investigate the effect of expanding the photosynthetic active spectral region from 600 to 750 nm. In this OR+FR light condition, *H. hongdechloris* retain both Chl *f* and phycobiliproteins (data not shown). However, the PC index decreased to around 0.5 ± 0.03 compared with that of cell grown under OR light/20 μE (0.62 ± 0.04) and Chl *f*/Chl *a* index decreased to about 0.20 ± 0.02 compared that of cell grown under FR light/20 μE (0.29 ± 0.03). Surprisingly, the coexistence of phycobiliproteins and Chl *f* does

not appear to benefit *H. hongdechloris* growth with an even slower k of 0.11 ± 0.01 day^{-1} compared to the k of 0.13 ± 0.01 day^{-1} when using OR light/20 μE or the k of 0.17 ± 0.01 day^{-1} using FR light/20 μE light. The results suggest that the main light harvesting strategies of *H. hongdechloris* grown under FR light compared with <700 nm light are different and not complementary corresponding to one another. Although the light-harvesting strategy of *H. hongdechloris* is currently undefined, our data presented here indicates that *H. hongdechloris* uses phycobiliproteins as its major antenna component when grown under light sources <700 nm, but uses Chl *f* to access light beyond 700 nm (i.e., grown under FR light). The relatively stable content of Chl *a* in *H. hongdechloris* under different light conditions strongly suggests that Chl *a* is the main photopigment in the photosystem reaction centers, although further experiments are required to confirm this hypothesis.

Previous results show that Chl *f* is a FR light induced chlorophyll (Akutsu et al., 2011; Chen et al., 2012) and phycobiliprotein contents increased dramatically in cell grown under WL, RL or OR light, which indicates photoacclimation between phycobiliproteins and chlorophyll-binding light-harvesting protein complexes (Gloag et al., 2007; Bibby et al., 2009). Both results were supported by confocal fluorescence results. **Figure 8A** illustrates that strong >692 nm fluorescence mainly came from Chl *f*, which was only detected in FR light-grown cells (Li et al., 2013). The much weaker but still visible >692 nm fluorescence observed in cells grown under WL, OR or RL light is most likely due to the presence of red-shifted Chl *a* in photosystems (Chen and Scheer, 2013). Fluorescence between 600 and 680 nm was observed strongly and uniformly around the periphery of cells grown under WL, RL or OR light, whereas in FR light-grown cells, this fluorescence was much weaker and concentrated at the septa (**Figure 9B**). Taken together with the pigment analyses (**Figure 6A**), the phycobiliprotein remanets in FR light grown cells seem predominantly localized at the septa of the cells or distributed between the plasma membrane and Th (**Figure 9B**). However, we cannot distinguish the different locations and correlation between phycobiliproteins and chlorophylls due to the resolution limits associated with confocal microscopy.

Halomicronema hongdechloris was isolated from a inner layer sediment of stromatolites which is a light filtered environment. Approximately 97% of light is attenuated through a 3 mm thick microbial mat (Brock, 1976; Al-Najjar et al., 2010). Therefore the light intensity inside stromatolites is expected to be extremely low, especially in the visible light spectral region. The photosynthetic microbial communities thriving in these unique niches have developed a capacity to flourish in such extreme light environment, which is consistent with the fact that *H. hongdechloris* prefers a lower light intensity and grows well under FR light.

Figure 4A illustrates that there were no significant reductions in growth rate when cells were grown at 27°C or 39°C compared with the optimal temperature 32°C ($F(2, 21) = 1.07$, $p = 0.3617 > 0.05$). However, these cells had approximately a week delay to reach the exponential phase when the temperature was decreased to 27°C (data not shown). In contrast, the cells grown at 39°C showed the similar growth profile as the cells at 32°C, but the growth rate was dropped dramatically after 10 days, without an obvious stationary phase (data not shown). One explanation for this observation is the reduced CO_2 solubility in aqueous solution at higher temperature. The solubility of CO_2 in water is about 1.45 g/L at 25°C; however, this decreases by more than 30% when the temperature is increased to 40°C (Carroll and Alan, 1992). This reduction in dissolved CO_2 may inhibit photosynthetic efficiency. The culture plates have limited volumes and the surface area (2 ml testing culture in 3.6 ml vial), which may result in a limited gas exchange rate leading to a decreased CO_2 concentration in the culture medium at higher temperatures.

Halomicronema hongdechloris grows well in 1 × seawater, but also tolerates higher salinity upto 4 × seawater. The initial cells are cultured under 1 × seawater control condition, therefore, the cells inoculated into 4 × seawater may face an osmotic shock. A long lag phase (∼2 weeks) was observed, but the cells started to grow after 16 days (data not shown). This phenomenon is also observed in the cells grown in 3 × seawater. The longer lag phase may represent the periods when cells prepare themselves for adapting such hypersaline conditions, albeit only after more than two weeks exposed to the high salt. In other words, *H. hongdechloris* demonstrates halotolerant characteristics, which is consistent with the feature observed in the *Halomicronema* strain TEFP, a moderately halophilic cyanobacterium growing within the salinity range of 40–132‰ (Abed et al., 2002). Unsurprisingly, *Halomicronema* strain TEFP is the closest identified relative of *H. hongdechloris* based on 16S rRNA classification. Previous studies reported that the ecological niche where *H. hongdechloris* was isolated (Hamelin Pool, Shark Bay, Western Australia) is hypersaline (Bauld, 1984; Papineau et al., 2005), owing to the restricted exchange of water between the open ocean and the shallow bay and a high net evaporation rate witnessed in the water at low tide during hot season. The reports also showed that several halophilic Archaea have been isolated from Hamelin Pool (Papineau et al., 2005; Goh et al., 2006). These evidences suggest that the microbial communities at Hamelin Pool must be able to adapt to the hypersaline coastal environment, which might explain the high salt tolerance observed in *H. hongdechloris*.

In this study, we focused on the requirements of *H. hongdechloris* for inorganic nitrogen and phosphorus. *H. hongdechloris* biomass reached a maximum of 35.7 mg cell wet weight per ml when the medium was supplemented with fivefold of both nitrogen and phosphorus (**Figure 5**). Diverse responses to differential nitrogen versus phosphorus concentration were observed. While the negative relationship between *H. hongdechloris* growth rate and the high N:P ratio of 780 or the low N:P ratio of 7.8 indicated the importance of correlation between nitrogen and phosphorus. Further investigation on the correlation between growth rate of *H. hongdechloris* and the additional organic form nutrients (carbon and nitrogen) is required.

CONCLUSION

In this study, we optimized the growth conditions for *H. hongdechloris*, both in terms of growth kinetics and Chl *f* content. We suggest the best culture conditions for *H. hongdechloris*, with a growth rate of 0.22 ± 0.02 day^{-1}, are: FR light with an intensity of 20 μE, at 32°C, pH 8.0, salinity of 33‰ in modified

K + ES seawater medium with increased nitrogen and phosphorus concentrations of 11.75 mM and 0.15 mM, respectively. *H. hongdechloris* cells are halotolerant, and do not grow in fresh water medium (salinity of 0‰). Sodium nitrate is the most favorable nitrogen sources among the tested inorganic nitrogen compounds. The greatest yield of Chl *f* is ∼10% of the total chlorophyll under these assigned optimal culture conditions. The cells grown under WL, OR and RL light showed a very similar content of phycobiliprotein with a PC index of ∼0.6. Fluorescence confocal microscopy reveals an unusual distinction in the distribution pattern of phycobiliproteins in Chl *f*-containing cells compared with those cells that do not have detectable Chl *f*. This result is supported by transmission electron microscopy analysis which shows a reduction in the number of phycobilisome-like structures present in a transverse section of Chl *f*-containing cells compared with cells that do not have Chl *f*. Different active O_2 evolution was observed between Chl *f* containing FR light-grown cells and WL light-grown cells, when illuminated by FR light, which confirms the spectral expansion of oxygenic photosynthesis afforded by the presence of Chl *f* in *H. hongdechloris*.

ACKNOWLEDGMENTS

Min Chen holds an Australian Research Council Future Fellowship and thanks the Australian Research Council for support. Yaqiong Li is the recipient of scholarship supported by the China Scholarship Council. Yuankui Lin would like to thank Dr. H. Liu and Ms. N. Gokoolparsadh for valuable discussion and assistance in transmission electron microscopy and sample preparation.

REFERENCES

Abed, R. M. M., Garcia-Pichel, F., and Hernández-Mariné, M. (2002). Polyphasic characterization of benthic, moderately halophilic, moderately thermophilic cyanobacteria with very thin trichomes and the proposal of *Halomicronema excentricum* gen. nov., sp. nov. *Arch. Microbiol.* 177, 361–370. doi: 10.1007/s00203-001-0390-2

Akutsu, S., Fujinuma1, D., Furukawa1, H., Watanabe, T., Ohkubo, S., and Miyashita, H. (2011). Pigment analysis of a chlorophyll f-containing cyanobacterium strain KC1 isolated from Lake Biwa. *Photomed. Photobiol.* 33, 35–40.

Al-Najjar, M. A. A., de Beer, D., Jørgensen, B. B., Kühl, M., and Polerecky, L. (2010). Conversion and conservation of light energy in a photosynthetic microbial mat ecosystem. *ISME J.* 4, 440–449. doi: 10.1038/ismej.2009.121

Bauld, J. (1984). "Microbial mats in marginal marine environments: Shark Bay, Western Australia, and Spencer Gulf, South Australia," in *Microbial Mats: Stromatolites*, eds Y. Cohen, R. W. Castenholz, and H. O. Halvorson (New York: Alan R. Liss), 39–58.

Bibby, T. S., Zhang, Y., and Chen M. (2009). Biogeography of photosynthetic light-harvesting genes in marina phytoplankton. *PLoS ONE* 4:e4601. doi: 10.1371/journal.pone.0004601

Blankenship, R. E. (2002). "Antenna complexes and energy transfer processes", in *Molecular Mechanisms of Photosynthesis*, ed. R. E. Blankenship (Oxford: Blackwell Science Ltd.), 124–157. doi: 10.1002/9780470758472.ch7

Brock, T. D. (1976). "Biological techniques for the study of microbial mats and living stromatolites," in *Developments in Sedimentology 20: Stromatolites*, ed. M. R. Walter (Amsterdam: Elsevier Scientific Pub. Co.), 21–30.

Carroll, J. J., and Alan, E. M. (1992). The system carbon dioxide-water and the Krichevsky–Kasarnovsky equation. *J. Sol. Chem.* 21, 607–621. doi: 10.1007/BF00650756

Chen, M., and Blankenship, R. E. (2011). Expanding the solar spectrum used by photosynthesis. *Trends Plant Sci.* 16, 427–431. doi: 10.1016/j.tplants.2011.03.011

Chen, M., Li, Y., Birch, D., and Willows, R. D. (2012). A cyanobacterium that contains chlorophyll f-a red-absorbing photopigment. *FEBS Lett.* 586, 3249–3254. doi: 10.1016/j.febslet.2012.06.045

Chen, M., and Scheer, H. (2013). Expanding the limits of natural photosynthesis and implications for technical light harvesting. *J. Porphyrins Phthalocyanines* 17, 1–15. doi: 10.1142/S1088424612300108

Chen, M., Schliep, M., Willows, R. D., Cai, Z. L., Neilan, B. A., and Scheer, H. (2010). A red-shifted chlorophyll. *Science* 329, 1318–1319. doi: 10.1126/science.1191127

Collins, A. M., Liberton, M., Jones, H. D. T., Garcia, O. F., Pakrasi, H. B., and Timlin, J. A. (2012). Photosynthetic pigment localization and yhylakoid membrane morphology are altered in *Synechocystis* 6803 phycobilisome mutants. *Plant Physiol.* 158, 1600–1609. doi: 10.1104/pp.111.192849

Dolman, A. M., Rücker, J., Frances, R., Fastner, J., Rohrlack, T., Mischke, U., et al. (2012). Cyanobacteria and cyanotoxins: the influence of nitrogen versus phosphorus. *PLoS ONE* 7:e38757. doi: 10.1371/journal.pone.0038757

Fogg, G. E., and Thake, B. (1987). "Culture of limited volume," in *Algal Cultures and Phytoplankton Ecology*, eds G. E. Fogg, and B. Thake (London: University of Wisconsin Press), 12–42.

Gloag, R. S., Ritchie, R. J., Chen, M., Larkum, A. W., and Quinnell, R. G. (2007). Chromatic photoacclimation, photosynthetic electron transport and oxygen evolution in the Chlorophyll d-containing oxyphotobacterium *Acaryochloris marina*. *Biochim. Biophys. Acta* 1767, 127–135. doi: 10.1016/j.bbabio.2006.11.014

Goh, F., Leuko, S., Allen, M. A., Bowman, J. P., Kamekura, M., Neilan, B. A., et al. (2006). *Halococcus hamelinensis* sp. nov., a novel halophilic archaeon isolated from stromatolites in Shark Bay, Australia. *Int. J. Syst. Evol. Microbiol.* 56, 1323–1329. doi: 10.1099/ijs.0.64180-0

Good, N. E., Winget, G. D., Winter, W., Connolly, T. N., Izawa, S., Singh, R. M., et al. (1966). Hydrogen ion buffer for biological research. *Biochemistry* 5, 467–477. doi: 10.1021/bi00866a011

Hansmann, E. (1973). "Growth measurement," in *Handbook of Phycological Methods–Culture Methods and Growth Measurements*, ed. J. R. Stein (Cambridge: Cambridge University Press), 359–368.

Hou, X., Raposo, A., and Hou, H. J. (2013). Response of chlorophyll d-containing cyanobacterium *Acaryochloris marina* to UV and visible irradiations. *Photosynth. Res.* 117, 497–507. doi: 10.1007/s11120-013-9946-7

Kenney, J. F., and Keeping, E. S. (1962). "Linear regression and correlation," in *Mathematics of Statistics*, 3rd Edn, Part 1, Chap. 15 (Princeton, NJ: Van Nostrand), 252–285.

Kühl, M., Min, C., Peter, R., Ulrich, S., and Anthony, L. (2005). A niche for cyanobacteria containing chlorophyll d. *Nature* 433, 820. doi: 10.1038/433820a

Lee, S., Prochaska, D. J., Fang, F., and Barnum, S. R. (1998). A 16.6-kilodalton protein in the cyanobacterium *Synechocystis* sp. PCC 6803 plays a role in the heat shock response. *Curr. Microbiol.* 37, 403–407. doi: 10.1007/s002849900400

Li, Y., Cai, Z.-L., and Chen, M. (2013). Spectroscopic properties of chlorophyll f. *J. Phys. Chem. B.* 117, 11309–11317. doi: 10.1021/jp402413d

Li, Y., Scales, N., Blankenship, R. E., Willows, R. D., and Chen, M. (2012). Extinction coefficient for red-shifted chlorophylls: chlorophyll d and chlorophyll f. *Biochim. Biophys. Acta* 1817, 1292–1298. doi: 10.1016/j.bbabio.2012.02.026

Loughlin, P. D., Lin, Y., and Chen, M. (2013). Chlorophyll d and *Acaryochloris marina*: current status. *Photosynth. Res.* 116, 277–293. doi: 10.1007/s11120-013-9829-y

Milligan, A. J., Berman-Frank, I., Gerchman, Y., Dismukes, G. C., and Falkowski1, P. G. (2007). Light dependent oxygen consumption in nitrogen fixing cyanobacteria plays a key role in nitrogenase protection. *J. Phycol.* 43, 845–852. doi: 10.1111/j.1529–8817.2007.00395.x

Miyashita, H., Ikemoto, H., Kurano, N., Adachi, B., Chihara, M., and Miyachiand, S. (1996). Chlorophyll d as a major pigment. *Nature* 383, 402. doi: 10.1038/383402a0

Miyashita, H., Ikemoto1, H., Kurano1, N., Miyachi1, S., and Chihara, M. (2003). *Acaryochloris marina* gen. et sp. nov. (cyanobacteria), an oxygenic photosynthetic prokaryote containing Chl d as a major pigment. *J. Phycol.* 39, 1247–1253. doi: 10.1111/j.0022-3646.2003.03–158.x

Moheimani, N. R., Borowitzka, M. A., and Isdepsky, A. (2013). "Standard methods for measuring growth of Algae and their composition," in *Algae for Biofuels and Energy*, eds M. A. Borowitzka and N. R. Moheimani (Dordrecht: Springer), 265–283.

Moisander, P. H., McClinton, E. III, and Paerl, H. W. (2002). Salinity effects on growth, photosynthetic parameters, and nitrogenase activity in estuarine planktonic cyanobacteria. *Microb. Ecol.* 43, 432–442. doi: 10.1007/s00248-001-1044-2

Papineau, D., Walker, J. J., Mojzsis, S. J., and Pace, N. R. (2005). Composition and structure of microbial communities from stromatolites of Hamelin Pool in Shark Bay, Western Australia. *Appl. Environ. Microbiol.* 71, 4822–4832. doi: 10.1128/AEM.71.8.4822–4832.2005

Pikuta, E. V., Hoover, R. B., and Tang, J. (2007). Microbial extremophiles at the limits of life. *Crit. Rev. Microbiol.* 33, 183–209. doi: 10.1080/10408410701451948

Saha, R., Verseput, A. T., Berla, B. M., Mueller, T. J., Pakrasi, H. B., and Maranas, C. D. (2012). Reconstruction and comparison of the metabolic potential of cyanobacteria *Cyanothece* sp. ATCC 51142 and *Synechocystis* sp. PCC 6803. *PLoS ONE* 7:e48285. doi: 10.1371/journal.pone.0048285

Singh, D. P. (2009). "Some secrets of ubiquity in cyanobacteria," in *Algal Biology and Biotechnology*, eds J. I. S. Khattat, D. P. Singh, and G. Kaur (India: I.K. International Publishing House Pvt. Ltd.), 57–62.

Smith, V. H. (1983). Low nitrogen to phosphorus ratios favor dominance by blue-green algae in lake phytoplankton. *Science* 225, 669–671. doi: 10.1126/science.221.4611.669

Smith, V. H. (1986). Light and nutrient effects on the relative biomass of blue-green algae in lake phytoplankton. *Can. J. Fish. Aquat. Sci.* 43,148–153. doi: 10.1139/f86-016

Stockner, G., and Shortreed, S. (1988). Response of Anabaena and Synechococcus to manipulation of N:P ratios in a lake fertilization experiment. *Limnol. Oceanogr.* 33, 1348–1361. doi: 10.4319/lo.1988.33.6.1348

Willows, R. D., Li, Y., Scheer, H., and Chen, M. (2013). Structure of chlorophyll f. *Org. Lett.* 15, 1588–1590. doi: 10.1021/ol400327j

Wood, A. M., Everroad, R. C., and Wingard, L. M. (2005). "Measuring growth rate in microalgal cultures," in *Algal Culturing Techniques*, ed. R. A. Anderson (UK: Elsevier Academic Press), 269–288.

Conflict of Interest Statement: The authors declare that the research was conducted in the absence of any commercial or financial relationships that could be construed as a potential conflict of interest.

Received: 27 December 2013; accepted: 07 February 2014; published online: 25 February 2014.

Citation: Li Y, Lin Y, Loughlin PC and Chen M (2014) Optimization and effects of different culture conditions on growth of Halomicronema hongdechloris – a filamentous cyanobacterium containing chlorophyll f. Front. Plant Sci. ***5****:1. doi: 10.3389/fpls.2014.00067*

This article was submitted to Plant Physiology, a section of the journal Frontiers in Plant Science.